Robust and Cooperative Formation Control of Nonlinear Multi-Agent Systems

by

Yang Fei

B Eng (Control Science and Engineering),
Harbin Institute of Technology, China, 2018

Thesis submitted for the degree of

Doctor of Philosophy

in

School of Electrical & Electronic Engineering
Faculty of Sciences, Engineering and Technology
The University of Adelaide, Australia

2022

Supervisors:

Prof. Peng Shi, School of Electrical & Electronic Engineering

Prof. Cheng-Chew Lim, School of Electrical & Electronic Engineering

© 2022
Yang Fei
All Rights Reserved

THE UNIVERSITY *of* ADELAIDE

Contents

Abstract

Compared with the conventional approach of controlling autonomous systems individually, building up a cooperative multi-agent structure is more robust and efficient for both research and industrial purposes. Among the many subbranches of multi-agent systems, formation control has been a popular research direction due to its close connection with complex missions such as spacecraft clustering and intelligent transportation. Hence, this thesis focuses on providing new robust formation control algorithms for first-order, second-order and mixed-order nonlinear multi-agent systems to construct and maintain stable system structure in practical scenarios.

System uncertainties and external disturbances are commonly seen factors that could negatively affect the formation tracking precision. Among the many popular tools of uncertainty estimation, the implementation of approaches including neural network adaptive estimation and observer-based approximation are discussed in this thesis.

Regarding the neural-based approximation process, different neural network structures including Chebyshev neural network, radial basis function neural network, two-layer artificial neural network and three-layer artificial neural network are tested and implemented. The merits and drawbacks of each network design in the field of control is then analysed. Apart from that, this thesis also offers detailed comparison between the cooperative tuning approach and the observer-based tuning approach regarding the neural network structure to find their corresponding applicable scenarios.

To ensure the safety of the formation control algorithms, the issues of obstacle avoidance and inter-agent collision avoidance are both considered. Although the method of constructing artificial potential fields is a popular approach in both the field of path planning and motion control, few have discussed the effect of the inter-agent communication on the collision avoidance scheme.

For the obstacle avoiding scenarios, the passive correcting behaviour of individual agent is defined and investigated. A new algorithm is then introduced to modify the reference of individual agents to act as the mitigation. The issue of insufficient information accessibility is then discussed for multi-agent systems with a static and uncompleted communication topology. A distance-based communication topology is proposed to create necessary information exchange channel for unconnected agent pairs that are close enough.

The actuator saturation issue is also considered for both first-order multi-agent systems and second-order multi-agent systems to increase the practicality of the formation control schemes. Apart from restricting the amplitudes of the control input, the effect of the input coupling phenomenon is investigated. The oscillation of states brought by the coupled and saturated control input is then summarised as the reverse effect. To attenuate the state oscillation, the methods of developing control input regulation algorithms and employing auxiliary compensator are discussed and validated.

The last technical problem to discuss is the hierarchical control scheme. The issue of how to decouple the inter-agent communication and the motion dynamics is discussed for both unified-order and mixed-order multi-agent systems. By using a hierarchical formation control structure, the inter-agent communication process is considered based on a group of virtual agents with ideal characteristics, which can significantly reduce the complexity of the system design. Adaptive hierarchical control schemes are then proposed and validated for both unified-order and mixed-order multi-agent systems through the examples of a multi-drone system and a multiple omni-directional robot system, respectively.

Statement of Originality

I certify that this work contains no material which has been accepted for the award of any other degree or diploma in my name, in any university or other tertiary institution and, to the best of my knowledge and belief, contains no material previously published or written by another person, except where due reference has been made in the text. In addition, I certify that no part of this work will, in the future, be used in a submission in my name, for any other degree or diploma in any university or other tertiary institution without the prior approval of the University of Adelaide and where applicable, any partner institution responsible for the joint award of this degree.

I acknowledges that copyright of published works contained within the thesis resides with the copyright holder(s) of those works.

I give permission for the digital version of my thesis to be made available on the web, via the University's digital research repository, the Library Search and also through web search engines, unless permission has been granted by the University to restrict access for a period of time.

Signed: .. ... Date: 24/06/2022 ....

Acknowledgements

I would like to express my sincere appreciation to my PhD supervisors, Professor Peng Shi and Professor Cheng-Chew Lim, for their kind encouragement, guidance and support throughout the past three years of my PhD journey.

I am so thankful that Professor Shi was kind enough to accept me as a part of the System and Control Group even though I shared no experience or ability in conducting research. When I struggled in my first period of study, Professor Shi was patient enough to comfort me and guide me on the road of exploring. As an old saying in Chinese, a great kid is usually raised by a loving mother and a solemn father. To me, Professor Shi is the "loving mother" who always encourages me during my journey of research.

Meanwhile, Professor Lim takes up the role of being a "solemn father" and keeps reminding me to be a rigorous researcher with precise and powerful words. Because of him, I learnt to always think twice before presenting any ideas.

I also greatly appreciate the support received from the School of Electrical and Electronic Engineering, the Faculty of Sciences, Engineering and Technology and the University of Adelaide for the outstanding research resources and the following financial support:

1. ECMS Faculty Divisional HDR Scholarship
2. Frank Perry Travelling Scholarship in Engineering 2020
3. ECMS HDR Travelling Scholarship 2021

I would like to thank the Institution of Engineering and Technology for recognising my research work through the following awards:

1. IET Presentation Around The World 2019 SA & NT Region Student Winner
2. IET Presentation Around The World 2019 SA & NT Region Audiences' Favourite

3. IET Presentation Around The World 2019 SA & NT Region Runner-up

4. IET Presentin10 2021 Digital Futures Topic Finalist

I also want to express my appreciation for all the help and encouragement received from my friends, Yuan Sun, Jingbo Fu, Di Shen, Jie Han, Qing Lu, Xiaolong You, Weijie Gao, Xin Yuan, Zhi Lian, Xiaoyang Yin, Dr. Siti Nailah Mastura Zainarry, Dr. Md. Saiful Islam, Yuan Yao, Zhi Cao and Hua Ma. I will treasure the valuable moments and our friendships forever.

I would also express my deep gratitude to two old friends back at China, Baozhao Ma and Jin Meng, who help me get through some hard time during the candidature with some heartwarming video chats.

Last but not the least, I want to express my heartfelt love and thanks to my family. They have been offering the strongest support and motivation since I left my hometown three years ago. I can never achieve where I am now without their endless encouragement and belief. I love you all and this thesis is a tribute to you all.

Thesis Conventions

The following conventions have been adopted in this Thesis:

Typesetting

This document was compiled using LaTeX2e. Texmaker 5.0.2 was used as text editor interfaced to LaTeX2e. Inkscape 0.92.2 was used to produce schematic diagrams and other drawings.

Spelling

Australian English spelling conventions have been used, as defined in the Macquarie English Dictionary (A. Delbridge (Ed.), Macquarie Library, North Ryde, NSW, Australia, 2001).

Referencing

The Harvard style is used for referencing and citation in this thesis.

System of Units

The units comply with the international system of units recommended in an Australian Standard: AS ISO 1000-1998 (Standards Australia Committee ME/71, Quantities, Units and Conversions 1998).

Publications

The majority of my work has been summarised into the following journal articles:

Journal publications

YANG FEI, PENG SHI, CHENG-CHEW LIM (2020). Neural network adaptive dynamic sliding mode formation control of multi-agent systems, *International Journal of Systems Science*, **51**(11), pp. 2025–2040.

YANG FEI, PENG SHI, CHENG-CHEW LIM (2021). Robust formation control for multi-agent systems: A reference correction based approach, *IEEE Transactions on Circuits and Systems I: Regular Papers*, **68**(6), pp. 2616-2625.

YANG FEI, PENG SHI, CHENG-CHEW LIM (2021). Robust and collision-free formation control of multiagent systems with limited information, *IEEE Transactions on Neural Networks and Learning Systems*, Accepted, doi: 10.1109/TNNLS.2021.3112679.

YANG FEI, YUAN SUN, PENG SHI (2022). Robust Hierarchical Formation Control of Unmanned Aerial Vehicles via Neural-Based Observers, *Drones*, **6**, pp. 40. (**Invited**)

YANG FEI, PENG SHI, CHENG-CHEW LIM (2022). Neural-based formation control of uncertain multi-agent systems with actuator saturation, *Nonlinear Dynamics*, **108**, pp. 3693–3709.

YANG FEI, PENG SHI, CHENG-CHEW LIM (2022). Robust formation control of saturated multi-agent systems via neural-based sliding mode observers and linear programming, *International Journal of Robust and Nonlinear Control*, revised version under review.

Some brief work is also published in the following conference proceedings:

Conference publications

YANG FEI, XIN YUAN, PENG SHI, CHENG-CHEW LIM (2020). Uncertainty-observer-based dynamic sliding mode formation control for multi-agent systems, *International Conference on Machine Learning and Cybernetics (ICMLC)*, Adelaide, Australia, DOI: 10.1109/ICMLC51923.2020.9469539.

YANG FEI, XIN YUAN, PENG SHI, CHENG-CHEW LIM (2021). Neural-based hierarchical formation control of mixed-order multi-agent systems, *International Conference on Machine Learning and Cybernetics (ICMLC)*, Adelaide, Australia, DOI: 10.1109/ICMLC54886.2021.9737151.

List of Acronyms

CNN .... Chebyshev neural network

DSM .... Dynamic sliding mode

ESO .... Extended state observer

FTDO .... Finite-time disturbance observer

MAS .... Multi-agent system

NN .... Neural network

ODR .... Omni-directional robot

SMC .... Sliding mode control

UAV .... Uncrewed aerial vehicle

UUB .... Uniformly ultimately bounded

Notation

G .... Graph

I_n .... Identity matrix with the dimension of n

$\mathbb{R}^n$ .... Set of $n \times 1$ real vectors

$\mathbb{R}^{m\times n}$ .... Set of $m \times n$ real matrices

$\overrightarrow{a_1 a_2}$ .... The vector pointing from point a_1 to point a_2

$\otimes$ .... Kronecker product

$\underline{\sigma}(\mathcal{B})$ .... The minimal eigenvalue of a square matrix $\mathcal{B}$

$\overline{\sigma}(\mathcal{B})$ .... The maximum eigenvalue of a square matrix $\mathcal{B}$

$\|\mathcal{B}\|$ .... The Euclidean norm of vector $\mathcal{B}$

$\|\mathcal{B}\|_F$ .... The Frobenius norm of matrix $\mathcal{B}$

$\mathcal{B}^{\mathrm{T}}$ .... Transpose of matrix $\mathcal{B}$

$\det(\mathcal{B})$ .... Determinant of matrix $\mathcal{B}$

List of Figures

List of Tables

Chapter 1

Introduction

CONSTRUCTING a multi-agent structure to form the collaboration among a cluster of intelligent robots is a promising choice to increase the capability and impact of each agent. It is undeniable that the robot cluster needs to move around in certain formation while carrying out different tasks. Hence, it is necessary to develop adaptive formation control algorithms to enhance the robustness of the multi-agent structure while moving. This chapter briefly introduces the research background, literature review, research questions in the field of formation control and the thesis outline.

1.1 Research background

Compared with the conventional approach of controlling autonomous systems individually, building up a cooperative multi-agent structure (Peydayesh and Arefi 2021, Shi and Yan 2020, Sun *et al.* 2021b, Yang *et al.* 2022) is more robust and efficient for both research (Olfati-Saber and Murray 2004) and industrial (Sharma *et al.* 2021) purposes. To illustrate the concept of multi-agent systems (MASs), it is necessary to first understand the concept of an agent.

In the field of artificial intelligence and electrical engineering (Wooldridge 2009), an agent is defined to have three important features, which are the ability to sense, decide and actuate:

1. Sense: An agent should be able to sense its local surroundings and localise itself.
2. Decide: An agent should be able to make self decisions and control its motion.
3. Actuate: An agent should be equipped with actuators that can allow itself to move around or interact with the local surroundings.

Decades ago, the concept of the multi-agent structure was developed based on the observations on the animal behaviours (Reynolds 1987). Animals usually choose to form up a team to conquer tasks far beyond their individual capabilities. Such observations then offer inspiration to the area of robotics and control engineering and further lead to the development of MAS.

Around the year of 2000, the concept of MAS and networked systems was introduced into the control society for their huge potential in the development of robotics (Olfati-Saber 2006, Anderson *et al.* 2008), micro-grids and traffic control (Choy *et al.* 2003). After many years of research, applying MASs is found to have the following merits over implementing single agents:

1. MASs have the ability of completing complex tasks such as building constructions (Lindsey *et al.* 2012) and have less time consumption.
2. Maintaining a MAS structure has lower energy cost for dynamic tasks such as cargo transportation (Chen and Cheng 2010), leading to higher efficiency.

3. MASs hold higher system redundancy, meaning that the multi-agent structure has higher chances of maintaining robustness and tolerating system faults.

The main focus of this thesis lies in the development of robust control techniques for MASs, which belongs to a subbranch of the ability to "decide". In general, there are two control structures for a MAS: centralised control and distributed control. The centralised approaches usually require the implementation of one control centre such as a central computer. The centre node is responsible for connecting individual agents and generating control commands. Although this structure is easy to employ in practice, such method is in fact fragile because of its over-dependence on the control centre.

On the contrary, there is no master that controls the entire system in a distributed structure. Each individual agent is offered the ability to make its own decisions, which remarkably increases the robustness of the system. Currently, there are four main control issues in the field of MASs:

1. Consensus control (Olfati-Saber and Murray 2004, Olfati-Saber *et al.* 2007, Gambuzza and Frasca 2020) that focuses on regulating the states of each individual agent to one or several unified values.

2. Formation control (Dong *et al.* 2016, Wang *et al.* 2019) that concentrates on the development of control schemes that can let MASs form up certain physical shapes such as circles and rectangles.

3. Containment control (Li *et al.* 2013) that investigates how to restrict the states of each agent within certain range that is correlated with one or several leaders.

4. Flocking and swarming (Olfati-Saber 2006, Kushleyev *et al.* 2013) that discusses the algorithms that can ensure static or dynamic gathering of a large number of agents.

Apart from the above four parts, there are also derivatives such as scaled consensus control (Roy 2015) and formation-containment control (Dong *et al.* 2018). In specific, The topic of cooperative formation control is chosen as the main concern of this thesis because of its close connection with practical applications including cooperative satellite clusters (Kang and Yeh 2002), intelligent transportation systems (Chen and Cheng 2010), and surveillance (Zhang *et al.* 2019).

1.2 Literature review

To dig out the potential issues to solve in the area of cooperative formation control, it is essential to review some past results. In this section, a brief overview of the consensus control problem is first given to offer fundamental knowledge for the formation control design. Some achievements and critical issues in the formation control society are then presented. After that, the basics of the sliding mode control (SMC) technique, the observer-based scheme and the neural-based adaptive control scheme are introduced.

1.2.1 Consensus control of multi-agent systems

Consensus is the most basic problem in the field of MAS because it is necessary to first let each individual agent agree on the mutual goal of the system so that they can cooperative with each other. As previously mentioned, the final goal of consensus control is to achieve the agreement of certain states for each agent (Ren and Beard 2005). Olfati-Saber first found that the states of a cluster of networked first-order agents will converge to a common value if the Laplacian matrix is applied in the control law design (Olfati-Saber and Murray 2004). The above work of Olfati-Saber's also pointed out two important factors in the control problem of networked MAS: communication topology and time delay.

The communication topology, which acts as the medium of the information exchange among agents, can be either static or time-varying depending on the specific application scenario. Hence, the consensus control problem is widely investigated for systems with both static communication topology (Ren *et al.* 2007) and switching communication topology (Ren and Beard 2005) . In recent years, the consensus issue is further extended to the scenario where the communication graph is partially unknown.

Time delay is also an important issue when communication exists. In the perspective of MASs, time delays exist in two formats: state delay and input delay (Richard 2003). Memoryless control schemes (Liang *et al.* 2014) are found effective for MAS with state delays, while constructing predictors is a more popular way for MAS with input delay (Wang *et al.* 2018a).

1.2.2 Formation control of multi-agent systems

The concept of formation control (Chen and Wang 2005) is also developed on the basis of the consensus theory. In general, there are four main approaches to investigate the formation control problem: the behaviour-based strategy (Balch and Arkin 1998), the virtual-structure-based scheme (Wiech *et al.* 2018), the leader-follower approach (Dong *et al.* 2016) and the distributed approach (Dong *et al.* 2018).

The behaviour-based strategy aims to define a finite set of possible behaviours for robots in advance, such as "avoid static obstacle", "avoid robot", "move to goal" and "maintain formation" (Balch and Arkin 1998), then each robot will calculate the control input for the actuators according to the combined results of the above behaviours.

Compared with the other methods, the virtual-structure-based strategy (Balch and Arkin 1998) is more intuitive. Virtual structures such as springs and dampers are placed between each pair of agent to maintain the desired relative distance. However, such method is not widely used because of its low robustness.

In the leader-follower structure, all agents are classified into two kinds: leaders and followers. The leaders are set with some predefined control scheme to act as the reference sources of the system formation status. Only a part of the followers can access the reference information from the leaders, and all followers use their local information to conduct formation tracking. In terms of the leader selection, both virtual leaders (Dong *et al.* 2016) and physical leaders (Yan *et al.* 2021) are applicable. Regarding the number of leaders, there are also available choices of having a single-leader structure (Dong *et al.* 2016) or constructing a multi-leader structure (Han *et al.* 2017). To ensure that the information of the leader can be obtained by each follower directly or through the communication with other followers, the communication topology is usually required to include at least a spanning tree from the cluster leader(s).

Compared with the leader-follower structure, all agents share the same role in the distributed structure (Fei *et al.* 2021a), meaning that each agent knows the exact desired position for itself to construct the system formation. In general, there are three ways to carry out a distributed formation tracking process (Oh *et al.* 2015):

1. Position-based control: Agents only make decisions according to the difference between their own positions and the corresponding references. This structure

requires no communication ability but lose the basic concept of having agents work cooperatively.

2. Displacement-based control: Agents make decisions based on the combination of both their own reference tracking errors and the ones from their neighbours (Fei *et al.* 2021b). This structure requires both distributed communication network and global sensing capabilities.

3. Distance-based control: Agents make decisions based on the relative distance and orientation between themselves and their current neighbours. This structure no longer requires the implementation of global sensing technologies but is heavily dependent on the communication technology. The communication graph needs to be rigid to ensure the successful construction of system formation (Sun *et al.* 2017).

This thesis focus on the development of robust displacement-based formation control algorithms, which currently contains three main directions (Hou and Wang 2013):

1. Model-based control: The dynamics of the MAS is perfectly known. Hence, simple structures such as the proportional controller or the proportional-derivative controller is sufficient (Dong *et al.* 2016, Dong *et al.* 2018).

2. Adaptive control and robust control: Part of the system dynamics (for example, the system order) is known during the controller design procedure and the uncertain terms are whether passively rejected (Yang *et al.* 2012) or actively estimated and compensated (Yu *et al.* 2018, Fei *et al.* 2020).

3. Model-less control: System dynamics is hard to develop or unavailable, indicating that the only possible way is to adjust the control input according to the available output data (Xiong and Hou 2021).

As mentioned, this thesis concentrates on the analysis and design of adaptive formation controller and robust formation controller, which include the designs based on the SMC technique, the observer-based control scheme and the neural-based adaptive control scheme.

1.2.3 Sliding mode control

The sliding mode technique (Shtessel *et al.* 2014) was brought up for the robust controller design of second-order and higher-order systems. To give direct illustration of this method, suppose there is a continuous-time second-order system as follows:

$$\begin{cases} \dot{x} = v \\ \dot{v} = u + w \end{cases}$$

where $x \in \mathbb{R}^n$ is the position state, $v \in \mathbb{R}^n$ is the velocity information, $u \in \mathbb{R}^n$ is the control input and $w \in \mathbb{R}^n$ is the system uncertainty.

If the reference state for the above system is given as $x_d \in \mathbb{R}^n$, then the following sliding variable is constructed to consider position tracking error and velocity tracking error simultaneously:

$$s = v - \dot{x}_d + \lambda(x - x_d)$$

where $\dot{x}_d \in \mathbb{R}^n$ is the velocity reference and λ represents the slope of the sliding surface.

In such way, the system error will converge exponentially in the following fashion if $\|s\| = 0$:

$$v - \dot{x}_d = \dot{x} - \dot{x}_d = -\lambda(x - x_d)$$

Therefore, the goal of sliding mode controller design is summarised as ensuring the convergence or boundedness of the sliding variable s. With the model being partially known, the time derivative of the sliding surface is given as

$$\dot{s} = u + w - \ddot{x}_d + \lambda(v - \dot{x}_d)$$

To ensure the boundedness of s, the sign function $\mathrm{sign}(\cdot)$ is employed (Liu and Wang 2012) to reject the uncertain factor and formulate the classic controller design as

$$u = \ddot{x}_d - \lambda(v - \dot{x}_d) - w_M \mathrm{sign}(s)$$

where $w_M \in \mathbb{R}^+$ is the boundary of the uncertain term.

Based on the above design, many modified versions of the sliding surface is developed to achieve different goals:

1. Integral sliding surface (Ma *et al.* 2017): The integration of the position error is included in the sliding surface design to compensate for the uncertain term to avoid the chattering phenomenon led by the switching function.

2. Terminal sliding surface (Zou *et al.* 2011): Terms with fractional order (less than 1) are introduced to increase the convergence speed around the equilibrium point.

3. Dynamic sliding surface (Liu and Wang 2012): An auxiliary variable is introduced to increase the order of the sliding surface to increase the robustness of the controller design.

Although many existed research work have introduced the sliding mode technique into the field of MAS, there are some potential gaps:

1. Certain sliding mode techniques have not yet been tested in the multi-agent cooperative control scenario (for example, the dynamic sliding mode technique).

2. Although the switching function can reject the effect of uncertain terms, it does introduce extra chattering phenomenon into the control input. Hence, it is necessary to find suitable substitutions for the switching function to maintain robustness with smooth control input.

1.2.4 Neural networks and observers

Other than disturbance rejection, another popular approach for robustness maintenance is to estimate the uncertain terms and make compensations when necessary. Currently, there are two commonly seen approaches for uncertainty approximation: observer estimation and neural-based estimation.

The core idea of the observer design is to build up a virtual system that share the same structure as the investigated system, then applying adaptive laws within the virtual structure to minimise the difference between the states of the virtual system and the corresponding ones of the actual system.

The concept of SMC is employed to construct finite-time disturbance observer (FTDO) that can estimate both matched and mismatched uncertainties simultaneously within finite time if the uncertain terms' Lipschitz constants are known in advance (Levant 2003, Chalanga *et al.* 2016).

For the case where only part of the system's state information is accessible, an auxiliary state (Yu *et al.* 2019) is defined to act as the estimation of the derivative of the uncertain term to construct extended state observers (ESOs). However, two of the following conditions must be satisfied to ensure the boundedness of the estimation error: (1) The uncertain term is energy bounded. (2) The value of the error amplifier in the last layer is chosen as infinity.

On the other hand, the neural-based estimation process is based on the concept of linearisation. According to the universal approximation rule (Liu *et al.* 2013), an m $(m \geq 2)$ layered neural network (NN) is able to estimate any function with bounded approximation error if the input vector of the NN is restricted to a certain compact set.

Different from deep NNs that are implemented in the field of image processing, two-layer NNs (Lewis *et al.* 2013) and three-layer NNs (Liu *et al.* 2013) are more common in control engineering (see Figure 1.1). In Figure 1.1, x is the input of NNs, $\varphi(\cdot)$ is the activation function in the first layer, $\widehat{W}_2$ is the weight in the hidden layer, $\sigma[\cdot]$ is the activation function in the second layer, $\widehat{W}_1$ is the weight for NN output and $\widehat{d}$ is the NN output. Note that the input layer is separated into two individual layers on purpose because different activation functions lead to different NN names in control. If the $\varphi(x)$ is chosen as a set of Chebyshev polynomials (Zou *et al.* 2013), then the corresponding two-layer NN is called Chebyshev neural network (CNN). Likewise, a two-layer NN is called radial basis function NN if $\varphi(\cdot)$ is chosen as the radial basis function (Zheng *et al.* 2021), and a two-layer NN is classified as fuzzy NN if $\varphi(\cdot)$ is a fuzzification function (Tsai *et al.* 2017).

Regarding the tuning approach of NNs, the cooperative tuning laws (Zou *et al.* 2013, Lewis *et al.* 2013) that are based on each agent's local information are widely studied. Other than that, there are also research works that discuss how to embed NNs into observers (Liu *et al.* 2013), leading to a new set of tuning laws that is independent from the reference tracking process.

The merits and drawbacks of the above three methods are summarised in Table 1.1. Based on the above discussions, there are several questions that are worthy of investigation in the field of adaptive estimation:

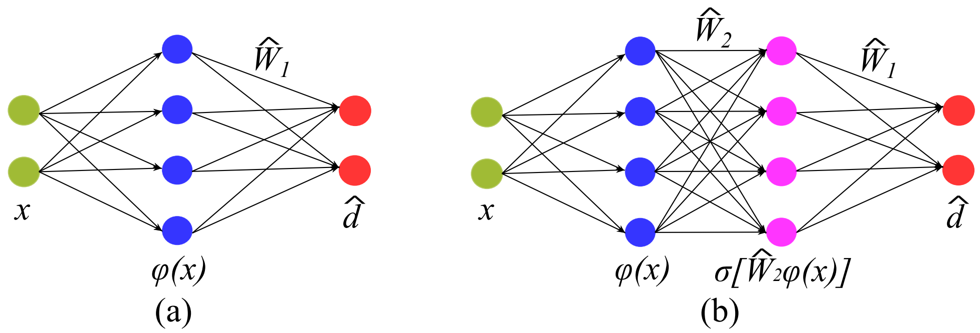

Figure 1.1. Illustration of NN Structures. (a) Two-layer NN (b) Three-layer NN

Table 1.1. Comparisons of two estimation approaches.

Criterias	FTDO	ESO	NNs
Estimate system states	No	Yes	No
Estimate matched uncertainties	Yes	Yes	Yes
Estimate mismatched uncertainties	Yes	No	No
Requirements for uncertainties	Yes (Lipschitz constants)	Yes (Energy bounded)	No
System states are required	Yes	No	Yes

1. Is the cooperative tuning approach (Lewis *et al.* 2013) the optimal method for all MASs?

2. Is it possible to achieve finite-time estimation in the neural-based observer structure (Liu *et al.* 2013)?

3. Is it possible to combine the sliding mode technique (Chalanga *et al.* 2016) and the NN-based estimation to find a fast NN tuning approach?

To give intuitive explanation of the literature review process, the overall mind map is given in Figure 1.2, where the topics discussed in this thesis are highlighted in pink.

1.3 Research questions

Motivated by the above discussions, this thesis provides answers to the following question:

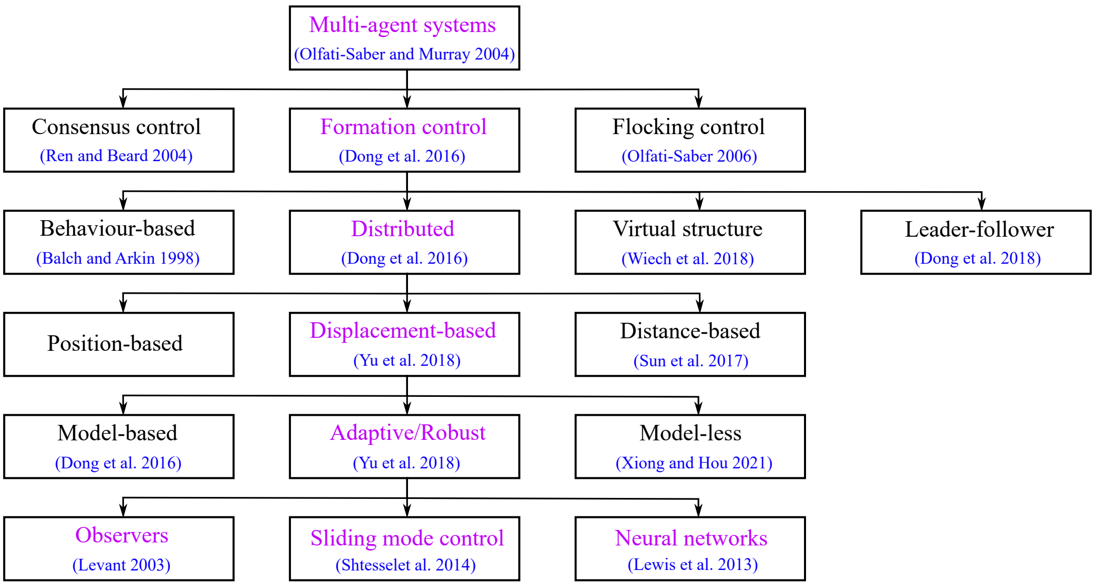

Figure 1.2. Mind map of the literature review.

How to ensure the safety and maintain the robust tracking behaviour of heterogeneous nonlinear MASs affected by factors including uncertainties, external disturbances and actuator saturation in time-varying formation tracking scenarios?

In specific, this thesis provides insights for the following research questions:

1. Regarding second-order nonlinear MASs with matched uncertainties and hysteresis phenomenon, how to design a robust and **smooth** formation controller to ensure the boundedness of the formation tracking error?

2. Regarding second-order nonlinear MASs with both matched and mismatched uncertainties, how to design a robust formation controller that can perform **obstacle avoidance** and **attenuate the passive correction** led by the cooperative information sharing?

3. Regarding second-order nonlinear MASs with limited system knowledge and matched uncertainties, how to estimate the unknown system information and further design a robust and **collision-free** formation controller?

4. Regarding first-order nonlinear MASs with actuator saturation and system uncertainties, how to find a **finite-time** tuning approach for **three-layer NNs** and attenuate the **reverse effect** caused by input coupling and input saturation.

5. Regarding second-order nonlinear MASs with actuator saturation and matched uncertainties, how to achieve **finite-time NN-based estimation** via sliding mode technique and further construct a robust formation controller that can **attenuate the state overshoot and oscillation**.

6. Regarding unfied-order MASs and heterogeneous mixed-order MASs, how to design **hierarchical formation control schemes** to avoid the negative effects of dynamics coupling and dynamics mismatch.

1.4 Thesis structure

To discuss the aforementioned questions, this thesis contains eight chapters.

In Chapter 1, the background introduction of the formation control problem of MASs, literature review, potential gaps and the outline of the thesis are provided.

In Chapter 2, the formation control problem for second-order nonlinear MASs with matched uncertainties and hysteresis phenomenon is discussed. The basics of the dynamic SMC technique is first introduced to offer a new perspective for the robust controller design. Both the FTDO-based and the CNN-based estimation methods are presented to estimate the matched uncertainties and their derivatives. To ensure the smoothness of the control input, the hysteresis inverse model is implemented to offer a robust way to design the time derivative of the control input.

In Chapter 3, the problem of obstacle avoidance is considered for a class of second-order nonlinear MASs with both matched and mismatched uncertainties. FTDOs are employed to estimate the system uncertainties within finite time. The APF technique is implemented to offer high potential energy to static obstacles so that the agents will be driven away from the virtual repulsive force to avoid collisions. The passive correcting behaviour caused by the cooperative information sharing is also studied and discussed. A new reference correction algorithm is developed to attenuate the corresponding passive corrections.

In Chapter 4, the robust formation control problem is extended for uncertain second-order MASs without velocity measurement. A new finite-time neural-based observer is developed to approximate the unknown velocity and the matched uncertainties simultaneously. To reduce the state oscillation in the NN output, a new fractional sensitivity parameter design is proposed. The essential issue of avoiding inter-agent collision is also considered, where both the APF technique and a distance-based communication topology is implemented to ensure the boundedness of the relative distance between an arbitrary pair of agents.

In Chapter 5, the actuator saturation phenomenon is included in the system modelling to enhance the practicality of the control scheme. The research focus of this chapter lies in the development of the adaptive three-layer NN tuning laws and the robust formation controller for uncertain first-order MASs. To avoid the potential divergence of the NN weights, a set of fully local-error-related tuning laws are developed for the cooperative tuning process. To ensure the finite-time convergence of the NN estimation error, a finite-time NN-based observer is then proposed for the uncertainty estimation. A new scheme is then provided to analyse the combined effect of input coupling and input saturation, then the corresponding issue is defined as the reverse effect. To attenuate the state oscillation led by the reverse effect, a new control input distribution algorithm is presented.

In Chapter 6, the input saturation phenomenon is discussed for second-order MASs in the formation control scenario. Virtual systems with dynamics identical to the actual agents are defined to share the concept of switching the estimation problem into a control problem. The new idea of employing the control input of the imaginary system as the final estimation result is developed to increase the estimation precision. To ensure the finite-time characteristics of the NN-based estimation process, the sliding mode technique is further embedded into the NN-based observer structure to shorten the error converging time. A new linear-programming-based control input regulation algorithm is then proposed to attenuate the state oscillation caused by the reverse effect.

In Chapter 7, instead of consider the multi-agent cooperation behaviour in the motion control layer, the inter-agent information exchange is embedded within the path planning section. The example of a cluster of uncrewed aerial vehicles (UAVs) is first used to represent MASs with strong dynamics coupling. A fully error-related tuning approach is proposed for NN-based sliding mode observer to estimate the unknown factors in the UAV dynamics. The sliding mode technique is then applied in both the path planning layer and the motion control layer to ensure the boundedness of the reference tracking error. Afterwards, the formation control issue is extended to a more complex situation where agents share different dynamics order. The correlated dynamics mismatch issue is analysed and defined for the conventional single-layer formation control scheme. To avoid the negative effect brought by dynamics mismatch, a NN-based hierarchical robust formation control scheme is then developed.

In Chapter 8, the work of this thesis is summarised and the final conclusions are drawn. Some open problems that are worthy of future discussion are also discussed.

To give direct illustration of the thesis structure, the relationships among chapters are briefly presented in Figure 1.3. The inherited methods or issues are given in purple, while the inspirations and the further discussed issues are illustrated in red.

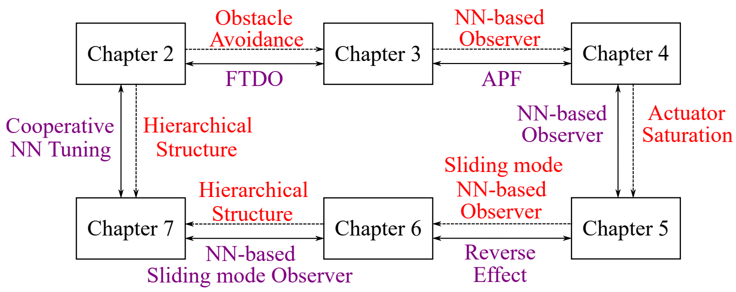

Figure 1.3. Correlations among chapters.

1.5 Chapter summary

The research background, recent literature, research questions and the structure of the thesis are given in this chapter.

In the next chapter, the basis of the dynamic sliding mode (DSM) control scheme is first explained to offer fundamental knowledge for its application under the topic of formation control. Both FTDOs and NNs are further introduced to act as the adaptive uncertainty estimator. Two DSM formation controllers are then developed for FTDOs with matched uncertainties.

Chapter 2

Formation Control via Dynamic Sliding Mode Scheme

ALTHOUGH sliding mode algorithms are famous for their high robustness, the classic switching-based design has received quite a few criticism for its impracticality for non-ideal actuators. In this chapter, two adaptive dynamic sliding mode formation control schemes are proposed for a class of second-order multi-agent systems with actuator hysteresis to achieve the boundedness of the tracking errors. First, a brief introduction of the dynamic sliding mode controller design is presented. To relieve the dependency of using fast switching function for uncertainties rejection, an observer-based approach is proposed for second-order multi-agent systems with ideal controllers. Furthermore, an adaptive method that is based on the application of Chebyshev neural network is further presented for a class of second-order multi-agent systems with actuator hysteresis. Simulations based on a group of omni-directional robots are given to illustrate the effectiveness of the proposed designs.

2.1 Introduction

The formation control problem is a topic worthy of investigation to apply cooperative MASs in practical scenarios like search and rescue (Meng *et al.* 2014), real-time surveillance and intelligent transportation (Chen and Cheng 2010).

The time-varying formation control problem was first discussed for a class of linear time-invariant MASs and the solution of an Riccati equation is employed to set up the formation controller (Dong *et al.* 2016, Dong *et al.* 2018). Although the stability of the above approach is validated by the Lyapunov stability theory, the corresponding results were obtained based on the assumption that all agents are ideally linear and free of unknown factors. Motivated by this gap, many researchers switch their focus to the robust controller design for MASs affected by dynamics uncertainties or external disturbances. Among the many robust control schemes, the sliding mode technique (Meng *et al.* 2014) is a popular choice due to its high robustness. However, the classic way of adopting switching functions in the control law will also introduce extensive chattering into the control input, making this approach less feasible for practical applications.

To ensure the smoothness of the control input, a high-order SMC algorithm with the name of DSM is proposed (Liu and Wang 2012). Instead of designing the value of control input directly, DSM offers us an alternative approach, which is designing the changing rate of the control input. Although the DSM approach is found to have higher robustness than the conventional sliding mode controllers, more assumptions regarding the system uncertainty's boundedness is required, which increases the design's conservatory. Hence, it is necessary to investigate how to integrate some popular uncertainty estimation methods such as observers (Shtessel *et al.* 2007) and NNs (Zou and Kumar 2012, Zou *et al.* 2013, Tsai *et al.* 2017) with the DSM technique to ensure adaptiveness and robustness simultaneously.

Meanwhile, the actuators in practical scenarios are usually not ideal. Nonlinear phenomenons including actuator hysteresis (Liu *et al.* 2015, Chen *et al.* 2016) are commonly seen for actuators that includes gears or similar structures. Over the different ways of describing the hysteresis effect, the Bouc-Wen model (Zhou *et al.* 2012) is found to have higher generality. Hence, it is necessary to find the mitigation to reduce the negative effect of the Bouc-Wen hysteresis phenomenon.

The following issues are addressed in this chapter:

1. How to integrate the uncertainty estimation methods (FTDO and CNN) with the DSM controller?
2. How to mitigate the negative effect of actuator hysteresis phenomenon in a DSM control scheme?
3. How to ensure the boundedness of each agent's local formation tracking error to achieve time-varying formation?

The contents in this chapter are organised as follows. The system modelling of a class of nonlinear MASs with hysteresis and the problem formulation are given Section 2.2. A brief introduction of the graph theory, the matrix theory, and the DSM technique is given in Section 2.3. A preliminary FTDO-based scheme is presented in Section 2.4 for uncertain MASs with ideal actuators. Modifications are then made to bring out the CNN-based formation controller Section 2.5 for uncertain MASs with actuator hysteresis. Simulations are conducted for both controller designs in their individual sections and the final conclusions are drawn in Section 2.6.

2.2 System modelling and problem formulation

In this chapter, consider a group of second-order nonlinear agents affected by the actuator hysteresis phenomenon, where the system dynamics of the ith agent is

$$\begin{cases} \dot{x}_i = v_i \\ \dot{v}_i = f_i(x_i, v_i) + h_i(u_i) + \bar{\omega}_i, \quad i = 1, 2, \ldots, N \end{cases} \tag{2.1}$$

where $x_i \in \mathbb{R}^n$ and $v_i \in \mathbb{R}^n$ are the position and velocity information of the ith agent, respectively, $f_i(x_i, v_i) \in \mathbb{R}^n$ is the unknown continuous system dynamics, $u_i \in \mathbb{R}^n$ is the control input, $\bar{\omega}_i \in \mathbb{R}^n$ is the external disturbance, $h_i(u_i) \in \mathbb{R}^n$ is the actuator hysteresis phenomenon (such as the ferromagnetic effect that exists in motor drive).

The Bouc-Wen hysteresis model (Zhou *et al.* 2012) is employed to describe the hysteresis phenomenon:

$$h_i(u_i) = \mu_i u_i + \bar{\mu}_i \zeta_i \tag{2.2}$$

where $\mu_i \in \mathbb{R}$ and $\bar{\mu}_i \in \mathbb{R}$ are positive constants related to the stiffness and pseudonatural frequency of the hysteresis, respectively, and $\zeta_i \in \mathbb{R}$ is an auxiliary vector whose jth element is written as

$$\dot{\zeta}_{i,j} = \dot{u}_{i,j} - \bar{\chi}_i |\dot{u}_{i,j}||\zeta_{i,j}|^{m_i - 1}\zeta_{i,j} - \chi_i \dot{u}_{i,j}|\zeta_{i,j}|^{m_i}, \quad \zeta_{i,j}(t_0) = 0 \tag{2.3}$$

where $j = 1, \ldots, n$, $m_i \geq 1$ is the smoothness of the initial slope, $\bar{\chi}_i$ and χ_i are the parameters related to the shape and amplitude of the hysteresis phenomenon that satisfy $\bar{\chi}_i > |\chi_i|$.

To show that (2.2) and (2.3) are able to model hysteresis, consider a one dimensional control input u, and choose the hysteresis parameters as $\mu_i = 1.5$, $\bar{\mu}_i = 3$, $\bar{\chi}_i = 1$, $\chi_i = 0.5$ and $m_i = 2$. Then the projection $u \to h(u)$ is illustrated as the curve in Figure 2.1.

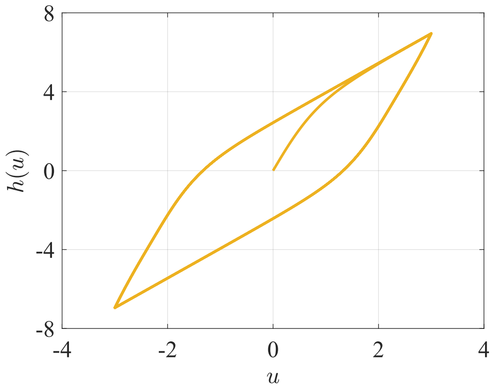

Figure 2.1. Illustration of the actuator hysteresis phenomenon.

To simplify the expression of the system dynamics, define $w_i = f_i(x_i, v_i) + \varpi_i$ to represent the overall uncertainty for the ith agent, then the simplified agent dynamics is obtained as

$$\begin{cases} \dot{x}_i = v_i \\ \dot{v}_i = h_i(u_i) + w_i, \quad i = 1, 2, \ldots, N \end{cases} \tag{2.4}$$

Define $x = [x_1^{\mathrm{T}}, x_2^{\mathrm{T}}, \ldots, x_N^{\mathrm{T}}]^{\mathrm{T}} \in \mathbb{R}^{nN\times 1}$ and $v = [v_1^{\mathrm{T}}, v_2^{\mathrm{T}}, \ldots, v_N^{\mathrm{T}}]^{\mathrm{T}} \in \mathbb{R}^{nN\times 1}$ as the position vector and velocity vector of the investigated MAS, respectively, then the cluster dynamics is obtained as follows:

$$\begin{cases} \dot{x} = v \\ \dot{v} = H + w \end{cases} \tag{2.5}$$

where H and w are given as

$$H = [h_1^{\mathrm{T}}(u_1), h_2^{\mathrm{T}}(u_2), \ldots, h_N^{\mathrm{T}}(u_N)]^{\mathrm{T}},\ w = [w_1^{\mathrm{T}}, w_2^{\mathrm{T}}, \ldots, w_N^{\mathrm{T}}]^{\mathrm{T}}$$

Definition 2.1. *Consider a state vector $X \in \mathbb{R}^n$, suppose there is a correlated continuous Lyapunov function $V(X)$. Then the vector X is said to be semi-globally uniformly ultimately bounded (UUB) if $V(X)$ satisfies $V(X) = 0$ only when $\|X\| = 0$, and there exists a positive boundary b_X and a time $t_X(X(t_0), b_X)$ such that $\|V(X)\| \leq b_X$ for all $t \geq t_0 + t_X$ and $X(t_0) \in \Omega_X^V$, where t_0 is the initial time, $X(t_0)$ is the initial value of X and Ω_X^V is a compact set of X.*

Lemma 2.1. (Ge *et al.* 2013) *Consider a vector X that satisfies $X(t_0) \in \Omega_X^V$ and its correlated continuous Lyapunov function $V(X)$, if $\dot{V}(X) < 0$ when $\|X\| > b_X$, then $\|X\|$ is said to be semi-globally UUB within the neighbourhood of $[0, b_X]$.*

The desired position for the ith agent to achieve can be specified as $x_{di} \in \mathbb{R}^n$ $(i = 1, 2, \ldots, N)$, where x_{di} is continuous and differentiable. The main goal of the to be proposed control schemes is to ensure the semi-global uniform ultimate boundedness of the ith agent's formation tracking error, which is specified as

$$\lim_{t\to\infty} ||x_i(t) - x_{di}(t)|| \leq \nu_\delta^s,\ \forall x_i(t_0) \in \Omega_x,\ i = 1, 2, \ldots, N \tag{2.6}$$

where Ω_x is a compact set of x_i and ν_δ^s is a small positive constant.

The following assumptions are made regarding system (2.5):

Assumption 2.1. *Both the reference vector x_{di} and its derivatives $\dot{x}_{di}$, $\ddot{x}_{di}$, $\dddot{x}_{di}$ are bounded and completely known.*

Assumption 2.2. *The Bouc-Wen model parameters $\bar{\mu}_i$, μ_i, $\bar{\chi}_i$, χ_i and m_i are known and bounded for each individual agent.*

2.3 Preliminaries

Before offering the technical contents of this chapter, it is necessary to introduce some preliminary results in the field of matrix theory, graph theory and DSM control that are useful for the upcoming contents.

2.3.1 Matrix theory

Define matrices $A = [a_{ij}] \in \mathbb{R}^{m_a \times n_a}$ and $B \in \mathbb{R}^{m_b \times n_b}$, where m_a, m_b, n_a and n_b are positive integers. Then the definition of the Kronecker product is given as

$$A \otimes B = \begin{bmatrix} a_{11}B & a_{12}B & \dots & a_{1n_a}B \\ a_{21}B & a_{22}B & \dots & a_{2n_a}B \\ \vdots & \vdots & \ddots & \vdots \\ a_{m_a1}B & a_{m_a2}B & \dots & a_{m_an_a}B \end{bmatrix} \in \mathbb{R}^{m_am_b \times n_an_b}$$

For matrices $A \in \mathbb{R}^{m_a \times n_a}$, $B \in \mathbb{R}^{m_b \times n_b}$, $C \in \mathbb{R}^{m_c \times n_c}$ and $D \in \mathbb{R}^{m_d \times n_d}$, where m_c, m_d, n_c and n_d are positive integers, then the following properties of the Kronecker product are given (Horn *et al.* 1994):

1. $A \otimes (B + C) = A \otimes B + A \otimes C$ if $m_b = m_c$ and $n_b = n_c$.
2. $(A \otimes B)(C \otimes D) = (AC) \otimes (BD)$ if $n_a = m_c$ and $n_b = m_d$.
3. $(A \otimes B)^{\mathrm{T}} = A^{\mathrm{T}} \otimes B^{\mathrm{T}}$.
4. $(A \otimes B)^{-1} = A^{-1} \otimes B^{-1}$ if A and B are both nonsingular square matrices.

To carry out further stability analysis, the definition of Hurwitz matrix is also provided:

Definition 2.2. *For square matrix A, if all the eigenvalues of A have negative real parts, then A is considered to be a Hurwitz matrix or stable matrix.*

2.3.2 Graph theory

In this thesis, graphs are used to illustrate the information exchange among the agents within the structure of MASs. In general, a graph is described as

$$G = \{\mathcal{R}(G), \mathcal{E}(G), \mathcal{A}(G)\}$$

where $\mathcal{R}(G) = \{r_1, r_2, \dots, r_N\}$ denotes the set of nodes, $\mathcal{E}(G) \subseteq \mathcal{R} \times \mathcal{R}$ is the set of edges, and $\mathcal{A}(G) = [a_{ij}] \in \mathbb{R}^{N \times N}$ is the adjacency matrix with nonnegative elements. An edge of the graph G is expressed as $e_{ij} = (r_i, r_j)$. Furthermore, $a_{ji} = 1$ if and only if $e_{ij} \in \mathcal{E}(G)$, and self loops are excluded by setting $a_{ii} = 0$.

Define $\deg_{\text{in}}(r_i) = \sum_{j=1}^{N} a_{ij}$ to be the in-degree of the node r_i, and the degree matrix of the graph is illustrated as $\mathcal{D}(G) = \text{diag}\{\deg_{\text{in}}(r_1), \deg_{\text{in}}(r_2), \ldots, \deg_{\text{in}}(r_N)\}$. The Laplacian matrix of the graph is defined as $L = \mathcal{D}(G) - \mathcal{A}(G)$.

The graph G is treated as an undirected graph if for any $e_{ij} \in \mathcal{E}(G)$, there is $e_{ji} \in \mathcal{E}(G)$ (see subfigure (a) in Figure 2.2). Otherwise, when e_{ij} and e_{ji} do not exist simultaneously, the graph G is considered to be a directed graph.

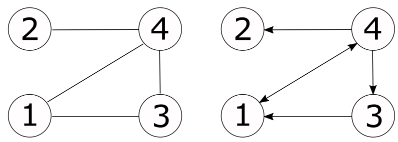

(a) (b)

Figure 2.2. Illustrations of two different graphs. (a) Undirected graph (b) Directed graph

For an undirected graph, if there always exists a path between an arbitrary pair of nodes (r_i, r_j), then the graph is called a connected graph. Similarly, if there always exists a directed path between any pair of nodes (r_i, r_j) for a directed graph, then the graph is said to be strongly connected.

Define a positive scalar b_i to represent the ith agent's sensitivity to its own tracking errors, then the local sensitivity matrix for the MAS is defined as a diagonal matrix $B = \text{diag}\{b_1, b_2, \ldots, b_N\}$. The following lemmas are helpful for illustrating the stability of the control schemes listed in the following chapters.

Lemma 2.2. (Zou *et al.* 2013) *Given an undirected and connected graph G and its associated Laplacian matrix L, the matrix $L + B$ is symmetric and positive definite for any non-negative diagonal matrix B with at least one positive element.*

Lemma 2.3. (Qu 2009) *Let the communication graph G be strongly connected and B be a non-negative diagonal matrix with at least one positive element. Then the matrix $(L + B)$ is an irreducible nonsingular M-matrix. If define*

$$q = [q_1\ q_2\ \ldots\ q_N]^{\mathrm{T}} = (L + B)^{-1} 1_{N \times 1}$$

then $P = \text{diag}\{p_i\} = \text{diag}\{1/q_i\}$ is a positive definite matrix. Then the matrix Q defined as follows is symmetric and positive definite.

$$Q = P(L + B) + (L + B)^{\mathrm{T}} P$$

2.3.3 Dynamic sliding mode control scheme

Before introducing the DSM formation controller designs for MASs, it is essential to first explain how DSM works in the perspective of one single agent. In this section, the actuator hysteresis phenomenon is ignored temporarily, which leads to the following system dynamics for the ith agent:

$$\begin{cases} \dot{x}_i = v_i \\ \dot{v}_i = u_i + w_i \end{cases} \tag{2.7}$$

To achieve goal (2.6), define the position tracking error δ_{xi} and the velocity tracking error δ_{vi} for the ith agent as follows:

$$\begin{cases} \delta_{xi} = x_i - x_{di} \\ \delta_{vi} = v_i - \dot{x}_{di} \end{cases} \tag{2.8}$$

To facilitate the design of a DSM (Liu and Wang 2012) controller, define an auxiliary variable ρ_i and the dynamic sliding variable ξ_i for the ith agent as

$$\begin{cases} \rho_i = \delta_{vi} + k_i \delta_{xi} \\ \xi_i = \dot{\rho}_i + \lambda_i \rho_i \end{cases} \tag{2.9}$$

where both $k_i \in \mathbb{R}$ and $\lambda_i \in \mathbb{R}$ are positive constants.

Then the time derivative of the dynamic sliding surface ξ_i is

$$\begin{aligned} \dot{\xi}_i &= \ddot{\delta}_{vi} + (k_i + \lambda_i)\dot{\delta}_{vi} + \lambda_i \delta_{vi} \\ &= (\ddot{v}_i - \dddot{x}_{di}) + (k_i + \lambda_i)(\dot{v}_i - \ddot{x}_{di}) + k_i \lambda_i (v - \dot{x}_{di}) \\ &= \dot{u}_i + \dot{w}_i - \dddot{x}_{di} + (k_i + \lambda_i)(u_i + w_i - \ddot{x}_{di}) + k_i \lambda_i (v - \dot{x}_{di}) \end{aligned}$$

If the overall uncertainty w_i is bounded such that $\|w_i\| \leq w_M^1$ and $\|\dot{w}_i\| \leq w_M^2$ are satisfied simultaneously, then there is a new perspective of designing $\dot{u}_i$ instead of the conventional u_i to increase the robustness of the controller:

$$\dot{u}_i = -w_M^2 \text{sign}(\xi_i) + \dddot{x}_{di} + (k_i + \lambda_i)(\ddot{x}_{di} - w_M^1 \text{sign}(\xi_i) - u_i) - k_i \lambda_i \delta_{vi} \tag{2.10}$$

Lemma 2.4. *Consider a nominal second-order system* (2.7), *by the sliding variables* (2.9) *and the nominal DSM controller* (2.10), *both the dynamic sliding variable ξ_i and the reference tracking error δ_{xi} are UUB.*

2.4 Formation control via finite-time observers

Although the stability of the controller design (2.10) is validated by the Lyapunov stability theorem, this approach still has the following shortcomings:

1. Holding the assumptions of $\|w_i\| \leq w_M^1$ and $\|\dot{w}_i\| \leq w_M^2$ are too conservative in the practical aspect.
2. Implementing the switching function sign$(\cdot)$ in the control input will introduce excessive chattering that is not suitable for practical systems.

Compared to the approach of passively reject the system uncertainty, estimating and compensating for the uncertainty in the controller design is a better choice. Before introducing the FTDO, it is necessary to have the following assumption:

Assumption 2.3. *The system uncertainty w_i is bounded and differentiable. Meanwhile, the term $\dot{w}_i$ has the Lipschitz constant $\beta_{i,w}$, where $\beta_{i,w}$ is a positive constant.*

2.4.1 Finite-time disturbance observers

Define $\mathrm{sgn}^{\beta}(\alpha) = \mathrm{diag}\{\mathrm{sign}(\alpha)\}|\alpha|^{\beta}$, where α is an arbitrary vector and β is a positive constant. Then the following FTDO (Shtessel *et al.* 2007) is constructed to observe w_i:

$$\begin{cases} \dot{\gamma}_{i,1} = \nu_{i,1} + u_i, \ \dot{\gamma}_{i,2} = \nu_{i,2}, \ \dot{\gamma}_{i,3} = \nu_{i,3} \\ \nu_{i,1} = -\alpha_{i,1}\beta_{i,w}^{\frac{1}{3}}\mathrm{sgn}^{\frac{2}{3}}(\gamma_{i,1} - v_i) + \gamma_{i,2} \\ \nu_{i,2} = -\alpha_{i,2}\beta_{i,w}^{\frac{1}{2}}\mathrm{sgn}^{\frac{1}{2}}(\gamma_{i,2} - \nu_{i,1}) + \gamma_{i,3} \\ \nu_{i,3} = -\alpha_{i,3}\beta_{i,w}\mathrm{sgn}(\gamma_{i,3} - \nu_{i,2}) \\ \widehat{v}_i = \gamma_{i,1}, \ \widehat{w}_i = \gamma_{i,2}, \ \widehat{\dot{w}}_i = \gamma_{i,3} \end{cases} \tag{2.11}$$

The following lemma is useful for the stability analysis of FTDO-based control designs.

Lemma 2.5. (Shtessel *et al.* 2007) *Regarding the FTDO* (2.11)*, if the parameter values are chosen reasonably, the observation error will converge to a very small value within a finite time t_o. In other words, there are $\|\widetilde{\gamma}_2\| = 0$ and $\|\widetilde{\gamma}_3\| = 0$ when $t \geq t_o$, where $\widetilde{\gamma}_2 = [(w_1 - \gamma_{1,2})^{\mathrm{T}}, (w_2 - \gamma_{2,2})^{\mathrm{T}}, \ldots, (w_N - \gamma_{N,2})^{\mathrm{T}}]^{\mathrm{T}}$ and $\widetilde{\gamma}_3 = [(\dot{w}_1 - \gamma_{1,3})^{\mathrm{T}}, (\dot{w}_2 - \gamma_{2,3})^{\mathrm{T}}, \ldots, (\dot{w}_N - \gamma_{N,3})^{\mathrm{T}}]^{\mathrm{T}}$.*

2.4.2 Robust formation control via finite-time disturbance observers

Regarding system (2.7), define $e_{xi} \in \mathbb{R}^n$ and $e_{vi} \in \mathbb{R}^n$ to be the local formation and velocity tracking error as follows:

$$\begin{cases} e_{xi} = \sum_{j=1}^{N} a_{ij}(\delta_{xi} - \delta_{xj}) + b_i\delta_{xi} = \sum_{j=1}^{N} l_{ij}\delta_{xj} + b_i\delta_{xi} \\ e_{vi} = \sum_{j=1}^{N} a_{ij}(\delta_{vi} - \delta_{vj}) + b_i\delta_{vi} = \sum_{j=1}^{N} l_{ij}\delta_{vj} + b_i\delta_{vi} \end{cases} \tag{2.12}$$

where l_{ij} is the element in the pre-defined Laplacian matrix and $b_i \in \mathbb{R}^+$ is the ith diagonal element in matrix B that represents the ith agent's sensitivity to its own reference tracking error.

Define $e_x = [e_{x1}^{\mathrm{T}}, e_{x2}^{\mathrm{T}}, \dots, e_{xN}^{\mathrm{T}}]^{\mathrm{T}}$ and $e_v = [e_{v1}^{\mathrm{T}}, e_{v2}^{\mathrm{T}}, \dots, e_{vN}^{\mathrm{T}}]^{\mathrm{T}}$, then the cluster expression is obtained as follows:

$$\begin{cases} e_x = (L+B) \otimes I_n(x - x_d) = (L+B) \otimes I_n\delta_x \\ e_v = (L+B) \otimes I_n(v - \dot{x}_d) = (L+B) \otimes I_n\delta_v \end{cases} \tag{2.13}$$

where $x_d = [x_{d1}^{\mathrm{T}}, x_{d2}^{\mathrm{T}}, \dots, x_{dN}^{\mathrm{T}}]^{\mathrm{T}}$, $\delta_x = [\delta_{x1}^{\mathrm{T}}, \delta_{x2}^{\mathrm{T}}, \dots, \delta_{xN}^{\mathrm{T}}]^{\mathrm{T}}$ and $\delta_v = [\delta_{v1}^{\mathrm{T}}, \delta_{v2}^{\mathrm{T}}, \dots, \delta_{vN}^{\mathrm{T}}]^{\mathrm{T}}$.

If the hysteresis phenomenon in (2.2) is disregarded, then the cluster local error dynamics is given as

$$\begin{cases} \dot{e}_x = e_v \\ \dot{e}_v = (L+B) \otimes I_n(-\ddot{x}_d + u + w) \end{cases}$$

where $u = [u_1^{\mathrm{T}}, u_2^{\mathrm{T}}, \dots, u_N^{\mathrm{T}}]^{\mathrm{T}}$.

Based on the discussion given in Section 2.3, the following auxiliary variable ρ_i and the dynamic sliding variable ξ_i based on the local tracking errors are constructed:

$$\begin{cases} \rho_i = e_{vi} + k_i e_{xi} \\ \xi_i = \dot{\rho}_i + \lambda_i\rho_i, \quad i = 1, 2, \dots, N \end{cases} \tag{2.14}$$

where both k_i and λ_i are positive constants.

Define $\xi = [\xi_1^{\mathrm{T}}, \xi_2^{\mathrm{T}}, \dots, \xi_N^{\mathrm{T}}]^{\mathrm{T}}$, then the time derivative of ξ is illustrated as

$$\begin{aligned} \dot{\xi} &= \ddot{e}_v + (K+\Lambda) \otimes I_n\dot{e}_v + K\Lambda \otimes I_n e_v \\ &= (L+B) \otimes I_n[\dot{u} + \dot{w} - \dddot{x}_d + (K+\Lambda) \otimes I_n(u + w - \ddot{x}_d) + K\Lambda \otimes I_n(v - \dot{x}_d)] \end{aligned}$$

where $K = \text{diag}\{k_1, k_2, \ldots, k_N\}$ and $\Lambda = \text{diag}\{\lambda_1, \lambda_2, \ldots, \lambda_N\}$.

Accordingly, the following FTDO-based DSM controller is proposed:

$$\dot{u}_i = -\gamma_{i,3} + \dddot{x}_d - (k_i + \lambda_i)(u_i + \gamma_{i,2} - \ddot{x}_d) + k_i\lambda_i\delta_{vi} - c_i\xi_i \tag{2.15}$$

where c_i is a positive constant. The control diagram of the FTDO-based approach is presented in Figure 2.3.

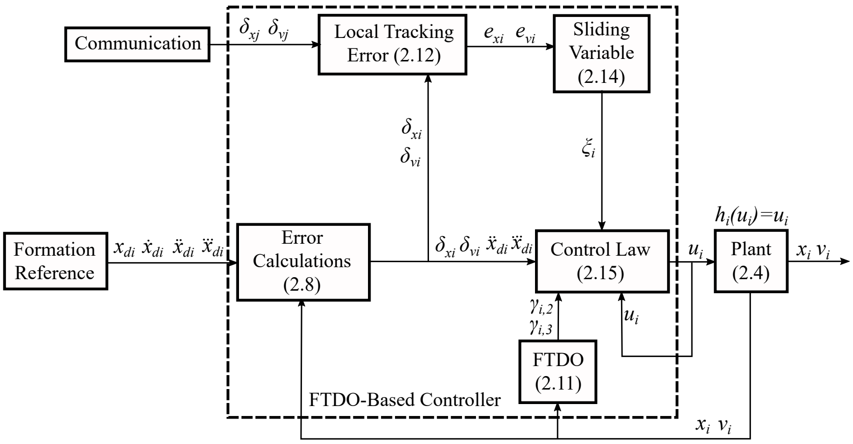

Figure 2.3. FTDO-based dynamic sliding mode formation control scheme.

The main result of the FTDO-based design when the actuator hysteresis (2.2) is not considered is given as the following theorem:

Theorem 2.1. *Consider system* (2.5) *where the actuator hysteresis* (2.2) *is ignored ($H = u$), suppose the communication topology L is an undirected graph and Assumptions 2.1-2.3 are satisfied, by the FTDO* (2.11), *the dynamic sliding variable design* (2.14) *and the DSM controller* (2.15), *the dynamic sliding variable ξ, local formation tracking error e_x and the reference tracking error δ_x are all semi-globally UUB.*

Proof. By Lemma 2.2, construct the following Lyapunov candidate:

$$V_{1,1} = \frac{1}{2}\xi^{\mathrm{T}}(L+B)^{-1} \otimes I_n \xi$$

The derivative of $V_{1,1}$ is given as

$$\begin{aligned}
\dot{V}_{1,1} &= \xi^{\mathrm{T}}(L+B)^{-1} \otimes I_n \dot{\xi} \\
&= \xi^{\mathrm{T}}[\dot{u} + \dot{w} - \dddot{x}_d + (K+\Lambda) \otimes I_n(u + w - \ddot{x}_d) + K\Lambda \otimes I_n(v - \dot{x}_d)] \\
&= \xi^{\mathrm{T}}[\widetilde{\gamma}_3 + (K+\Lambda) \otimes I_n\widetilde{\gamma}_2 - C \otimes I_n\xi]
\end{aligned}$$

where $C = \text{diag}\{c_1, c_2, \ldots, c_N\}$.

By Lemma 2.5, the simplified version of $\dot{V}_{1,1}$ is given as follows when $t \geq t_o$:

$$\dot{V}_{1,1} \leq -\underline{\sigma}(C)\|\xi\|^2$$

Hence, the value of $\dot{V}_{1,1}$ will remain negative until the value of $\|\xi\|$ is settled as $\|\xi_i\| = 0$. By Lemma 3.1, the uniform ultimate boundedness of ξ is achieved. By the expression of $\xi_i = \dot{\rho}_i + \lambda_i \rho_i$ and the Laplace final value theorem, the following equation is obtained after applying the Laplace transformation:

$$\lim_{t\to\infty} \|\rho(t)\| \leq \lim_{s\to 0} \sum_{i=1}^{N} |sL(\rho_i)| \leq \lim_{s\to 0} \sum_{i=1}^{N} \left| \frac{s}{s+\lambda_i}(L(\xi_i) - \rho_i(0)) \right| = 0$$

Similarly, we also have

$$\lim_{t\to\infty} \|e_x(t)\| \leq \lim_{s\to 0} \sum_{i=1}^{N} |sL(e_{xi})| \leq \lim_{s\to 0} \sum_{i=1}^{N} \left| \frac{s}{s+k_i}(L(\rho_i) - e_{xi}(0)) \right| = 0$$

According to the definition of local error vectors, one has

$$\lim_{t\to\infty} \|\delta_x(t)\| \leq \frac{\|e_x\|}{\underline{\sigma}(L+B)} = 0$$

By Lemma 3.1, the error-related vectors ξ, e_x and δ_x are all UUB. Hence, the proof is completed. □

Remark 2.1. *The FTDO-based design is able to guarantee the global uniform ultimate boundedness of $\|\delta_{xi}\|$ because its implementation does not require that the initial value of the system state is bounded within a compact set. If the state of an arbitrary system is UUB, it is semi-globally UUB as well. Hence, the FTDO-based design will still achieve our goal in* (2.6).

Remark 2.2. *Although the value of $\|\xi\|$, $\|\rho\|$, $\|e_x\|$ and $\|\delta_x\|$ will achieve 0 ultimately in theory, their values can not converge exactly to 0 in practice. Instead, the expected convergence boundaries of the above vector norms should be a really small positive number.*

Remark 2.3. *Note that the separation principle is a very important concept in the development of observer-based control schemes. In this thesis, the stability of the proposed observer designs are not affected by the controller. Normally, analysis regarding the closed-loop that contains both the observer and the controller is required to prove the stability of the entire system. Although the corresponding descriptions have been omitted for some of the observer-based designs in both this chapter and the upcoming technical chapters, the stability of the designs presented in this thesis is still valid because of the boundedness of both the observation errors and the tracking errors.*

2.4.3 Simulation results and discussion

To verify the effectiveness of the proposed observer-based DSM control scheme, simulations based on a group of three-wheel omni-directional robots (ODRs) are conducted (Fei *et al.* 2020).

First, it is necessary to analyse if the system dynamics of a three-wheel ODR matches the nominal second-order model presented in (2.7). Define $x_i = [p_i^x, p_i^y, \theta_i]^{\mathrm{T}}$ and $v_i = [v_i^x, v_i^y, \omega_i]$ to act as the position vector and the velocity vector of the ith robot, respectively. Then the dynamics of the ith ODR subjected to external disturbances ϖ_i is

$$\begin{cases} \dot{x}_i = v_i \\ \dot{v}_i = M_i T_s(\theta_i, R_i) F_i^m + \varpi_i \end{cases} \tag{2.16}$$

where $M_i = \mathrm{diag}\{1/m_i, 1/m_i, 1/I_i\}$, m_i is the mass of the ith robot, I_i is the inertia of the ith robot, R_i is the radius of the ith robot, $F_i = [F_i^1, F_i^2, F_i^3]^{\mathrm{T}}$ and $T_s(\theta_i, R_i)$ is the transformation matrix with the following expression:

$$T_s(\theta_i, R_i) = \begin{bmatrix} -\sin(\theta_i) & -\sin(\pi/3 - \theta_i) & \sin(\pi/3 + \theta_i) \\ \cos(\theta_i) & -\cos(\pi/3 - \theta_i) & -\cos(\pi/3 + \theta_i) \\ R_i & R_i & R_i \end{bmatrix}$$

The structure of the ith ODR is given in Figure 2.4.

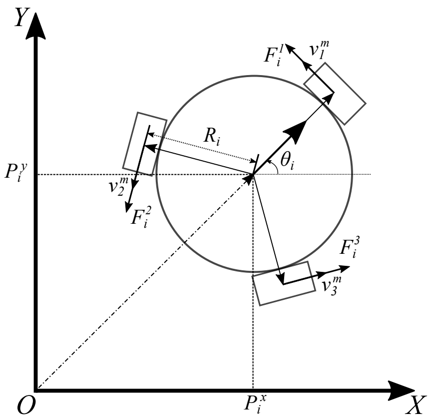

Figure 2.4. Physical structure of an ODR.

If each robot is equipped with direct current motors, then the force vector F_i^m has the following expression (Dinh *et al.* 2012):

$$F_i^m = \alpha_i U_i - \beta_i v_i^w$$

Table 2.1. ODR parameter values.

Robot number	m_i(kg)	R_i(m)	$I_i(\mathrm{kg}\cdot\mathrm{m}^2)$	$\beta_{i,j}$(N/v)
1	4.5	0.20	0.22	11.4
2	5.2	0.24	0.24	11.6
3	4.8	0.22	0.23	11.8
4	5.5	0.26	0.25	12.0

where $\alpha_i \in \mathbb{R}^{3\times 3}$ and $\beta_i \in \mathbb{R}^{3\times 3}$ are the diagonal matrices that contain the characteristic coefficients, $U_i \in \mathbb{R}^3$ is the voltage applied to the motors and $v_i^w \in \mathbb{R}^3$ is the linear speed of the wheels.

Based on Figure 2.4, the relationship between the linear speed of the wheels and the speed of the robot is expressed as

$$v_i = T_f(\theta_i, R_i)v_i^m$$

where $T_f(\theta_i, R_i)$ is the speed rotational matrix defined as

$$T_f(\theta_i, R_i) = \begin{bmatrix} -\sin(\theta_i) & -\sin(\pi/3-\theta_i) & \sin(\pi/3+\theta_i) \\ \cos(\theta_i) & -\cos(\pi/3-\theta_i) & -\cos(\pi/3+\theta_i) \\ 1/R_i & 1/R_i & 1/R_i \end{bmatrix}$$

Consequently, one has

$$\begin{cases} \dot{x}_i = v_i \\ \dot{v}_i = -\beta_i M_i T_s(\theta_i, R_i) T_f^{-1}(\theta_i, R_i) v_i + \alpha_i M_i T_s(\theta_i, R_i) U_i + \bar{w}_i \end{cases} \tag{2.17}$$

where $\alpha_i = \mathrm{diag}\{\alpha_{i,1}, \alpha_{i,2}, \alpha_{i,3}\}$ and $\beta_i = \mathrm{diag}\{\beta_{i,1}, \beta_{i,2}, \beta_{i,3}\}$. If applying $w_i = \bar{w}_i - \beta_i M_i T_s(\theta_i, R_i) T_f^{-1}(\theta_i, R_i) v_i$ and $u_i = \alpha_i M_i T_s(\theta_i, R_i) U_i$, then the simplified dynamics of the ith ODR is obtained as

$$\begin{cases} \dot{x}_i = v_i \\ \dot{v}_i = u_i + w_i \end{cases}$$

Hence, the model of ODR is suitable for the simulation of our proposed controllers. Consider a system with four ODRs, whose parameters are given in Table 2.1.

Table 2.2. Initial states of the ODRs for the FTDO-based controller.

Robot number	p_i^x(m)	p_i^y(m)	$\theta_i(\mathrm{kg}\cdot\mathrm{m}^2)$
1	2.3	-0.5	$\pi/4$
2	-1.0	1.5	$\pi/6$
3	-3.4	1.5	$-\pi/6$
4	0.8	-3.3	$-\pi/4$

To validate the effectiveness of the FTDO-based approach, the initial states of the ODRs are set as what's given in Table 2.2. The initial states of FTDOs are set with the same values as the actual states in Table 2.2.

The formation reference of the ith agent is given as

$$x_{di} = \left[3\cos\left(\frac{t}{10} + \frac{i-1}{2}\pi\right),\ 3\sin\left(\frac{t}{10} + \frac{i-1}{2}\pi\right),\ 0\right]^{\mathrm{T}}, \quad i = 1, 2, 3, 4$$

Meanwhile, the external disturbance w_i is chosen as

$$d_i(t) = \left[\frac{3}{10}p_i^x \sin\left(t + \frac{i\pi}{3}\right) + 2, \frac{1}{5}p_i^y \cos\left(2t + \frac{i\pi}{3}\right) + \frac{3}{2}, \frac{1}{10}\theta_i \sin\left(\frac{4}{5}t + \frac{i\pi}{3}\right) + 1\right]^{\mathrm{T}}$$

The undirected communication topology of the system is given in Figure 2.5.

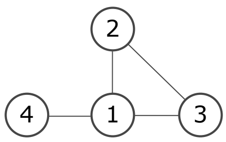

Figure 2.5. Communication topology of 4 ODRs.

The parameters of the FTDO is chosen as $\alpha_{i,1} = 3$, $\alpha_{i,2} = 6$, $\alpha_{i,3} = 3$ and $\beta_{i,w} = 10$. The parameters in the control law (2.15) are given as $k_i = 3$, $\lambda_i = 3$ and $c_i = 3$.

Accordingly, the propagation of each ODR's $\|\delta_{xi}\|$ is presented in Figure 2.6, where the uniform ultimate boundedness of δ_{xi} is validated for each agent. Similar results are also obtained for the dynamic sliding variable ξ_i, whose curves are given in Figure 2.7. In specific, the bounded region of $\|\delta_{xi}\|$ and $\|\xi_i\|$ are 2.5×10^{-3} and 9×10^{-2}, respectively.

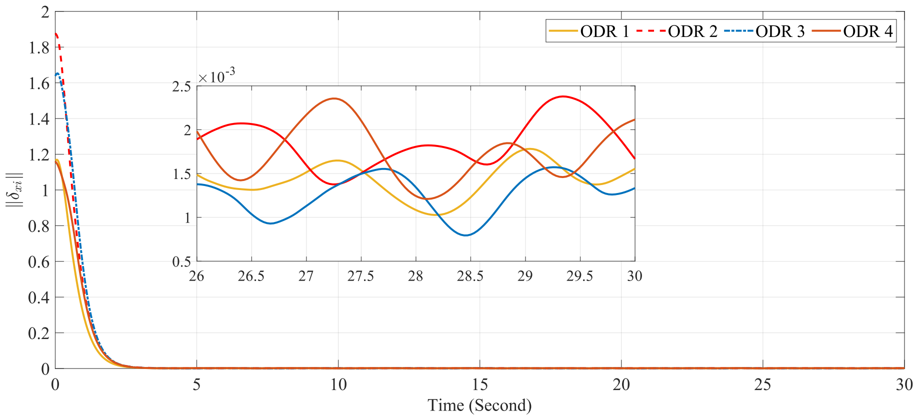

Figure 2.6. $\|\delta_{xi}\|$ of individual ODRs (FTDO-based design).

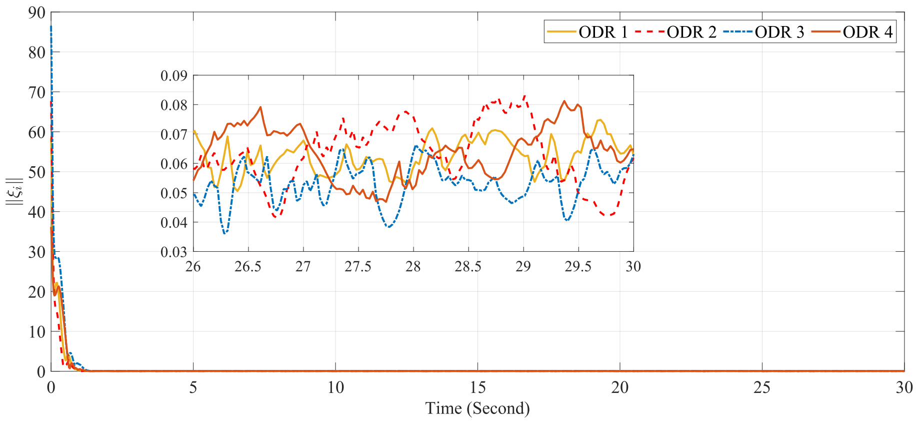

Figure 2.7. $\|\xi_i\|$ of individual ODRs (FTDO-based design).

To prove that the DSM design will reduce the chattering phenomenon in the control input, the curves of u_i are given in Figure 2.8. It is observed that the control input are smooth, which illustrates the effectiveness of the FTDO-based design in (2.15).

Furthermore, the trajectories of each ODR throughout the formation tracking mission are presented in Figure 2.9. We can see that all four ODRs are able to track their position reference smoothly to form a circular formation that is rotating anti-clockwise, indicating the the validity of Theorem 2.1.

2.5 Formation control via Chebyshev neural networks

Although the controller design (2.15) can ensure the uniform ultimate boundedness of error-related states, Assumption 2.3 is still quite conservative for practical scenarios. To remove this assumption, the CNN-based method is proposed.

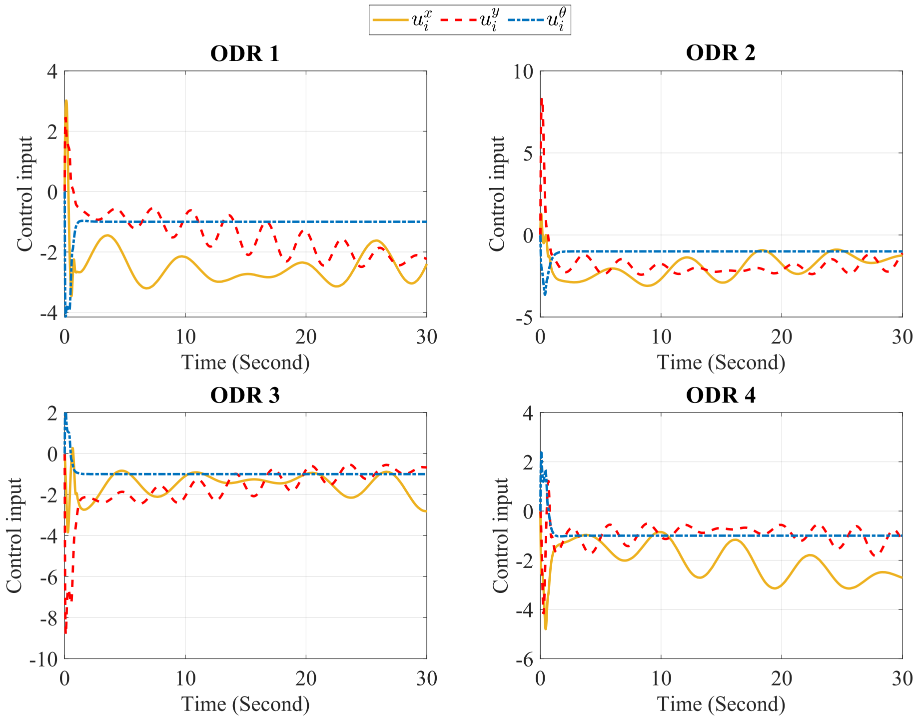

Figure 2.8. Control input of individual ODRs (FTDO-based design).

2.5.1 Chebyshev neural networks

It is found that a general function can be estimated by a linear combination of a set of its related variables' Chebyshev polynomials (Lee and Jeng 1998) when the input of the NN is restricted to a compact set. Therefore, the CNN was proposed for the purpose of unknown function approximation (Zou *et al.* 2011, Zou and Kumar 2012). CNN is usually designed to be a single layered functional link network with Chebyshev polynomials as its input. Chebyshev polynomials are a set of orthogonal polynomials that can be obtained by using the following recursive function:

$$T_{i+1}(y) = 2yT_i(y) - T_{i-1}(y),\ T_0(y) = 1$$

where $y \in \mathbb{R}$ and $T_1(y)$ can be defined as y, $2y$, $2y-1$ or $2y+1$. In this chapter, set $T_1(y) = y$. For a given vector $Y = [y_1, y_2, \ldots, y_q]^{\mathrm{T}} \in \mathbb{R}^q$, the Chebyshev-polynomial-based activation function for the vector is defined as

$$\varphi(Y) = [1, T_1(y_1), \ldots, T_1(y_q), \ldots, T_{N_c}(y_1), \ldots, T_{N_c}(y_q)]^{\mathrm{T}} \tag{2.18}$$

where N_c is the order of the Chebyshev polynomials, and $T_i(y_j)$ $(i = 1, \ldots, N_c, j = 1, \ldots, q)$ represents the Chebyshev polynomial for variable y_j with order i.

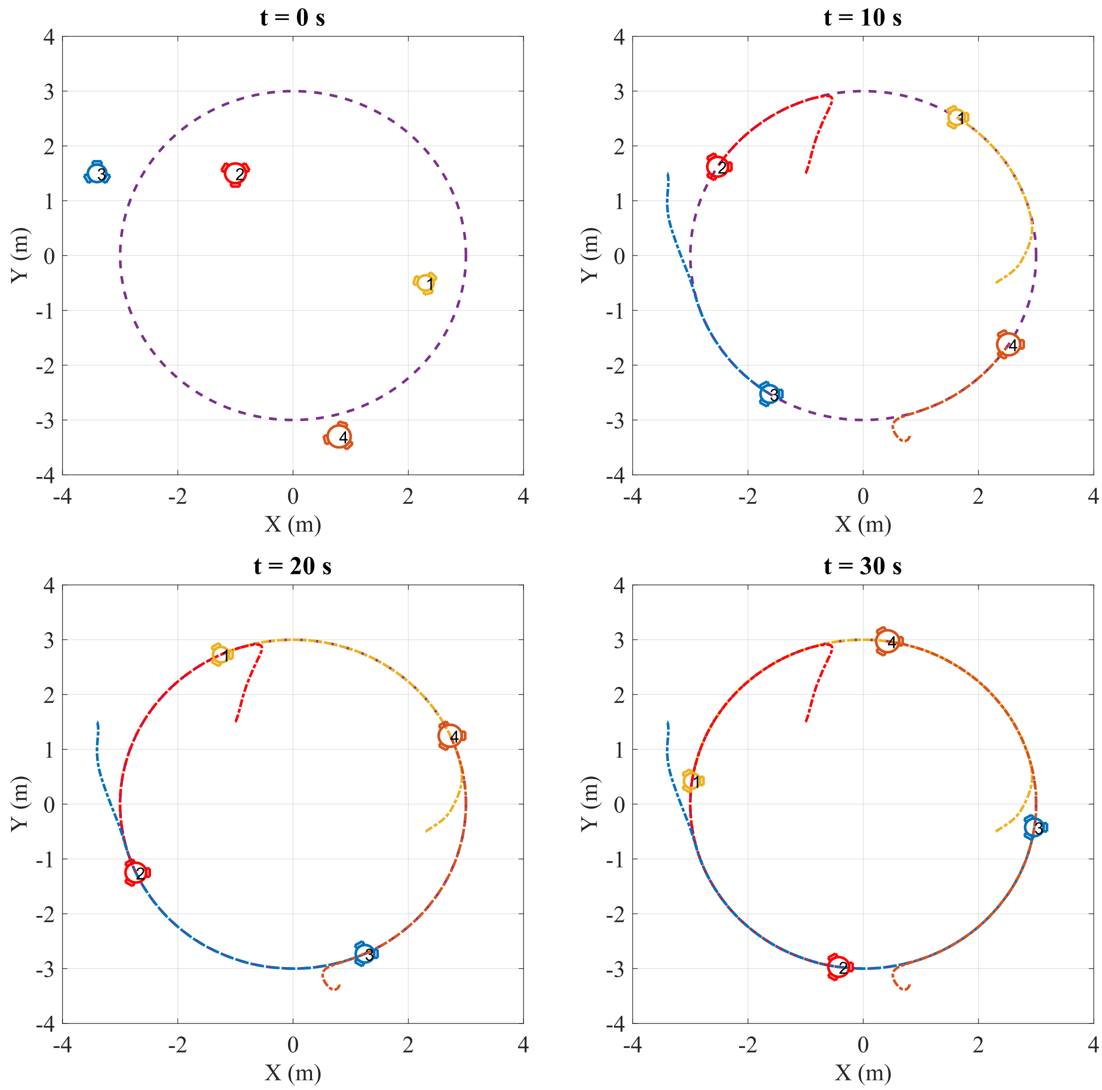

Figure 2.9. Trajectories of individual ODRs (FTDO-based design).

As previously mentioned, the terms $\dot{w}_i$ and $(k_i + \lambda_i)w_i$ are both unknown. Because both $\dot{w}_i$ and w_i can be seen as a function that uses x_i and v_i as its variables, it is reasonable to combine these two terms as $E_i = \dot{w}_i + (k_i + \lambda_i)w_i$ for the CNN-based estimation. According to the universal approximation rule, an unknown function can be estimated by an NN when the network compact set condition is satisfied such that the function is bounded or the network input is restricted to its compact set. Hence, the unknown nonlinear function E_i can be expressed as follows:

$$E_i = W_i^{\mathrm{T}} \varphi(Y_i) + \epsilon_i,\ i \in [1, N] \tag{2.19}$$

where $W_i \in \mathbb{R}^{(2nN_c+1)\times n}$ is the optimal weight matrix, $Y_i = [x_i, v_i]^{\mathrm{T}}$ and $\epsilon_i \in \mathbb{R}^n$ is the bounded estimation error. Define $\widehat{W}_i \in \mathbb{R}^{(2nN_c+1)\times n}$ to be the estimated weight matrix, then the following CNN-based approximation procedure is given as

$$\widehat{E}_i = \widehat{W}_i^{\mathrm{T}} \varphi(Y_i) \tag{2.20}$$

Define $\widetilde{W}_i = W_i - \widehat{W}_i$ as the neural weight estimation error, then the CNN-based estimation error is defined as

$$\widetilde{E}_i = E_i - \widehat{E}_i = \widetilde{W}_i^{\mathrm{T}} \varphi(Y_i) + \epsilon_i$$

Meanwhile, to ensure that all elements in the estimated weight matrix $\widehat{W}_i$ are bounded throughout the estimation process, a smooth projection law $\tau_i(\widehat{W}_i) = \widehat{W}_{i\tau}$ (Zou and Kumar 2012) as follows is applied to every weight matrix:

$$\tau_i(\widehat{W}_i(j,k)) = \begin{cases} W_i^M + \psi_W \left[1 - \exp\left(\dfrac{W_i^M - \widehat{W}_i(j,k)}{\psi_W}\right)\right], & \text{if } \widehat{W}_i(j,k) > W_i^M \\ \widehat{W}_i(j,k), & \text{if } |\widehat{W}_i(j,k)| \leq W_i^M \\ \psi_W \left[\exp\left(\dfrac{\widehat{W}_i(j,k) + W_i^M}{\psi_W}\right) - 1\right] - W_i^M, & \text{if } \widehat{W}_i(j,k) < -W_i^M \end{cases} \tag{2.21}$$

where $W_i^M \in \mathbb{R}^+$ is the expected bounded value of $\widehat{W}_i(j,k)$, ψ_W is a very small positive constant, $\widehat{W}_i(j,k)$ is the element on the jth row and the kth column in matrix $\widehat{W}_i$ and $\tau_i(\widehat{W}_i(j,k))$ is the element on the jth row and the kth column in matrix $\widehat{W}_{i\tau}$. Accordingly, the value of $\tau_i(\widehat{W}_i(j,k))$ satisfies $\tau_i(\widehat{W}_i(j,k)) \in [-W_i^M - \psi_W, W_i^M + \psi_W]$.

2.5.2 Robust formation control via Chebyshev neural networks

Consider the MAS (2.5) with actuator hysteresis (2.2), the updated version of $\dot{\xi}$ is given as

$$\dot{\xi} = (L + B) \otimes I_n[\dot{H} + \dot{w} - \dddot{x}_d + (K + \Lambda) \otimes I_n(H + w - \ddot{x}_d) + K\Lambda \otimes I_n(v - \dot{x}_d)]$$

Regarding the actuator hysteresis phenomenon, the controller design in (2.15) is inadequate. Hence, the following modified formation controller design is proposed:

$$\dot{u}_i = \frac{\dot{\pi}_i}{\mu_i + \bar{\mu}_i g(\bar{\zeta}_i, \frac{\dot{\pi}_i}{\mu_i})} \tag{2.22}$$

where

$$\dot{\pi}_i = -\widehat{W}_{i\tau}^T \varphi_i(Y_i) + \dddot{x}_{di} + (k_i + \lambda_i)\ddot{x}_{di} - (k_i + \lambda_i)\pi_i - k_i\lambda_i(v_i - \dot{x}_{di}) - c_i\xi_i$$

$$g\left(\bar{\zeta}_i, \frac{\dot{\pi}_i}{\mu_i}\right) = 1 - \bar{\chi}\text{sign}\left(\frac{\dot{\pi}_i}{\mu_i}\right)|\bar{\zeta}_i|^{m_i-1}\bar{\zeta}_i - \chi_i|\bar{\zeta}_i|^{m_i},\ \dot{\bar{\zeta}}_i = \frac{\dot{\pi}_i}{\mu_i + \bar{\mu}_i g(\bar{\zeta}_i, \frac{\dot{\pi}_i}{\mu_i})} g\left(\bar{\zeta}_i, \frac{\dot{\pi}_i}{\mu_i}\right)$$

$$\pi_i(t_0) = \mathbf{0}_n,\ \dot{\pi}_i(t_0) = \mathbf{0}_n,\ \bar{\zeta}_i(t_0) = \mathbf{0}_n,\ \dot{\bar{\zeta}}_i(t_0) = \mathbf{0}_n,\ u_i(t_0) = \mathbf{0}_n$$

The adaptive weight tuning law is chosen as

$$\dot{\widehat{W}}_i = \eta_1 \varphi_i(Y_i)\xi_i^{\mathrm{T}} \tag{2.23}$$

Based on the above discussion, the control diagram of the CNN-based control approach is presented in Figure 2.10.

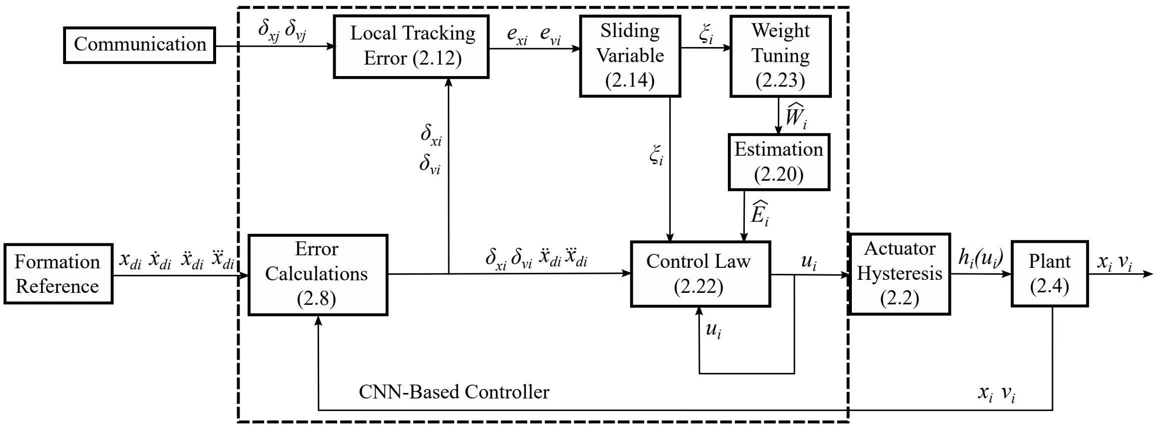

Figure 2.10. CNN-based dynamic sliding mode formation control scheme.

Before presenting the main results, let us recall the following results.

Lemma 2.6. (Zou and Kumar 2012) *Define $\widetilde{W}_{i\tau} = W_i - \widehat{W}_{i\tau}$, then the following function*

$$V_W^i = \sum_{j=1}^{2nN_c+1}\sum_{k=1}^{n}\int_0^{\widetilde{W}_i(j,k)} (W_i(j,k) - \tau_i(W_i(j,k) - v))\,dv,\ i = 1, 2, \ldots, N \tag{2.24}$$

is positive definite.

Lemma 2.7. (Zhou *et al.* 2012) *For variables ζ_i and $\bar{\zeta}_i$ that are defined in* (2.3) *and* (2.22)*, if the initial values of ζ_i and $\bar{\zeta}_i$ satisfies $\bar{\zeta}_i(t_0) = \zeta_i(t_0) = 0$, then the following equation is valid for all $t \geq t_0$*

$$\frac{1}{2}(\zeta_i(t) - \bar{\zeta}_i(t))^2 \leq \frac{1}{2}(\zeta_i(t_0) - \bar{\zeta}_i(t_0))^2 = 0,\ i = 1, 2, \ldots, N \tag{2.25}$$

Lemma 2.8. (Lee and Jeng 1998) *For a continuous nonlinear function E_i, the NN estimation error ϵ_i is bounded such that $\|\epsilon\| \leq \epsilon_M$, where ϵ_M is a positive constant and $\epsilon = [\epsilon_1^{\mathrm{T}}, \epsilon_2^{\mathrm{T}}, \ldots, \epsilon_N^{\mathrm{T}}]^{\mathrm{T}}$.*

The main result of the CNN-based controller design is presented as the following theorem:

Theorem 2.2. *Consider the MAS* (2.5) *with known Bouc-Wen hysteresis nonlinearity* (2.2), *where Assumptions 2.1-2.1 hold, by the DSM variable* (2.14), *the smooth projection function* (2.21), *the CNN-based controller* (2.22), *and the adaptive weight tuning law* (2.23), *then the dynamic sliding variable ξ, the formation tracking error e_x and the reference tracking error δ_x are all semi-globally UUB if the compact set conditions of the CNNs are satisfied such that either $E_i \in \Omega_E$ or $Y_i \in \Omega_Y$ is satisfied when $t \geq t_0$, where Ω_E and Ω_Y are compact sets for E_i and Y_i, respectively.*

Proof. To prove the effectiveness of the proposed control law, consider the following Lyapunov function:

$$V_{1,2} = \frac{1}{2}\xi^{\mathrm{T}}(L+B)^{-1} \otimes I_n \xi + \sum_{i=1}^{N} \frac{1}{\eta_1} V_W^i$$

According to Lemmas 2.2 and 2.6, both $L+B$ and V_{W_i} are positive definite, which indicates that $V_{i,2}$ is nonnegative. The time derivative of $V_{i,2}$ is given as

$$\begin{aligned}\dot{V}_{1,2} &= \xi^{\mathrm{T}}(L+B)^{-1} \otimes I_n \dot{\xi} - \sum_{i=1}^{N} \sum_{j=1}^{2nN_c+1} \sum_{k=1}^{n} \frac{1}{\eta_1} \widetilde{W}_{i\tau}(j,k)\dot{\widehat{W}}_i(j,k) \\ &= \xi^{\mathrm{T}}[\dot{H} + \dot{w} - \dddot{x}_d + (K+\Lambda) \otimes I_n(H + w - \ddot{x}_d) + K\Lambda \otimes I_n(v - \dot{x}_d)] \\ &\quad - \frac{1}{\eta_1}\mathrm{tr}\{\widetilde{W}_\tau^T \dot{\widehat{W}}\}\end{aligned} \tag{2.26}$$

where $\widetilde{W}_\tau = \mathrm{diag}\{\widetilde{W}_{1\tau}, \widetilde{W}_{2\tau}, \ldots, \widetilde{W}_{N\tau}\}$ and $\widehat{W} = \mathrm{diag}\{\widetilde{W}_1, \widetilde{W}_2, \ldots, \widetilde{W}_N\}$.

Substituting (2.2) and (2.3) into (2.26), then one has

$$\begin{aligned}\dot{V}_{1,2} &= \xi^{\mathrm{T}}[\mu\dot{u} + \bar{\mu}\dot{\zeta} + \dot{w} - \dddot{x}_d + K\Lambda \otimes I_n(v - \dot{x}_d)] - \frac{1}{\eta_1}\mathrm{tr}\{\widetilde{W}_\tau^{\mathrm{T}} \dot{\widehat{W}}\} \\ &\quad + \xi^{\mathrm{T}}[(K+\Lambda) \otimes I_n(\mu u + \bar{\mu}\zeta + w - \ddot{x}_d)] \\ &= \xi^{\mathrm{T}}[\dot{\pi} + \bar{\mu}(\dot{\zeta} - \dot{\hat{\zeta}}) + \dot{w} - \dddot{x}_d + K\Lambda \otimes I_n(v - \dot{x}_d)] - \frac{1}{\eta_1}\mathrm{tr}\{\widetilde{W}_\tau^{\mathrm{T}} \dot{\widehat{W}}\}\end{aligned}$$

$$
\begin{aligned}
&+ \xi^{\mathrm{T}}[(K+\Lambda)\otimes I_n(\pi+\bar{\mu}(\zeta-\bar{\zeta})+w-\ddot{x}_d)] \\
&= \xi^{\mathrm{T}}\left[\dot{\pi}+\bar{\mu}\left(\dot{u}g(\zeta,\dot{u})-\frac{\dot{\pi}g(\bar{\zeta},\frac{\pi}{\mu})}{\mu+\bar{\mu}g(\bar{\zeta},\frac{\pi}{\mu})}\right)+\dot{w}-\dddot{x}_d+K\Lambda\otimes(v-\dot{x}_d)\right] \\
&+ \xi^{\mathrm{T}}\bar{\mu}\left[\zeta(t_0)+\int_{t_0}^{t}\dot{u}g(\zeta,\dot{u})\,dt-\bar{\zeta}(t_0)-\int_{t_0}^{t}\frac{\dot{\pi}g(\bar{\zeta},\frac{\pi}{\mu})}{\mu+\bar{\mu}g(\bar{\zeta},\frac{\pi}{\mu})}\,dt\right] \\
&+ \xi^{\mathrm{T}}[(K+\Lambda)(\pi+w-\ddot{x}_d)]-\frac{1}{\eta_1}\mathrm{tr}\{\widetilde{W}_\tau^{\mathrm{T}}\dot{\hat{W}}\}
\end{aligned}
$$

where

$$
\begin{aligned}
&\rho=[\rho_1,\rho_2,\ldots,\rho_N]^{\mathrm{T}},\ \bar{\zeta}=[\bar{\zeta}_1,\bar{\zeta}_2,\ldots,\bar{\zeta}_N]^{\mathrm{T}},\ \zeta=[\zeta_1,\zeta_2,\ldots,\zeta_N]^{\mathrm{T}} \\
&\mu=\mathrm{diag}\{\mu_1,\mu_2,\ldots,\mu_N\}\otimes I_n,\ \bar{\mu}=\mathrm{diag}\{\bar{\mu}_1,\bar{\mu}_2,\ldots,\bar{\mu}_N\}\otimes I_n
\end{aligned}
$$

By Lemma 2.7, when conditions $\zeta_i(t)=\bar{\zeta}_i(t)$ and $\dot{\zeta}_i(t)=\dot{\bar{\zeta}}_i(t)$ are given, the expression of $\dot{V}_{1,2}$ is further modified as

$$
\begin{aligned}
\dot{V}_{1,2} &= \xi^{\mathrm{T}}[\dot{\pi}+\dot{w}-\dddot{x}_d+K\Lambda\otimes I_n(v-\dot{x}_d)]-\frac{1}{\eta_1}\mathrm{tr}\{\widetilde{W}_\tau^{\mathrm{T}}\dot{\hat{W}}\} \\
&\quad+\xi^{\mathrm{T}}[(K+\Lambda)\otimes(\pi+w-\ddot{x}_d)] \\
&= \xi^{\mathrm{T}}[\dot{w}+(K+\Lambda)\otimes w+\dot{\pi}-\dddot{x}_d+(K+\Lambda)\otimes I_n(\pi-\ddot{x}_d)] \\
&\quad+\xi^{\mathrm{T}}[K\Lambda\otimes I_n(v-\dot{x}_d)]-\frac{1}{\eta_1}\mathrm{tr}\{\widetilde{W}_\tau^{\mathrm{T}}\dot{\hat{W}}\} \\
&= \xi^{\mathrm{T}}[W^{\mathrm{T}}\varphi+\epsilon-\widehat{W}_\tau^{\mathrm{T}}\varphi-C\otimes I_n\xi]-\frac{1}{\eta_1}\mathrm{tr}\{\widetilde{W}_\tau^{\mathrm{T}}\dot{\hat{W}}\} \\
&= -\xi^{\mathrm{T}}C\otimes I_n\xi+\xi^{\mathrm{T}}[\widetilde{W}_\tau^{\mathrm{T}}\varphi+\epsilon]-\frac{1}{\eta_1}\mathrm{tr}\{\widetilde{W}_\tau^{\mathrm{T}}\dot{\hat{W}}\} \\
&= -\xi^{\mathrm{T}}C\otimes I_n\xi+\xi^{\mathrm{T}}\epsilon+\frac{1}{\eta_1}\mathrm{tr}\{\widetilde{W}_\tau^{\mathrm{T}}(\eta_1\varphi\xi^{\mathrm{T}}-\dot{\hat{W}})\} \\
&= -\xi^{\mathrm{T}}C\otimes I_n\xi+\xi^{\mathrm{T}}\epsilon
\end{aligned}
$$

where $C=\mathrm{diag}\{c_1,c_2,\ldots,c_N\}$ and $\varphi=[\varphi_1^{\mathrm{T}},\varphi_2^{\mathrm{T}},\ldots,\varphi_N^{\mathrm{T}}]^{\mathrm{T}}$.

By Lemma 2.8, the following inequality is obtained:

$$
\dot{V}_{1,2}\le-\underline{\sigma}(C)\|\xi\|^2+\epsilon_M\|\xi\| \tag{2.27}
$$

where ϵ_M is a positive constant that satisfies $\|\epsilon_i\|\le\epsilon_M$, further leading to the conclusion that $\dot{V}_{1,2}$ would remain negative outside the compact set Ω_ξ^1:

$$
\Omega_\xi^1=\left\{\xi(t)\,\middle|\,\|\xi(t)\|\le\frac{\epsilon_M}{\underline{\sigma}(C)}\right\} \tag{2.28}
$$

Hence, the dynamic sliding variable ξ will keep decreasing until $\|\xi\|$ is within the compact set Ω_{ξ}^{1}. By Lemma 2.1, ξ is semi-globally UUB.

Regarding an arbitrary vector, its norm satisfies the following inequality (Lewis *et al.* 2013):

$$\|\xi\|_1 = \sum_{i=1}^{N} |\xi_i| \geq \|\xi\|_2 \geq \|\xi\|_\infty$$

By applying the final value theorem of Laplace transform, the following equation is obtained

$$\lim_{t\to\infty} \|\xi(t)\| \leq \lim_{t\to\infty} \sum_{i=1}^{N} |\xi_i(t)| = \lim_{s\to 0} \sum_{i=1}^{N} s|L(\xi_i)| \leq \frac{\epsilon_M}{\underline{\sigma}(C)} \tag{2.29}$$

By applying Laplace transformation to (2.14), one has

$$L(\xi_i) = sL(\rho_i) + \rho_i(0) + \lambda_i L(\rho_i)$$
$$L(\rho_i) = sL(e_{xi}) + e_{xi}(0) + k_i L(e_{xi})$$

which is equivalent to

$$L(\rho_i) = \frac{1}{s+\lambda_i}(L(\xi_i) - \rho_i(0))$$
$$L(e_{xi}) = \frac{1}{s+k_i}(L(\rho_i) - e_{xi}(0))$$

Accordingly, there are

$$\lim_{t\to\infty} \|\rho(t)\| \leq \lim_{t\to\infty} \sum_{i=1}^{N} |\rho_i(t)| = \lim_{s\to 0} \sum_{i=1}^{N} s|L(\rho_i)| \leq \frac{\epsilon_M}{\underline{\sigma}(C\Lambda)}$$
$$\lim_{t\to\infty} \|e_x(t)\| \leq \lim_{t\to\infty} \sum_{i=1}^{N} |e_{xi}(t)| = \lim_{s\to 0} \sum_{i=1}^{N} s|L(e_{xi})| \leq \frac{\epsilon_M}{\underline{\sigma}(C\Lambda K)}$$

By the definition of local tracking errors in (2.12), one also has

$$\lim_{t\to\infty} \|\delta_x(t)\| \leq \lim_{t\to\infty} \|(L+B)^{-1} \otimes I_n e_x\| \leq \frac{\epsilon_M}{\underline{\sigma}(C\Lambda K)\underline{\sigma}(L+B)}$$

As a result, both e_x and δ_x are semi-globally UUB, which completes the proof. □

Remark 2.4. *If the initial formation tracking error of the system is too large, the high value of dynamic sliding variable will cause rapid and severe oscillation during the weight tuning process. The unstable weight values can potentially result in an unregulated output of the NN,*

Table 2.3. Initial states of the ODRs for the CNN-based controller.

Robot number	p_i^x(m)	p_i^y(m)	$\theta_i(\mathrm{kg}\cdot\mathrm{m}^2)$
1	2.0	3.0	0
2	−0.5	2.0	$\pi/4$
3	0.5	0.0	$2\pi/3$
4	1.5	−3.3	$5\pi/4$

which will jeopardise the performance of the designed controller. Hence, the smooth projection law (2.21) *is employed in this design to restrict the weight matrix and estimation error in the unstable period to prevent system failure.*

Remark 2.5. *It is found that the value of tuning rate* η_1 *in* (2.23) *should be chosen critically because high value can not only lead to high sensitivity of errors and precision, but also cause chattering in estimation error* $\widetilde{E}$*, which makes it hard to converge. Besides, if the value of* η_1 *is too low, the NN will become insensitive and estimation error* $\widetilde{E}$ *will not converge as well.*

2.5.3 Simulation results and discussion

To illustrate the stability of the controller design in (2.22), a numerical simulation based on the a group of ODRs is conducted. The model of the ODR is still set as (2.17) and the parameters of the ODRs remain the same as what's given in Table 2.1. The initial states of the ODRs are altered into the values in Table 2.3.

The external disturbance stays the same as the FTDO case and the formation reference is changed to

$$x_{di}(t) = \left[2\cos\left(\frac{-t}{10}+\frac{\pi}{4}\right)+\cos\left(\frac{t}{10}+\frac{i\pi}{2}\right), 2\sin\left(\frac{-t}{10}+\frac{\pi}{4}\right)+\sin\left(\frac{t}{10}+\frac{i\pi}{2}\right), \frac{i\pi}{4}\right]^{\mathrm{T}} \tag{2.30}$$

The parameters in (2.22) are set as $k_i = 2.5$, $\lambda_i = 2.5$ and $c_i = 10$. The order of the CNN is chosen as $N_c = 3$. The weight matrices of the CNN are set as $\mathbf{0}_{19\times 3}$ and the error sensitivity is chosen as $\eta_1 = 0.1$. The curves of $\|\delta_{xi}\|$, $\|\xi_i\|$ and u_i are shown in Figures 2.11-2.13, respectively.

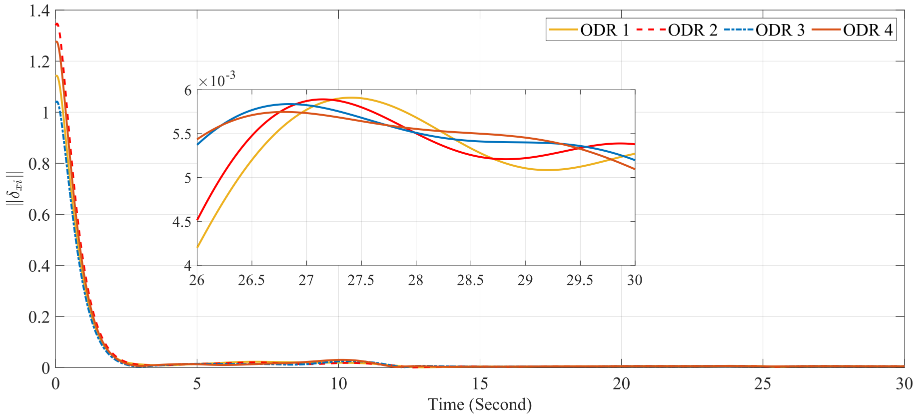

Figure 2.11. $\|\delta_{xi}\|$ of individual ODRs (CNN-based design).

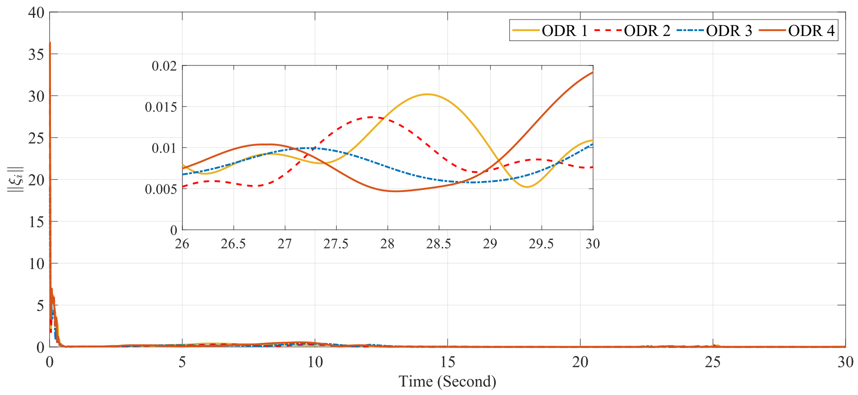

Figure 2.12. $\|\xi_i\|$ of individual ODRs (CNN-based design).

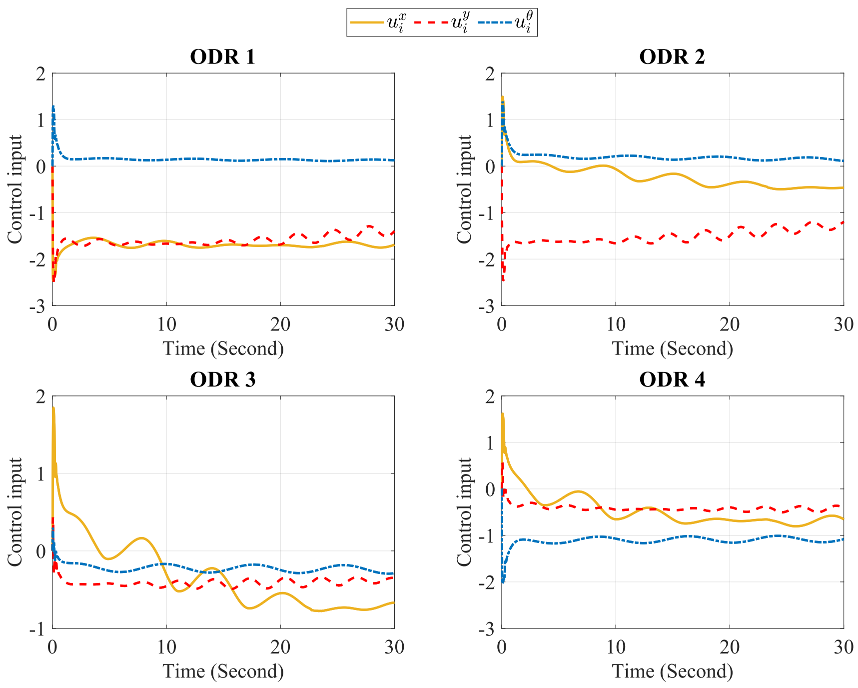

Figure 2.13. Control input of individual ODRs (CNN-based design).

Similar to the FTDO-based design, both $\|\delta_{xi}\|$ and $\|\xi_i\|$ are semi-globally UUB within the region of 8.8×10^{-3} and 1.6×10^{-3}, respectively. The control input of each individual ODR is still smooth, which matches the characteristics of the DSM technique.

The norm of the CNN estimation error is also given in Figure 2.14, where the error norm is found to be semi-globally UUB within the value of 0.4 for each individual agent.

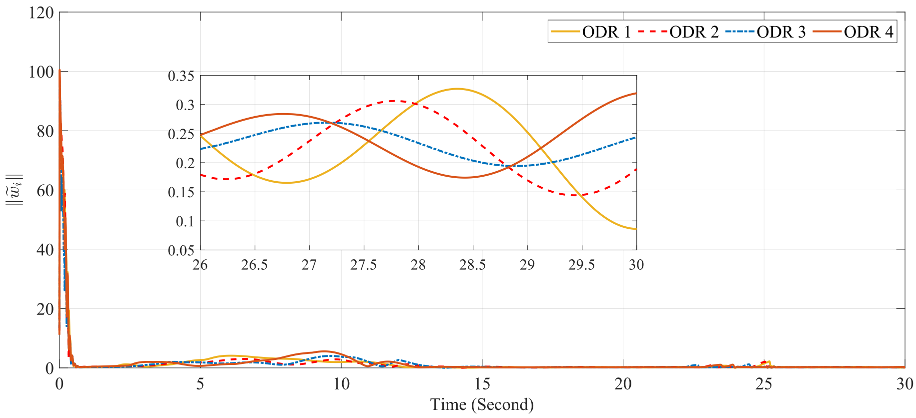

Figure 2.14. CNN estimation error.

The system trajectories and formation status are recorded in Figure 2.15. The formation reference given in (2.30) is a time-varying circular formation (see the green dashed circle) that performs self-rotation while its centre travels on another circular trajectory (purple dashed circle). It is observed in Figure 2.15 that all four ODRs are able to track their references (dotted-dashed lines) to form the expected formation.

2.6 Chapter summary

This chapter focuses on the implementation of the DSM technique in multi-agent scenarios. A brief introduction of the DSM theory is first given to clarify the conditions and controller design procedures for nominal second-order systems. The FTDO structure is then employed to perform finite-time estimation of the system uncertainty, and the stability of the corresponding FTDO-based DSM formation controller is validated by both theoretical analysis and a numerical simulation. To reduce our assumption on the system uncertainty, the CNN approximation mechanism is introduced and integrated with the DSM technique to obtain an adaptive formation control scheme. The

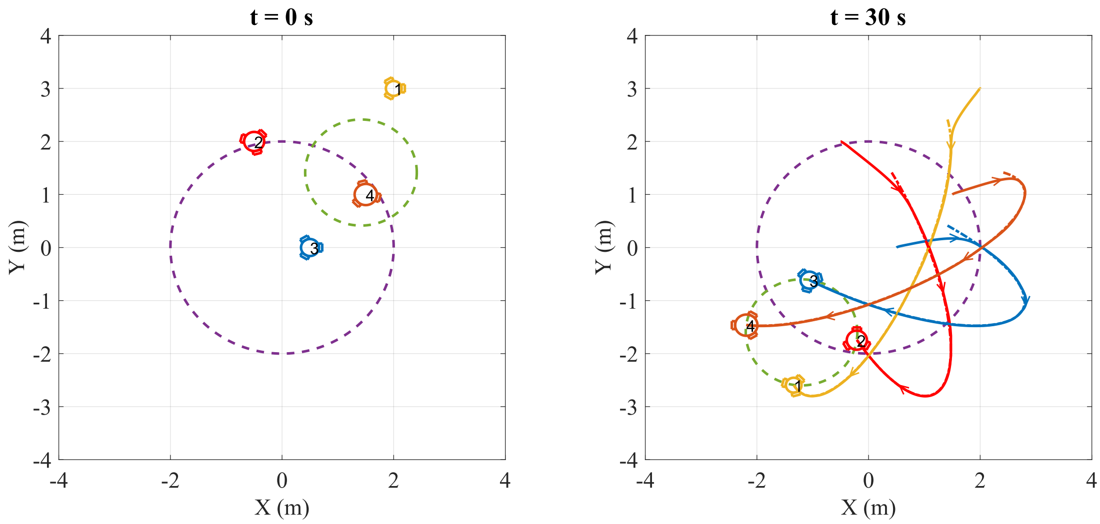

Figure 2.15. Trajectories of individual ODRs (CNN-based design).

semi-global uniform ultimate boundedness of error-related states in the CNN-based design is also illustrated by a numerical simulation. Both control designs are found to have smooth control input signals, which matches our expectation.

In the next chapter, the issue of obstacle avoidance will be considered to ensure the safty of MASs during the formation tracking process. A reference correction algorithm is developed to deal with the passive correction led by the unreachable reference scenario. An observer-based formation controller is further proposed for MASs with both matched and mismatched uncertainties.

Chapter 3

Robust Formation Control with Obstacle Avoidance

OTHER than ensuring the boundedness of each agent's tracking error to guarantee a robust formation status, it is also necessary to design obstacle avoidance algorithms to maintain the safety of each robot. In this chapter, an observer-and-algorithm-based formation controller is proposed for second-order multi-agent systems to achieve time-varying formation without having collision with obstacles. First, a new sliding surface design is proposed for second-order multi-agent systems with both matched and mismatched disturbances. The artificial potential field technique is then integrated with the sliding mode control scheme to develop a robust formation controller. To attenuate the passive corrections led by the inter-agent communication, a new reference correction algorithm is further developed. Comparative simulations based on a group of omni-directional robots are given to illustrate the effectiveness of the robust formation controller and the new algorithm.

3.1 Introduction

To carry out practical formation tracking tasks such as real-time surveillance, we usually need to employ autonomous UAVs (Dong *et al.* 2018), uncrewed grounded vehicles (Wang *et al.* 2019) or uncrewed underwater vehicles (Li *et al.* 2019b) in non-ideal environments. It is common sense that the practical environments are usually filled with obstacles, which indicates the necessity of considering the obstacle avoidance issue in the field of MASs.

The obstacle avoidance issue is more challenging for multi-agent applications compared to single-agent systems because interactions among agents can largely increase the complexity of the system. One popular approach to solve the obstacle avoidance issue is optimal control. A distributed optimal control law that only requires local information was implemented to achieve high obstacle avoidance capability for linear MASs (Chen and Sun 2016). To ensure that each agent can move along the optimal trajectory, the theory of model predictive control was employed to perform simultaneous optimisation without colliding into any obstacles (Dai *et al.* 2017).

Apart from the optimisation perspective, artificial potential field (APF) is one famous approach that is widely used for both path planning and motion control to achieve real-time collision avoidance (Wen *et al.* 2017, Li *et al.* 2018, Sharma *et al.* 2021). A potential function based sliding mode surface was first designed by Li et al. to handle the local minima issue of APF with the assumption that the reference trajectory should remain outside the collision regions (Li *et al.* 2018). To deal with the obstacle avoidance problem of a group of stochastic second-order agents, the APF technique was employed with a proportional-derivative formation controller to ensure the boundedness of the expectation of formation tracking error (Wen *et al.* 2017). However, the effect of interactions among agents was often ignored among the aforementioned articles.

For example, the results obtained by Wen et al, illustrate that when one agent needs to move away from its reference trajectory to avoid an obstacle, there are sudden boosts in the reference tracking errors of the other agents, leading to chaotic system formations. Therefore, how to ensure the robustness of the system's formation when part of the agents need to avoid obstacles is a gap to be filled.

System uncertainty is another factor that is worth considering in the formation control community due to its tight link with the robustness of system formations. Most research works only focused on matched uncertainties that exist in the same channel as control input (Zou and Kumar 2012, Wen *et al.* 2017), leaving problems related to mismatched uncertainties unsolved.

Mismatched uncertainties usually refer to the uncertain factors caused by parameter perturbations, external winds or mismodelled dynamics that affect the system through channels different from control input (Chen *et al.* 2015). The most suitable method to estimate the mismatched uncertainty is to employ observers (Ma *et al.* 2017, Mondal *et al.* 2017b). The ESO structure was proved to be effective by Ma et al. to achieve adaptive consensus control for second-order MASs with mismatched disturbances (Ma *et al.* 2017). A new homogeneous disturbance observer was developed by Mondal et al. to construct the sliding mode consensus controller for high-order MASs. An observer-based sliding mode controller (Mondal *et al.* 2017b) was further designed by Mondal et al. to achieve the state consensus of heterogeneous MASs. However, no previous work has yet discussed the problem of obstacle avoidance for MASs with mismatched disturbances, which leads to a considerable challenge.

The following issues are addressed in this chapter:

1. How to ensure each agent's safety by avoiding collisions with static obstacles when the agent is affected by both matched and mismatched disturbances?

2. How to guarantee the uniform ultimate boundedness of each agent's reference tracking error with the existence of matched and mismatched disturbances?

3. How to ensure the robustness of the overall system formation while a part of the agents need to move away from the desired position to avoid obstacles?

The contents in this chapter are organised as follows. The system modelling of a class of nonlinear MASs with both matched and mismatched disturbances and the problem formulation are given Section 3.2. A brief introduction of the APF technique is given in Section 3.3. The development of the observer-based sliding mode formation controller and the reference correction algorithm (RCA) are presented in Section 3.4, where numerical simulation results are given to illustrate the effectiveness of the proposed control scheme. The final conclusions are drawn in Section 3.5.

3.2 System modelling and problem formulation

In this chapter, consider a group of second-order nonlinear agents affected by both matched and mismatched disturbances, where the system dynamics of the ith agent is given as

$$\begin{cases} \dot{x}_i = v_i + d_i \\ \dot{v}_i = f_i(x_i, v_i) + g_i u_i + \varpi_i, \quad i = 1, 2, \ldots, N \end{cases} \tag{3.1}$$

where $x_i = [x_{i,p}^{\mathrm{T}}, x_{i,a}^{\mathrm{T}}]^{\mathrm{T}} \in \mathbb{R}^n$ and $v_i = [v_{i,p}^{\mathrm{T}}, v_{i,a}^{\mathrm{T}}]^{\mathrm{T}} \in \mathbb{R}^n$ are the position and velocity information of the ith agent, respectively, $x_{i,p} \in \mathbb{R}^{n_1}$ is the agent's coordinates in the global frame, $x_{i,a} \in \mathbb{R}^{n_2}$ is the agent's angular status, $v_{i,p} \in \mathbb{R}^{n_1}$ is the agent's linear velocity, $v_{i,a} \in \mathbb{R}^{n_2}$ is the agent's angular velocity, $f_i(x_i, v_i) \in \mathbb{R}^n$ is the unknown continuous system dynamics, $u_i \in \mathbb{R}^n$ is the control input, $g_i \in \mathbb{R}^{n \times n}$ is the known coupling matrix for the control input, $d_i \in \mathbb{R}^n$ is the mismatched disturbance and $\varpi_i \in \mathbb{R}^n$ is the matched disturbance. The parameters mentioned above satisfy the conditions that $n_1 \geq 2$, $n_2 \geq 0$ and $n_1 + n_2 = n$.

Define $w_i = f_i(x_i, v_i) + \varpi_i$ to be the overall matched uncertainty of the ith agent, then we have the simplified version of (3.1) as follows:

$$\begin{cases} \dot{x}_i = v_i + d_i \\ \dot{v}_i = g_i u_i + w_i, \quad i = 1, 2, \ldots, N \end{cases} \tag{3.2}$$

Accordingly, we have the following cluster expression:

$$\begin{cases} \dot{x} = v + d \\ \dot{v} = g u + w \end{cases} \tag{3.3}$$

where

$$x = [x_1^{\mathrm{T}}, x_2^{\mathrm{T}}, \ldots, x_N^{\mathrm{T}}]^{\mathrm{T}} \in \mathbb{R}^{nN \times 1},\ v = [v_1^{\mathrm{T}}, v_2^{\mathrm{T}}, \ldots, v_N^{\mathrm{T}}]^{\mathrm{T}} \in \mathbb{R}^{nN \times 1},\ d = [d_1^{\mathrm{T}}, d_2^{\mathrm{T}}, \ldots, d_N^{\mathrm{T}}]^{\mathrm{T}}$$
$$g = \mathrm{diag}\{g_1, g_2, \ldots, g_N\},\ u = [u_1^{\mathrm{T}}, u_2^{\mathrm{T}}, \ldots, u_N^{\mathrm{T}}]^{\mathrm{T}},\ w = [w_1^{\mathrm{T}}, w_2^{\mathrm{T}}, \ldots, w_N^{\mathrm{T}}]^{\mathrm{T}}$$

Definition 3.1. (Lewis *et al.* 2013) *Consider a state vector $X \in \mathbb{R}^n$, suppose there is a correlated continuous Lyapunov function $V(X)$. Then the vector X is said to be UUB if $V(X)$ satisfies $V(X) = 0$ only when $\|X\| = 0$, and there exists a positive boundary b_X and a time $t_X(X(t_0), b_X)$ such that $\|V(X)\| \leq b_X$ for all $t \geq t_0 + t_X$, where t_0 is the initial time and $X(t_0)$ is the initial value of X.*

Lemma 3.1. (Lewis *et al.* 2013) *Consider a positive definite function $V(X)$, if there is a positive boundary b_X such that $\dot{V}(X)$ is expected to remain negative when $\|X\| > b_X$, then the uniform ultimate boundedness of the state X is guaranteed.*

The desired position for the ith agent is specified as $x_{di} \in \mathbb{R}^n$ $(i = 1, 2, \ldots, N)$, where x_{di} is continuous and differentiable. The main goal of the to be proposed control scheme is to ensure the uniform ultimate boundedness of the ith agent's formation tracking error, which is specified as

$$\lim_{t\to\infty} ||x_i(t) - x_{di}(t)|| \leq \nu_\delta^g, \; i = 1, 2, \ldots, N \tag{3.4}$$

where ν_δ^g is a small positive constant.

The communication topology of system (3.3) is given as a directed graph (see Section 2.3) and the following assumptions are made:

Assumption 3.1. *The formation reference vector x_{di} for the ith agent is second-order differentiable and its time derivatives $\dot{x}_{di}$ and $\ddot{x}_{di}$ are bounded and known.*

Assumption 3.2. (Shtessel *et al.* 2007) *For the above mentioned second-order agents, suppose both the mismatched uncertainty d_i and matched uncertainty w_i are bounded and differentiable. Also, the uncertainties $\dot{d}_i$ and $\dot{w}_i$ have Lipschitz constants $\beta_{i,d}$ and $\beta_{i,w}$, respectively.*

3.3 Artificial potential fields

To achieve the goal of obstacle avoidance, APFs are employed in this chapter to offer high potential to each obstacle, which can further generate the repulsive forces to drive the agents away from the obstacles.

The operating space of the MAS contains N_o fixed obstacles. Each obstacle can be described as an element of the set $\mathbb{O} = \{(p_{o,k}, r_{o,k}), k = 1, 2, \ldots, N_o\}$, where $p_{o,k}$ denotes the Cartesian position of the centre of the kth obstacle, and $r_{o,k}$ is the radius of the kth obstacle. Without the loss of generality, the obstacle avoidance problem is discussed on the basis of two-dimensional space in latter parts, if not stated otherwise.

Define $z_{i,k}$ to be the relative position vector between the ith agent and the kth obstacle that can be expressed as:

$$z_{i,k} = x_{i,p} - p_{o,k} = \overrightarrow{p_{o.k} x_{i,p}}$$

Assumption 3.3. *In this chapter, each agent can be modelled as a circle and the radius of the ith agent is expressed as $r_{a,i}$, where $i = 1, 2, \ldots, N$.*

Now, we define the repulsive potential function $\Phi(\|z_{i,k}\|)$ between the ith agent and the kth obstacle as follows:

Definition 3.2. (Wen *et al.* 2017) *The potential function $\Phi(\|z_{i,k}\|)$ is a nonnegative, differentiable and monotonically decreasing function that satisfies the following conditions*

1. $\Phi(\|z_{i,k}\|) \to +\infty$ *when* $\|z_{i,k}\| \to \underline{r}_{i,k}$, *where* $\underline{r}_{i,k} = \epsilon_1(r_{a,i} + r_{o,k})$ *is the minimal safe distance between the centre of the ith agent and the centre of the kth obstacle, and* ϵ_1 *is a constant that satisfies* $\epsilon_1 > 1$.
2. $\Phi(\|z_{i,k}\|) \to 0$ *when* $\|z_{i,k}\| \to \bar{r}_{i,k}$, *and* $\Phi(\|z_{i,k}\|) = 0$ *when* $\|z_{i,k}\| \geq \bar{r}_{i,k}$, *where* $\bar{r}_{i,k} = \epsilon_2(r_{a,i} + r_{o,k})$ *represents the outer edge of the artificial potential field, and* ϵ_2 *is a constant that satisfies* $\epsilon_2 > \epsilon_1$.

Assumption 3.4. *The information set $(p_{o,k}, r_{o,k})$ of the kth obstacle is known or can be obtained from detection when $\|z_{i,k}\| \geq \bar{r}_{i,k}$.*

Define the total potential function for the ith agent as

$$\Phi_i = \sum_{k=1}^{N_o} \Phi(\|z_{i,k}\|) \tag{3.5}$$

The repulsive force between the ith agent and the kth obstacle is obtained as the negative gradient of the potential function $\Phi(\|z_{i,k}\|)$ as follows:

$$f_{i,k} = -\nabla_{z_{i,k}} \Phi(\|z_{i,k}\|) = -\nabla_{x_{i,p}} \Phi(\|z_{i,k}\|)$$

Then the combined repulsive force f_i which is applied to the ith agent is given as

$$f_i = \sum_{k=1}^{N_o} f_{i,k} = -\sum_{k=1}^{N_o} \nabla_{z_{i,k}} \Phi(\|z_{i,k}\|) \tag{3.6}$$

Remark 3.1. *To offer additional safety, the parameter is chosen with the condition of $\epsilon_1 > 1$. Hence, if the norm of the distance vector $z_{i,k}$ is guaranteed to be larger than $\underline{r}_{i,k}$, then the collision between the ith agent and the kth obstacle can be sufficiently avoided.*

3.4 Robust formation control with reference correction

3.4.1 Observer-based sliding mode formation controller

By the definition of δ_{xi} and δ_{vi} in Chapter 2, we have the reference tracking error dynamics of the system (3.3) as

$$\begin{cases} \dot{\delta}_x = \delta_v + d \\ \dot{\delta}_v = -\ddot{x}_d + gu + w \end{cases}$$

To estimate the matched and mismatched uncertainties, the FTDO structure (Yang *et al.* 2013) is implemented:

$$\begin{cases} \dot{\gamma}_{i,1} = \nu_{i,1} + v_i,\ \dot{\gamma}_{i,2} = \nu_{i,2},\ \dot{\gamma}_{i,3} = \nu_{i,3},\ \dot{\gamma}_{i,4} = \nu_{i,4} + g_i u_i,\ \dot{\gamma}_{i,5} = \nu_{i,5},\ \dot{\gamma}_{i,6} = \nu_{i,6} \\ \nu_{i,1} = -\alpha_{i,1}\beta_{i,d}^{\frac{1}{3}}\mathrm{sgn}^{\frac{2}{3}}(\gamma_{i,1} - x_i) + \gamma_{i,2},\ \nu_{i,2} = -\alpha_{i,2}\beta_{i,d}^{\frac{1}{2}}\mathrm{sgn}^{\frac{1}{2}}(\gamma_{i,2} - \nu_{i,1}) + \gamma_{i,3} \\ \nu_{i,3} = -\alpha_{i,3}\beta_{i,d}\mathrm{sgn}(\gamma_{i,3} - \nu_{i,2}),\ \nu_{i,4} = -\alpha_{i,4}\beta_{i,w}^{\frac{1}{3}}\mathrm{sgn}^{\frac{2}{3}}(\gamma_{i,4} - v_i) + \gamma_{i,5} \\ \nu_{i,5} = -\alpha_{i,5}\beta_{i,w}^{\frac{1}{2}}\mathrm{sgn}^{\frac{1}{2}}(\gamma_{i,5} - \nu_{i,4}) + \gamma_{i,6},\ \nu_{i,6} = -\alpha_{i,6}\beta_{i,w}\mathrm{sgn}(\gamma_{i,6} - \nu_{i,5}) \\ \widehat{x}_i = \gamma_{i,1},\ \widehat{d}_i = \gamma_{i,2},\ \widehat{\dot{d}}_i = \gamma_{i,3},\ \widehat{v}_i = \gamma_{i,4},\ \widehat{w}_i = \gamma_{i,5},\ \widehat{\dot{w}}_i = \gamma_{i,6} \end{cases} \tag{3.7}$$

where $\widehat{d}_i$ and $\widehat{w}_i$ are the estimation value for the ith agent's matched and mismatched uncertainties d_i and w_i, respectively, and the expression of $\mathrm{sgn}(\cdot)$ is as explained in Section 2.4.1.

Then define the uncertainty observation errors of the ith agent as

$$\begin{cases} \widetilde{d}_i = \widehat{d}_i - d_i \\ \widetilde{w}_i = \widehat{w}_i - w_i \end{cases} \tag{3.8}$$

To facilitate the controller design, define the local mismatched uncertainty sum e_{di} and the local mismatched uncertainty observation sum $\widehat{e}_{di}$ for agent i as follows:

$$\begin{cases} e_{di} = \sum_{j=1}^{N} a_{ij}(d_i - d_j) + b_i d_i = \sum_{j=1}^{N} l_{ij} d_j + b_i d_i \\ \widehat{e}_{di} = \sum_{j=1}^{N} a_{ij}(\widehat{d}_i - \widehat{d}_j) + b_i \widehat{d}_i = \sum_{j=1}^{N} l_{ij} \widehat{d}_j + b_i \widehat{d}_i \end{cases} \tag{3.9}$$

If define $e_d = [e_{d1}^{\mathrm{T}}, e_{d2}^{\mathrm{T}}, \ldots, e_{dN}^{\mathrm{T}}]^{\mathrm{T}}$ and $\widehat{e}_d = [\widehat{e}_{d1}^{\mathrm{T}}, \widehat{e}_{d2}^{\mathrm{T}}, \ldots, \widehat{e}_{dN}^{\mathrm{T}}]^{\mathrm{T}}$ to act as the cluster expression, we then have

$$\begin{cases} e_d = (L+B) \otimes I_n d \\ \widehat{e}_d = (L+B) \otimes I_n \widehat{d} \end{cases}$$

Based on the definition of local errors (2.12), the local formation tracking error dynamics is further obtained as

$$\begin{cases} \dot{e}_x = e_v + e_d \\ \dot{e}_v = (L+B) \otimes I_n(-\ddot{x}_d + gu + w) \end{cases}$$

To ensure the sliding motion with the existence of mismatched uncertainties, define the modified sliding surface for the ith agent as

$$s_i = e_{vi} + \widehat{e}_{di} + \lambda_i e_{xi} \tag{3.10}$$

where λ_i is a positive constant.

Accordingly, if define $S = [s_1^{\mathrm{T}}, s_2^{\mathrm{T}}, \ldots, s_N^{\mathrm{T}}]^{\mathrm{T}}$, then the time derivative of the modified sliding variable is obtained as

$$\begin{aligned} \dot{S} &= \dot{e}_v + \dot{\widehat{e}}_d + \Lambda \otimes I_n \dot{e}_x \\ &= (L+B) \otimes I_n(\dot{\delta}_v + \dot{\widehat{d}} + \Lambda \otimes I_n \dot{\delta}_x) \\ &= (L+B) \otimes I_n(-\ddot{x}_d + gu + w + \dot{\widehat{d}} + \Lambda \otimes I_n(\delta_v + d)) \end{aligned}$$

where $\Lambda = \mathrm{diag}\{\lambda_1, \lambda_2, \ldots, \lambda_N\}$.

Define $\Delta r_{i,k} = \overline{r}_{i,k} - \underline{r}_{i,k}$ to represent the width of the potential field, then the artificial potential function between the ith agent and the kth obstacle is chosen as follows according to Definition 3.2:

$$\Phi(\|z_{i,k}\|) = \begin{cases} \alpha\left(\ln\left(\dfrac{\|z_{i,k}\| - \underline{r}_{i,k}}{\Delta r_{i,k}}\right) + \dfrac{\overline{r}_{i,k} - \|z_{i,k}\|}{\|z_{i,k}\| - \underline{r}_{i,k}}\right), & \|z_{i,k}\| \in (\underline{r}_{i,k}, \overline{r}_{i,k}] \\ 0, & \text{otherwise} \end{cases} \tag{3.11}$$

where α is a positive constant.

By using the chain rule of calculus, the repulsive force generated by the artificial potential field is obtained as the following equation:

$$f_{i,k} = \begin{cases} \alpha \dfrac{\overline{r}_{i,k} - \|z_{i,k}\|}{(\|z_{i,k}\| - \underline{r}_{i,k})^2} \dfrac{z_{i,k}}{\|z_{i,k}\|}, & \|z_{i,k}\| \in (\underline{r}_{i,k}, \overline{r}_{i,k}] \\ 0, & \text{otherwise} \end{cases} \tag{3.12}$$

Based on the previous analysis related to the APF (3.12), disturbance observer (3.7) and modified sliding variable (3.10), the proposed distributed observer based sliding mode formation controller is designed as

$$u_i = g_i^{-1}(-c_i s_i - \widehat{w}_i - \widehat{\dot{d}}_i - \lambda_i \delta_{vi} - \lambda_i \widehat{d}_i - \delta_{xi} + \ddot{x}_{di} + F_i) \tag{3.13}$$

where $F_i = [f_i^{\mathrm{T}}, 0_{1\times n_2}]^{\mathrm{T}}$ and $c_i \in \mathbb{R}^+$.

Remark 3.2. *The artificial potential function is chosen as* (3.11) *so that the potential function* $\Phi(\|z_{i,k}\|)$ *and the norm* $\|f_{i,k}\|$ *will achieve* 0 *simultaneously when* $\|z_{i,k}\| = \bar{r}_{i,k}$, *which further ensures the continuity of both functions.*

Remark 3.3. *In terms of the usage of the APF, it is not necessary to illustrate the APF function* (3.11) *because it will not be directly used during the controller design. With Assumption 3.4 guaranteeing that the essential knowledge of the obstacles can be obtained forehand, a simpler way to implement APF is to calculate the repulsive force regarding each obstacle as* (3.12) *and perform summation as* (3.6) *to obtain* F_i *that acts as the overall repulsive force for the ith agent.*

3.4.2 Reference correction algorithm

During a formation control process, the position reference distributed to each agent can be unreachable when the agent is expected to encounter collision with obstacles at the very position, which can lead to the problem of unreachable references.

To simplify the discussion by treating each agent as a point, we define the circle centred in $p_{o,k}$ with the radius of $\underline{r}_{i,k}$ to be the inner boundary of the kth obstacle's potential field regarding the ith agent, and the circle centred in $p_{o,k}$ with the radius of $\bar{r}_{i,k}$ to be the outer boundary of the kth obstacle's potential field regarding the ith agent. Now, we are ready to give a clear definition of the unreachable reference scenarios as follows:

Definition 3.3. *Consider a plane that contains the ith agent and the kth obstacle (see Figure 3.1), the tangents of the inner boundary of the obstacle's potential field that go through the centre of the agent can separate the plane into five regions: a (beyond the intersection angle of tangents), b (within tangents intersection angle and in the opposite direction of obstacle), c (within tangents intersection and between the agent and obstacle), d (within the inner radius of APF) and e (within tangents intersection and behind the obstacle). If the current desired position of the agent lies in regions d and e, then the current position reference is considered to be unreachable.*

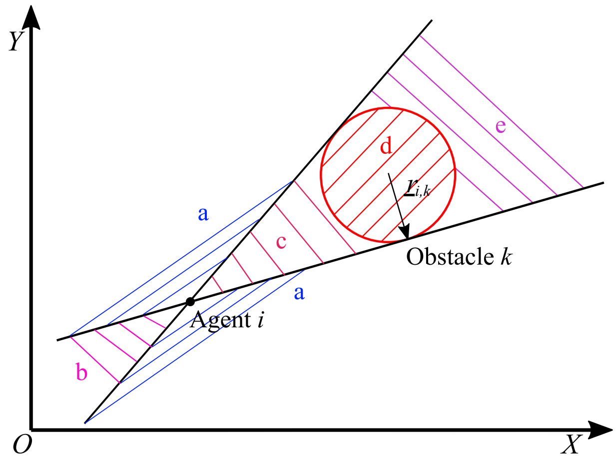

Figure 3.1. Unreachable reference scenarios.

Assumption 3.5. *For the ith agent, the outer boundaries of the obstacles' artificial potential fields do not overlap, the initial position of each agent does not lie inside the inner boundaries of the potential fields, and the given position reference vector x_{di} does not permanently stay inside the inner boundaries of the potential fields.*

Different from the obstacle avoidance of independent systems, the effect of communications among agents needs to be considered for the obstacle avoidance of MASs. According to (2.12) and (3.10), the local formation tracking error and sliding variable of the ith agent are affected by the reference tracking errors of both itself and the agents whose information is accessible. Therefore, if one agent suffers from the unreachable reference scenario and has to move away from the reference trajectory to avoid collision with an obstacle, the agents that have access to its current state will perform passive corrections and move away from the desired trajectories to decrease the values of variables defined in (2.12) and (3.10), which can jeopardise the system's performance.

Hence, a distributed reference correction algorithm is proposed in this section to attenuate the passive correcting behaviours caused by the unreachable reference issue and avoid the local minima problem when the agent faces single obstacle. The detailed steps of the algorithm are illustrated in Algorithm 1. To sum up, the controller design of the reference correction algorithm based sliding mode controller can be illustrated by Figure 3.2, where $i = 1, 2, \ldots, N$.

Remark 3.4. *The purpose of making Assumption 3.5 is to rule out the local minima issue that is caused by multiple obstacles. Furthermore, it also ensures that the reference trajectories for agents will not stay unreachable.*

3.4.2 Reference correction algorithm

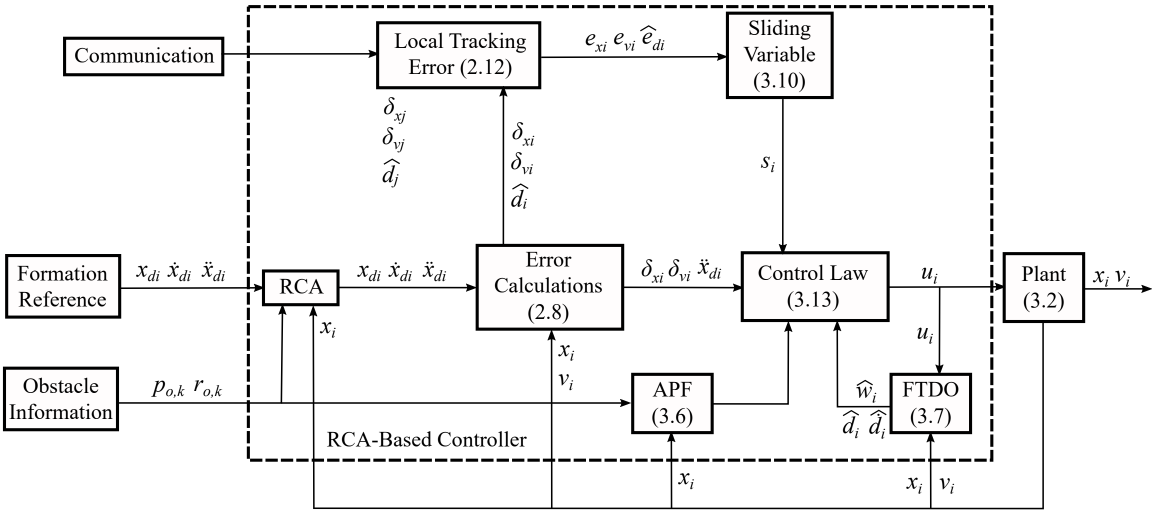

Figure 3.2. RCA-based robust controller.

Algorithm 1: Reference correction algorithm

Input: x_{pi},$\mathbb{O}$,x_{di},$\dot{x}_{di}$,$\ddot{x}_{di}$

Output: x_{di},$\dot{x}_{di}$,$\ddot{x}_{di}$

$k_i^o = 0$;

$k = \arg\min_k \|\overrightarrow{x_{p,i}p_{o,k}}\|$;

if $\|\overrightarrow{x_{p,i}p_{o,k}}\| \in (\underline{r}_{i,k}, \overline{r}_{i,k}]$ **then**

  if $\sin(<\overrightarrow{x_{pi}p_{o,k}}, \overrightarrow{x_{pi}x_{di}}>)\|\overrightarrow{x_{p,i}p_{o,k}}\| \in [0, \underline{r}_{i,k}]$ & $\cos(<\overrightarrow{x_{pi}p_{o,k}}, \overrightarrow{x_{pi}x_{di}}>) \geq 0$ **then**

    if $\sqrt{\|\overrightarrow{x_{pi}p_{o,k}}\|^2 - \underline{r}_{i,k}^2} \leq \|\overrightarrow{x_{pi}x_{di}}\|$ or $\|\overrightarrow{x_{di}p_{o,k}}\| \leq \underline{r}_{i,k}$ **then**

      Find the kth obstacle's inner boundary's tangent that crosses x_{pi};

      Find the tangent T_i that has a point x_c that minimize the value of $\|\overrightarrow{x_{di}x_c}\|$;

      $x_{di} \leftarrow x_c$;

      Obtain the projection of $\dot{x}_{di}$ and $\ddot{x}_{di}$ on tangent T_i: $\dot{\mathcal{X}}_{di}$ and $\ddot{\mathcal{X}}_{di}$;

      $\dot{x}_{di} \leftarrow \dot{\mathcal{X}}_{di}$;

      $\ddot{x}_{di} \leftarrow \ddot{\mathcal{X}}_{di}$;

      $k_i^o = k$;

    end

  end

end

Return $x_{di}, \dot{x}_{di}, \ddot{x}_{di}$;

3.4.3 Stability analysis of the algorithm-and-observer-based scheme

Before presenting the stability analysis for the proposed control scheme, it is necessary to first recall the following useful results:

Lemma 3.2. (Li *et al.* 2018) *If a given agent's state will not cross the inner boundary of any obstacle's potential field, then its total potential function* (3.5) *can be considered to be bounded throughout the tracking control process.*

Lemma 3.3. (Yang *et al.* 2013) *For a second-order system with mismatched uncertainties, if the disturbance observer is designed in the form given in* (3.7)*, then the observation errors that were defined in* (3.8) *will converge to zero within a finite time* t_o*.*

Now, we are ready to present the main result of this chapter.

Theorem 3.1. *Consider a second-order MAS* (3.3) *affected by both matched and mismatched uncertainties, where Assumptions 3.1-3.5 hold. By the artificial potential field* (3.11)*, the RCA (Algorithm 1), the finite-time disturbance observer* (3.7) *and the distributed control law* (3.13)*, the sliding variable* S*, the local formation tracking error* e_x*, and the position tracking error* δ_x *are all UUB.*

Proof. The proof contains two parts, the first part illustrates that each agent is able to avoid the collision with any given obstacle with the existence of both mismatched and matched uncertainties, while the uniform ultimate boundedness of the system states are proved in the second part.

Part 3.1.1. In this part, the effectiveness of obstacle avoidance is analysed between the ith agent and the kth obstacle. The same result can also be extended to the other cases.

Construct an energy Lyapunov function as the following equation regarding the ith agent and the kth obstacle:

$$V_{i,k} = \frac{1}{2} z_{i,k}^{\mathrm{T}} z_{i,k} + \frac{1}{2} v_i^{\mathrm{T}} v_i$$

Then its time derivative is expressed as

$$\begin{aligned}
\dot{V}_{i,k} &= z_{i,k}^{\mathrm{T}} \dot{x}_{pi} + v_i^{\mathrm{T}} \dot{v}_i \\
&= z_{i,k}^{\mathrm{T}} (v_{pi} + d_{pi}) + v_i^{\mathrm{T}} (-\bar{c} s_i - \widehat{w}_i - \dot{\widehat{d}}_i - \lambda_i \delta_{vi} - \lambda_i \widehat{d}_i - \delta_{xi} + \ddot{x}_{di} + F_i + w_i) \\
&= z_{i,k}^{\mathrm{T}} (v_{pi} + d_{pi}) - \bar{c} v_i^{\mathrm{T}} s_i - v_i^{\mathrm{T}} (\widetilde{w}_i - \ddot{x}_{di} + \dot{\widehat{d}}_i + \lambda_i \widehat{d}_i) - v_i^{\mathrm{T}} (\lambda_i \delta_{vi} + \delta_{xi}) + v_i^{\mathrm{T}} F_i
\end{aligned}$$

$$= z_{i,k}^{\mathrm{T}}(v_{pi} + d_{pi}) - \bar{c}v_i^{\mathrm{T}}s_i - v_i^{\mathrm{T}}(\widetilde{w}_i - \ddot{x}_{di} + \dot{\widehat{d}}_i + \lambda_i \widehat{d}_i) - v_i^{\mathrm{T}}(\lambda_i \delta_{vi} + \delta_{xi}) + v_{pi}^{\mathrm{T}} f_{i,k}$$

Since the formation reference is continuous and bounded, terms including $z_{i,k}^{\mathrm{T}}(v_{pi} + d_{pi})$, $\bar{c}v_i^{\mathrm{T}}s_i$, $v_i^{\mathrm{T}}(\widetilde{w}_i - \ddot{x}_{di} + \dot{\widehat{d}}_i + \lambda_i \widehat{d}_i)$, and $v_i^{\mathrm{T}}(\lambda_i \delta_{vi} + \delta_{xi})$ are all bounded. Thus, if the ith agent is moving toward the kth obstacle, the agent can be considered as moving toward the gradient direction of the potential function $\Phi(\|z_{i,k}\|)$. According to Definition 3.2, we can obtain that if $\|z_{i,k}\| \to \underline{r}_{i,k}$, $v_{pi}^{\mathrm{T}} f_{i,k} \to +\infty$. Therefore, the following inequality sufficiently holds if the ith agent is about to collide into the kth obstacle:

$$\begin{aligned} v_{pi}^{\mathrm{T}} f_{i,k} > & - z_{i,k}^{\mathrm{T}}(v_{pi} + d_{pi}) + \bar{c}v_i^{\mathrm{T}}s_i + v_i^{\mathrm{T}}(\lambda_i \delta_{vi} + \delta_{xi}) - v_i^{\mathrm{T}}(\widetilde{w}_i + \ddot{x}_{di} + \dot{\widehat{d}}_i + \lambda_i \widehat{d}_i) \\ & + \frac{\eta_v}{2} z_{i,k}^{\mathrm{T}} z_{i,k} + \frac{\eta_v}{2} v_i^{\mathrm{T}} v_i \end{aligned}$$

where η_v is a positive number which is big enough. Based on the above condition, the following equation can be obtained:

$$\dot{V}_{i,k} > \eta_v V_{i,k}$$

Hence, we obtain the following equation

$$\|z_{i,k}\|^2 > 2e^{\eta_v(t-t_c)} V_{i,k}(t_c) - \|v_i\|^2$$

where t_c represents the time when the agent i is about to have collision with the kth obstacle.

With η_v being a positive number that is big enough, the condition $\|z_{i,k}\| > \underline{r}_{i,k}$ is guaranteed. By Lemma 3.2, we also get that both the potential function $\Phi(\|z_{i,k}\|)$ and the norm $\|F_i\|$ of the ith agent remain bounded throughout the formation tracking process.

Part 3.1.2. Choose the Lyapunov candidate as the following equation:

$$V_{2,1} = \frac{1}{2} S^{\mathrm{T}} P \otimes I_n S + \frac{1}{2} e_x^{\mathrm{T}} P \otimes I_n e_x$$

The time derivative of the Lyapunov candidate is given as

$$\begin{aligned} \dot{V}_{2,1} &= S^{\mathrm{T}} P \otimes I_n \dot{S} + e_x^{\mathrm{T}} P \otimes I_n \dot{e}_x \\ &= S^{\mathrm{T}}[P(L+B)] \otimes I_n[\dot{\delta}_v + \dot{\widehat{d}} + \Lambda \otimes I_n(\widehat{d} + \delta_v)] + e_x^{\mathrm{T}} P \otimes I_n(S - \widehat{e}_d - \Lambda \otimes I_n e_x + e_d) \\ &= e_x^{\mathrm{T}} P \otimes I_n S + S^{\mathrm{T}}[P(L+B)] \otimes I_n[-\ddot{x}_d + gu + w + \dot{\widehat{d}} + \Lambda \otimes I_n(\widehat{d} + \delta_v)] \\ &\quad - e_x^{\mathrm{T}}[P(L+B)] \otimes I_n \widetilde{d} - e_x^{\mathrm{T}}(P\Lambda) \otimes I_n e_x \end{aligned}$$

By Lemma 2.3, the following alternative expression of $\dot{V}_{2,1}$ is obtained:

$$\begin{aligned}\dot{V}_{2,1} &= -\frac{1}{2}S^{\mathrm{T}}(CQ)\otimes I_n S - e_x^{\mathrm{T}}(P\Lambda)\otimes I_n e_x + \frac{1}{2}S^{\mathrm{T}}Q\otimes I_n(F+\widetilde{w}) - \frac{1}{2}e_x^{\mathrm{T}}Q\otimes I_n\widetilde{d} \\ &\leq -\begin{bmatrix}\|e_x\| & \|S\|\end{bmatrix}\begin{bmatrix}\underline{\sigma}(P)\underline{\sigma}(\Lambda) & 0 \\ 0 & \frac{1}{2}\underline{\sigma}(CQ)\end{bmatrix}\begin{bmatrix}\|e_x\| \\ \|S\|\end{bmatrix} \\ &\quad + \begin{bmatrix}\frac{\overline{\sigma}(Q)}{2}\|\widetilde{d}\| & \frac{\overline{\sigma}(Q)}{2}(\|F\|+\|\widetilde{w}\|)\end{bmatrix}\begin{bmatrix}\|e_x\| \\ \|S\|\end{bmatrix}\end{aligned} \tag{3.14}$$

where $C = \mathrm{diag}\{c_1, c_2, \ldots, c_N\}$.

By Lemma 3.3, if the parameters of the disturbance observer are chosen properly, then the observation errors $\widetilde{w}$ and $\widetilde{d}$ will converge to zero within the finite time of t_o. Therefore, (3.14) can be rewritten as follows when $t > t_o$:

$$\dot{V}_{2,1} \leq -\begin{bmatrix}\|e_x\| & \|S\|\end{bmatrix}\begin{bmatrix}\underline{\sigma}(P)\underline{\sigma}(\Lambda) & 0 \\ 0 & \frac{1}{2}\underline{\sigma}(CQ)\end{bmatrix}\begin{bmatrix}\|e_x\| \\ \|S\|\end{bmatrix} + \begin{bmatrix}0 & \frac{\overline{\sigma}(Q)}{2}\|F\|\end{bmatrix}\begin{bmatrix}\|e_x\| \\ \|S\|\end{bmatrix} \tag{3.15}$$

Define

$$H_{2,1} = \begin{bmatrix}\underline{\sigma}(P)\underline{\sigma}(\Lambda) & 0 \\ 0 & \frac{1}{2}\underline{\sigma}(CQ)\end{bmatrix},\ h_{2,1} = \begin{bmatrix}0 & \frac{\overline{\sigma}(Q)}{2}\|F\|\end{bmatrix},\ \chi_{2,1} = \begin{bmatrix}\|e_x\| \\ \|S\|\end{bmatrix}$$

then (3.15) is rewritten as

$$\dot{V}_{2,1} \leq -\chi_{2,1}^{\mathrm{T}}H_{2,1}\chi_{2,1} + h_{2,1}\chi_{2,1}$$

When every agent is outside the outer APF boundary of each obstacle, the combination of the repulsive forces for the ith agent will remain $F_i = 0 (i = 1, 2, \ldots, N)$. Then one has

$$\dot{V}_{2,1} \leq -\chi_{2,1}^{\mathrm{T}}H_{2,1}\chi_{2,1} \leq -\bar{c}V_{2,1} \tag{3.16}$$

where $\bar{c} = 2\underline{\sigma}(H_{2,1})/\overline{\sigma}(P)$. Hence, both e_x and S are expected to converge exponentially after time t_o when there are no obstacles to avoid.

Otherwise when $\|F\| \neq 0$, the time derivative of the Lyapunov function $\dot{V}_{2,1}$ will remain negative when $\|\chi_{2,1}\| > \overline{\delta}(h_{2,1})/\underline{\delta}(H_{2,1})$. Therefore, we can get that

$$\begin{aligned}\|e_x\| \leq \|\chi\| &\leq \frac{\overline{\sigma}(Q)F_M}{\min(2\underline{\sigma}(P)\underline{\sigma}(\Lambda), \underline{\sigma}(CQ))} \\ \|S\| \leq \|\chi\| &\leq \frac{\overline{\sigma}(Q)F_M}{\min(2\underline{\sigma}(P)\underline{\sigma}(\Lambda), \underline{\sigma}(CQ))}\end{aligned}$$

where $\|F\| \leq F_M$ and $F_M \in \mathbb{R}^+$. Thus, both S and e_x are bounded. Based on (2.12), we have

$$\|e_x\| \geq \frac{\underline{\sigma}(Q)}{2\overline{\sigma}(P)}\|\delta_x\| \tag{3.17}$$

which further leads to the following equation:

$$\|\delta_x\| \leq \frac{2\overline{\sigma}(P)}{\underline{\sigma}(Q)}\|e_x\| \leq \frac{2\overline{\sigma}(Q)\overline{\sigma}(P)F_M}{\min(2\underline{\sigma}(P)\underline{\sigma}(\Lambda), \bar{c}\underline{\sigma}(Q))\underline{\sigma}(Q)}$$

By Lemmas 3.1, δ_x, e_x and S are UUB within the following regions, respectively:

$$\Omega_\delta^1 = \left\{\delta_x \middle| \|\delta_x\| \leq \frac{2\overline{\sigma}(Q)\overline{\sigma}(P)F_M}{\min(2\underline{\sigma}(P)\underline{\sigma}(\Lambda), \bar{c}\underline{\sigma}(Q))\underline{\sigma}(Q)}\right\}$$
$$\Omega_e^1 = \left\{e_x \middle| \|e_x\| \leq \frac{\overline{\sigma}(Q)F_M}{\min(2\underline{\sigma}(P)\underline{\sigma}(\Lambda), \underline{\sigma}(CQ))}\right\}$$
$$\Omega_S^1 = \left\{S \middle| \|S\| \leq \frac{\overline{\sigma}(Q)F_M}{\min(2\underline{\sigma}(P)\underline{\sigma}(\Lambda), \underline{\sigma}(CQ))}\right\}$$

which completes the proof.

□

3.4.4 Simulation results and discussion

To illustrate the effectiveness of the proposed sliding mode controller design (3.13), simulations based on a multi-ODR system is conducted.

Consider the three-wheel ODR mentioned in Chapter 2, we can make some simplifications based on the model in (2.17) to get the following second-order dynamics (Fei *et al.* 2021b):

$$\begin{cases} \dot{x}_i = v_i + d_i \\ \dot{v}_i = M_i T_s(\theta_i, R_i)u_i + w_i \end{cases}$$

where $x_i = [p_i^x, p_i^y, \theta_i]^{\mathrm{T}}$, $M_i = \mathrm{diag}\{1/m_i, 1/m_i, 1/I_i\}$, m_i is the mass of the robot, I_i is the inertia of the robot, $u_i = [F_i^1, F_i^2, F_i^3]^{\mathrm{T}}$ is the force vector of the three motors, and R_i is the radius of the robot. The system contains five heterogeneous omni-directional robots, whose model parameters and initial states are given in Table 3.1.

The communication topology of the multi-robot system is chosen as the one shown in Figure 3.3 so that ODRs can have in-degrees of one, two and three for the sake of diversity.

Table 3.1. Parameters and initial states of ODRs with mismatched disturbances.

Robot number	Model parameters			Initial states		
	m_i(kg)	R_i(m)	$I_i(\text{kg}\cdot\text{m}^2)$	p_i^x(m)	p_i^y(m)	θ_i(rad)
1	4.8	0.24	0.15	0	0.8	$\pi/6$
2	4.5	0.23	0.12	-1.3	1.4	$\pi/3$
3	5.5	0.30	0.25	-1.4	-1.2	$-\pi/4$
4	5.3	0.28	0.21	0	-0.6	$-\pi/6$
5	5.0	0.25	0.15	0.8	0.3	$\pi/4$

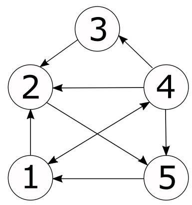

Figure 3.3. Communication topology of the multi-ODR cluster.

The formation pattern is chosen as a time-varying circular formation (each ODR moves in a sine-wave trajectory while the relative distance between each pair of ODRs stays the same to form a radial-fixed circle), which can be abstracted as:

$$x_{di} = \left[\frac{3}{2}\cos\left(\frac{2i}{5}\pi\right) + \frac{3}{20}t, \frac{3}{2}\sin\left(\frac{2i}{5}\pi\right) + \sin\left(\frac{3}{10}t\right), 0\right]^{\mathrm{T}}, \ i \in [1,5] \tag{3.18}$$

The matched and mismatched nonlinear uncertainties are chosen as the following equations, respectively

$$d_i = \left[\frac{3}{10}\sin\left(t + \frac{i}{5}\pi\right) + \frac{1}{5}, \frac{1}{10}\cos\left(\frac{3}{2}t + \frac{i}{4}\pi\right) + \frac{1}{5}, \frac{1}{5}\sin\left(\frac{6}{5}t + \frac{i}{3}\pi\right) + \frac{1}{10}\right]^{\mathrm{T}}$$
$$w_i = \left[\frac{1}{2}\sin\left(\frac{3}{2}t + \frac{i}{4}\pi\right) + 2, \frac{3}{5}\sin\left(2t + \frac{i}{3}\pi\right) + \frac{3}{2}, \frac{1}{2}\sin\left(\frac{4}{5}t + \frac{i}{5}\pi\right) + 1\right]^{\mathrm{T}}$$

The parameters for the finite time disturbance observer are chosen as $\alpha_{i,1} = 4$, $\alpha_{i,2} = 8$, $\alpha_{i,3} = 4$, $\alpha_{i,4} = 6$, $\alpha_{i,5} = 12$, $\alpha_{i,6} = 6$, $\beta_{i,d} = 0.7$ and $\beta_{i,w} = 5$ for $i \in [1,5]$. The parameter values for the APF are set as $\epsilon_1 = 1.1$ and $\epsilon_2 = 2$, respectively. The parameters in the sliding mode controller (3.13) are chosen as $c_i = 2$ and $\lambda_i = 2$ for $i \in [1,5]$. Two obstacles are chosen and their corresponding information is given as $p_{o,1} = [2.9, 2.0]$, $p_{o,2} = [1.8, -1.6]$, $r_{o,1} = 0.3$ and $r_{o,2} = 0.25$.

The reference tracking errors and sliding variables of all ODRs are shown in Figures 3.4 and 3.5, respectively, where the boundedness of each ODR's position tracking error and sliding variable is illustrated.

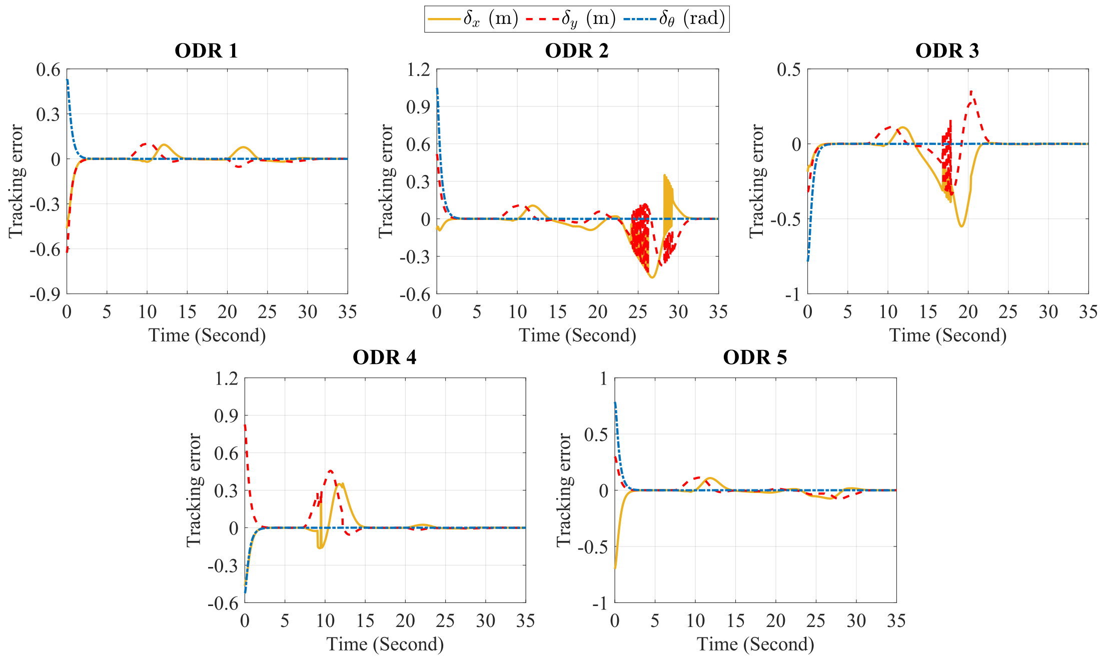

Figure 3.4. Reference tracking errors of the RCA-based robust controller.

Two snapshots of the system formation status are given in Figure 3.6. It is clear that when the outputs of disturbance observer are stabilised and there are no obstacles to avoid, the position reference tracking errors and sliding variables of all five ODRs will converge to a small neighbourhood around zero.

Chattering phenomenons are observed in each ODR's position tracking error and sliding variable during obstacle avoidance procedure. One main reason is that the proposed reference correction algorithm might provide reference points with relatively large distance between each control iteration comparing with the given reference $\dot{x}_{di}$. Such problem can be considered as a future aspect to work on to improve the performance of the algorithm.

Alternatively, after conducting a comparison between the results of ODR two and ODR four, it is found out that as the distance between the reference trajectory and the centre of the obstacle decreases, the chattering phenomenon appears to be more severe.

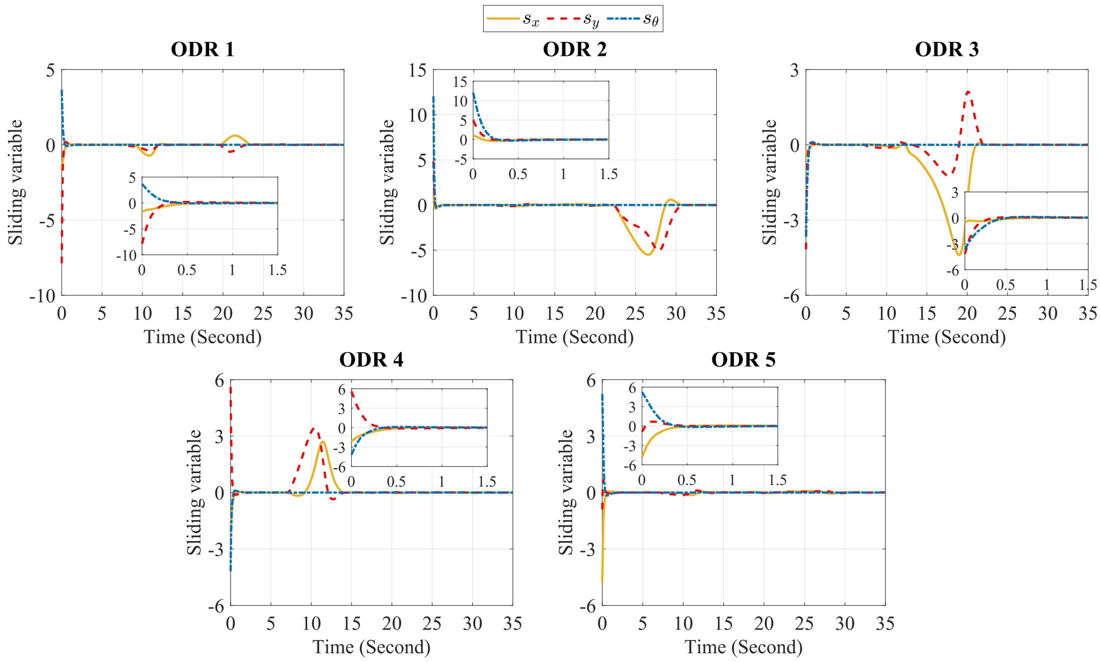

Figure 3.5. Sliding variables of the RCA-based robust controller.

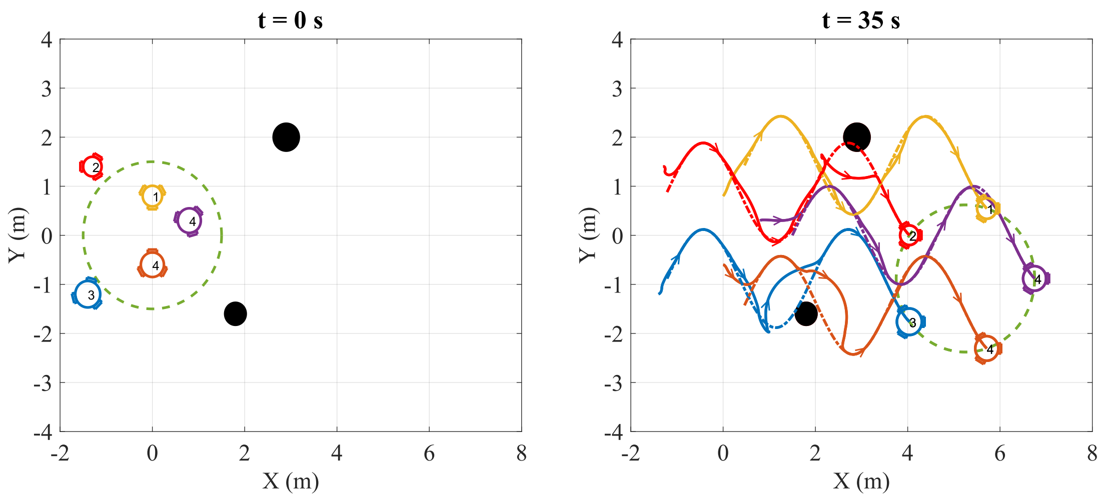

Figure 3.6. Trajectories of individual ODRs (RCABSMC).

Moreover, for a trajectory that enters the inner boundary of one obstacle's potential field, the smaller the distance between the entrance point (where trajectory enters the boundary) and the exit point (where trajectory leaves the boundary) is, the more obvious the chattering is. Specifically, for the sine wave references that we use during this simulation, more chattering can be observed for those that have to avoid obstacles on wave peak or valley (see ODRs two and three) comparing with the one that needs to avoid the obstacle in somewhere between the peak and valley (see ODR four).

Apart from that, no collisions are observed between any pair of ODR and obstacle according to the trajectories of each ODR in Figure 3.6, indicating that the goal of obstacle avoidance is fulfilled.

To test whether the proposed reference correction algorithm can attenuate the passive corrections in the system, define a scalar Δ_i to be the absolute position reference tracking error of the ith ODR as

$$\Delta_i = \int_0^{t_n} \|\delta_{xi}(\tau)\|_1 d\tau \tag{3.19}$$

where t_n represents the current time.

Then we are able to compare the performance of the robust SMC scheme (3.13) and the reference correction algorithm based sliding mode controller (RCABSMC). The comparisons in the absolute reference tracking error Δ_i are illustrated in Figure 3.7.

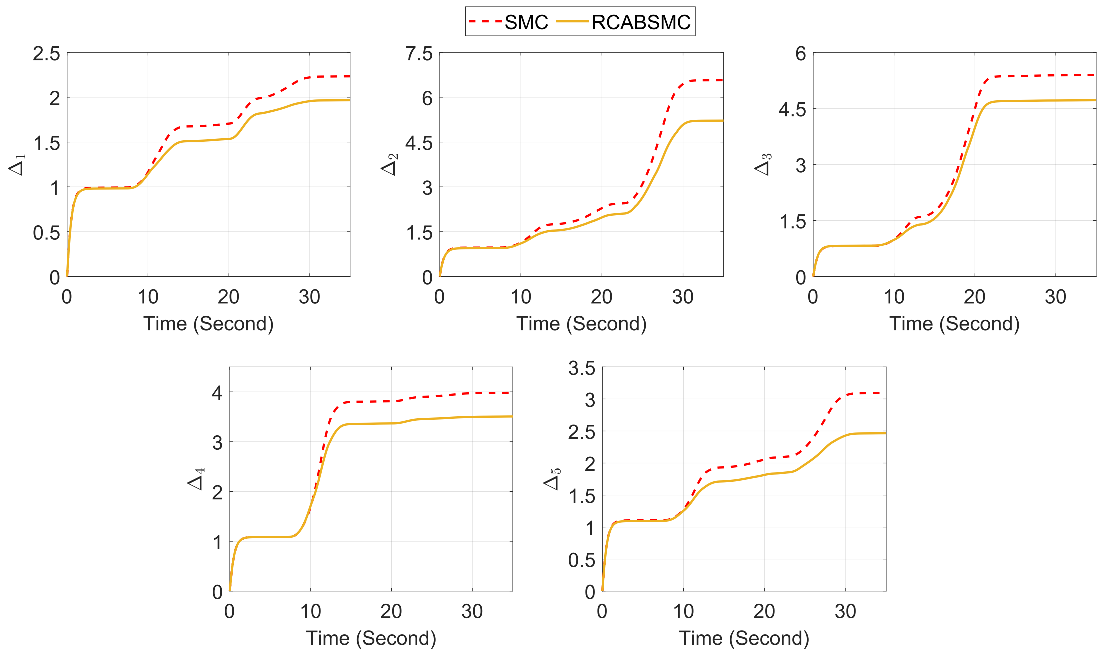

Figure 3.7. Comparison of absolute position reference tracking errors.

Meanwhile, the trigger flag k_i^o of the ith ODR's reference correction algorithm is also given in Figure 3.8 to justify that the RCA works during the formation tracking process. For ODRs that do not need to avoid obstacles (see ODR one and ODR five), remarkable declines can be observed in their absolute position reference tracking error, meaning the passive correction phenomenon is attenuated. Similar trends is also spotted for the ODRs that are involved in obstacle avoidance (see ODRs two, three and four).

To sum up, the stability of the sliding mode controller (3.13) and the performance of the reference correction algorithm (Algorithm 1) are both proved.

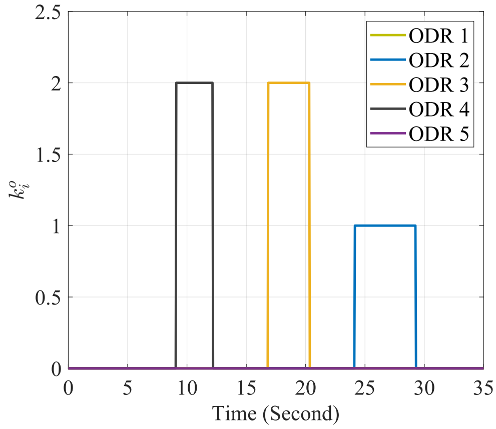

Figure 3.8. RCA flags of ODRs 1-5.

3.5 Chapter summary

In this chapter, the formation control problem for nonlinear second-order MASs with issues including mismatched uncertainties and obstacle avoidance is considered. Sliding mode surface is first updated to ensure cooperative error convergence with mismatched disturbances. A novel observer-based SMC scheme is then proposed to ensure the uniform ultimate boundedness of the position tracking error and sliding variable of each agent. APFs are also implemented to drive agents away from obstacles. A distributed reference correction algorithm is also proposed to deal with the newly defined unreachable reference scenario and its related passive correcting phenomenon. The stability of the proposed control scheme and the validity of the obstacle avoidance scheme are illustrated by both the Lyapunov stability theory and numerical simulations. The effectiveness of the proposed reference correction algorithm is also demonstrated by the comparative studies conducted based on the absolute reference tracking error.

In the next chapter, the collision avoidance issue will be investigated for a class of MASs with limited information. A new neural-based observer is developed to estimate the unknown velocity and the system uncertainty simultaneously to further construct a robust formation control scheme. An observer-based collision-free control scheme is further proposed to achieve robust formation control.

Chapter 4

Robust Formation Control with Limited Information

ALTHOUGH the sliding mode technique is a popular choice to ensure the robustness of the system performance, most of the controller designs are based on the assumption that the controller can gain access to all the system states and the reference states. Therefore, it is necessary to discuss the feasibility of designing a sliding mode controller when only part of the necessary information is available. In this chapter, an observer-based formation controller is proposed for second-order multi-agent systems with limited information to ensure both the convergence of the system's tracking error and the boundedness of the relative distance between each pair of agents. First, two new finite-time neural-based observer designs are introduced to estimate both the agent velocity and the system uncertainty. The sliding mode differentiator is then employed for every agent to approximate the unknown derivatives of the formation reference to further construct the limited-information-based sliding mode controller. To ensure that the system is collision-free, artificial potential fields are introduced along with a time-varying topology. An example of a multiple robot system is used to conduct numerical simulations, and necessary comparisons are made to justify the effectiveness of the proposed limited-information-based control scheme.

4.1 Introduction

According to the concept of MASs, each intelligent agent within the system shall possess the ability to sense, make decision and actuate. In practice, the implementation of MASs usually involves the development of real-time and embedded systems such as intelligent rovers (Sharma *et al.* 2021) that only contains a limited amount of resources (such as space, weight, computational power, etc.). Hence, it is hard to expect that every agent can be equipped with enough number of sensors to acquire its own system states, and how to maintain the robustness of the system with limited system information becomes one problem worthy of investigation.

Various robust control methods have been proposed to ensure system stability when uncertainty exists. A Q-learning-based approach was proposed by Radac and Lala to perform optimal robust control for nonlinear systems (Radac and Lala 2020). An observer based H_∞ approach (Li *et al.* 2018) was presented for a class of quantised networked control systems to ensure robustness with the existence of randomly occurring uncertainties. For second order systems, SMC (Lin *et al.* 2019, Chu *et al.* 2019, Fei *et al.* 2020) is one popular method to achieve fast error convergence and maintain system robustness.

Global sliding mode scheme (Chu *et al.* 2019) was used with a recurrent NN to perform adaptive control for dynamic systems. An adaptive dynamic SMC scheme was proposed by Fei et al. to regulate system formations (Fei *et al.* 2020). However, most results are inapplicable if either system states or state references are not completely known, leading to a lack of robustness. Hence, how to perform SMC with limited information in both system states and their references becomes one big gap to fill.

For practical systems with restricted sensing capabilities, observers (Hu and Jiang 2017, Yu *et al.* 2019) are usually employed to estimate the inaccessible system states. ESOs were implemented by Yu et al. to approximate the uncertainties of followers and the unknown control input of the leader for the formation tracking of high-order MASs (Yu *et al.* 2019). A type of observer was constructed for rigid spacecrafts to achieve finite-time convergence of the estimation error (Hu and Jiang 2017). However, observers with similar structure are only capable to approximate energy-bounded uncertainties, and the high gain design is hard to realise for practical implementations.

To face the aforementioned issues, the idea of neural-based observer was first brought up by Kim et al., where a dynamic recurrent neural-based observer was developed (Kim *et al.* 1997). radial basis function NNs were then used by Chen et al. to build up adaptive observers to perform backstepping control (Chen *et al.* 2017). Currently, one unsolved challenge for the neural-based observer is that no existing design can guarantee finite-time characteristics.

With part of the necessary system information being unknown, there is a high chance that agents will collide into each other before the control input is stabilised. Therefore, collision avoidance techniques are essential to avoid inter-agent collisions. For ideal and completely known systems, the dynamic window approach (Lee *et al.* 2021) is commonly used to generate smooth and optimal trajectories for robots. However, motion control approaches such as APF (Sharma *et al.* 2021) are more suitable for systems with uncertainties.

A collision-free consensus algorithm was proposed for autonomous underwater vehicles with static communication topology (Li and Wang 2013). The problem of connectivity assurance was further considered along with collision avoidance issue by Sharma et al. for a group of mobile robots (Sharma *et al.* 2021). However, such results are far from satisfactory because potential collisions are still expected for agent pairs without direct communication if the system topology is assumed to be static. Hence, how to ensure that every agent pair is collision-free becomes an important issue.

Motivated by the above discussions, the following issues are investigated in this chapter:

1. How to estimate the unknown agent velocity and the system uncertainty simultaneously?

2. How to construct a sliding mode controller when the velocity reference is unknown to each agent?

3. How to ensure that an arbitrary pair of agents are collision free when each agent is affected by the above unknown factors?

The contents in this chapter are organised as follows. The system modelling of a class of nonlinear MASs with limited information and the problem formulation are given in Section 4.2. A brief introduction about the distance-related communication topology, the radial basis function NN estimation and the inter-agent APF construction is given in Section 4.3. The development of the finite-time neural-based observers and the limited-information-based sliding mode formation controller are presented in Section 4.4, where numerical simulation results are given to illustrate the effectiveness of the proposed control scheme. The final conclusions are drawn in Section 4.5.

4.2 System modelling and problem formulation

Consider a group of nonlinear agents with second-order dynamics that is written as

$$\begin{cases} \dot{x}_i = v_i \\ \dot{v}_i = f_i(x_i, v_i) + g_i u_i + \bar{w}_i, \quad i = 1, 2, \ldots, N \end{cases} \tag{4.1}$$

where $x_i = [x_{i,p}^{\mathrm{T}}, x_{i,a}^{\mathrm{T}}]^{\mathrm{T}} \in \mathbb{R}^n$ is the observable position information, $v_i = [v_{i,p}^{\mathrm{T}}, v_{i,a}^{\mathrm{T}}]^{\mathrm{T}} \in \mathbb{R}^n$ is the inaccessible velocity information, $x_{i,p} \in \mathbb{R}^{n_1}$ is the agent's coordinates in the global frame, $x_{i,a} \in \mathbb{R}^{n_2}$ is the agent's angular status, $v_{i,p} \in \mathbb{R}^{n_1}$ is the agent's linear velocity, $v_{i,a} \in \mathbb{R}^{n_2}$ is the agent's angular velocity, $f_i(x_i, v_i) \in \mathbb{R}^n$ is the unknown system dynamics, $\bar{w}_i \in \mathbb{R}^n$ is the external disturbance, $g_i \in \mathbb{R}^{n \times n}$ is the known nonlinear control gain matrix and $u_i \in \mathbb{R}^n$ represents the control input. The aforementioned parameters satisfy the conditions that $n_1 \geq 2$, $n_2 \geq 0$, and $n_1 + n_2 = n$. If define $w_i = f_i(x_i, v_i) + \bar{w}_i$ to represent the overall uncertainty, (4.1) has the following alternative form:

$$\begin{cases} \dot{x}_i = v_i \\ \dot{v}_i = g_i u_i + w_i, \quad i = 1, 2, \ldots, N \end{cases} \tag{4.2}$$

Similar to the discussion we had in Chapter 3, the cluster dynamics is obtained as

$$\begin{cases} \dot{x} = v \\ \dot{v} = gu + w \end{cases} \tag{4.3}$$

where

$$x = [x_1^{\mathrm{T}}, x_2^{\mathrm{T}}, \ldots, x_N^{\mathrm{T}}]^{\mathrm{T}}, \qquad v = [v_1^{\mathrm{T}}, v_2^{\mathrm{T}}, \ldots, v_N^{\mathrm{T}}]^{\mathrm{T}}$$
$$w = [w_1^{\mathrm{T}}, w_2^{\mathrm{T}}, \ldots, w_N^{\mathrm{T}}]^{\mathrm{T}}, \qquad g = \mathrm{diag}\{g_1, g_2, \ldots, g_N\}$$

The position reference for the ith agent is illustrated as $x_{di} \in \mathbb{R}^n$ $(i = 1, 2, \dots, N)$. The aim of this chapter is to provide a robust formation controller that can achieve the semi-global uniform ultimate boundedness of each agent's position tracking error, which is specified as

$$\lim_{t \to \infty} ||x_i(t) - x_{di}(t)|| \leq \nu_\delta^s,\ \forall x_i(t_0) \in \Omega_x,\ i = 1, 2, \dots, N \tag{4.4}$$

The following assumption is made regarding the unified model (4.3):

Assumption 4.1. *The ith agent can get access to its position reference. The norm $\|x_{di} - x_{dj}\| (j \in [1, N])$ remains bounded. Furthermore, x_{di} is at least second-order differentiable but its time derivatives are not directly provided to the agent. The variable $\ddot{x}_{di}$ has a known Lipschitz constant $\beta_{i,x}$.*

4.3 Preliminaries

4.3.1 Distance-related communication topology

In this chapter, the communication topology of the MAS is described by a time-varying weighted directed graph $G = \{\mathcal{R}(G), \mathcal{E}(G), \mathcal{A}(G)\}$, where $\mathcal{R}(G) = \{r_1, r_2, \dots, r_N\}$ is the set of nodes, $\mathcal{E}(G) \subseteq R \times R$ represents the set of edges, and $\mathcal{A}(G) = [a_{ij}] \in \mathbb{R}^{N \times N}$ is the adjacency matrix with nonnegative elements. The overall communication graph G consists of two subgraphs G_1 and G_2 that satisfy $\mathcal{A}(G) = \mathcal{A}_1 + \mathcal{A}_2$, where $\mathcal{A}_k$ $(k = 1, 2)$ is the adjacency matrix for graph G_k. G_1 is a static directed graph that represents the distance-invariant communication topology and G_2 is a time-varying graph that illustrates the information exchange achieved by limited range communication approaches.

We use terms a_{ji}^k and e_{ji}^k to represent the element in the jth row and ith column of matrix A_k, and the directed edge from r_j to r_i in graph G_k for $i, j \in [1, N]$, respectively. We consider $a_{ii}^k = 0$ for both subgraphs. In graph G_k, node r_j is considered as the neighbour of r_i if and only if the directed edge e_{ji}^k exists. The element a_{ji}^1 satisfies $a_{ji}^1 = 1$ if and only if the edge e_{ij}^1 exists. In G_2, the edge e_{ij}^2 is built when the relative distance between the node pair (r_i, r_j) is not larger than R_c if and only if e_{ij}^1 does not exist, which leads to

$$a_{ji}^2 = \begin{cases} f(\|z_{i,j}\|), & \|z_{i,j}\| \leq R_c\ ,\ a_{ji}^1 = 0 \text{ and } i \neq j \\ 0, & \text{otherwise} \end{cases} \tag{4.5}$$

where $z_{i,j} = x_{i,p} - x_{j,p}$, $R_c \in \mathbb{R}^+$ represents the outer boundary of the distance-based communication range and $f(\|z_{i,j}\|)$ is a continuous function whose value is contained within the region of $[0, 1]$.

The degree matrix $\mathcal{D}(G)$ of graph G is defined as $\mathcal{D}(G) = \text{diag}\{\sum_{j=1}^{N}(a_{ij}^1 + a_{ij}^2), i \in [1, N]\}$. The Laplacian matrix of the graph G is written as $L(G) = \mathcal{D}(G) - \mathcal{A}(G)$. Based on $A = A_1 + A_2$, we have $\mathcal{D}(G) = \mathcal{D}_1 + \mathcal{D}_2$ and $L(G) = L_1 + L_2$, where $\mathcal{D}_k = \text{diag}\{\sum_{j=1}^{N} a_{ij}^k, i \in [1, N]\}$ and $L_k = \mathcal{D}_k - \mathcal{A}_k$ represent the degree matrix and Laplacian matrix of graph G_k, respectively. Graph G_k is considered to be strongly connected if there always exists a directed path from a given node r_i to any other nodes in G_k. Graph G_1 is assumed to be static and strongly connected in this design.

Assumption 4.2. *Matrix L_2 and its time derivative $\dot{L}_2$ are bounded such that $\|L_2\|_F \leq L_M^1$ and $\|\dot{L}_2\|_F \leq L_M^2$ are satisfied simultaneously, where L_M^1 and L_M^2 are both positive constants.*

Remark 4.1. *The static communication graph G_1 is constructed to ensure that the overall topology G remains strongly connected, which further guarantees the robustness of the formation tracking process. Instead of relying on static communication topology (Sharma* et al. *2021), the distance-related communication topology G_2 is defined so that each agent can obtain necessary information of the nearby agents to avoid potential collisions.*

4.3.2 Radius basis function neural networks

In this chapter, the radial basis function NN (Zheng *et al.* 2021) is implemented in the state observer to approximate uncertain function w_i:

$$w_i = W_i^{\mathrm{T}} \varphi(Y_i) + \epsilon_i,\ i \in [1, N] \tag{4.6}$$

where $Y_i \in \mathbb{R}^{m_1}$ is the input vector of the radial basis function NN of the ith agent, $\varphi(Y_i) = [\varphi_1(Y_i), \varphi_2(Y_i), \ldots, \varphi_m(Y_i)]^{\mathrm{T}} \in \mathbb{R}^m$ is the Gaussian activation function, $W_i \in \mathbb{R}^{m \times n}$ is the optimal weight and ϵ_i is the network bias. The Gaussian activation function $\varphi(Y_i)$ is expressed as

$$\varphi_j(Y_i) = \exp\left[\frac{-(Y_i - d_j)^{\mathrm{T}}(Y_i - d_j)}{\mu_G^2}\right],\ j = 1, 2, \ldots, m \tag{4.7}$$

where $d_j = [d_{j,1}, d_{j,2}, \ldots, d_{j,m_1}]^{\mathrm{T}}$ is the centre of receptive field and μ_G denotes the width of the Gaussian function.

The estimation procedure of the radial basis function NN is given as

$$\widehat{w}_i = \widehat{W}_i^{\mathrm{T}} \varphi(Y_i)$$

where $\widehat{W}_i \in \mathbb{R}^{m\times n}$ is the estimated weight matrix. The following lemma concerning radial basis function NNs is important for our later designs:

Lemma 4.1. (Zheng *et al.* 2021) *When the approximated function w_i is bounded, the estimation error ϵ_i is expected to be bounded by a positive constant ϵ_M such that $\|\epsilon_i\| \leq \epsilon_M$ is satisfied.*

4.3.3 Artificial potential fields among agents

In this design, APFs are implemented for all agents so that they can avoid colliding into each other. It is first assumed that the ith agent can be illustrated by a circle centred at x_{pi} with the radius of r_{ai}.

Now, we are ready to define the repulsive potential function $\Phi(\|z_{i,j}\|)$ between the ith and the jth agent as follows:

Definition 4.1. (Sharma *et al.* 2021) *$\Phi(\|z_{i,j}\|)$ is a nonnegative, differentiable and monotonically decreasing function that satisfies:*

1. *$\Phi(\|z_{i,j}\|) \to +\infty$ when $\|z_{i,j}\| \to \underline{r}_{i,j}$, where $\underline{r}_{i,j} = \epsilon_1(r_{a,i} + r_{a,j})$ is the minimal safe distance between the agent pair $\{i,j\}$, and ϵ_1 is a constant that satisfies $\epsilon_1 > 1$.*

2. *$\Phi(\|z_{i,j}\|) \to 0$ when $\|z_{i,j}\| \to \bar{r}_{i,j}$, and $\Phi(\|z_{i,j}\|) = 0$ when $\|z_{i,j}\| \geq \bar{r}_{i,j}$, where $\bar{r}_{i,j} = \epsilon_2(r_{a,i} + r_{a,j})$ represents the outer boundary of the APF, and ϵ_2 is a constant that satisfies $\bar{r}_{i,j} \in (\underline{r}_{i,j}, R_c]$ and $\bar{r}_{i,j} < \|x_{di} - x_{dj}\|$.*

Based on the above discussion, the relationship between the APF and the limited range communication is given as what is shown in Figure 4.1.

The repulsive force generated between the ith and the jth agents is obtained as the negative gradient of $\Phi(\|z_{i,j}\|)$, and the repulsive force posed on the ith agent is obtained as

$$f_{i,j} = -\nabla_{z_{i,j}} \Phi(\|z_{i,j}\|)$$

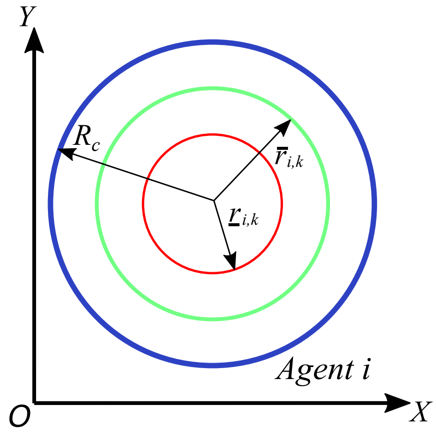

Figure 4.1. Communication and APF ranges of the ith agent.

Then we have the combined repulsive force f_i applied to the ith agent as

$$f_i = \sum_{j \in N_i} f_{i,j} = -\sum_{j \in N_i} \nabla_{z_{i,j}} \Phi(\|z_{i,j}\|)$$

where N_i is the neighbour set of the ith agent in graph G.

In this chapter, the potential function is chosen as

$$\Phi(\|z_{i,j}\|) = \begin{cases} \alpha \ln\left(\dfrac{\|z_{i,j}\| - \underline{r}_{i,j}}{\overline{r}_{i,j} - \underline{r}_{i,j}}\right) + \alpha \dfrac{\overline{r}_{i,j} - \|z_{i,j}\|}{\|z_{i,j}\| - \underline{r}_{i,j}}, & \text{for } \|z_{i,j}\| \in (\underline{r}_{i,j}, \overline{r}_{i,j}] \\ 0, & \text{otherwise} \end{cases} \tag{4.8}$$

Accordingly, the repulsive force is obtained as

$$f_{i,j} = \begin{cases} \alpha \dfrac{\overline{r}_{i,j} - \|z_{i,j}\|}{(\|z_{i,j}\| - \underline{r}_{i,j})^2} \dfrac{z_{i,j}}{\|z_{i,j}\|}, & \text{for } \|z_{i,j}\| \in (\underline{r}_{i,j}, \overline{r}_{i,j}] \\ 0, & \text{otherwise} \end{cases} \tag{4.9}$$

Remark 4.2. *The outer boundary of the APF is chosen as $\overline{r}_{i,j} \leq R_c$ to ensure that necessary position information is already obtained for each agent before generating the repulsive force f_i. The purpose of applying condition $\overline{r}_{i,j} < \|x_{di} - x_{dj}\|$ is that no redundant repulsive force is generated to disturb the system formation.*

4.4 Observer-based collision-free formation controller

The main results of this chapter include two parts, designs and analysis of the finite-time neural-based observer are presented in Section 4.4.1, while the robust limited-information-based sliding mode formation controller is illustrated in Section 4.4.2.

4.4.1 Finite-time neural-based state observer design

Motivated by the previous neural-based observer design (Kim *et al.* 1997, Liu *et al.* 2013), we propose a finite-time neural-based state observer that can estimate both unknown system state and disturbance for agents with second order dynamics (4.2) as

$$\begin{cases} \dot{\widehat{x}}_i = \widehat{v}_i + \alpha_1 \mathrm{sgn}^{\beta_1}(x_i - \widehat{x}_i) \\ \dot{\widehat{v}}_i = \alpha_2 \mathrm{sgn}^{\beta_2}(x_i - \widehat{x}_i) + g_i u_i + \widehat{W}_i^{\mathrm{T}} \varphi(Y_i) \end{cases} \tag{4.10}$$

where $\widehat{x}_i \in \mathbb{R}^n$ is the estimated position information, $\widehat{v}_i \in \mathbb{R}^n$ is the estimated velocity information, $Y_i = [x_i^{\mathrm{T}}, \widehat{v}_i^{\mathrm{T}}]^{\mathrm{T}}$, $\alpha_1, \alpha_2 \in \mathbb{R}^+$ and $\beta_2 = 2\beta_1 - 1 > 0$. According to the approximating properties of radial basis function NNs, we have the expression of the estimation error as

$$\widetilde{w}_i = W_i^{\mathrm{T}} \varphi(Y_i) + \epsilon_i - \widehat{W}_i^{\mathrm{T}} \varphi(Y_i) = \widetilde{W}_i^{\mathrm{T}} \varphi(Y_i) + \epsilon_i \tag{4.11}$$

where $\widetilde{W}_i = W_i - \widehat{W}_i$ denotes the weight estimation error.

With $\widetilde{x}_i = x_i - \widehat{x}_i$ and $\widetilde{v}_i = v_i - \widehat{v}_i$, we obtain the error dynamics of the neural-based observer as follows:

$$\begin{cases} \dot{\widetilde{x}}_i = \widetilde{v}_i - \alpha_1 \mathrm{sgn}^{\beta_1}(\widetilde{x}_i) \\ \dot{\widetilde{v}}_i = \widetilde{w}_i - \alpha_2 \mathrm{sgn}^{\beta_2}(\widetilde{x}_i) \end{cases} \tag{4.12}$$

where the expression of $\mathrm{sgn}(\cdot)$ is as explained in Section 2.4.1.

Define $\bar{Z}_i = [\mathrm{sgn}^{\beta_1}(\widetilde{x}_i^{\mathrm{T}}), \widetilde{v}_i^{\mathrm{T}}]^{\mathrm{T}}$, then we are able to obtain the time derivative of the $\bar{Z}_i$ as

$$\begin{aligned} \dot{\bar{Z}}_i &= \begin{bmatrix} \beta_1 \mathrm{diag}(|\widetilde{x}_i|^{\beta_1 - 1})(-\alpha_1 \mathrm{sgn}^{\beta_1}(\widetilde{x}_i) + \widetilde{v}_i) \\ -\alpha_2 \mathrm{sgn}^{\beta_2}(\widetilde{x}_i) \end{bmatrix} + \begin{bmatrix} 0 \\ \widetilde{w}_i \end{bmatrix} \\ &= \mathcal{Z}_i A_o \bar{Z}_i + B_o \widetilde{w}_i \end{aligned}$$

where the following equations are applied:

$$\mathcal{Z}_i = \mathrm{diag}([|\widetilde{x}_i^{\mathrm{T}}|^{\beta_1 - 1}, |\widetilde{x}_i^{\mathrm{T}}|^{\beta_1 - 1}]), \ A_o = \begin{bmatrix} -\alpha_1 \beta_1 I_n & \beta_1 I_n \\ -\alpha_2 I_n & 0_{n \times n} \end{bmatrix}, \ B_o = \begin{bmatrix} 0_{n \times n} \\ I_n \end{bmatrix}$$

To ensure the boundedness of the observation error, the online weight tuning law of the radial basis function NN is chosen as follows:

$$\dot{\widehat{W}}_i = \eta_1 \varphi(Y_i) \mathrm{sgn}^{\beta_1}(\widetilde{x}_i^{\mathrm{T}}) - \eta_2 \| \mathrm{sgn}^{\beta_1}(\widetilde{x}_i^{\mathrm{T}}) \| \widehat{W}_i \tag{4.13}$$

The following lemmas are helpful for the stability analysis of the neural-based observer.

Lemma 4.2. (Li *et al.* 2019a) *If A_o is a Hurwitz matrix, there always exists a symmetric positive definite matrix P_2 such that*

$$A_o{}^{\mathrm{T}}P_2 + P_2A_o = -Q_2$$

where Q_2 is a symmetric positive definite matrix.

Lemma 4.3. (Hu and Jiang 2017) *Consider a continuous positive definite Lyapunov candidate $V(\widetilde{x}_i, \widetilde{v}_i)$ for a nonlinear agent* (4.2)*, if its time derivative satisfies the condition that*

$$\dot{V} \leq -\bar{\beta}_1 V^{\bar{\alpha}_1} + \bar{\beta}_2 V^{\bar{\alpha}_2}$$

where $0 < \bar{\alpha}_2 < \bar{\alpha}_1 < 1$, $\bar{\beta}_1, \bar{\beta}_2 > 0$, then the error states $\widetilde{x}_i$ and $\widetilde{v}_i$ are both finite-time UUB. The function $V(\widetilde{x}_i, \widetilde{v}_i)$ is contained within the attraction region of

$$\Omega_V = \left\{ (\widetilde{x}_i, \widetilde{v}_i) \;\middle|\; V(\widetilde{x}_i, \widetilde{v}_i) \leq \sqrt[\bar{\alpha}_1 - \bar{\alpha}_2]{\bar{\beta}_2/\bar{\beta}_3} \right\}$$

where $\bar{\beta}_3 \in (0, \bar{\beta}_1)$. With t_0 acting as the initial time, the boundary of the settling time is obtained as

$$T \leq V^{1-\bar{\alpha}_2}(t_0)/[(\bar{\beta}_1 - \bar{\beta}_3)(1-\bar{\alpha}_1)]$$

Theorem 4.1. *Consider the ith nonlinear agent* (4.2)*, by the neural-based observer* (4.10) *and the neural weight update law* (4.13)*, then we have that both $\widetilde{W}_i$ and $\bar{Z}_i$ are semi-globally UUB and $\bar{Z}_i$ is semi-globally finite-time UUB if the following conditions are met simultaneously:*

1. *The parameters are chosen reasonably within the constrains of $\alpha_1, \alpha_2 > 0$, $0.5 < \beta_1 < 1$ and $\beta_2 = 2\beta_1 - 1$*

2. *The compact set conditions of the radial basis function NNs are satisfied such that we have $w_i \in \Omega_w$ or $Y_i \in \Omega_Y$ when $t \geq t_0$, where Ω_w is a compact set of w_i.*

Proof. The characteristic polynomial of A_o is obtained as

$$\det(\lambda I_2 - A_o) = \lambda^2 + \alpha_1\beta_1\lambda + \alpha_2\beta_1$$

which indicates that A_o is a Hurwitz matrix. Define the following continuous Lyapunov candidate V_o:

$$V_o = \frac{1}{2}\bar{Z}_i^{\mathrm{T}}P_2\bar{Z}_i + \frac{1}{2}\mathrm{tr}\{\widetilde{W}_i^{\mathrm{T}}\widetilde{W}_i\} \tag{4.14}$$

By Lemma 4.2, if we define $C_o = [I_n, 0_{n\times n}]$, we are able to obtain the time derivative of V_o as

$$\begin{aligned}
\dot{V}_o &= -\frac{1}{2}\bar{Z}_i^{\mathrm{T}}\mathcal{Z}_iQ_2\bar{Z}_i - \bar{Z}_i^{\mathrm{T}}P_2B_o\widetilde{w}_i - \mathrm{tr}\{\widetilde{W}_i^{\mathrm{T}}\dot{\hat{W}}_i\} \\
&= -\frac{1}{2}\bar{Z}_i^{\mathrm{T}}\mathcal{Z}_iQ_2\bar{Z}_i - \bar{Z}_i^{\mathrm{T}}P_2B_o(\widetilde{W}_i^{\mathrm{T}}\varphi(Y_i)+\epsilon_i) + \eta_1\mathrm{tr}\{\widetilde{W}_i^{\mathrm{T}}\varphi(Y_i)(C_o\bar{Z}_i)^{\mathrm{T}}\} \\
&\quad + \eta_2\mathrm{tr}\{\widetilde{W}_i^{\mathrm{T}}\|C_o\bar{Z}_i\|(W_i-\widetilde{W}_i)\}
\end{aligned} \tag{4.15}$$

By Lemma 4.1, if we apply the inequalities that $\|W_i\|_F \le W_M$, $\mathrm{tr}\{\widetilde{W}_i(W_i-\widetilde{W}_i)\} \le W_M\|\widetilde{W}_i\|_F - \|\widetilde{W}_i\|_F^2$ and $\varphi(Y_i) \le \varphi_M$, we can rewrite (4.15) into the following equations:

$$\begin{aligned}
\dot{V}_o &\le -\frac{1}{2}\underline{\sigma}(Q_2)\|\bar{Z}\|^{3-1/\beta_1} + \overline{\sigma}(P_2)\epsilon_M\|\bar{Z}\| + \bar{Z}^{\mathrm{T}}P_2B_o\widetilde{W}\varphi(\bar{z}) + \eta_1\varphi^{\mathrm{T}}(\bar{z})\widetilde{W}^{\mathrm{T}}C_o\bar{Z} \\
&\quad + \eta_2\|C_o\|\|\bar{Z}\|\|\widetilde{W}\|_F(W_M - \|\widetilde{W}\|_F) \\
&\le -\frac{1}{2}\underline{\sigma}(Q_2)\|\bar{Z}_i\|^{3-1/\beta_1} + (k_3 + k_2\|\widetilde{W}_i\|_F)\|\bar{Z}_i\| - \eta_2k_1\|\bar{Z}_i\|\|\widetilde{W}_i\|_F^2
\end{aligned} \tag{4.16}$$

where $k_1 = \|C_o\|_F$, $k_2 = \varphi_M\max(|\overline{\sigma}(\mathcal{P}_1)|, |\underline{\sigma}(\mathcal{P}_1)|) + \eta_2k_1W_M$, $\mathcal{P}_1 = P_2B_o + \eta_1C_o$ and $k_3 = \overline{\sigma}(P_2)\epsilon_M$. Then we have

$$\begin{aligned}
\dot{V}_o &\le -\frac{1}{2}\underline{\sigma}(Q_2)\|\bar{Z}_i\|^{3-1/\beta_1} + \left[-k_1\eta_2\left(\|\widetilde{W}_i\|_F - \frac{k_2}{2k_1\eta_2}\right)^2 + k_3 + \frac{k_2^2}{4k_1\eta_2}\right]\|\bar{Z}_i\| \\
&\le -\frac{1}{2}\underline{\sigma}(Q_2)\|\bar{Z}_i\|^{3-1/\beta_1} + \left(k_3 + \frac{k_2^2}{4k_1\eta_2}\right)\|\bar{Z}_i\|
\end{aligned}$$

Therefore, the negativeness of function $\dot{V}_o$ is guaranteed when $\|\bar{Z}_i\| > K_o$, where $K_o = ((4k_1k_3\gamma_2 + k_2^2)/(2k_1\gamma_2\underline{\sigma}(Q_2)))^{2-1/\beta_1}$. Because the radial basis function NN can only guarantee semi-global stability, by Lemma (2.1), we have that the $\|\bar{Z}_i\|$ is semi-globally UUB within the following neighbourhood:

$$\Omega_z = \left\{\bar{Z}_i \middle| \|\bar{Z}_i\| \le K_o\right\} \tag{4.17}$$

Similarly, the weight estimation error $\widetilde{W}_i$ is also semi-globally UUB according to a standard Lyapunov theory extension (Kim and Lewis 1999).

Consider another function V_z as follows:

$$V_z = \frac{1}{2}\bar{Z}_i^{\mathrm{T}}P_2\bar{Z}_i \tag{4.18}$$

If the weight estimation error is bounded such that $\|\widetilde{W}_i\|_F \le \widetilde{W}_M$, the time derivative of V_z is obtained as

$$\begin{aligned}\dot{V}_z &= \frac{1}{2}\bar{Z}_i^{\mathrm{T}}\mathcal{Z}_i(A_o^{\mathrm{T}}P_2 + P_2A_o)\bar{Z}_i - \bar{Z}_i^{\mathrm{T}}P_2B_o\widetilde{w}_i \\ &= -\frac{1}{2}\bar{Z}_i^{\mathrm{T}}\mathcal{Z}_iQ_2\bar{Z}_i - \bar{Z}_i^{\mathrm{T}}P_2B_o(\widetilde{W}_i^{\mathrm{T}}\varphi(Y_i) + \epsilon_i) \\ &\le -\frac{1}{2}\underline{\sigma}(Q_2)\|\bar{Z}_i\|^{3-1/\beta_1} + k_4\|\bar{Z}_i\|\end{aligned} \tag{4.19}$$

where $k_4 = \overline{\sigma}(P_2)\epsilon_M + \overline{\sigma}(P_2B_o)\widetilde{W}_M\varphi_M$. By the inequality that $\underline{\sigma}(P_2)\|\bar{Z}_i\|^2/2 \le V_z \le \overline{\sigma}(P_2)\|\bar{Z}_i\|^2/2$, one has

$$\dot{V}_z \le -k_5V_z^{(3\beta_1-1)/2\beta_1} + k_6V_z^{1/2} \tag{4.20}$$

where equations $k_5 = (\overline{\sigma}(P_2)/2)^{(1-3\beta_1)/2\beta_1}\underline{\sigma}(Q_2)/2$ and $k_6 = k_4(2/\underline{\sigma}(P_2))^{1/2}$ are applied.

Because the radial basis function NN only guarantees semi-global stability, by Lemma 4.3, the error vector $\bar{Z}_i$ of the proposed observer (4.10) is semi-globally finite-time UUB, which completes the proof. □

Notice that inequality (4.16) used in the proof of Theorem 4.1 can be rewritten as follows:

$$\begin{aligned}\dot{V}_o &\le -\frac{1}{2}\underline{\sigma}(Q_2)\|\bar{Z}_i\|^{1-1/\beta_1}\|\bar{Z}_i\|^2 + k_2\|\widetilde{W}_i\|_F\|\bar{Z}_i\| + k_3\|\bar{Z}_i\| - \eta_2\|\bar{Z}_i\|\|\widetilde{W}_i\|_F^2 \\ &\le -\chi_o^{\mathrm{T}}H_o\chi_o + \mathcal{H}_o\chi_o\end{aligned} \tag{4.21}$$

where

$$\chi_o = \begin{bmatrix}\|\bar{Z}_i\| \\ \|\widetilde{W}_i\|_F\end{bmatrix},\ \mathcal{H}_o = \begin{bmatrix}k_3 & 0\end{bmatrix},\ H_o = \begin{bmatrix}\underline{\sigma}(Q_2)\|\bar{Z}_i\|^{1-1/\beta_1}/2 & -k_2/2 \\ -k_2/2 & \eta_2\|\bar{Z}_i\|\end{bmatrix}$$

It is observed in (4.21) that the positiveness of H_o is determined by the value of the matrix determinant that $\det(H_o) = \underline{\sigma}(Q_2)\eta_2\|\bar{Z}_i\|^{2-1/\beta_1}/2 - k_2^2/4$. Theoretically, we need to offer high values to η_1 and η_2 so that the matrix H_o is positive definite to further guarantee the convergence of $\bar{Z}_i$.

However, high values of η_1 and η_2 will also introduce high error-sensitivity in (4.13) and lead to oscillations or even instability when the value of $\|\bar{Z}_i\|$ is too high. Therefore, the performance of the observer is unsatisfactory if we only have static weight tuning parameters. Hence, a new varying-parameter neural-based observer is further introduced.

Because the vector $\bar{Z}_i$ is not completely known to the agent, it is necessary to find a substitute for it. According to our previous design of the NN tuning law in (4.13), we can treat the parameters η_1 and η_2 as the amplifiers of the value of $\|\text{sgn}^{\beta_1}(\tilde{z}_1)\|$. Hence, it is reasonable to choose the value of $\|\text{sgn}^{\beta_1}(\tilde{z}_1)\|$ as the criterion to set the values of η_1 and η_2. For analysing, after slicing the value region of $\|\text{sgn}^{\beta_1}(\tilde{z}_1)\|$ exponentially into $n_v(n_v \in \mathbb{R}^+)$ parts, we define the value sets $\bar{\eta}_1$ and $\bar{\eta}_2$ as follows:

$$\bar{\eta}_i = [\bar{\eta}_{i,1}, \bar{\eta}_{i,2}, \ldots, \bar{\eta}_{i,n_v}], \quad i = 1, 2$$

By defining a constant $c_v \in \mathbb{R}$, we present the fractional parameter design as

$$\eta_i = \begin{cases} \bar{\eta}_{i,1} & \|\text{sgn}^{\beta_1}(\tilde{z}_1)\| \in [10^{c_v-1}, +\infty) \\ \bar{\eta}_{i,2} & \|\text{sgn}^{\beta_1}(\tilde{z}_1)\| \in [10^{c_v-2}, 10^{c_v-1}) \\ \vdots & \vdots \\ \bar{\eta}_{i,j} & \|\text{sgn}^{\beta_1}(\tilde{z}_1)\| \in [10^{c_v-j}, 10^{c_v-j+1}) \\ \vdots & \vdots \\ \bar{\eta}_{i,n_v} & \|\text{sgn}^{\beta_1}(\tilde{z}_1)\| \in [0, 10^{c_v-n_v+1}) \end{cases} \tag{4.22}$$

where $j = 1, 2, \ldots, n_v$.

Hence, a new parameter design regarding the neural-based observer is proposed:

Theorem 4.2. *Consider the ith nonlinear agent* (4.2)*, by the neural-based observer* (4.10) *and the neural weight update law* (4.13)*, we have that both $\widetilde{W}_i$ and $\bar{Z}_i$ are semi-globally UUB and $\bar{Z}_i$ is semi-globally finite-time UUB if the following conditions are met:*

1. *The parameters of the observer are chosen reasonably within the constrains of $\alpha_1, \alpha_2 > 0$, $0.5 < \beta_1 < 1$ and $\beta_2 = 2\beta_1 - 1$.*
2. *The sets $\bar{\eta}_1$ and $\bar{\eta}_2$ are chosen properly within the following region:*

$$\Omega_{\bar{\eta}} = \begin{cases} \left\{ (\bar{\eta}_{1,j}, \bar{\eta}_{2,j}) \middle| \bar{\mathcal{K}} < 10^{c_v-j} \right\} & j \in [1, n_v) \\ \left\{ (\bar{\eta}_{1,j}, \bar{\eta}_{2,j}) \middle| \bar{\mathcal{K}} < 10^{c_v-n_v+1} \right\} & j = n_v \end{cases} \tag{4.23}$$

3. *The compact set conditions of the radial basis function NNs are satisfied such that we have $w_i \in \Omega_w$ or $Y_i \in \Omega_Y$ when $t \geq t_0$.*

Proof. According to (4.17), if we have $\eta_1 = \bar{\eta}_{1,j}$ and $\eta_2 = \bar{\eta}_{2,j}$ when $j \in [1, n_v - 1]$, then the following inequality is obtained:

$$\sqrt[2-1/\beta_1]{\frac{4k_1k_3\eta_2 + k_2^2}{2k_1\eta_2\underline{\sigma}(Q_2)}} < 10^{c_v - j}$$

which indicates that $\|\bar{Z}_i\|$ will further converge to the $(j+1)$th fractional region mentioned in (4.22).

Otherwise for $j = n_v$, we have $\eta_1 = \bar{\eta}_{1,n_v}$ and $\eta_2 = \bar{\eta}_{2,n_v}$ that further lead to

$$\sqrt[2-1/\beta_1]{\frac{4k_1k_3\eta_2 + k_2^2}{2k_1\eta_2\underline{\sigma}(Q_2)}} < 10^{c_v - n_v + 1}$$

we can then guarantee that $\|\bar{Z}_i\|$ is restricted within the n_vth fractional region, which leads to the conclusion that both $\|\bar{Z}_i\|$ and $\|\widetilde{W}_i\|_F$ are semi-globally UUB. The proof of the finite-time characteristic of $\|\bar{Z}_i\|$ is similar to the one of Theorem 4.1. Hence, the proof is completed. □

Remark 4.3. *We choose the radial basis function NN because its Gaussian activation function can ensure the boundedness of vector $\varphi(Y_i)$ regardless of the value of our estimation $\widehat{v}_i$, which further decreases the chance of having oscillations in its output. Theoretically, the finite-time neural-based observer design can also be extended to fit higher-order systems.*

4.4.2 Robust sliding mode controller with limited information

Regarding the definition of the ith agent's position and velocity tracking errors mentioned in (2.8), we have the error dynamics of the cluster as

$$\begin{cases} \dot{\delta}_x = \delta_v \\ \dot{\delta}_v = -\ddot{x}_d + gu + w \end{cases} \tag{4.24}$$

where $\delta_x = [\delta_{x1}^{\mathrm{T}}, \delta_{x2}^{\mathrm{T}}, \ldots, \delta_{xN}^{\mathrm{T}}]^{\mathrm{T}}$, $\delta_v = [\delta_{v1}^{\mathrm{T}}, \delta_{v2}^{\mathrm{T}}, \ldots, \delta_{vN}^{\mathrm{T}}]^{\mathrm{T}}$, and $x_d = [x_{d1}^{\mathrm{T}}, x_{d2}^{\mathrm{T}}, \ldots, x_{dN}^{\mathrm{T}}]^{\mathrm{T}}$.

With the definition of local formation tracking errors as mentioned in (2.12), we have the sliding variable s_i for agent i as

$$s_i = e_{vi} + \lambda_i e_{xi} \tag{4.25}$$

where $\lambda_i \in \mathbb{R}^+$ represents the slope of the sliding surface.

Then the sliding vector for the cluster is expressed as

$$S = e_v + \Lambda \otimes I_n e_x = (L + B) \otimes I_n(\delta_v + \Lambda \otimes I_n \delta_x) \tag{4.26}$$

where the following terms are applied:

$$\begin{aligned} e_x &= [e_{x1}^{\mathrm{T}}, e_{x2}^{\mathrm{T}}, \ldots, e_{xN}^{\mathrm{T}}]^{\mathrm{T}}, \quad & e_v &= [e_{v1}^{\mathrm{T}}, e_{v2}^{\mathrm{T}}, \ldots, e_{vN}^{\mathrm{T}}]^{\mathrm{T}} \\ S &= [s_1^{\mathrm{T}}, s_2^{\mathrm{T}}, \ldots, s_N^{\mathrm{T}}]^{\mathrm{T}}, & \Lambda &= \mathrm{diag}\{\lambda_1, \lambda_2, \ldots, \lambda_N\} \end{aligned}$$

To estimate the first-order and second-order derivatives of the position reference x_{di}, a four-layer sliding mode differentiator (Levant 2003) is employed for each agent:

$$\begin{cases} \dot{\gamma}_{i,1} = \nu_{i,1}, \ \dot{\gamma}_{i,2} = \nu_{i,2}, \ \dot{\gamma}_{i,3} = \nu_{i,3}, \ \dot{\gamma}_{i,4} = \nu_{i,4} \\ \nu_{i,1} = -\alpha_{i,1}\beta_{i,x}^{\frac{1}{4}}\mathrm{sgn}^{\frac{3}{4}}(\gamma_{i,1} - x_{di}) + \gamma_{i,2} \\ \nu_{i,2} = -\alpha_{i,2}\beta_{i,x}^{\frac{1}{3}}\mathrm{sgn}^{\frac{2}{3}}(\gamma_{i,2} - \nu_{i,1}) + \gamma_{i,3} \\ \nu_{i,3} = -\alpha_{i,3}\beta_{i,x}^{\frac{1}{2}}\mathrm{sgn}^{\frac{1}{2}}(\gamma_{i,3} - \nu_{i,2}) + \gamma_{i,4} \\ \nu_{i,4} = -\alpha_{i,4}\beta_{i,x}\mathrm{sgn}(\gamma_{i,4} - \nu_{i,3}) \end{cases} \tag{4.27}$$

where $\widehat{x}_{di}^{(j-1)} = \gamma_{i,j}$ $(j = 1, 2, 3, 4)$ stands for the estimation of the $(j-1)$th time derivative of x_{di}, and the expression of $\mathrm{sgn}(\cdot)$ is as explained in Section 2.4.1. With the implementation of the finite-time neural-based observer (4.10), we have the approximated velocity tracking error, local velocity tracking error and sliding variable as

$$\widehat{\delta}_{vi} = \widehat{v}_i - \gamma_{i,2}, \ \widehat{e}_{vi} = \sum_{j=1}^{N} l_{ij}\widehat{\delta}_{vj} + b_i\widehat{\delta}_{vi}, \ \widehat{s}_i = \widehat{e}_{vi} + \lambda_i e_{xi} \tag{4.28}$$

Then the estimated sliding vector for the entire system is written as:

$$\widehat{S} = \widehat{e}_v + \Lambda \otimes I_n e_x = (L + B) \otimes I_n(\widehat{\delta}_v + \Lambda \otimes I_n \delta_x) \tag{4.29}$$

According to (4.26), the time derivative of S is obtained as follows:

$$\dot{S} = (L + B) \otimes I_n(-\ddot{x}_d + gu + w + \Lambda \otimes I_n \delta_v) + \dot{L}_2 \otimes I_n(\delta_v + \Lambda \otimes I_n \delta_x) \tag{4.30}$$

Based on the discussions about the APF (4.9), the neural-based observer (4.10), the sliding mode differentiator (4.27) and the limited-information-based sliding variable

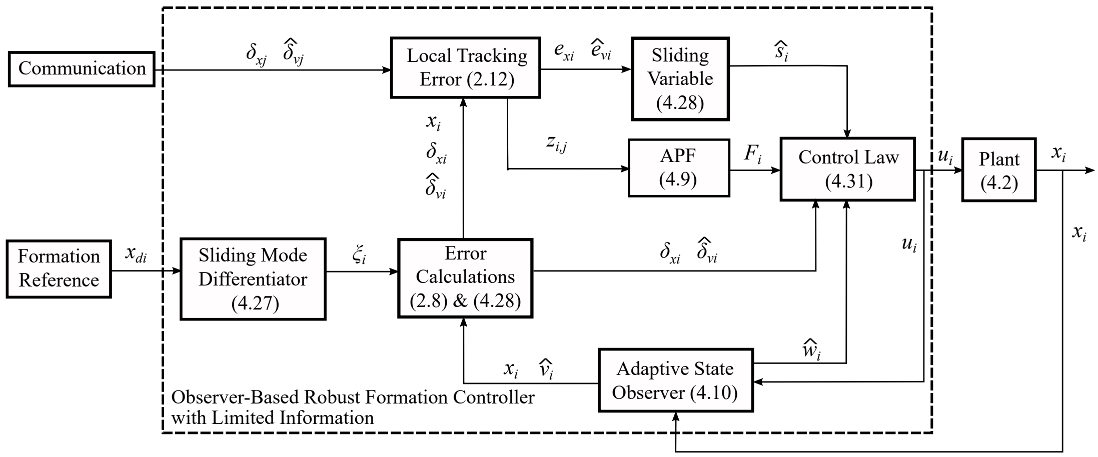

Figure 4.2. Limited-information-based formation control scheme.

(4.28), we are ready to present the limited-information-based formation controller design for the ith agent as

$$u_i = g_i^{-1}(-c_i\hat{s}_i - \hat{w}_i - \lambda_i\hat{\delta}_{vi} - \delta_{xi} + \gamma_{i,3} + F_i) \tag{4.31}$$

where $F_i = [f_i^{\mathrm{T}}, 0_{1\times n_2}]^{\mathrm{T}}$ and $c_i \in \mathbb{R}^+$. Based on the above discussions, the system design is illustrated as the diagram in Figure 4.2.

The following lemma is helpful for the stability proof of the limited-information-based controller design:

Lemma 4.4. (Levant 2003) *With the parameters properly chosen for the sliding mode differentiator* (4.27)*, if there is no input noise regarding the implemented differentiator, the following equations are true for agent i within a finite-time t_d:*

$$\gamma_{i,j} = x_{di}^{(j-1)},\ i = 1, 2, \ldots, n,\ j = 1, 2, 3, 4$$

Now we are ready to present our controller design:

Theorem 4.3. *Consider a second-order MAS* (4.3) *with limited information under Assumptions 4.1-4.2, by the finite-time neural-based observer* (4.10)*, the sliding mode differentiator* (4.27)*, the APF between pairs of agents* (4.8) *and the limited-information-based formation control law* (4.31)*, then the states S, e_x and δ_x are all semi-globally UUB if the following conditions are met:*

1. *The parameters in the controller satisfy $\underline{\sigma}(CQ_1)/2 - \overline{\sigma}(P_1)L_M^2/\underline{\sigma}(L_1 + B) > 0$ and $\underline{\sigma}(\Lambda) - L_M^2/\underline{\sigma}(L_1 + B) > 0$, where $C = \mathrm{diag}\{c_1, c_2, \ldots, c_N\}$.*

2. *The compact set conditions of the radial basis function NNs are satisfied such that we have $w_i \in \Omega_w$ or $Y_i \in \Omega_Y$ when $t \geq t_0$.*

Proof. This is a two-parted proof, where the effectiveness of the collision avoidance scheme and the formation controller are proved, respectively.

Part 1. In this part, we offer analysis regarding the proposed collision avoidance mechanism. For simplicity, the proof of collision is conducted on the agent pair $\{i,j\}$, where $i,j \in [1,N]$ and $i \neq j$. The same result can also be extended to any other agent pairs.

Consider an energy-based Lyapunov function as follows:

$$V_{i,j} = \frac{1}{2} z_{i,j}^{\mathrm{T}} z_{i,j} + \frac{1}{2} v_i^{\mathrm{T}} v_i + \frac{1}{2} v_j^{\mathrm{T}} v_j \tag{4.32}$$

Accordingly, its time derivative is obtained as

$$\dot{V}_{i,j} = z_{i,j}^{\mathrm{T}}(v_{i,p} - v_{j,p}) + \sum_{k=i,j} v_k^{\mathrm{T}}(-c_k \widehat{s}_k + \widetilde{w}_k - \lambda_k \widehat{\delta}_{vk} - \delta_{xk} + \gamma_{k,3}) + \sum_{k=i,j} v_{k,p}^{\mathrm{T}} f_k \tag{4.33}$$

By Assumption 4.1 and the compact set conditions of the radial basis function NNs, we have that terms $\sum_{k=i,j} v_k^{\mathrm{T}}(-c_k \widehat{s}_k + \widetilde{w}_k - \lambda_k \widehat{\delta}_{vk} - \delta_{xk} + \gamma_{k,3})$ and $z_{i,j}^{\mathrm{T}}(v_{i,p} - v_{j,p})$ should be bounded in any time. For the scenario where the ith agent is running toward the jth agent, with the condition that $\sum_{k=i,j} v_{k,p}^{\mathrm{T}} f_k \to +\infty$ when $\|z_{i,j}\| \to \underline{r}_{i,j}$, we always get that $\dot{V}_{i,j} \to +\infty$ when $\|z_{i,j}\|$ is small enough. Such result will further lead to a boost of $\|z_{i,j}\|$ that indicates the separation of the agent pair $\{i,j\}$.

Meanwhile, we obtain the following equation based on the condition that $\|x_{di} - x_{dj}\| > \bar{r}_{i,j}$:

$$\lim_{t \to +\infty} \|F_i\| = 0,\ i = 1, 2, \ldots, N \tag{4.34}$$

Part 2. To prove the semi-global uniform ultimate boundedness of the sliding variable S and local formation tracking error e_x, construct the following Lyapunov function:

$$V_{3,1} = \frac{1}{2} S^{\mathrm{T}} P_1 \otimes I_n S + \frac{1}{2} e_x^{\mathrm{T}} P_1 \otimes I_n e_x \tag{4.35}$$

Motivated by the work of Chen et al. (Chen *et al.* 2019), the time derivative of $V_{3,1}$ is further obtained as

$$\begin{aligned} \dot{V}_{3,1} = {} & S^{\mathrm{T}}[P_1(L+B)] \otimes I_n[-\ddot{x}_d - C \otimes I_n \widehat{S} - \widetilde{w} - \delta_x + \gamma_3 + F + \Lambda \otimes I_n(\delta_v - \widehat{\delta}_v)] \\ & + e_x^{\mathrm{T}} P_1 \otimes I_n S - e_x^{\mathrm{T}}(P_1 \Lambda) \otimes I_n e_x + S^{\mathrm{T}}(P_1 \dot{L}_2) \otimes I_n(\delta_v + \Lambda \otimes I_n \delta_x) \\ & + e_x^{\mathrm{T}}(P_1 \dot{L}_2) \otimes I_n \delta_x \end{aligned} \tag{4.36}$$

Define $\widetilde{\gamma}_3 = \gamma_3 - \ddot{x}_d$, $\widetilde{\gamma}_2 = \eta_2 - \dot{x}_d$, $\widetilde{v} = \widehat{v} - v$, $\widetilde{w} = \widehat{w} - w$, $\widehat{v} = [\widehat{v}_1^{\mathrm{T}}, \widehat{v}_2^{\mathrm{T}}, \ldots, \widehat{v}_N^{\mathrm{T}}]^{\mathrm{T}}$ and $\widehat{w} = [\widehat{w}_1^{\mathrm{T}}, \widehat{w}_2^{\mathrm{T}}, \ldots, \widehat{w}_N^{\mathrm{T}}]^{\mathrm{T}}$. By Lemma 4.4, we get that both $\widetilde{\gamma}_2$ and $\widetilde{\gamma}_3$ will converge to 0 after finite time t_d. By Lemma 2.3, we further obtain

$$
\begin{aligned}
\dot{V}_{3,1} = & S^{\mathrm{T}}[P_1(L+B)] \otimes I_n\{F - \widetilde{w} - C \otimes I_n S - [C(L+B)] \otimes I_n \widetilde{v} - \Lambda \otimes I_n \widetilde{v}\} \\
& + S^{\mathrm{T}}[P_1 \dot{L}_2 (L+B)^{-1}] \otimes I_n S - e_x^{\mathrm{T}}(P_1 \Lambda) \otimes I_n e_x + e_x^{\mathrm{T}}[P_1 \dot{L}_2 (L+B)^{-1}] \otimes I_n e_x \\
\leq & -[\underline{\sigma}(CQ_1)/2 - \overline{\sigma}(P_1) L_M^2 / \underline{\sigma}(L_1+B)]\|S\|^2 + \overline{\sigma}(P_1)\mathcal{K}_1[\overline{\sigma}(\Lambda) + \overline{\sigma}(C)\mathcal{K}_1]\|\widetilde{v}\|\|S\| \\
& + [\overline{\sigma}(P_1) L_M^1 + \overline{\sigma}(Q_1)/2](\|\widetilde{w}\| + \|F\|)\|S\| - \underline{\sigma}(P_1)[\underline{\sigma}(\Lambda) - L_M^2/\underline{\sigma}(L_1+B)]\|e_x\|^2 \\
\leq & (\mathcal{K}_3(\widetilde{w}_M + \|F\|) + \mathcal{K}_4 \widetilde{v}_M)\|S\| - \mathcal{K}_2\|S\|^2 - \mathcal{K}_5\|e_x\|^2 \\
\leq & -\begin{bmatrix} \|S\| & \|e_x\| \end{bmatrix} \begin{bmatrix} \mathcal{K}_2 & 0 \\ 0 & \mathcal{K}_5 \end{bmatrix} \begin{bmatrix} \|S\| \\ \|e_x\| \end{bmatrix} + \begin{bmatrix} \mathcal{K}_6 & 0 \end{bmatrix} \begin{bmatrix} \|S\| \\ \|e_x\| \end{bmatrix}
\end{aligned}
$$

where $\mathcal{K}_1 = \overline{\sigma}(L+B)$, $\mathcal{K}_2 = \underline{\sigma}(CQ_1)/2 - \overline{\sigma}(P_1)L_M^2/\underline{\sigma}(L_1+B)$, $\mathcal{K}_3 = (\overline{\sigma}(P_1)L_M^1 + \overline{\sigma}(Q_1)/2)$, $\mathcal{K}_4 = \overline{\sigma}(P_1)\mathcal{K}_1(\overline{\sigma}(\Lambda) + \overline{\sigma}(C)\mathcal{K}_1)$, $\mathcal{K}_5 = \underline{\sigma}(P_1)(\underline{\sigma}(\Lambda) - L_M^2/\underline{\sigma}(L_1+B))$, $\mathcal{K}_6 = \mathcal{K}_3(\widetilde{w}_M + \|F\|) + \mathcal{K}_4\widetilde{v}_M$, $\|\widetilde{w}\| \leq \widetilde{w}_M$ and $\|\widetilde{v}\| \leq \widetilde{v}_M$ are applied.

By the inequality of $\underline{\sigma}(L+B) \geq \underline{\sigma}(L_1+B)$, the following inequalities are ensured when $\|F\| = 0$:

$$
\|S\| \leq \frac{\mathcal{K}_7}{\min(\mathcal{K}_2, \mathcal{K}_5)}, \; \|e_x\| \leq \frac{\mathcal{K}_7}{\min(\mathcal{K}_2, \mathcal{K}_5)}, \; \|\delta_x\| \leq \frac{\mathcal{K}_7}{\underline{\sigma}(L_1+B)\min(\mathcal{K}_2, \mathcal{K}_5)} \tag{4.37}
$$

where $\mathcal{K}_7 = \mathcal{K}_3\widetilde{w}_M + \mathcal{K}_4\widetilde{v}_M$.

Particularly, if the formation reference satisfies $\min_{(i,j)}\|x_{di} - x_{dj}\| > R_c$, we have the distance-based communication that satisfies

$$
\lim_{t\to\infty}(||L_2(t)|| + ||\dot{L}_2(t)||) = 0
$$

By Lemma 2.1, we have that $\|S\|$, $\|e_x\|$ and δ_x are semi-globally UUB within the following neighbourhood ultimately:

$$
\begin{aligned}
\Omega_S^2 &= \left\{ \|S\| \middle| \|S\| \leq \frac{\overline{\sigma}(Q_1)(\widetilde{w}_M + (c\overline{\sigma}(L_1+B) + \overline{\sigma}(\Lambda))\widetilde{v}_M)}{\min(c\underline{\sigma}(Q_1), 2\underline{\sigma}(Q_1)\underline{\sigma}(\Lambda)} \right\} \\
\Omega_e^2 &= \left\{ \|e_x\| \middle| \|e_x\| \leq \frac{\overline{\sigma}(Q_1)(\widetilde{w}_M + (c\overline{\sigma}(L_1+B) + \overline{\sigma}(\Lambda))\widetilde{v}_M)}{\min(c\underline{\sigma}(Q_1), 2\underline{\sigma}(Q_1)\underline{\sigma}(\Lambda)} \right\} \\
\Omega_\delta^2 &= \left\{ \|\delta_x\| \middle| \|\delta_x\| \leq \frac{\overline{\sigma}(Q_1)(\widetilde{w}_M + (c\overline{\sigma}(L_1+B) + \overline{\sigma}(\Lambda))\widetilde{v}_M)}{\underline{\sigma}(L_1+B)\min(c\underline{\sigma}(Q_1), 2\underline{\sigma}(Q_1)\underline{\sigma}(\Lambda)} \right\}
\end{aligned} \tag{4.38}
$$

which completes the proof. $\square$

Table 4.1. Parameters and initial states of ODRs with limited information.

Robot number	Model parameters			Initial states					
	m_i(kg)	R_i(m)	$I_i(\mathrm{kg}\cdot\mathrm{m}^2)$	p_i^X(m)	p_i^y(m)	θ_i(rad)	$\widehat{p}_i^x$(m)	$\widehat{p}_i^y$(m)	$\widehat{\theta}_i$(rad)
1	4.8	0.24	0.15	1.8	0.1	0	1.5	0.4	0
2	5.5	0.30	0.25	-0.9	0.6	$\pi/3$	-0.7	0.3	$\pi/4$
3	4.5	0.23	0.12	-0.7	2.3	$-\pi/3$	-0.2	1.9	$-\pi/2$
4	5.8	0.31	0.29	0.8	-0.5	$\pi/2$	0.6	-0.3	$7\pi/12$
5	5.3	0.28	0.21	-0.1	-1.3	$\pi/4$	0	-1.1	$\pi/3$
6	5.0	0.25	0.15	1.5	1.5	$-\pi/4$	1.2	1.7	$-\pi/3$

Remark 4.4. *According to* (4.37) *and* (4.38)*, the convergence boundaries of the system states can be reduced if we properly increase the value of c_i and λ_i. Therefore, the upper-limits of the convergence neighbourhood can be manually designed regardless of each agent's initial states.*

4.4.3 Simulation results and discussion

To justify the performance of the proposed neural-based observer design (4.10) and the limited-information-based sliding mode controller (4.31), numerical simulations based on a multiple ODR system are conducted.

Consider a cluster of three-wheel ODRs (Fei *et al.* 2021a), where the dynamics of the ith agent is written as

$$\begin{cases} \dot{x}_i = v_i \\ \dot{v}_i = M_i T_S(\theta_i, R_i) u_i + w_i \end{cases} \tag{4.39}$$

where $x_i = [p_i^x, p_i^y, \theta_i]^{\mathrm{T}}$, $M_i = \mathrm{diag}\{1/m_i, 1/m_i, 1/I_i\}$, m_i is the mass of the robot, I_i is the inertia of the robot, $u_i = [F_i^1, F_i^2, F_i^3]^{\mathrm{T}}$ is the force vector of the three motors, and R_i is the radius of the robot. The dynamics related parameters, the initial system states and the initial observer states are chosen as shown in Table 4.1.

The static topology L_1 is selected as the directed graph in Figure 4.3 and $b_i = 2$ for $i \in [1, 6]$.

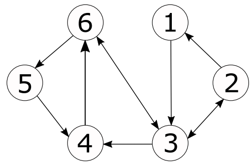

Figure 4.3. Static communication topology L_1.

The position reference for the ith agent is chosen as

$$x_{di} = \left[\frac{9}{5}\cos\left(\frac{i\pi}{3}\right) + \frac{1}{5}t, \frac{9}{5}\sin\left(\frac{i\pi}{3}\right) + \sin\left(\frac{3}{10}t\right), 0\right]^{\mathrm{T}} \tag{4.40}$$

The time-varying communication function $f(\|z_{i,j}\|)$ for the distance-related communication is chosen in the form of

$$f(\|z_{i,j}\|) = \begin{cases} \dfrac{e^{-14(\|z_{i,j}\|-1.1)}}{5+5e^{-14(\|z_{i,j}\|-1.1)}} & \|z_{i,j}\| \in [0, R_c] \\ 0 & \|z_{i,j}\| \in (R_c, +\infty) \end{cases}$$

where the communication boundary is set as $R_c = 1.5$ m. The values of $f(\|z_{i,j}\|)$ and its derivative $df/d\|z_{i,j}\|$ are illustrated by Figure 4.4, which justifies the validity of Assumption 4.2. The APF for each agent is constructed with the value selection of $\alpha = 2$, $\epsilon_1 = 1.1$ and $\epsilon_2 = 2$.

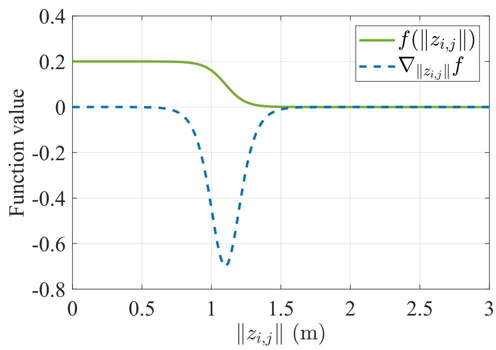

Figure 4.4. Illustration of $f(\|z_{i,j}\|)$ and its gradient.

The parameters of the sliding mode differentiator are set as $\alpha_{i,1} = \alpha_{i,4} = 6$ and $\alpha_{i,2} = \alpha_{i,3} = 8$. By Theorem 4.3, the parameters of the sliding mode controller are set as $\lambda_i = 2$ and $c_i = 2$ for each agent. The uncertainty w_i is chosen as

$$\begin{aligned} w_i = [&0.5\sin(p_{xi}) + \tanh(p_{xi}) + 0.6\sin(0.6t + i\pi/5), \\ &0.3\sin(p_{yi}) - 1.4e^{-|p_{yi}|-1} + 0.8\sin(0.4t + i\pi/5), \\ &0.2\cos(\theta_i) + \sin(0.5t + i\pi/5)]^{\mathrm{T}} \end{aligned}$$

4.4.3 Simulation results and discussion

Firstly, we define the following three error norms to illustrate the amount of estimation error for each method to further justify our designs of the finite-time neural-based observer:

$$\mathcal{N}_x = \sum_{i=1}^{6} \|\widetilde{x}_i\|,\ \mathcal{N}_v = \sum_{i=1}^{6} \|\widetilde{v}_i\|,\ \mathcal{N}_w = \sum_{i=1}^{6} \|\widetilde{w}_i\|$$

By Theorem 4.1, the basic parameters for the observers are chosen as $\beta_1 = 2/3$, $\alpha_1 = 8$ and $\alpha_2 = 8$. For radial basis function NNs, the number of neurons is chosen as $m = 8$, the receptive field centres are chosen as $d_j = (j-3)\mathbf{1}_{2n}(j \in [1, m])$, and the width of the Gaussian function is set as $\mu_G = 8$. Here, we choose the following three designs for the performance comparison regarding the values of $\mathcal{N}_x$, $\mathcal{N}_v$ and $\mathcal{N}_w$:

1. The original finite-time observer (OFTO) (Li *et al.* 2019a):
$$\begin{cases} \dot{\widehat{x}}_i = \widehat{v}_i - \alpha_1 \mathrm{sgn}^{\beta_1}(\widetilde{x}_i) \\ \dot{\widehat{v}}_i = \widehat{w}_i - \alpha_2 \mathrm{sgn}^{\beta_2}(\widetilde{x}_i) + g_i u_i \\ \dot{\widehat{w}}_i = -\alpha_3 \mathrm{sgn}^{\beta_2}(\widetilde{x}_i) \end{cases} \tag{4.41}$$
with the parameter α_3 chosen as $\alpha_3 = 6$.

2. The neural-based observer (4.10) with static parameters (NBOSP), where the neural weight tuning parameters in (4.13) are chosen as $\eta_1 = 200$ and $\eta_2 = 20$.

3. The neural-based observer (4.10) with varying parameters (NBOVP), where $c_v = 1$ and the neural weight tuning parameters in (4.13) are chosen as follows by Theorem 4.2:
$$\begin{aligned} \bar{\eta}_1 &= [1, 5, 50, 200, 10000] \\ \bar{\eta}_2 &= [0.05, 0.25, 5, 20, 100] \end{aligned} \tag{4.42}$$

The comparative results of three observer designs are presented in Figure 4.5, and the bounded regions of $\mathcal{N}_x$, $\mathcal{N}_v$ and $\mathcal{N}_w$ are provided in Table 4.2. Although the OFTO can achieve boundedness of $\|\widetilde{x}_i\|$, $\|\widetilde{v}_i\|$ and $\|\widetilde{w}_i\|$, the estimation accuracy is comparatively low ($\mathcal{N}_w$ can only be bounded within 4.1).

However, the estimation precision is found to be significantly improved if the radial basis function NN is introduced into the observer design (see the results of NBOSP), which validates the necessity of designing the neural-based observer. Compared to the NBOSP design, the NBOVP design not only increases the estimation precision by 50%

(the value of $\mathcal{N}_w$ drops from 2.3 to 1.1), but also shortens the error converging time from 4s to 2.3s, which proves the validity of Theorem 4.1.

Moreover, the NBOVP design can also attenuate the oscillation of the radial basis function NN output (see when $t \in [0, 4]$ in Figure 4.5), illustrating the effectiveness of having a fractional parameter design as described in Theorem 4.2.

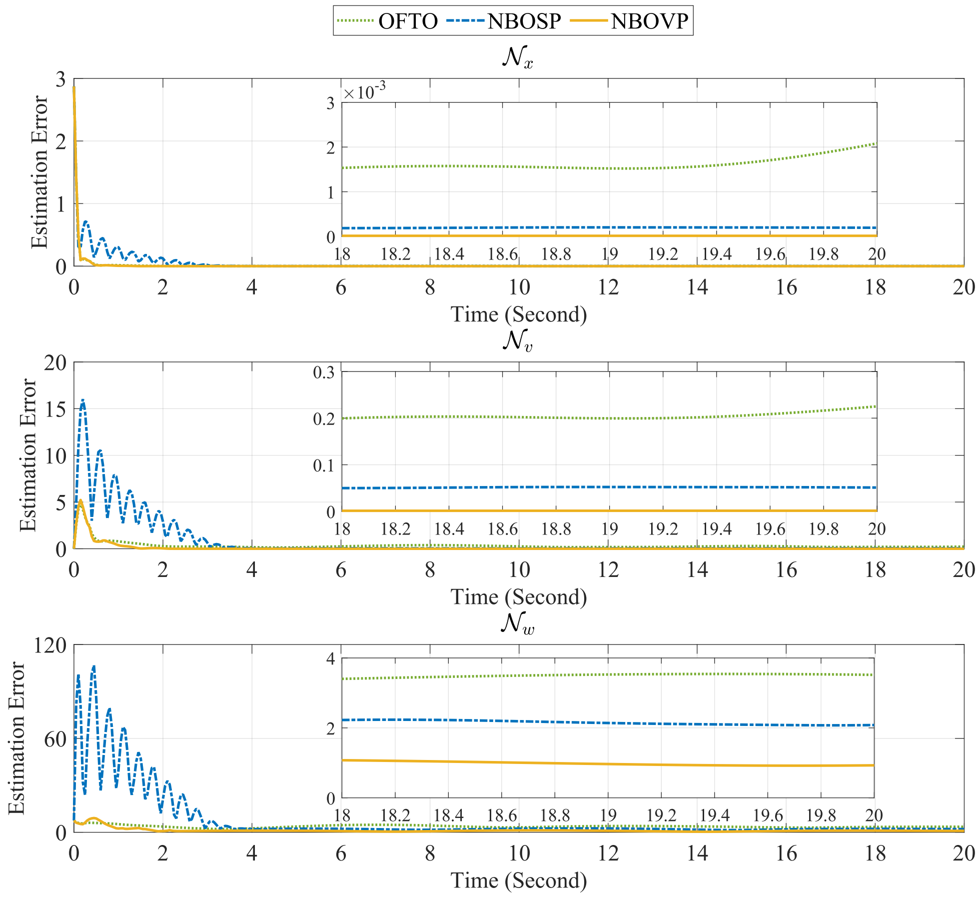

Figure 4.5. Performance comparisons among three observer designs.

Since the NBOVP design is proved to have higher estimation accuracy, it is employed in all later comparative simulations, if not specially stated otherwise. To illustrate that the range-based communication topology G_2 is helpful for avoiding potential collisions, the following three scenarios where (4.31) is implemented are chosen for further comparisons:

1. The APF in (4.8) is implemented along with the static topology (ST) that satisfies $L = L_1$.
2. The APF is disabled ($\|F_i\| = 0$) while the time-varying topology (TVT) that satisfies $L = L_1 + L_2$ is employed.

Table 4.2. Observer accuracy comparisons.

Criteria	Observer designs		
	OFTO	NBOSP	NBOVP
$\mathcal{N}_x$	4.2×10^{-3}	2.1×10^{-4}	1.5×10^{-5}
$\mathcal{N}_v$	2.3×10^{-1}	5.3×10^{-2}	1.7×10^{-3}
$\mathcal{N}_w$	4.1	2.3	1.1

3. The APF is implemented along with the time-varying topology (APFTVT) that satisfies $L = L_1 + L_2$.

By defining $r_{i,j}^{col} = R_i + R_j$ to be the relative distance of the agent pair $\{i, j\}$ when collision happens, we then have the relative distance between different pairs of agents as shown in Figure 4.6.

Although the APF technique is employed in the ST design, such structure can only ensure safety for the pairs of agents that have static communication in G_1, leaving potential safety issue for agents that are not connected initially (see Agent pair (1,6) in Figure 4.6). Such results point out that the ST design is insufficient, which further indicates the necessity of introducing the distance-based communication described by G_2.

However, collisions are observed for all three pairs if the APF technique is turned off (see TVT). Hence, the MAS (4.3) is considered as collision-free if and only if we employ both the APF and the range-based communication, indicating the necessity and effectiveness of having the APFTVT design. It is measured that the APFTVT method can guarantee inequalities $\|z_{i,j}\| > \underline{r}_{i,j}$ and $\|z_{i,j}\| \geq r_{i,j}^{col} + 0.1$ in this simulation. The propagation of three related elements in the adjacency matrix A_2 is also given in Figure 4.7, where we observe that necessary edges (see a_{16}^2 and a_{54}^2) are formed when potential collision is expected, but no new edge is generated when the connection has already existed in the static graph G_1 (see a_{23}^2), which matches our design rule in (4.5).

The norms of system states are presented in Figure 4.8, where it is observed that $\|\delta_x\|_2$ is bounded within 0.016, $\|e_x\|_2$ is bounded within 0.057, and the values of $\|S\|_2$ and

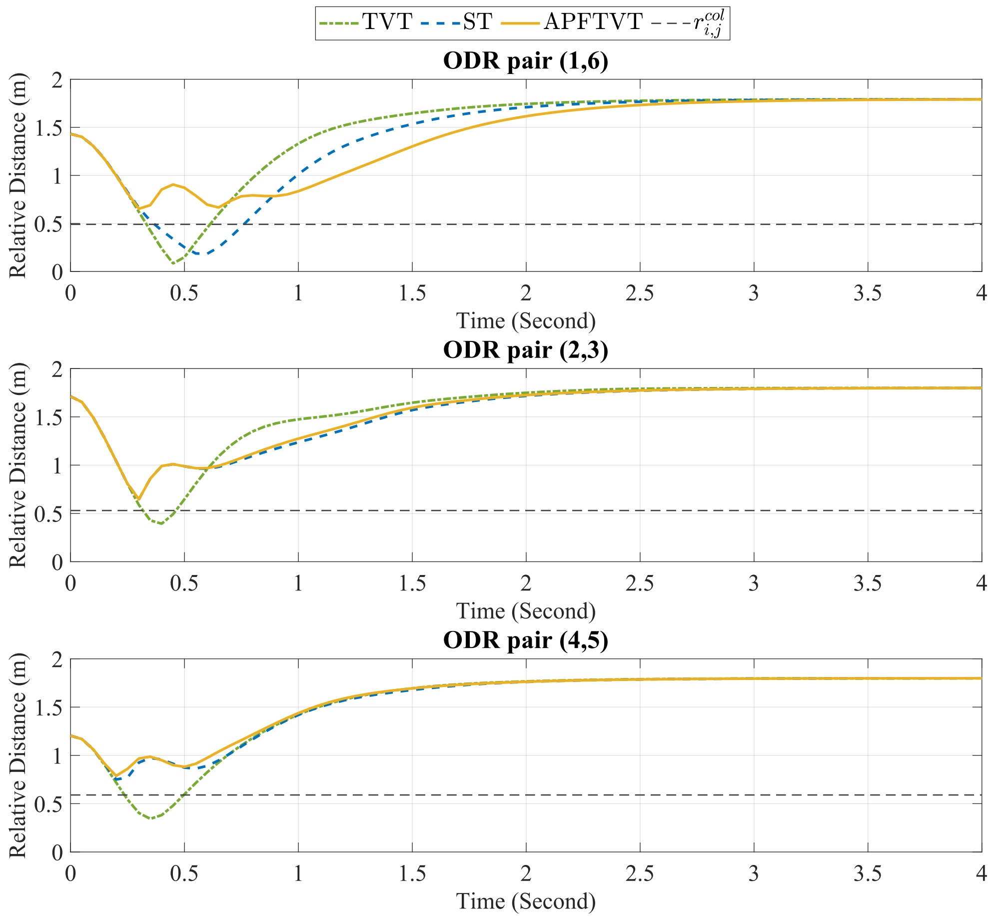

Figure 4.6. Effectiveness of the collision avoidance scheme.

$\|\widehat{S}\|_2$ are bounded within 0.12 simultaneously. The trajectories of all agents are presented in Figure 4.9 to illustrate the movement and formation status of the entire system. According to (4.40), the formation reference is a circular formation whose centre moves in a sine-wave trajectory (purple circle). It is observed that each agent follows its reference trajectory (dotted line) with bounded tracking error and compose the expected formation successfully, which illustrates the effectiveness of the proposed distributed formation controller (4.31).

Remark 4.5. *For a formation tracking task where there is at least one channel of the agent's position state whose norm is expected to have a linear relationship with time like* (4.40)*, we need to enlarge the width of the Gaussian function by increasing the value of μ. Otherwise, potential divergence issue will occur when t is large enough because $\varphi(Y_i)$ will lose sensitivity to Y_i if $\|Y_i - d_j\|$ is too large.*

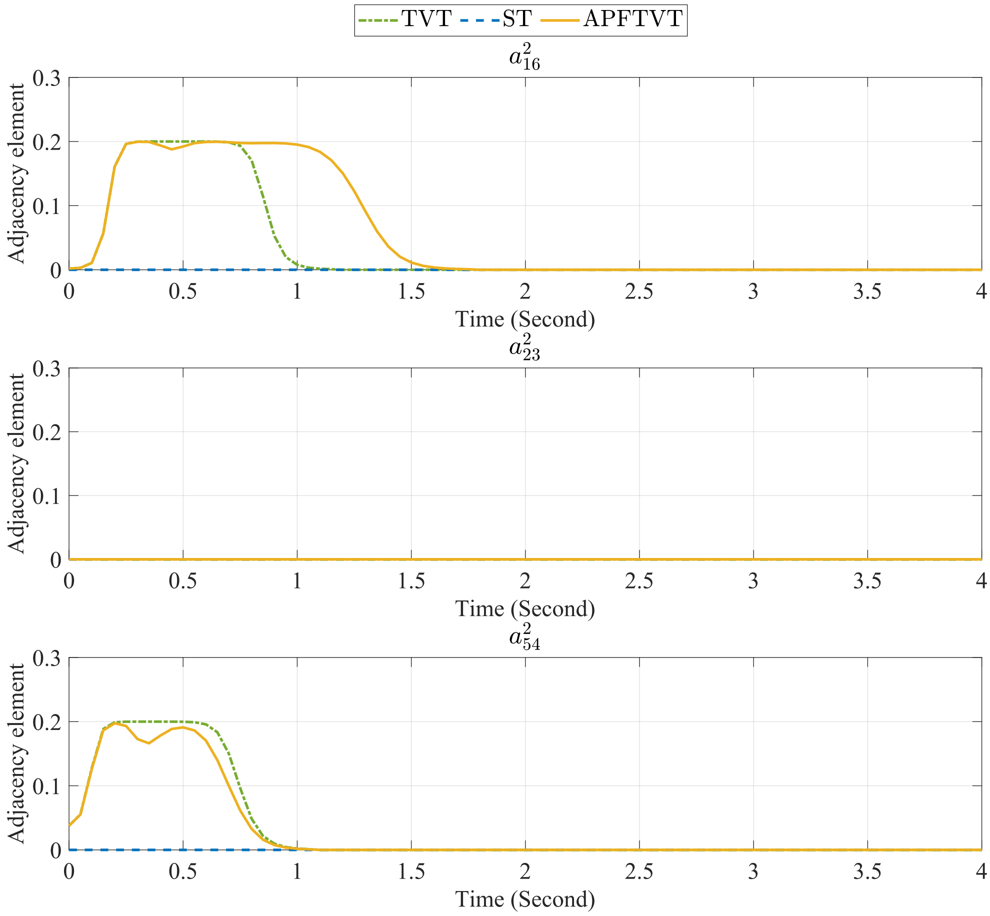

Figure 4.7. Propagation of adjacency elements in A_2.

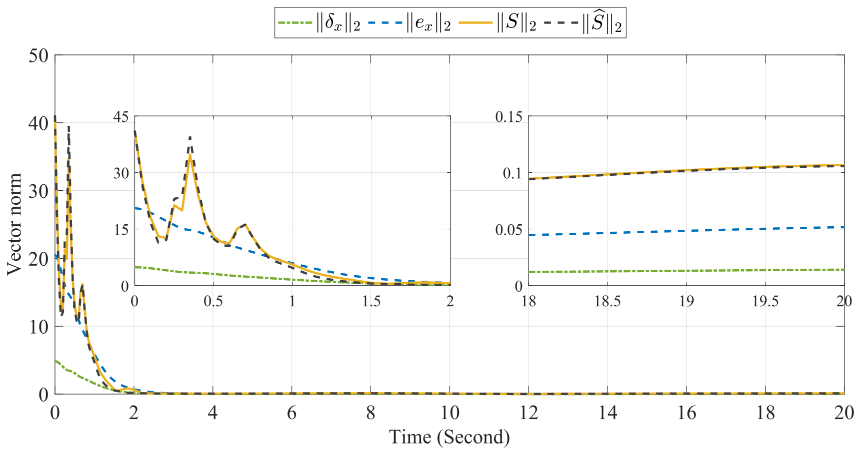

Figure 4.8. Performance of the limited-information-based formation controller.

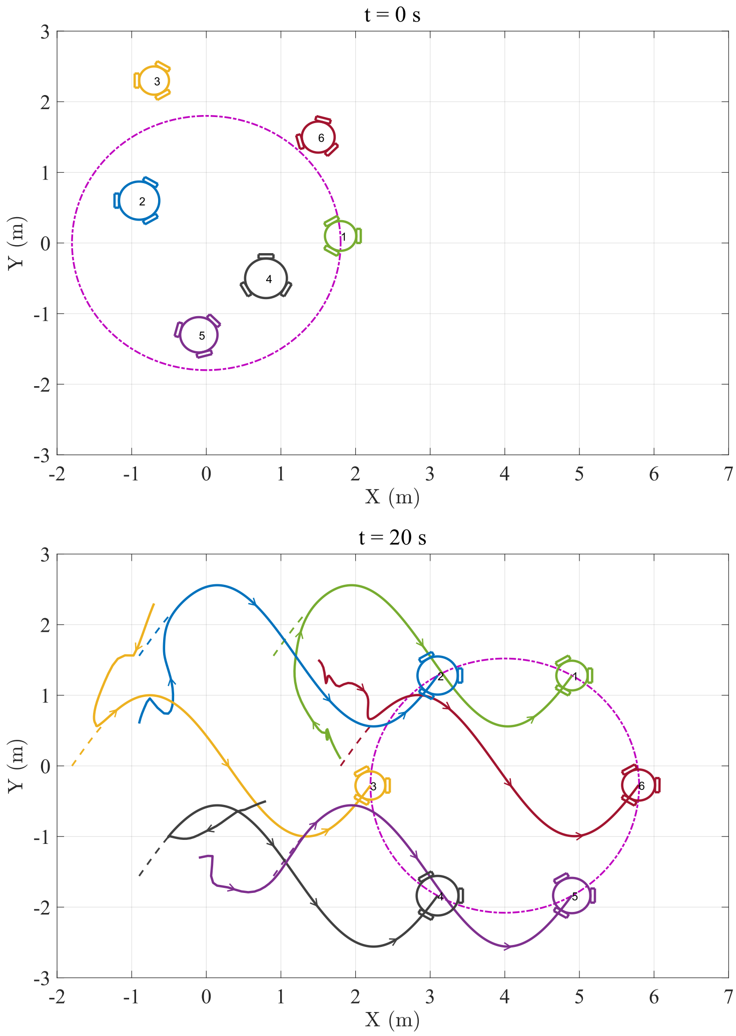

Figure 4.9. Trajectories of the system while applying the limited-information-based formation controller.

4.5 Chapter summary

In this chapter, the robust and collision-free formation control problem for second-order MASs with limited information was investigated. A new finite-time neural-based state observer was first designed to estimate the unknown velocity and the system uncertainty simultaneously. Furthermore, an error-related observer parameter design was proposed to attenuate the chattering phenomenon and increase approximation precision. By introducing a distance-related directed topology, agents are able to obtain each other's position to generate repulsive force to avoid collision. A distributed robust SMC scheme was then proposed to ensure the semi-global uniform ultimate boundedness of the system's formation tracking error. The validity of each design is first guaranteed by the Lyapunov stability theory, and further illustrated by simulations and comparisons.

In the next chapter, the actuator saturation phenomenon is considered to enhance the practicality of the formation control algorithms. Analysis regarding the joint effect of actuator saturation and input coupling is also discussed. To attenuate the state oscillation and maintain the robustness of the system simultaneously, an observer-and-algorithm-based formation control law is proposed for first-order agent clusters.

Chapter 5

Formation Control of First-Order Agents with Input Saturation

TO ensure the practicality of the formation control scheme, it is essential to consider the issue of actuator saturation. In this chapter, the robust formation control problem of a cluster of nonlinear first-order agents is investigated. A new cooperative tuning scheme for three-layer neural networks is first proposed for first-order agents without input constraints. To ensure that the neural estimation error can be bounded within finite-time regardless of the actuator saturation phenomenon, a neural-based observer structure is then proposed to further construct an observer-based controller. To attenuate the state fluctuation brought by coupled and saturated control input, a control input distribution algorithm is presented. In order to extend the stability of the uncertainty estimation process into a global perspective, a new adaptive observer is developed along with an auxiliary control compensation term to achieve robust formation tracking. The compensated controller is then validated through both simulations and physical experiments.

5.1 Introduction

Although multiple neural-based designs are validated through both the Lyapunov stability theory and comparative simulations, both the CNN (Zou and Kumar 2012) and the radial basis function NN (Zheng *et al.* 2021) are two-layer NNs. According to Liu et al., the approximation precision of an NN will be improved after introducing more hidden layer into the network design. Hence, one of the main focuses in this chapter is to explore a suitable way to employ three-layer NNs in multi-agent formation tracking scenarios.

In terms of the tracking problem of single systems, the dynamic programming approach was used along with a three-layer NN to perform optimal control (Liu *et al.* 2013). When it comes to the multi-agent scenarios, the cooperative tuning design is one popular approach. To estimate the uncertain nonlinearities and external disturbances in each individual agent, three-layer NNs were tuned based on the formation tracking error to perform formation tracking for a group of autonomous underwater vehicles (Elhaki and Shojaei 2018).

However, the cooperative weight tuning law proposed by Elhaki and Shojaei is not fully error-related, which will lead to the potential divergence of weight values. Hence, how to obtain a fully local-error-related cooperative tuning law has become a considerable challenge for multi-agent scenarios.

In the area of control engineering, it is also vital to consider the actuator saturation phenomenon when justifying the applicability of one control scheme. Currently, a convenient way to deal with the saturation effect is to treat it as a bounded disturbance and make corresponding compensation while designing the controller (Gao and Selmic 2006, Shojaei 2016). The three-layer NN was first used by Gao and Selmic to approximate the effect of saturation phenomenon (Gao and Selmic 2006). However, the network weight in the hidden layer is set to be constant, which leads to a lack of adaptiveness. The adaptiveness of the three-layer NN is further improved by constructing adaptive tuning law for the weight matrix in the hidden layer (Shojaei 2016).

Although the tracking-error-based weight tuning approach mentioned by Shojaei is proved to be effective for both saturated and unsaturated systems, the convergence time of the NN estimation error will increase along with the system's initial tracking error. Furthermore, the neural estimation error will not settle before the tracking error converges. Such features expose the drawbacks of employing variables related to the reference tracking error as the weight tuning criterion in systems with actuator saturation. Therefore, it is necessary to develop a finite-time tuning approach that adjusts the neural weights regardless of the tracking error.

Besides, although the NNs are proved to have high estimation accuracy for nonlinear functions, such result is based on the assumption that the input of the NN is restricted within a compact set. However, the NN estimation process in adaptive control usually requires the system states as the network input because of their correlation with the system uncertainty, which means that the stability of the NNs only exists semi-globally. Hence, it is also necessary to find an estimation structure that possesses global stability to be used in the practical scenarios.

To ensure that the amplitude of the control input is restricted within the saturation limitation, many researchers choose to implement smooth and bounded functions within the controller design (Huang *et al.* 2016, Liu *et al.* 2019, Li *et al.* 2019b). Currently, plenty of results have been obtained for systems without input coupling effect (Huang *et al.* 2016, Bai *et al.* 2019). An adaptive reaching-law-based SMC approach was developed for formation tracking of electromagnetic systems by Huang et al. to achieve finite-time and chattering-free error convergence (Huang *et al.* 2016). A compensation term was introduced along with an auxiliary system for a class of discrete-time system by Bai et al. to perform adaptive control based on reinforcement learning (Bai *et al.* 2019),

Similarly, saturation functions are also applied in the controller design of coupled systems. For example, a saturation function was added into the controller by Fu and Yu to deal with the input saturation problem of a cluster of marine surface vehicles (Fu and Yu 2018). Additional control terms were introduced by Li et al. to deal with the input saturation issue of underwater vehicles (Li *et al.* 2019b).

However, obvious oscillations of system states were observed in the results obtained by Fu and Yu, while chattering phenomenons were also recorded for control inputs by Li et al. Such observations indicate that the amplitude limitation of control input is not the only concern for systems that have both coupled and saturated actuators. Hence, it is essential to investigate the joint effect of actuator saturation and input coupling effect.

Motivated by the above discussions, the following issues are investigated in this chapter:

1. How to settle the three-layer NN tuning process within finite time when the actuator is affected by input saturation?

2. How to analyse and attenuate the joint effect of input coupling and actuator saturation?

3. How to design an adaptive observer structure that ensures global stability and can be employed in practice?

The contents in this chapter are organised as follows. The system modelling of a class of first-order nonlinear MASs with actuator saturation and the problem formulation are given Section 5.2. A brief introduction of three-layer NNs and two corresponding neural-based formation controller is given in Section 5.3. A new adaptive observer structure with global stability is then presented in Section 5.4, where physical experiments are carried out to validate the practicality of the observer-based scheme. The summary of this chapter's work is presented in Section 5.5.

5.2 System modelling and problem formulation

Consider a distributed nonlinear multi-agent system consists of N first-order agents, and the dynamics of the ith agent is given as

$$\dot{x}_i = f_i(x_i) + g_i(x_i, \mathbf{P}_i)\mathcal{S}(u_i, U_{Mi}) + \varpi_i,\ i = 1, 2, \ldots, N \tag{5.1}$$

where $x_i \in \mathbb{R}^n$ is the position information of the ith agent, $g_i(x_i, \mathbf{P}_i) \in \mathbb{R}^{n\times n}$ is the nonlinear control gain matrix, $\mathbf{P}_i$ represents the model parameter set, $u_i \in \mathbb{R}^n$ is the control input, $f_i(x_i) \in \mathbb{R}^n$ is the unknown dynamics of the system, $\bar{\varpi}_i \in \mathbb{R}^n$ represents the external disturbance, and $\mathcal{S}(u_i, U_{Mi}) \in \mathbb{R}^n$ is the saturated control input. The jth element of $\mathcal{S}(u_i, U_{Mi})$ is expressed as

$$\mathcal{S}(u_i(j), U_{Mi}) = \begin{cases} u_i(j) & |u_i(j)| \leq U_{Mi} \\ \mathrm{sign}(u_i(j))U_{Mi} & |u_i(j)| > U_{Mi} \end{cases} \tag{5.2}$$

where $u_i(j)$ is the jth element of u_i and $U_{Mi} \in \mathbb{R}^+$ is the saturation limit. Obtaining the value of $g_i(x_i, \mathbf{P}_i)$ is necessary for controller design, but it is hard to obtain the precise value of $\mathbf{P}_i$ with the existence of measurement error. If define $\widehat{\mathbf{P}}_i$ to be our measurement of the parameter set, then the control gain matrix obtained through calculation is

$\widehat{g}_i(x_i, \widehat{\mathbf{P}}_i) \in \mathbb{R}^{n\times n}$, and the parameter estimation error is given as $\widetilde{\mathbf{P}}_i = \mathbf{P}_i - \widehat{\mathbf{P}}_i$. Define $\widetilde{g}_i(x_i, \widetilde{\mathbf{P}}_i) = g_i(x_i, \mathbf{P}_i) - \widehat{g}_i(x_i, \widehat{\mathbf{P}}_i)$ to represent the modelling error of the input coupling matrix, the simplified model is given as

$$\dot{x}_i = \widehat{g}_i(x_i, \widehat{\mathbf{P}}_i)\mathcal{S}(u_i, U_{Mi}) + E_i \tag{5.3}$$

where $E_i = \widetilde{g}_i(x_i, \widetilde{\mathbf{P}}_i)\mathcal{S}(u_i, U_{Mi}) + \varpi_i + f_i(x_i)$ represents the combination of unknown factors. For simplicity, terms g_i and $\widehat{g}_i$ are used in the rest of this chapter to represent $g_i(x_i, \mathbf{P}_i)$ and $\widehat{g}_i(x_i, \widehat{\mathbf{P}}_i)$, respectively, unless specially stated.

Then the cluster dynamics is obtained as follows:

$$\dot{x} = \widehat{g}\mathcal{S}(u) + E \tag{5.4}$$

where

$$\begin{aligned}
&x = [x_1^{\mathrm{T}}, x_2^{\mathrm{T}}, \ldots, x_N^{\mathrm{T}}]^{\mathrm{T}} \in \mathbb{R}^{nN},\ \widehat{g} = \mathrm{diag}\{\widehat{g}_1, \widehat{g}_2, \ldots, \widehat{g}_N\} \in \mathbb{R}^{nN\times nN} \\
&\mathcal{S}(u) = [\mathcal{S}^{\mathrm{T}}(u_1, U_{M1}), \mathcal{S}^{\mathrm{T}}(u_2, U_{M2}), \ldots, \mathcal{S}^{\mathrm{T}}(u_N, U_{MN})]^{\mathrm{T}} \in \mathbb{R}^{nN} \\
&E = [E_1^{\mathrm{T}}, E_2^{\mathrm{T}}, \ldots, E_N^{\mathrm{T}}]^{\mathrm{T}} \in \mathbb{R}^{nN}
\end{aligned}$$

The position and velocity references of the ith agent are described by $x_{di} \in \mathbb{R}^n$ and $\dot{x}_{di} \in \mathbb{R}^n$, respectively. The main purpose of the controller design is to ensure the semi-global uniform ultimate boundedness of each uncertain agent's reference tracking error with the actuator saturation (5.2), which is illustrated as

$$\lim_{t\to\infty} \|x_i(t) - x_{di}(t)\| \leq \nu_\delta^s,\ \forall x_i(t_0) \in \Omega_x,\ i = 1, 2, \ldots, N \tag{5.5}$$

Assumption 5.1. *The state references x_{di} and $\dot{x}_{di}$ are known and bounded when $t \geq t_0$. The parameter measurement error $\widetilde{\mathbf{P}}_i$ is also bounded. The initial state of the ith agent is bounded such that $x_i(t_0) \in \Omega_x$ is satisfied.*

Assumption 5.2. *There is a known positive constant τ_i and a finite time t_s for the ith agent such that the following inequality is satisfied when $t \geq t_s$*

$$|g_i^{-1}(t)(\dot{x}_{di}(t) - f_i(x_i(t)) - \varpi_i(t))| \leq \tau_i \mathbf{1}_{n\times 1}$$

where $\tau_i < U_{Mi}$ and $\mathbf{1}_{n\times 1}$ is an n-dimensional column vector whose every entry is 1.

Remark 5.1. *Notice that Assumption 5.2 is made to ensure that the formation tracking process is feasible to the saturated agents in* (5.1) *after a finite amount of time. In an ideal situation* *where* $u_i = g_i^{-1}(t)(\dot{x}_{di}(t) - f_i(x_i(t)) - \bar{w}_i(t))$*, one has* $\dot{x}_i = \dot{x}_{di}$*, meaning that the agent can successfully track the velocity reference. However, it is still necessary to have a residual amount of control input to reduce the value of* $\|x_i(t) - x_{di}(t)\|$ *when* $\|x_i(t_0) - x_{di}(t_0)\| > \nu_\delta^s$*, where* $x_i(t_0)$ *and* $x_{di}(t_0)$ *are the initial system state and the initial position reference. Hence, the inequality of* $\tau_i < U_{Mi}$ *is given to offer the redundancy in the control input. The time* t_s *is defined to mark the time when the formation tracking task is feasible to each agent in* (5.4).

5.3 Formation control via three-layer neural networks

This section focuses on the NN-based formation controller design for saturated first-order MASs. A fully error-related cooperative tuning approach is first proposed for first-order MASs without actuator saturation, To achieve finite-time convergence of the estimation error when the actuator is saturated, a NN-based observer is then proposed. Afterwards, the combined effect of actuator saturation and input coupling is analysed and summarised as the reverse effect. To attenuate the state oscillation, a new control input algorithm is provided.

5.3.1 Three-layer neural networks

In this section, three-layer NNs are implemented to approximate the unknown nonlinear function E_i and act as a part of the adaptive control law. According to the universal approximation rule (Liu *et al.* 2013), an m $(m \geq 3)$ layered NN is able to estimate any unknown function with high precision if the input vector of the NN is restricted to its compact set. If the compact set conditions of the network are satisfied, then the NN-based estimation of E_i is written as

$$E_i = W_i^{\mathrm{T}} \mathcal{T}(J_i^{\mathrm{T}} y_i) + \epsilon_i, \ i = 1, 2, \ldots, n$$

where $J_i \in \mathbb{R}^{2n \times \bar{n}}$ and $W_i \in \mathbb{R}^{\bar{n} \times n}$ are the optimal weight matrices, $y_i = [x_i^{\mathrm{T}}, u_i^{\mathrm{T}}]^{\mathrm{T}} \in \mathbb{R}^{2n}$ is the input vector of the three-layer NN, $\bar{n} \in \mathbb{R}$ is the number of neurons in the hidden layer, $\epsilon_i \in \mathbb{R}^n$ is the network bias and $\mathcal{T}(\cdot)$ is the hyperbolic tangent activation function of the hidden layer. Define $\bar{y}_j$ as the jth element of the vector $J_i^{\mathrm{T}} y_i$, then the jth element of $\mathcal{T}(J_i^{\mathrm{T}} y_i)$ has the following expression:

$$\mathcal{T}(\bar{y}_j) = \frac{e^{\bar{y}_j} - e^{-\bar{y}_j}}{e^{\bar{y}_j} + e^{-\bar{y}_j}}$$

The estimation process of a three-layer NN is

$$\widehat{E}_i = \widehat{W}_i^{\mathrm{T}} \mathcal{T}(\widehat{J}_i^{\mathrm{T}} y_i) \tag{5.6}$$

where $\widehat{J}_i$ and $\widehat{W}_i$ are the estimated weight matrices.

The estimation error of the three-layer NN is given as

$$\widetilde{E}_i = E_i - \widehat{E}_i = \widetilde{W}_i^{\mathrm{T}} \mathcal{T}(\widehat{J}_i^{\mathrm{T}} y_i) + \bar{\epsilon}_i(y_i)$$

where $\bar{\epsilon}_i(y_i) = W_i^{\mathrm{T}}[\mathcal{T}(J_i^{\mathrm{T}} y_i) - \mathcal{T}(\widehat{J}_i^{\mathrm{T}} y_i)] + \epsilon_i$ and $\widetilde{W}_i = W_i - \widehat{W}_i$.

Assumption 5.3. *The neighbourhood of $[-U_{Mi}, U_{Mi}]$ is included in the approximation compact set Ω_u for each individual agent.*

Assumption 5.4. *The weight matrices W, J and the estimation error ϵ are bounded such that there are positive constants W_M, J_M and ϵ_M that satisfy*

$$\|W\|_F \leq W_M, \; \|J\|_F \leq J_M, \; \|\epsilon\| \leq \epsilon_M$$

where

$$\begin{aligned} &\epsilon = [\epsilon_1^{\mathrm{T}}, \epsilon_2^{\mathrm{T}}, \ldots, \epsilon_N^{\mathrm{T}}]^{\mathrm{T}} \in \mathbb{R}^{nN}, \; W = \mathrm{diag}\{W_1, W_2, \ldots, W_N\} \in \mathbb{R}^{\bar{n}N \times nN} \\ &J = \mathrm{diag}\{J_1, J_2, \ldots, J_N\} \in \mathbb{R}^{2nN \times \bar{n}N} \end{aligned}$$

Lemma 5.1. (Liu *et al.* 2013) *Based on the boundedness of the activation function $\mathcal{T}(\cdot)$, the three-layer NN approximation error ϵ and the optimal weight matrices W and J, there exist positive constants $\mathcal{T}_{Mi}$, $\bar{\epsilon}_{Mi}$, $\mathcal{T}_M$ and $\bar{\epsilon}_M$ such that:*

$$\|\mathcal{T}(\widehat{J}_i^{\mathrm{T}} y_i)\| \leq \mathcal{T}_{Mi}, \quad \|\bar{\epsilon}_i(y_i)\| \leq \bar{\epsilon}_{Mi}, \; \|\mathcal{T}(\widehat{J}^{\mathrm{T}} y)\| \leq \mathcal{T}_M, \quad \|\bar{\epsilon}(y)\| \leq \bar{\epsilon}_M$$

where $\bar{\epsilon}(y) = [\bar{\epsilon}_1^{\mathrm{T}}(y_1), \bar{\epsilon}_2^{\mathrm{T}}(y_2), \ldots, \bar{\epsilon}_N^{\mathrm{T}}(y_N)]^{\mathrm{T}}$.

5.3.2 Neural adaptive formation control via cooperative tuning

In this subsection, the saturation phenomenon is removed by setting $U_{Mi} = +\infty$. According to the agent dynamics (5.3), one has

$$\delta_{xi} = x_i - x_{di} \tag{5.7}$$

where $\delta_{xi} \in \mathbb{R}^n$ is the position tracking error of the ith agent.

Then the global form is obtained as follows:

$$\delta_x = x - x_d \tag{5.8}$$

where

$$\delta_x = [\delta_{x1}^{\mathrm{T}}, \delta_{x2}^{\mathrm{T}}, \ldots, \delta_{xN}^{\mathrm{T}}]^{\mathrm{T}} \in \mathbb{R}^{nN},\ x_d = [x_{d1}^{\mathrm{T}}, x_{d2}^{\mathrm{T}}, \ldots, x_{dN}^{\mathrm{T}}]^{\mathrm{T}} \in \mathbb{R}^{nN}$$

Define $b_i \in \mathbb{R}^+$ to be the ith diagonal element of B, the local formation tracking error of the ith agent is obtained as

$$e_{xi} = \sum_{j=1}^{N} a_{ij}(\delta_{xi} - \delta_{xj}) + b_i\delta_{xi} = \sum_{j=1}^{N} l_{ij}\delta_{xj} + b_i\delta_{xi} \tag{5.9}$$

where l_{ij} is the element on the ith row and jth column of L. In (5.9), the practical meaning of b_i is the ith agent's sensitivity on its own reference tracking error δ_{xi}. Define $e_x = [e_{x1}^{\mathrm{T}}, e_{x2}^{\mathrm{T}}, \ldots, e_{xN}^{\mathrm{T}}]^{\mathrm{T}}$, then the following global form is obtained:

$$e_x = (L + B) \otimes I_n\delta_x \tag{5.10}$$

The time derivative of (5.10) is obtained as

$$\dot{e}_x = (L + B) \otimes I_n(\widehat{g}u + E - \dot{x}_d) \tag{5.11}$$

To perform adaptive estimation, the weight tuning law set of a three-layer NN is usually chosen as follows (Elhaki and Shojaei 2018, Wu *et al.* 2020):

$$\begin{cases} \dot{\widehat{W}}_i = \Gamma_1 G_W(e_{xi}, \widehat{J}_i, \widehat{W}_i, y_i) - \Gamma_2\widehat{W}_i \\ \dot{\widehat{J}}_i = \Gamma_3 G_J(e_{xi}, \widehat{J}_i, \widehat{W}_i, y_i) - \Gamma_4\widehat{J}_i \end{cases}$$

where $\Gamma_i \in \mathbb{R}^+ (i \in [1, 4])$ are the error-invariant tuning gains, and G_W and G_J represent the related tuning functions that satisfy $\|G_W\|_F = \|G_J\|_F = 0$ when $\|e_{xi}\| = 0$ (G_W and G_J will no longer affect W_i when there is no error).

In the work of (Elhaki and Shojaei 2018), parameters Γ_2 and Γ_4 are set to be static. Although it is reasonable to include terms like $-\Gamma_2\widehat{W}_i$ and $-\Gamma_4\widehat{J}_i$ to prevent the oscillation of neural weights when the value of $\|e_{xi}\|$ is high, such terms will also lead to contradictions that $\dot{\widehat{W}}_i = -\Gamma_2\widehat{W}_i$ and $\dot{\widehat{J}}_i = -\Gamma_4\widehat{J}_i$ when $\|e_{xi}\| = 0$, meaning that a potential divergence of estimation error always exists unless $\|W_i\|_F = \|J_i\|_F = 0$ or $\Gamma_2 = \Gamma_4 = 0$.

To deal with the estimation error divergence issue, the idea of selecting Γ_2 and Γ_4 as time-related exponentially decreasing functions is proposed (Wu *et al.* 2020). Although such approach is found to be effective, it does introduce the danger that the three-layer NN will lose the protection from $-\Gamma_2\widehat{W}_i$ and $-\Gamma_4\widehat{J}_i$ after certain period of time, leading to potential chattering or oscillation.

To maintain the protection of $-\Gamma_2\widehat{W}_i$ and $-\Gamma_4\widehat{J}_i$ while avoiding the divergence issue, a fully error-related tuning approach was then proposed (Liu *et al.* 2013). However, this approach is never investigated in a cooperative way for multi-agent systems. Therefore, a set of fully local-error-related tuning laws of $\widehat{W}_i$ and $\widehat{J}_i$ is proposed as

$$\begin{cases} \dot{\widehat{W}}_i = \eta_1 \mathcal{T}(\widehat{J}_i^{\mathrm{T}} y_i) e_{xi}^{\mathrm{T}} - \eta_2 \|e_{xi}\| \widehat{W}_i \\ \dot{\widehat{J}}_i = \dfrac{\eta_3}{2nN} \mathrm{sign}(y_i) e_{xi}^{\mathrm{T}} \widehat{W}_i^{\mathrm{T}} (I_{\bar{n}} - \alpha(\widehat{J}_i^{\mathrm{T}} y_i)) - \eta_4 \|e_{xi}\| \widehat{J}_i \end{cases} \tag{5.12}$$

where $\alpha(\widehat{J}_i^{\mathrm{T}} y_i) = \mathrm{diag}\{\mathcal{T}_j^2(\widehat{J}_i^{\mathrm{T}} y_i)\}, j \in [1, \bar{n}]$ and $\eta_i \in \mathbb{R}^+$ $(i = 1, 2, 3, 4)$. Then one has $\|\dot{\widehat{W}}_i\|_F = \|\dot{\widehat{J}}_i\|_F = 0$ when $\|e_{xi}\| = 0$, while $-\eta_2\|e_{xi}\|\widehat{W}_i$ and $-\eta_4\|e_{xi}\|\widehat{J}_i$ remain to be the counter parts to reduce the chattering in the network output without triggering the divergence of the three-layer NN estimation error. Accordingly, the following global form is obtained:

$$\begin{cases} \dot{\widehat{W}} = \eta_1 \mathcal{T}(\widehat{J}^{\mathrm{T}} y) e_x^{\mathrm{T}} - \eta_2 \Delta_e \otimes I_{\bar{n}} \widehat{W} \\ \dot{\widehat{J}} = \dfrac{\eta_3}{2nN} \mathrm{sign}(y) e_x^{\mathrm{T}} \widehat{W}^{\mathrm{T}} (I_{\bar{n}N} - \alpha(\widehat{J}^{\mathrm{T}} y)) - \eta_4 \Delta_e \otimes I_{2n} \widehat{J} \end{cases} \tag{5.13}$$

where the following equations are applied:

$$\widehat{W} = \mathrm{diag}\{\widehat{W}_1, \widehat{W}_2, \ldots, \widehat{W}_N\} \in \mathbb{R}^{\bar{n}N \times nN}, \qquad \widehat{J} = \mathrm{diag}\{\widehat{J}_1, \widehat{J}_2, \ldots, \widehat{J}_N\} \in \mathbb{R}^{2nN \times \bar{n}N}$$
$$\Delta_e = \mathrm{diag}\{\|e_{x1}\|, \|e_{x2}\|, \ldots, \|e_{xN}\|\} \in \mathbb{R}^{N \times N}, \quad y = [y_1^{\mathrm{T}}, y_2^{\mathrm{T}}, \ldots, y_N^{\mathrm{T}}]^{\mathrm{T}} \in \mathbb{R}^{2nN \times 1}$$

Based on the NN-based estimation (7.9) and the weight tuning law set (5.13), the cooperative formation controller is designed as

$$u_i = \widehat{g}_i^{-1}(\dot{x}_{di} - \widehat{E}_i - k_i e_{xi}) \tag{5.14}$$

The following theorem summarises the fully error-related cooperative tuning law set design for the three-layer NN:

Theorem 5.1. *Consider system* (5.4) *without actuator saturation ($U_{Mi} = +\infty$), and Assumptions 5.1 and 5.4 hold. By the three-layer NN-based estimation* (7.9)*, the weight tuning law set* (5.12)*, and the formation controller* (5.14)*, the system states e_x, δ_x, $\widetilde{W}$ and $\widetilde{J}$ are semi-globally UUB if the following conditions are met:*

1. *The parameters η_2, η_3 and η_4 in* (5.12) *and* (5.13) *satisfy $\eta_2 > \eta_3/2$ and $\eta_4 > \eta_3/2$.*

2. *The compact set conditions of the NNs hold such that either $E_i \in \Omega_E$ or $y_i \in \Omega_y$ is satisfied when $t \geq t_0$, where Ω_y is a compact set of y_i and $\Omega_u \subset \Omega_y$.*

Proof. Define $\widetilde{W} = W - \widehat{W}$ and $\widetilde{J} = J - \widehat{J}$, then consider the following Lyapunov function candidate:

$$V_{4,1} = \frac{1}{2}e_x^{\mathrm{T}}\mathcal{P}e_x + \frac{1}{2}\mathrm{tr}\{\widetilde{W}^{\mathrm{T}}\widetilde{W}\} + \frac{1}{2}\mathrm{tr}\{\widetilde{J}^{\mathrm{T}}\widetilde{J}\} \tag{5.15}$$

where $\mathcal{P} = P \otimes I_n$. By Lemma 2.3, the time derivative of $V_{4,1}$ is obtained as

$$\begin{aligned}
\dot{V}_{4,1} &= e_x^{\mathrm{T}}\mathcal{P}[(L+B)\otimes I_n]\dot{\delta}_x - \mathrm{tr}\{\widetilde{W}^{\mathrm{T}}\dot{\widehat{W}}\} - \mathrm{tr}\{\widetilde{J}^{\mathrm{T}}\dot{\widehat{J}}\} \\
&= \frac{1}{2}e_x^{\mathrm{T}}\mathcal{Q}\bar{\epsilon} + \eta_4\mathrm{tr}\{\widetilde{J}^{\mathrm{T}}\Delta_e \otimes I_{2n}(J-\widetilde{J})\} - \mathrm{tr}\left\{\widetilde{J}^{\mathrm{T}}\frac{\eta_3}{2nN}\mathrm{sign}(y)e_x^{\mathrm{T}}\widehat{W}^{\mathrm{T}}(I_{N\bar{n}} - \alpha(\widehat{J}^{\mathrm{T}}y))\right\} \\
&\quad + \mathrm{tr}\left\{\widetilde{W}^{\mathrm{T}}\mathcal{T}(\widehat{J}^{\mathrm{T}}y)e_x^{\mathrm{T}}\left(\frac{1}{2}\mathcal{Q} - \eta_1 \otimes I_{nN}\right)\right\} + \eta_2\mathrm{tr}\{\widetilde{W}^{\mathrm{T}}\Delta_e \otimes I_{\bar{n}}(W-\widetilde{W})\} - \frac{1}{2}e_x^{\mathrm{T}}\mathcal{Q}Ke_x
\end{aligned}$$

where $K = \mathrm{diag}\{k_1, k_2, \ldots, k_N\} \otimes I_n$ and $\mathcal{Q} = (P(L+B)) \otimes I_n$. With the following inequalities:

$$\begin{aligned}
&\mathrm{tr}\{\widetilde{W}^{\mathrm{T}}(W-\widetilde{W})\} \leq W_M\|\widetilde{W}\|_F - \|\widetilde{W}\|_F^2, \quad && \Delta_e \leq \|e_x\| \otimes I_N \\
&\mathrm{tr}\{\widetilde{J}^{\mathrm{T}}(J-\widetilde{J})\} \leq J_M\|\widetilde{J}\|_F - \|\widetilde{J}\|_F^2, && \left\|\frac{1}{2nN}\mathrm{sign}(y)\right\| \leq 1
\end{aligned}$$

the expression of $\dot{V}_{4,1}$ is further modified as

$$\begin{aligned}
\dot{V}_{4,1} &\leq -\frac{1}{2}\underline{\sigma}(\mathcal{Q}K)\|e_x\|^2 - \eta_2\|\widetilde{W}\|_F^2\|e_x\| + \frac{1}{2}\overline{\sigma}(\mathcal{Q})\bar{\epsilon}_M\|e_x\| + \eta_2 W_M\|\widetilde{W}\|_F\|e_x\| \\
&\quad + \eta_3\|\widetilde{J}\|_F\|e_x\|(W_M + \|\widetilde{W}\|_F)\|\mathcal{T}(\widehat{J}^{\mathrm{T}}y)\|\overline{\sigma}(\frac{1}{2}\mathcal{Q} - \eta_1 \otimes I_{nN})\|\widetilde{W}\|_F\|e_x\| \\
&\quad + \eta_4 J_M\|\widetilde{J}\|_F\|e_x\| - \eta_4\|\widetilde{J}\|_F^2\|e_x\| \\
&\leq (r_1\|\widetilde{W}\|_F + r_2 - \eta_2\|\widetilde{W}\|_F^2 + r_3\|\widetilde{J}\|_F + \eta_3\|\widetilde{W}\|_F\|\widetilde{J}\|_F - \eta_4\|\widetilde{J}\|_F^2)\|e_x\| \\
&\quad - \frac{1}{2}\underline{\sigma}(\mathcal{Q}K)\|e_x\|^2
\end{aligned} \tag{5.16}$$

where $r_1 = \overline{\sigma}(\mathcal{Q}/2 - \eta_1 \otimes I_{nN})\mathcal{T}_M + \eta_2 W_M$, $r_2 = \overline{\sigma}(\mathcal{Q})\bar{\epsilon}_M/2$ and $r_3 = \eta_3 W_M + \eta_4 J_M$.

With the parameters chosen as $\eta_2 > \eta_3/2$ and $\eta_4 > \eta_3/2$, (5.16) can be rewritten into the following form:

$$\begin{aligned}\dot{V}_{4,1} \leq & -\frac{1}{2}\underline{\sigma}(QK)\|e_x\|^2 - \frac{\eta_3}{2}\|e_x\|(\|\widetilde{W}\|_F - \|\widetilde{J}\|_F)^2 - (\eta_2 - \frac{\eta_3}{2})\|e_x\|(\|\widetilde{W}\|_F - \frac{r_1}{2\eta_2 - \eta_3})^2 \\ & - (\eta_4 - \frac{\eta_3}{2})\|e_x\|(\|\widetilde{J}\|_F - \frac{r_3}{2\eta_4 - \eta_3})^2 + \left(\frac{r_3^2}{2(2\eta_4 - \eta_3)} + \frac{r_1^2}{2(2\eta_2 - \eta_3)} + r_2\right)\|e_x\| \\ \leq & -\frac{1}{2}\underline{\sigma}(QK)\|e_x\|^2 + r_4\|e_x\|\end{aligned} \tag{5.17}$$

where $r_4 = r_3^2/(4\eta_4 - 2\eta_3) + r_1^2/(4\eta_2 - 2\eta_3) + r_2$. Hence, $\dot{V}_{4,1}$ will remain negative when e_x belongs to the following region:

$$\Omega_e^3 = \left\{ e_x \middle| \|e_x\| > \frac{2r_4}{\underline{\sigma}(QK)} \right\} \tag{5.18}$$

By (5.10), the reference tracking error is semi-globally UUB within the following neighbourhood:

$$\Omega_\delta^3 = \left\{ \delta_x \middle| \|\delta_x\| \leq \frac{2r_4}{\underline{\sigma}(QK)\underline{\sigma}(L+B)} \right\}$$

By the Lyapunov theory extension (Kim and Lewis 1999), both $\widetilde{W}$ and $\widetilde{J}$ are semi-globally UUB, which completes the proof. □

Although the cooperative tuning approach (5.12) can guarantee the semi-global uniform ultimate boundedness of the error states e_x and δ_x, its performance is questionable when there exists the actuator saturation phenomenon (5.2).

Theoretically, the error related weight tuning procedure (5.12) will not settle before $\|e_{xi}\|$ converges to a neighbourhood around zero. Correspondingly, the settling time for the weight tuning process is expected to be prolonged along with the increment in each agent's initial local formation tracking error because of the actuator saturation in (5.2). Hence, further investigation is essential to explore a more suitable way to implement three-layer NNs when the system is affected by input saturation.

5.3.3 Issues correlated with actuator saturation

Now, consider the MASs with saturated actuators. In most of the previous research works (Cui *et al.* 2016, Huang *et al.* 2016, Fu and Yu 2018, Han *et al.* 2019, Zhou *et al.*

2020), the only issue regarding saturation is considered as restricting the amplitude of each element in the control input within the saturation limitation U_{Mi}. However, such results are far from sufficient for a system that has coupled and saturated control inputs like (5.3).

To point out the potential issue, an example of a two-dimensional system is picked. Consider the following nominal first-order system:

$$\begin{bmatrix} \dot{X} \\ \dot{Y} \end{bmatrix} = \begin{bmatrix} \cos(\theta_1) & \cos(\theta_2) \\ \sin(\theta_1) & \sin(\theta_2) \end{bmatrix} \mathcal{S}(u_i, U_{Mi}) \tag{5.19}$$

where $u_i = [\|U_1\|, \|U_2\|]^{\mathrm{T}}$ is the nominal control input vector, U_1 and U_2 are two vectors, $\theta_1 \in (-\pi, \pi]$ is the included angle between U_1 and the X axis, and $\theta_2 \in (-\pi, \pi]$ is the included angle between U_2 and the X axis. Suppose that in one certain moment, the desired U_1 and U_2 is obtained based on the calculation of a stable nominal controller as the dashed vectors shown in Figure 5.1(a), where the circle with the radius of U_{Mi} represents the actuator saturation limit. To ensure that the amplitudes of U_1 and U_2 do not exceed U_{Mi}, the saturation operation (5.2) is obtained, which further leads to $\bar{U}_1$ and $\bar{U}_2$ (see the solid vectors in Figure 5.1(b)).

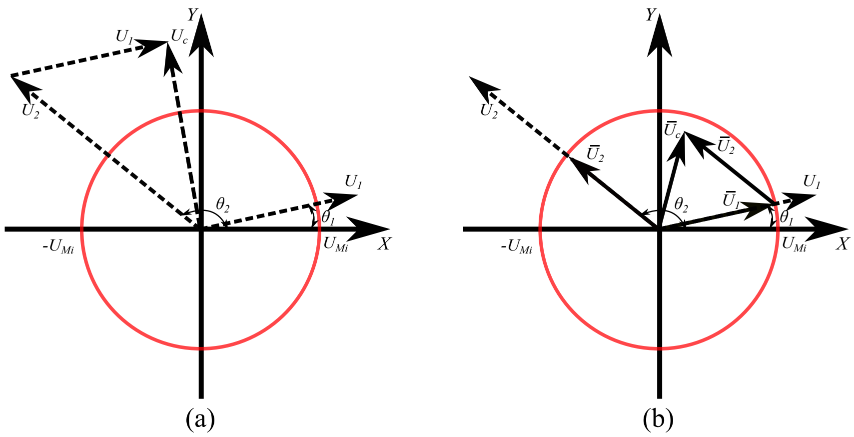

Figure 5.1. Saturation's effect on coupled control input. (a) Combined effect of nominal control input (U_c). (b) Combined effect of saturated control input ($\bar{U}_c$).

According to the nominal system dynamics in (5.19), the following results are obtained:

$$\begin{bmatrix} \cos(\theta_1) & \cos(\theta_2) \\ \sin(\theta_1) & \sin(\theta_2) \end{bmatrix} u_i = U_c, \quad \begin{bmatrix} \cos(\theta_1) & \cos(\theta_2) \\ \sin(\theta_1) & \sin(\theta_2) \end{bmatrix} \mathcal{S}(u_i, U_{Mi}) = \bar{U}_c$$

After comparing Figure 5.1(a) with Figure 5.1(b), it is found that the overall effect of the saturated control input ($\bar{U}_c$) is different from the one of the nominal controller (U_c).

Such circumstances will lead to elevations or fluctuations of the error-related states. Before conducting further discussions, it is necessary to offer the definition of the aforementioned issue. In this thesis, the corresponding phenomenon is defined as the reverse effect of coupled actuator saturation phenomenons as follows:

Definition 5.1. *For a system where control input is coupled and saturated as* (5.3), *suppose there is a nominal controller u_i, then the control input is said to be affected by the reverse effect when the following condition is met:*

$$\mathrm{sign}(g_i u_i) \neq \mathrm{sign}(g_i \mathcal{S}(u_i))$$

Moreover, as mentioned in Section 5.3.2, the saturation phenomenon will also delay the cooperative neural tuning procedure (5.12) because the output of the three-layer NN cannot be fully reflected by the control input due to the saturation phenomenon. It is unreasonable to employ a weight tuning process (5.12) that cannot guarantee the semi-global uniform ultimate boundedness of $\widetilde{W}$ and $\widetilde{J}$ before the convergence of e_x and δ_x. As a result, apart from the aim to make the control input bounded, two more problems correlated with the saturation phenomenon are worthy of further discussion:

Problem 5.1. *How to have a finite-time NN-based estimation of system uncertainties regardless of the reference tracking errors δ_{xi} and e_{xi}?*

Problem 5.2. *How to ensure that the coupled controller can provide control inputs with correct combined control direction to attenuate the reverse effect?*

5.3.4 Observer design via the three-layer neural network structure

Regarding the first problem, the method of reconstructing the previous three-layer NN into a finite-time observer is proposed (Liu *et al.* 2013):

$$\dot{\widehat{x}}_i = \widehat{g}_i u_i + \widehat{E}_i + \gamma_i \mathrm{diag}\{\mathrm{sign}(\widetilde{x}_i)\}|\widetilde{x}_i|^{\beta_i} \tag{5.20}$$

where $\widetilde{x}_i = x_i - \widehat{x}_i$, $\gamma_i \in \mathbb{R}^{n\times n}$ is a positive definite constant diagonal matrix and β_i is a real number that satisfies $\beta_i \in (0.5, 1)$.

The weight tuning law set of the three-layer NN is chosen as

$$\begin{cases} \dot{\widehat{W}}_i = \eta_1 \mathcal{T}(\widehat{J}_i^{\mathrm{T}} y_i)\widetilde{x}_i^{\mathrm{T}} - \eta_2 \|\widetilde{x}_i\| \widehat{W}_i \\ \dot{\widehat{J}}_i = \dfrac{\eta_3}{\|\mathrm{sign}(y_i)\|} \mathrm{sign}(y_i)\widetilde{x}_i^{\mathrm{T}} \widehat{W}_i^{\mathrm{T}} (I_{\bar{n}} - \alpha(\widehat{J}_i^{\mathrm{T}} y_i)) - \eta_4 \|\widetilde{x}_i\| \widehat{J}_i \end{cases} \tag{5.21}$$

Then the error dynamics of the neural-based observer is obtained as

$$\dot{\tilde{x}}_i = \widetilde{E}_i - \gamma_i \text{diag}(|\tilde{x}_i|^{\beta_i - 1})\tilde{x}_i + \widehat{g}_i(\mathcal{S}(u_i, U_{Mi}) - u_i) \tag{5.22}$$

The following assumption is made to ensure the boundedness of the initial error in (5.20).

Assumption 5.5. *The error states $\tilde{x}_i$, $\widetilde{W}_i$ and $\widetilde{J}_i$ are all bounded such that*

$$\tilde{x}_i^{\mathrm{T}}(t_0)\tilde{x}_i(t_0) + \mathrm{tr}\{\widetilde{W}_i^{\mathrm{T}}(t_0)\widetilde{W}_i(t_0)\} + \mathrm{tr}\{\widetilde{J}_i^{\mathrm{T}}(t_0)\widetilde{J}_i(t_0)\} \leq \mathcal{V}_e$$

where $\mathcal{V}_e$ is a positive constant.

Before presenting the theorem for the observer design, let us first recall one useful result:

Lemma 5.2. (Hu and Jiang 2017) *For a continuous Lyapunov function $V(X)$ that satisfies:*

$$\dot{V} \leq -\rho_1 V^{\bar{\rho}}(t) + \rho_2 V^{1/2}(t)$$

the state X is globally finite-time UUB within the region of $\Omega_V = \{X | V(X)^{\bar{\rho}-1/2} < \rho_2/\bar{\rho}_1\}$, where $\bar{\rho}_1 \in (0, \rho_1)$, $\bar{\rho} > 1/2$, $\rho_1, \rho_2 > 0$. The settling time T is bounded by:

$$T \leq \frac{V^{1-\bar{\rho}}(t_0)}{(\rho_1 - \bar{\rho_1})(1 - \bar{\rho})}$$

Then the final result result on the finite-time observer design is given as the following theorem:

Theorem 5.2. *Consider system* (5.3) *with actuator saturation* (5.2), *where Assumptions 5.1, 5.3, 5.4 and 5.5 hold. By the neural-based observer* (5.20), *and the weight tuning law set* (5.21), *the semi-global uniform ultimate boundedness of $\tilde{x}_i$, $\widetilde{W}_i$ and $\widetilde{J}_i$ is guaranteed if the following conditions are met:*

1. *The control input satisfies $|u_i| \leq U_{Mi}\mathbf{1}_{n\times 1}$.*

2. *The parameters η_2, η_3 and η_4 in* (5.21) *satisfy $\eta_2 > \eta_3/2$ and $\eta_4 > \eta_3/2$.*

3. *The compact set conditions of the three-layer NNs hold such that either $E_i \in \Omega_E$ or $y_i \in \Omega_y$ is satisfied when $t \geq t_0$*

Furthermore, the observation error $\widetilde{x}_i$ is semi-globally finite-time UUB.

Proof. Consider a Lyapunov candidate as follows:

$$V_{4,2} = \frac{\eta_1}{2}\widetilde{x}_i^{\mathrm{T}}\widetilde{x}_i + \frac{1}{2}\mathrm{tr}\{\widetilde{W}_i^{\mathrm{T}}\widetilde{W}_i\} + \frac{1}{2}\mathrm{tr}\{\widetilde{J}_i^{\mathrm{T}}\widetilde{J}_i\} \tag{5.23}$$

With the control input satisfies $|u_i| \leq U_{Mi}\mathbf{1}_{n\times 1}$, one has $\mathcal{S}(u_i, U_{Mi}) = u_i$, which further leads to

$$\begin{aligned}
\dot{V}_{4,2} &= \eta_1\widetilde{x}_i^{\mathrm{T}}\dot{\widetilde{x}}_i + \mathrm{tr}\{\widetilde{W}_i^{\mathrm{T}}\dot{\widetilde{W}}_i\} + \mathrm{tr}\{\widetilde{J}_i^{\mathrm{T}}\dot{\widetilde{J}}_i\} \\
&= \eta_1\widetilde{x}_i^{\mathrm{T}}(\widetilde{W}_i^{\mathrm{T}}\mathcal{T}(\widehat{J}_i^{\mathrm{T}}y_i) + \bar{\epsilon}_i(y_i)) - \gamma_i\eta_1\widetilde{x}_i^{\mathrm{T}}\mathrm{diag}\{\mathrm{sign}(\widetilde{x}_i)\}|\widetilde{x}_i|^{\beta_i} - \eta_1\mathrm{tr}\{\widetilde{W}_i^{\mathrm{T}}\mathcal{T}(\widehat{J}_i^{\mathrm{T}}y_i)\widetilde{x}_i^{\mathrm{T}}\} \\
&\quad - \eta_3\mathrm{tr}\left\{\widetilde{J}_i^{\mathrm{T}}\frac{\mathrm{sign}(y_i)}{\|\mathrm{sign}(y_i)\|}\widetilde{x}_i^{\mathrm{T}}\widehat{W}_i^{\mathrm{T}}(I_n - \alpha(\widehat{J}_i^{\mathrm{T}}y_i))\right\} + \eta_4\mathrm{tr}\{\widetilde{J}_i^{\mathrm{T}}\|\widetilde{x}_i\|\widehat{J}_i\} + \eta_2\mathrm{tr}\{\widetilde{W}_i^{\mathrm{T}}\|\widetilde{x}_i\|\widehat{W}_i\} \\
&\leq -\underline{\sigma}(\gamma_i)\eta_1\|\widetilde{x}_i\|^{1+\beta_i} + \eta_3\|\widetilde{J}_i\|_F\|\widetilde{x}_i\|(W_{Mi} + \|\widetilde{W}_i\|_F) - \eta_2\|\widetilde{W}_i\|_F^2\|\widetilde{x}_i\| - \eta_4\|\widetilde{J}_i\|_F^2\|\widetilde{x}_i\| \\
&\quad + \eta_1\|\widetilde{x}_i\|\bar{\epsilon}_{Mi} + \eta_4 J_{Mi}\|\widetilde{J}_i\|_F\|\widetilde{x}_i\| + \eta_2 W_{Mi}\|\widetilde{W}_i\|_F\|\widetilde{x}_i\|
\end{aligned}$$

where $\|W_i\| \leq W_{Mi}$ and $\|J_i\| \leq J_{Mi}$ are applied based on Lemma 5.1.

Similar to the proof of Theorem 5.1, if define $r_5 = \eta_2 W_{Mi}$ and $r_6 = \eta_3 W_{Mi} + \eta_4 J_{Mi}$, there is

$$\dot{V}_{4,2} \leq -\|\widetilde{x}_i\|\left[\eta_1(\underline{\sigma}(\gamma_i)\|\widetilde{x}_i\|^{\beta_i} - \bar{\epsilon}_{Mi}) - \frac{r_5^2}{2(2\eta_2 - \eta_3)} - \frac{r_6^2}{2(2\eta_4 - \eta_3)}\right]$$

Then the semi-globally UUB region of $\|\widetilde{x}_i\|$ is given as follows:

$$\|\widetilde{x}_i\| \leq \left[\frac{1}{2\eta_1\underline{\sigma}(\gamma_i)}\left(\frac{r_5^2}{(2\eta_2 - \eta_3)} + \frac{r_6^2}{(2\eta_4 - \eta_3)} + 2\eta_1\bar{\epsilon}_{Mi}\right)\right]^{1/\beta_i} \tag{5.24}$$

By the Lyapunov theory extension (Kim and Lewis 1999), $\widetilde{W}$ and $\widetilde{J}$ are both semi-globally UUB. Alternatively, select the following Lyapunov candidate:

$$V_{4,3} = \frac{1}{2}\widetilde{x}_i^{\mathrm{T}}\widetilde{x}_i$$

Then the time derivative of $V_{4,3}$ is obtained as

$$\begin{aligned}
\dot{V}_{4,3} &= \widetilde{x}_i^{\mathrm{T}}\dot{\widetilde{x}}_i \\
&= -\gamma_i\widetilde{x}_i^{\mathrm{T}}\mathrm{diag}\{\mathrm{sign}(\widetilde{x}_i)\}|\widetilde{x}_i|^{\beta_i} + \widetilde{x}_i^{\mathrm{T}}(\widetilde{W}_i^{\mathrm{T}}\mathcal{T}(\widehat{J}_i^{\mathrm{T}}y_i) + \bar{\epsilon}_i(y_i)) \\
&\leq -\underline{\sigma}(\gamma_i)\|\widetilde{x}_i\|^{\beta_i+1} + \|\widetilde{x}_i\|\widetilde{w}_M
\end{aligned}$$

where $\|\widetilde{W}_i^{\mathrm{T}}\mathcal{T}(\widehat{J}_i^{\mathrm{T}}y_i) + \bar{\epsilon}_i(y_i)\| \leq \widetilde{w}_M$ and $\widetilde{w}_M$ is a positive constant because the NN estimation error is semi-globally UUB.

Define $r_7 = \underline{\sigma}(\gamma_i)\sqrt{2^{\beta_i+1}}$ and $r_8 = \sqrt{2}\widetilde{w}_M$, we have

$$\dot{V}_{4,3} \leq -r_7 V_3^{(\beta_i+1)/2} + r_8 V_3^{1/2} \tag{5.25}$$

By Lemma 5.2, $\widetilde{x}_i$ is finite-time UUB. However, because the input of the NN needs to satisfy $x_i \in \Omega_x$ and $u_i \in \Omega_u$, $\widetilde{x}_i$ is considered to be semi-globally finite-time UUB, and the finite-time characteristics of $\|\widetilde{x}_i\|$ remains until it reaches the following neighbourhood:

$$\Omega_{\widetilde{x}}^1 = \left\{ \widetilde{x}_i \middle| \|\widetilde{x}_i\| \leq \left(\frac{\widetilde{w}_M}{\underline{\sigma}(\gamma_i)} \right)^{1/\beta_i} \right\} \tag{5.26}$$

which completes the proof. □

After constructing the finite-time neural-based observer (5.20), Problem 5.1 is solved. Now, it is vital to consider Problem 5.2.

5.3.5 Observer-based formation controller via control input distribution algorithm

To attenuate the previously defined reverse effect of actuator saturation, let us first decompose the previous controller design (5.14) for our analysis:

$$u_i = u_{t,i} + u_{d,i} + u_{e,i} \tag{5.27}$$

where $u_{t,i} = \widehat{g}_i^{-1}\dot{x}_{di}$ is the control input to maintain the velocity tracking behaviour, $u_{d,i} = -\widehat{g}_i^{-1}\widehat{E}_i$ is the control input to compensate for the estimated system uncertainties, and $u_{e,i} = -k_i\widehat{g}_i^{-1}e_{xi}(k_i \in \mathbb{R}^+)$ is the control input for formation error reduction.

It is observed that both $u_{t,i}$ and $u_{d,i}$ are consistently needed throughout the formation tracking process. By Assumption 5.2, there is

$$\lim_{t\to t_s} |\widehat{g}_i^{-1}(t)(\dot{x}_{di}(t) - \widehat{E}_i)| \leq \tau_i \mathbf{1}_{n\times 1}$$

which indicates that the combination of $u_{t,i}$ and $u_{d,i}$ is bounded after t_s.

By Assumption 5.5 and Theorem 5.2, there is a finite time t_o and three positive constants E_M, $\bar{E}_M$ and $\widetilde{E}_M$ that satisfy

$$|E_i| \le E_M \mathbf{1}_{n\times 1},\ |E_i - \widehat{E}_i| \le \bar{E}_M \mathbf{1}_{n\times 1},\ \lim_{t\to t_o} |E_i(t) - \widehat{E}_i(t)| \le \widetilde{E}_M \mathbf{1}_{n\times 1}$$

Based on the obtained boundedness conditions, the following smooth projection function (Fei *et al.* 2020) $\bar{\mathcal{S}}(\mathcal{V}, \tau_M, \psi_M)$ is introduced to improve the performance of the proposed controller:

$$\bar{\mathcal{S}}(\mathcal{V}(j), \tau_M, \psi_M) = \begin{cases} \tau_M + \psi_M(1 - \mathrm{e}^{(\tau_M - \mathcal{V}(j))/\psi_M}), & \text{if } \mathcal{V}(j) > \tau_M \\ \mathcal{V}(j), & \text{if } |\mathcal{V}(j)| \le \tau_M \\ \psi_M(\mathrm{e}^{(\tau_M + \mathcal{V}(j))/\psi_M} - 1) - \tau_M & \text{if } \mathcal{V}(j) < -\tau_M \end{cases} \tag{5.28}$$

where $\mathcal{V}(j)$ denotes the jth element of the column vector $\mathcal{V}$, τ_M is a positive constant, and ψ_M denotes a small positive constant. Then define $u_{m,i} \in \mathbb{R}^n$ to be the control input to maintain the velocity tracking behaviour for the ith agent:

$$u_{m,i} = \widehat{g}_i^{-1}(\dot{x}_{di} - \bar{\mathcal{S}}(\widehat{E}_i, E_M, \psi_E)) \tag{5.29}$$

where ψ_E is a small positive constant.

To attenuate the reverse effect of saturation phenomenon, we propose a control input distribution algorithm (CIDA) that generates a positive variable $\bar{\xi}_i$ to shrink $u_{e,i}$ as shown in Algorithm 2. The CIDA keeps monitoring if the nominal control input $u^i_{\text{nom}} = u_{m,i} + u_{e,i}$ triggers the reverse effect. If the nominal control input does not exceed the saturation limit, then the controller will run at its maximum effort within the saturation limitation. Otherwise, a series of calculation is performed to generate a shrinking factor $\bar{\xi}_i \in (0, 1]$ for each agent to reduce the scenarios where $\text{sign}(\widehat{g}_i u_i) \neq \text{sign}(\widehat{g}_i \mathcal{S}_i(u_i))$. Based on the discussions about the neural-based observer (5.20), the weight tuning law set (5.21), the formation maintaining control input (5.29), and Algorithm 2, the final controller design is given as

$$\bar{u}_i = \bar{\mathcal{S}}(u_{m,i}, \tau_i, \psi_u) + \bar{\xi}_i u_{e,i} \tag{5.30}$$

where $\mathcal{S}(\bar{u}_i, U_{Mi}) = \bar{u}_i$ is guaranteed by Algorithm 2.

Based on the results of neural-based observer and the CIDA, the final system design of this section is given in Fig. 5.2.

The results on the new saturated formation controller design is given as the following theorem:

Algorithm 2: Control Input Distribution Algorithm

Input: $\bar{\mathcal{S}}(u_{m,i}, \tau_i, \psi_u)$,$u_{e,i}$,$U_{Mi}$

Output: $\bar{\xi}_i$

$\bar{\xi}_{min} = 1$;

$u^i_{\text{nom}} = \bar{\mathcal{S}}(u_{m,i}, \tau_i, \psi_u) + u_{ei}$;

$u^i_{\text{sat}} = \bar{\mathcal{S}}(u^i_{\text{nom}}, U_{Mi}, 0)$;

if $u^i_{\text{nom}} \neq u^i_{\text{sat}}$ **then**

  $u_{up} = U_{Mi}\mathbf{1}_{n\times 1} - \bar{\mathcal{S}}(u_{m,i}, \tau_i, \psi_u)$;

  $u_{lo} = -U_{Mi}\mathbf{1}_{n\times 1} - \bar{\mathcal{S}}(u_{m,i}, \tau_i, \psi_u)$;

  for $j = 1 : n$ **do**

    if $u_{e,i}(j) = 0$ **then**

      $\bar{\xi}_i = 1$;

    else

      if $u_{e,i}(j) > 0$ **then**

        $\bar{\xi}_i = u_{up}(j)/u_{e,i}(j)$;

      else

        $\bar{\xi}_i = u_{lo}(j)/u_{e,i}(j)$;

      end

    end

    $\bar{\xi}_{min} = \min(\bar{\xi}_i, \bar{\xi}_{min})$;

  end

end

$\bar{\xi}_i = \bar{\xi}_{min}$;

Return $\bar{\xi}_i$;

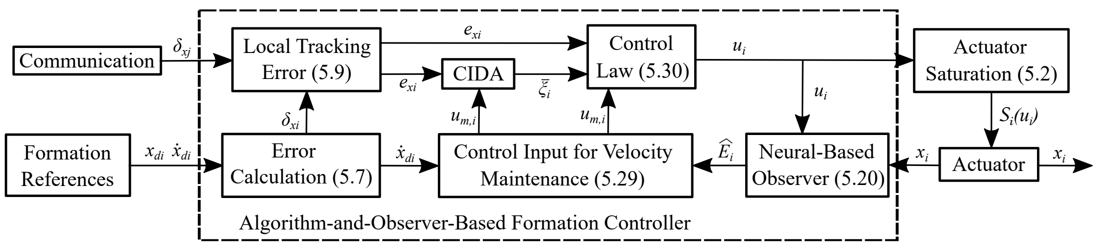

Figure 5.2. Algorithm-and-observer-based formation controller.

Theorem 5.3. *Consider system* (5.4) *with actuator saturation* (5.2), *and Assumptions 5.1-5.5 hold. By the finite-time neural-based observer* (5.20), *the weight tuning law set* (5.21), *the formation control law* (5.30), *and the CIDA (Algorithm 2), the error states* e_x *and* δ_x *are* *semi-globally UUB within the following regions, respectively*

$$\|e_x\| \leq \frac{\overline{\sigma}(Q)\widetilde{E}_M nN}{\bar{k}\underline{\sigma}(Q)}, \ \|\delta_x\| \leq \frac{\overline{\sigma}(Q)\widetilde{E}_M nN}{\bar{k}\underline{\sigma}(Q)\underline{\sigma}(L+B)} \tag{5.31}$$

if the following conditions are met simultaneously:

1. η_2, η_3 *and* η_4 *in* (5.21) *satisfy* $\eta_2 > \eta_3/2$ *and* $\eta_4 > \eta_3/2$
2. k_i *in* (5.30) *satisfies* $k_i = \bar{k} > 0 (i = 1, 2, \dots, N)$
3. ψ_u *in* (5.30) *satisfies* $\psi_u < \bar{U}_{Mi} - \widetilde{E}_M - \epsilon_E$
4. *The compact set conditions of the NNs hold such that either* $E_i \in \Omega_E$ *or* $y_i \in \Omega_y$ *is satisfied when* $t \geq t_0$

Proof. With the implementation of the shrinking factor $\bar{\xi}_i$ generated by Algorithm 2, it is hard to use Lyapunov functions to directly obtain a result for the stability analysis. Therefore, it is essential to first illustrate that the value of $\bar{\xi}_i$ will converge to one within finite time for each individual agent. Afterwards, the Lyapunov stability theory is employed to prove that e_x is semi-globally UUB.

The formation tracking procedure of the ith agent is divided into the following three stages:

1. When $t \leq t_f = \max(t_s, t_o)$ and $\bar{\xi}_i \in [0, 1)$.
2. When $t > t_f = \max(t_s, t_o)$ and $\bar{\xi}_i \in [0, 1)$.
3. When $t > t_f = \max(t_s, t_o)$ and $\bar{\xi}_i = 1$.

To analyse the transformation from one stage to another, the following Lyapunov function is constructed regarding the formation tracking error of system (5.4):

$$V_{4,4} = \frac{1}{2} e_x^{\mathrm{T}} P \otimes I_n e_x$$

Then the time derivative is obtained as

$$\dot{V}_{4,4} = e_x^{\mathrm{T}} P (L+B) \otimes I_n (\widehat{g}\mathcal{S}(\bar{u}) + E - \dot{x}_d)$$

where $\bar{u} = [\bar{u}_1^{\mathrm{T}}, \bar{u}_2^{\mathrm{T}}, \ldots, \bar{u}_N^{\mathrm{T}}]^{\mathrm{T}}$. Based on the knowledge of $\mathcal{S}(\bar{u}_i, U_{Mi}) = \bar{u}_i$, one has

$$\dot{V}_{4,4} = e_x^{\mathrm{T}} P(L+B) \otimes I_n(\hat{g}\bar{u} + E - \dot{x}_d) \tag{5.32}$$

For the first stage, consider one extreme circumstance that equations $\bar{\xi}_i = 0$ and $|\widetilde{E}_i| = \bar{E}_M \mathbf{1}_{n\times 1}$ remain true until time t_f, when the neural-based observer is settled and the formation tracking task is achievable. With $|\bar{\mathcal{S}}(u_{m,i}, \tau_i, \psi_u)| \leq |u_{m,i}|$, the following equation is obtained:

$$\dot{e}_x = (L+B) \otimes I_n(\bar{E}_M \mathbf{1}_{nN\times 1})$$

With $(L \otimes I_n)\bar{E}_M \mathbf{1}_{nN\times 1} = \mathbf{0}_{nN\times 1}$, one has $|\dot{e}_x| \leq \overline{\sigma}(B)\bar{E}_M \mathbf{1}_{nN\times 1}$, which further leads to

$$|e_x(t_f)| \leq |e_x(t_0)| + t_f \overline{\sigma}(B)\bar{E}_M \mathbf{1}_{nN\times 1}$$

After the finite time t_f, the system (5.4) is at the second stage, where (5.32) is expressed as

$$\dot{V}_{4,4} = e_x^{\mathrm{T}} P(L+B) \otimes I_n(\widetilde{E} - \bar{k}\bar{\xi} \otimes I_n e_x)$$

where

$$\bar{\xi} = \mathrm{diag}\{\bar{\xi}_1, \bar{\xi}_2, \ldots, \bar{\xi}_N\},\ \widetilde{E} = [\widetilde{E}_1^{\mathrm{T}}, \widetilde{E}_2^{\mathrm{T}}, \ldots, \widetilde{E}_N^{\mathrm{T}}]^{\mathrm{T}}$$

If define $\bar{U}_{Mi} = U_{Mi} - \tau_i$ to represent the minimum amplitude of the accessible control input for error reduction, it is reasonable to have $\widetilde{E}_M < \bar{U}_{Mi}$ for every agent when $t \geq t_f$.

Define $\underline{e}_x = \min(|e_x|)$ and $\bar{e}_x = \max(|e_x|)$ to represent channels with the lowest and the highest amplitude in vector e_x, respectively. By $\psi_u < \bar{U}_{Mi} - \widetilde{E}_M$, if define $\widetilde{U}_{Mi} = \bar{U}_{Mi} - \widetilde{E}_M - \psi_u$ to represent the least amount of residual control input for each agent, it is confident to say that the available control input can reduce the amplitude $\bar{e}_x$ with the speed of

$$\frac{d|\bar{e}_x|}{dt} \leq -\underline{\sigma}(L+B)\widetilde{U}_{Mi}$$

For other channels, consider the extreme scenario where $\dot{e}_{xi}(j)e_{xi}(j) > 0$ is satisfied when $|e_{xi}(j)| < |\bar{e}_x|$. Because the controller parameter k_i is chosen as $k_i = \bar{k}$ for each individual agent, $|e_{xi}(j)|$ will increase until $|e_{xi}(j)| = |\bar{e}_x|$, leading to

$$\begin{cases} \dot{e}_{xi}(j) \leq -\underline{\sigma}(L+B)\widetilde{U}_{Mi}, & \text{if } \bar{e}_x \geq 0 \\ \dot{e}_{xi}(j) \geq \underline{\sigma}(L+B)\widetilde{U}_{Mi}, & \text{if } \bar{e}_x < 0 \end{cases}$$

Thus, the parameter $\bar{\xi}_i$ is expected to converge to 1 within the finite time of

$$t_{\bar{\xi}} = \frac{|\bar{e}_x(t_0)| + t_f \overline{\sigma}(L+B)\bar{E}_M - \widetilde{U}_{Mi}/\bar{k}}{\underline{\sigma}(L+B)\widetilde{U}_{Mi}}$$

Finally, every agent will achieve the third stage after the finite time of $t_f + t_{\bar{\xi}}$ to have the following results:

$$\begin{aligned} \dot{V}_{4,4} &= e_x^{\mathrm{T}} P(L+B) \otimes I_n(-\bar{k}e_x + \widetilde{E}) \\ &= -\frac{\bar{k}}{2} e_x^{\mathrm{T}} Q \otimes I_n e_x + \frac{1}{2} e_x^{\mathrm{T}} Q \otimes I_n \widetilde{E} \\ &\leq -\frac{\bar{k}}{2} \underline{\sigma}(Q)\|e_x\|^2 + \frac{1}{2}\overline{\sigma}(Q)\|e_x\|\|\widetilde{E}\| \end{aligned} \tag{5.33}$$

Hence, $\dot{V}_{4,4}$ will remain negative unless the following equations are satisfied:

$$\|e_x\| \leq \frac{\overline{\sigma}(Q)\widetilde{E}_M nN}{\bar{k}\underline{\sigma}(Q)}, \ \|\delta_x\| \leq \frac{\overline{\sigma}(Q)\widetilde{E}_M nN}{\bar{k}\underline{\sigma}(Q)\underline{\sigma}(L+B)} \tag{5.34}$$

Note that the neural-based observer (5.20) only holds semi-global stability. Hence, by Lemma 2.1, both e_x and δ_x are semi-globally UUB, which completes the proof. □

Remark 5.2. *In* (5.21)*, parameters η_1 and η_3 both act as the NN's sensitivity to the observation error $\widetilde{x}_i$. Hence, if the values of η_1 and η_3 are increased, the convergence neighbourhood of $\|\widetilde{x}_i\|$* (5.24) *will shrink in theory. However, if the values of η_1 and η_3 are set to be very high, the NN in* (7.9) *will be over-sensitive to errors, leading to oscillations in its output. On the other hand, both η_2 and η_4 act as the damper to stop the weight matrix from changing rapidly. Hence, increasing the values of η_2 and η_4 will decrease the amount of chattering in network output, but it will also extend the convergence time of the observation error.*

Remark 5.3. *The constant matrix γ_i in* (5.20) *acts as the observer's sensitivity to the error-related term* $\mathrm{diag}\{\mathrm{sign}(\widetilde{x}_i)\}|\widetilde{x}_i|^{\beta_i}$*. By both* (5.24) *and* (5.26)*, it is expected that the convergence region of $\|\widetilde{x}_i\|$ will shrink if the value of $\underline{\sigma}(\gamma_i)$ is increased. The effect of β_i is comparatively complex. When $\|\widetilde{x}_i\| \leq 1$, setting β_i close to* 0.5 *will bring faster convergence speed. However, due to the characteristics of the fractional-order term, choosing β_i close to* 1 *will lead to a faster convergence when $|\widetilde{x}_i| > \mathbf{1}_{n\times 1}$.*

Remark 5.4. *The purpose of employing the smooth projection law in* (5.29) *is to restrict the effect of $\widehat{E}_i$, which will attenuate chattering in the control input u_i and system state x_i if the states in the neural-based observer are experiencing oscillation. Regarding the proportional parameter k_i in term $u_{e,i}$, a rise in its value will result in a decrease in the ultimate convergence region of both δ_x and e_x (see* (5.34)*).*

Remark 5.5. *The purpose of Assumption 5.5 is to ensure that the initial estimation error of the neural-based observer is bounded. Related parameters are also useful to prove the finite-time convergence of observation error $\widetilde{x}_i$ and the shrinking factor $\bar{\xi}_i$.*

5.3.6 Simulation results and discussions

To justify the performances of the proposed neural-based observer (5.20), the CIDA (Algorithm 2) and the distributed formation control law (5.30), simulations and comparisons regarding a multi-robot system are provided.

Consider a multi-robot system that contains six ODRs (Fei *et al.* 2022a), and the dynamics of the ith robot is given as the following equation as mentioned in Chapter 2:

$$\dot{x}_i = T_f(\theta_i, R_i)u_i + \bar{\omega}_i$$

where $x_i = [p_i^x, p_i^y, \theta_i]^{\mathrm{T}}$ denotes the state vector that contains the position and orientation information of the robot, $u_i = [u_i^1, u_i^2, u_i^3]^{\mathrm{T}}$ represents the speed vector of the robot's motors and $\bar{\omega}_i$ is the external disturbance vector.

With the existence of measurement error, it is hard for us to get the precise value of R_i. Hence, the parameter value that is measured and employed in the controller design process is illustrated as $\widehat{R}_i$. The value of R_i, $\widehat{R}_i$ and the initial state values are provided in Table 5.1. The actuator saturation limit is set as $U_{Mi} = 0.25$ by Assumption 5.2.

The communication topology is chosen as Fig. 5.3 and $b_i = 2$. The system uncertainties and formation references are chosen as follows, respectively:

$$\begin{aligned} \bar{\omega}_i = {} & [0.02\cos(0.5t + \pi/2) + 0.03e^{-|p_i^x|-1}, 0.03\sin(0.2t) + 0.02\tanh(p_i^y), \\ & 0.04\sin(0.1t + \theta_i) + 0.01\tanh(\theta_i)]^{\mathrm{T}}, \\ x_{di} = {} & [2\cos(-0.15t + \pi) + 2\cos(i\pi/3) - 1, 2\sin(i\pi/3) + 2\sin(-0.15t + \pi), 0]^{\mathrm{T}}, \\ & i = 1, 2, \ldots, 6 \end{aligned} \tag{5.35}$$

To justify the effectiveness of our designs, simulations based on the following four controller designs are conducted:

1. The cooperatively tuned formation controller design (CTFC) that uses (5.12) as the weight tuning law. The control input is chosen as $u_i = \bar{\mathcal{S}}(u_{c,i}, \bar{\tau}_i, \bar{\psi}_i)$, where $u_{c,i} = \widehat{g}_i^{-1}(\dot{x}_{di} - \widehat{E}_i - k_i e_{xi})$, $\bar{\tau}_i = 0.24$ and $\bar{\psi}_i = 0.01$.

Table 5.1. Model parameters and initial states of six saturated first-order ODRs.

Robot number	Model parameters		Initial states					
	R_i(m)	$\widehat{R}_i$(m)	p_i^x(m)	p_i^y(m)	θ_i(rad)	$\widehat{p}_i^x$(m)	$\widehat{p}_i^y$(m)	$\widehat{\theta}_i$(rad)
1	0.24	0.21	-0.2	-0.7	$-\pi/4$	0	-0.3	$-\pi/5$
2	0.23	0.25	1.6	3.6	$-\pi/5$	1.4	3.3	$-\pi/6$
3	0.30	0.33	-4	-2.4	$\pi/3$	-3.7	-2.1	$\pi/4$
4	0.28	0.24	-1.9	-1.1	$\pi/4$	-1.6	-0.8	$\pi/6$
5	0.25	0.28	-1.6	-4.6	$-\pi/3$	-1.1	-4.1	$-\pi/4$
6	0.32	0.29	3.6	-1.5	$-\pi/6$	3.9	-1.9	$-\pi/5$

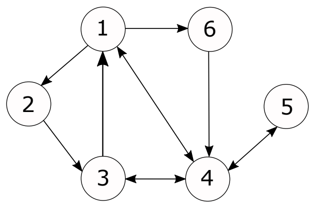

Figure 5.3. The strongly connected topology of the multi-ODR system.

2. The restricted cooperatively tuned formation controller design (RCTFC) that uses (5.12) as the weight tuning law. The control input is chosen as $u_i = \bar{\mathcal{S}}(u_{c,i}, \bar{\tau}_i, \bar{\psi}_i)$, where $u_{c,i} = u_{m,i} + u_{e,i}$, $E_M = 0.10$, $\bar{\tau}_i = 0.24$ and $\bar{\psi}_i = \psi_E = 0.01$.

3. The observer-based formation controller design (OBFC) that implements the proposed neural-based observer (5.20) and the weight tuning law (5.21). Algorithm 2 is not applied and the controller is chosen as $u_i = \bar{\mathcal{S}}(u_{o,i}, \bar{\tau}_i, \bar{\psi}_i)$, where $u_{o,i} = u_{e,i} + \bar{\mathcal{S}}(u_{m,i}, \tau_i, \psi_i)$, $\bar{\tau}_i = 0.24$, $\tau_i = 0.22$, $E_M = 0.10$ and $\psi_i = \psi_E = \bar{\psi}_i = 0.01$.

4. The algorithm-and-observer-based formation cont-roller design (AOBFC) that has the neural-based observer (5.20) tuned by (5.21). Algorithm 2 is implemented to generate the shrinking factor $\bar{\xi}_i$ and the controller is designed as (5.30), where $\tau_i = 0.22$, $E_M = 0.10$ and $\psi_E = \psi_u = 0.01$.

The tuning parameters of the NN are chosen as $\eta_1 = 15$, $\eta_2 = 0.1$, $\eta_3 = 0.1$ and $\eta_4 = 0.06$ in all simulations. Initially, $\widehat{J}_i(0)$ is chosen as a random 6×5 matrix with

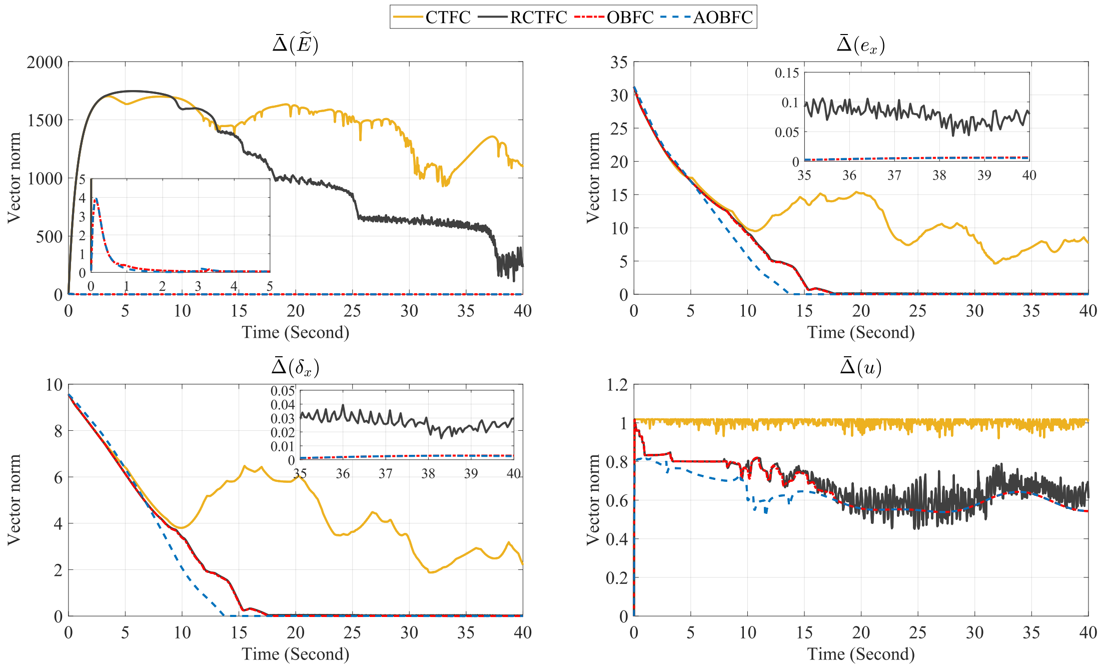

Figure 5.4. Merits of using the neural-based observer over using the cooperative tuning design.

elements whose norms are less than 1 and $\widehat{W}_i(0)$ is chosen as a 5×3 zero matrix. For the designs that employ neural-based observer (5.20), the parameters are chosen as $\beta_i = 0.9$ and $\gamma_i = \text{diag}\{12, 12, 18\}$.

The proportional parameter k_i in $u_{e,i}$ is chosen as $k_i = \bar{k} = 3$ for every agent in each simulation. To compare the performance of different designs, define the Euclidean-norm calculation of an arbitrary column vector $\mathcal{V}$ as $\bar{\Delta}(\mathcal{V}) = \sqrt{\mathcal{V}^{\mathrm{T}}\mathcal{V}}$. To illustrate the merits of the neural-based observer (Theorem 5.2) over the cooperative tuning approach (Theorem 5.1), the trends of $\bar{\Delta}(\widetilde{E})$, $\bar{\Delta}(e_x)$, $\bar{\Delta}(\delta_x)$ and $\bar{\Delta}(u)$ are provided in Fig. 5.4. The semi-globally UUB region and convergence time of each method are recorded in Table 5.2.

Although the norm of e_x and δ_x are both semi-globally UUB for the CTFC design, it is hard to say that the system error states converged due to the high value of $b_{\widetilde{E}}$ (over 1000). Adding an extra smooth projection function to restrict the amplitudes of the NN output can lead to a success converge for both e_x and δ_x in RCTFC, but the accuracy of the NN is far from sufficient ($\bar{\Delta}(\widetilde{E}) \geq 100$). Furthermore, the control input of the RCTFC is also filled with chattering (see $\bar{\Delta}(u)$ in Fig. 5.4), which indicates the cooperative tuning method (5.12) is not suitable when the actuators are restricted by saturation phenomenon.

Table 5.2. Performance comparison of four control schemes.

Design	Semi-globally UUB region				Convergence time			
	$b_{\widetilde{E}}$	b_{e_x}	b_{δ_x}	b_u	$t_{\widetilde{E}}$	t_{e_x}	t_{δ_x}	t_u
CTFC	1.4×10^3	8.5	3.1	1.1	–	–	–	–
RCTFC	4.2×10^2	1.5×10^{-1}	5.5×10^{-2}	8.0×10^{-1}	37.7 s	17.6 s	17.6 s	10.1 s
OBFC	4.8×10^{-2}	1.5×10^{-2}	5.0×10^{-3}	6.5×10^{-1}	13.2 s	16.0 s	17.8 s	17.0 s
AOBFC	5.3×10^{-2}	1.5×10^{-2}	5.0×10^{-3}	6.5×10^{-1}	4.2 s	14.0 s	14.3 s	10.0 s

On the contrary, $\bar{\Delta}(\widetilde{E})$ of the neural-based observer (5.20) in AOBFC is bounded within the region of 0.053 in 4.2 seconds, which proves the validity of the finite-time characteristics claimed in Theorem 5.2. Besides, the local formation tracking error e_x and the reference tracking error δ_x are semi-globally UUB within 0.015 and 0.005, respectively. As a result, the existence of Problem 5.1 and the validity Theorem 5.2 are both illustrated. Hence, the neural-based observer design (5.20) is a method more suitable than the cooperative tuning design (5.12) for systems with actuator saturation.

To verify the existence of the reverse effect mentioned in Problem 5.2, the values of each agent's local formation tracking error e_{xi} in the first 20 seconds are recorded and presented in Fig. 5.5. It is observed that every agent with the OBFC design experiences oscillation in the value of e_θ and part of the agents have fluctuated trends in e_x (ODRs one, three, four and six) and e_y (ODRs two, five and six), which indicates the existence of the reverse effect. In comparison, most of the state fluctuations are attenuated in the AOBFC design. To validate that the CIDA algorithm is also capable to restrict the amplitudes of the control input within the saturation limit to satisfy $\mathcal{S}(\bar{u}_i, U_{Mi}) = \bar{u}_i$, the curves of each agent's control input are shown in Fig. 5.6.

The evolution of the shrinking factor $\bar{\xi}_i$ in Algorithm 2 is provided in Fig. 5.7, where it is observed that each $\bar{\xi}_i$ converges to one within the finite time of 13.8 seconds, illustrating the validity of Theorem 5.3. However, the proposed CIDA algorithm cannot completely avoid the reverse effect mentioned in Problem 5.2 (see ODR three in Fig. 5.5). As stated in the proof of Theorem 5.3, the factor $\bar{\xi}_i$ is determined by both the accessible control input amplitude $\bar{U}_{Mi}$ and the maximum error amplitude in e_{xi}. Hence,

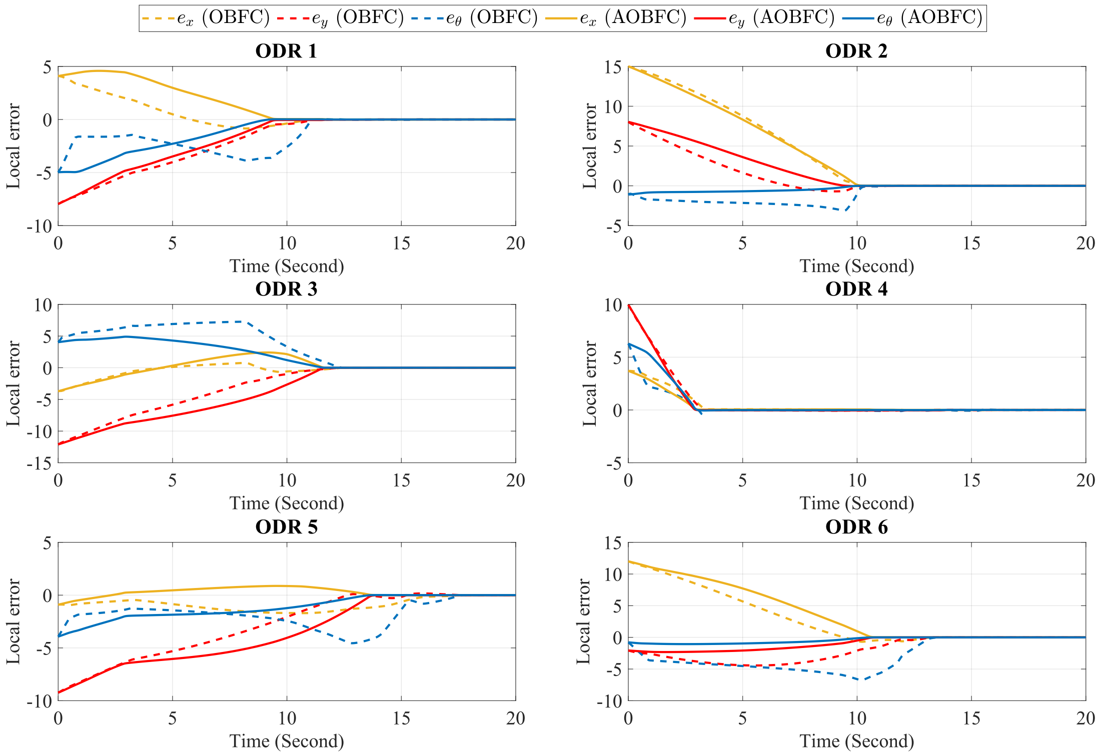

Figure 5.5. Illustration of the reverse effect and the merits of implementing CIDA.

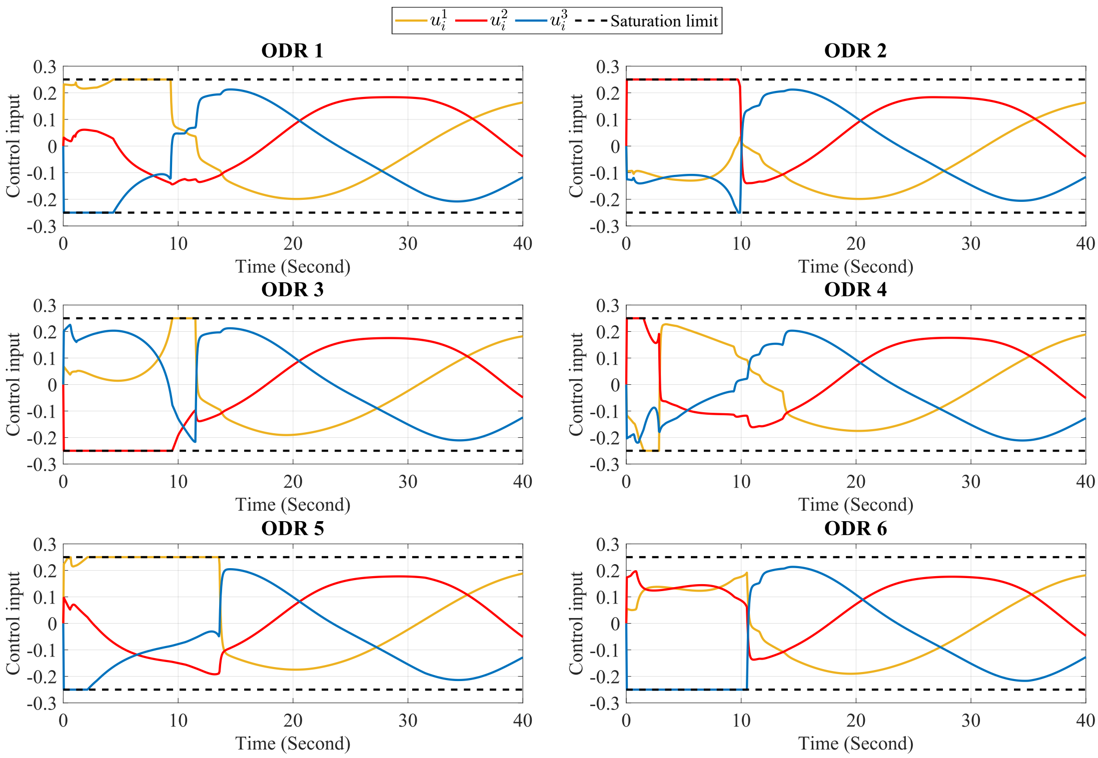

Figure 5.6. Evolution of control inputs in AOBFC.

when one channel (p_i^y channel in e_{x3}) has a significant amount of error over other channels (p_i^x channel in e_{x3}), the channels with small error amplitudes can be overshadowed due to a low value of $\bar{\xi}_i$, which leads to an increment of e_x. This circumstance is eased when the amplitude of different channels in the error vector achieves similar values or the shrinking factor $\bar{\xi}_i$ rises to higher values (see ODR three in Fig. 5.5 and Fig. 5.7 around ten seconds).

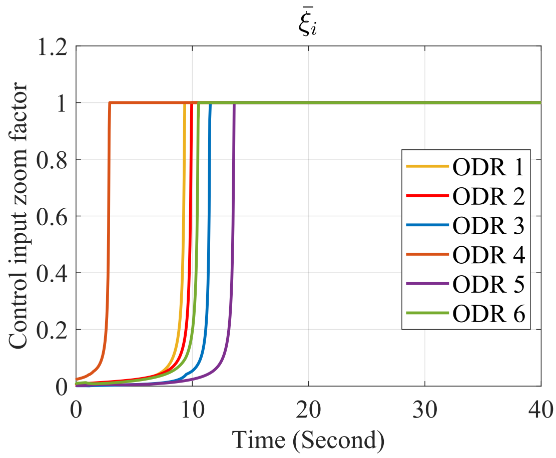

Figure 5.7. Shrinking factor $\bar{\xi}_i$.

To monitor the formation tracking behaviour of the system (5.4), the trajectories of all agents are recorded in Fig. 5.8. It is observed that the entire system is able to track the desired time-varying circular formation (5.35) (a circular formation whose centre is moving in a circular trajectory) with the existence of model uncertainty, external disturbances and actuator saturation, which concludes the effectiveness of the proposed formation control scheme (5.30) and the CIDA (Algorithm 2).

Remark 5.6. *In all simulations, the system uncertainty is chosen as* (5.35)*, which is a function related to both the system state x_i and the task time t. In practice, the relationship between the actual system state x_i and the task time t should be a continuous but unknown function $x_i = \mathcal{F}(t)$. In theory, the task time t can be seen as an unknown function whose variable is system state x_i, further leading to $t = \mathcal{G}(x_i)$. Hence, both the system uncertainty $\bar{w}_i$ and the overall system uncertainty E_i can be treated as an unknown function that use x_i as the variable, which indicates that the estimation process* (7.9) *is valid.*

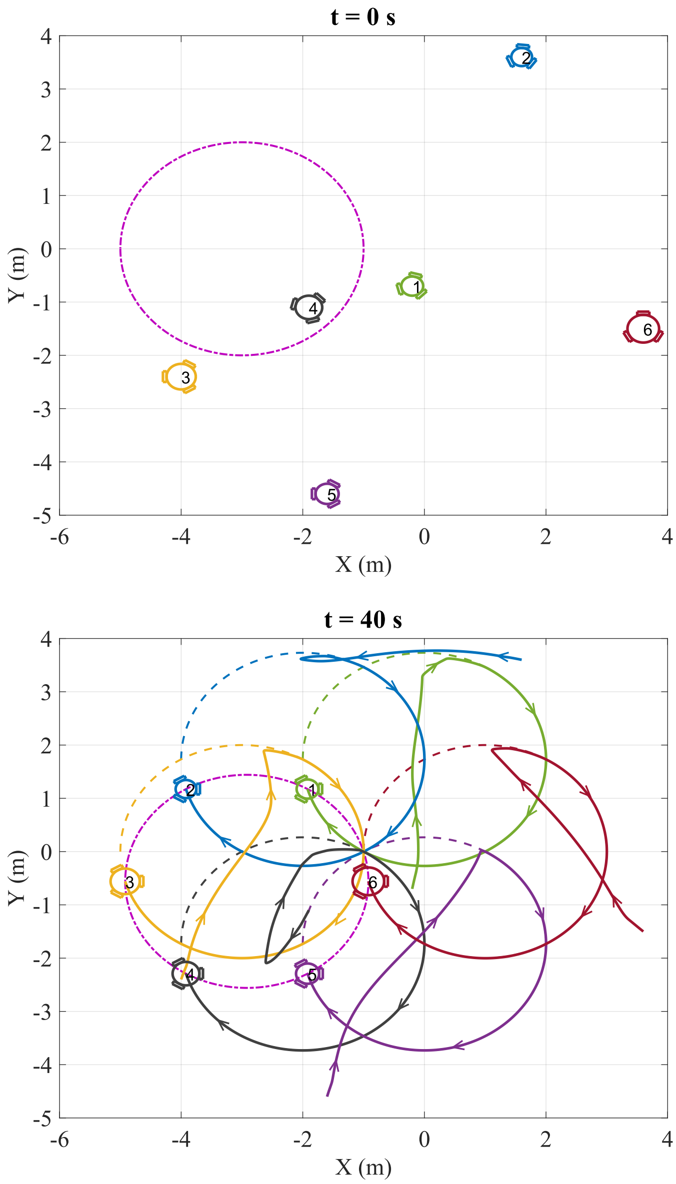

Figure 5.8. Trajectories of the multi-robot system while applying the AOBFC design.

5.4 Practical formation control of multi-robot systems

Although the NN-based estimation process is able to approximate the unknown factors within bounded error, such complex structure does increase the computational burden of each agent. Hence, it is necessary to develop an adaptive estimation structure with less complexity.

In this section, a new adaptive observer design is proposed to obtain global stability in both the estimation process and the control process. The CIDA structure will also be modified to check if there is an alternative approach to design a saturated controller.

5.4.1 Adaptive observer design with global stability

To ensure global stability, the method of employing the NN structure is no longer available. Instead of relying on one particular kind of estimation tool, it is also reasonable to consider the uncertainty approximation issue in the perspective of controller design. To illustrate such idea, construct the following imaginary system according to the dynamics of the individual agents (5.3):

$$\dot{\widehat{x}}_i = \widehat{g}_i u_i + \widehat{u}_i \tag{5.36}$$

where $\widehat{u}_i \in \mathcal{R}^n$ is the control input of the imaginary system.

Then the error dynamics of the imaginary system is given as

$$\dot{\widetilde{x}}_i = E_i - \widehat{u}_i \tag{5.37}$$

Accordingly, when $\widetilde{x}_i$ achieve the equilibrium point to have $\|\widetilde{x}_i\| = 0$, the condition of $E_i = \widehat{u}_i$ is also satisfied. Hence, it is reasonable to transfer the above uncertainty approximation problem into the controller design problem of (5.36). The following assumption is made to establish the observers with global stability:

Assumption 5.6. *The uncertain factor E_i is bounded such that $\|E_i\| \leq E_M^1$ and $\|\dot{E}_i\| \leq E_M^2$ are satisfied simultaneously. The control gain matrix is bounded such that there are positive constants g_M^1 and g_M^2 that satisfy the following inequalities:*

$$\|\widehat{g}\|_F \leq g_M^1, \; \|\dot{\widehat{g}}\|_F \leq g_M^2$$

Based on the designs proposed in the previous part of the thesis, the control input $\widehat{u}_i$ can be designed in an adaptive way as follows:

$$\widehat{u}_i = \widehat{E}_i + \widetilde{k}_i \widetilde{x}_i \tag{5.38}$$

where the term $\widehat{E}_i$ is defined as an adaptive term that is sensitive to $\widetilde{x}_i$ and $\widetilde{k}_i$ is a positive definite diagonal matrix. Inspired by the tuning laws of NNs, the self adaptive law of $\widehat{E}_i$ is given as

$$\dot{\widehat{E}}_i = \eta_5 \widetilde{x}_i - \eta_6 \widehat{E}_i \tag{5.39}$$

where η_5 and η_6 are both positive definite diagonal matrices. To illustrate the estimation error regarding E_i, define $\widetilde{E}_i = E_i - \widehat{E}_i$.

The results on the adaptive observer with global stability is given as the following theorem:

Theorem 5.4. *Consider system* (5.3) *with actuator saturation* (5.2)*, where Assumptions 5.1 and 5.6 hold. By the imaginary system* (5.36)*, the imaginary control input* (5.38)*, and the adaptive law* (5.39)*, the uniform ultimate boundedness of $\widetilde{x}_i$ and $\widetilde{E}_i$ is guaranteed if the control input satisfies $u_i = \mathcal{S}(u_i, U_{Mi})$.*

Proof. Consider the following Lyapunov candidate for the ith agent:

$$V_{4,5} = \frac{1}{2}\widetilde{x}_i^{\mathrm{T}}\eta_5\widetilde{x}_i + \frac{1}{2}\widetilde{E}_i^{\mathrm{T}}\widetilde{E}_i$$

Then the time derivative of $V_{4,5}$ is given as

$$\begin{aligned}
\dot{V}_{4,5} &= \widetilde{x}_i^{\mathrm{T}}\eta_5\dot{\widetilde{x}}_i + \widetilde{E}_i^{\mathrm{T}}\dot{\widetilde{E}}_i \\
&= \widetilde{x}_i^{\mathrm{T}}\eta_5(E_i - \widehat{u}_i) + \widetilde{E}_i^{\mathrm{T}}(\dot{E}_i - \dot{\widehat{E}}_i) \\
&= \widetilde{x}_i^{\mathrm{T}}\eta_5(\widetilde{E}_i - \widetilde{k}_i\widetilde{x}_i) + \widetilde{E}_i^{\mathrm{T}}\dot{E}_i - \widetilde{E}_i^{\mathrm{T}}(\eta_5\widetilde{x}_i - \eta_6\widehat{E}_i) \\
&= -\widetilde{x}_i^{\mathrm{T}}\eta_5\widetilde{k}_i\widetilde{x}_i + \widetilde{E}_i^{\mathrm{T}}\dot{E}_i - \widetilde{E}_i^{\mathrm{T}}\eta_6\widetilde{E}_i + \widetilde{E}_i^{\mathrm{T}}\eta_6 E_i
\end{aligned}$$

By Assumption 5.6, an alternative version of $\dot{V}_{4,5}$ is given as

$$\begin{aligned}
\dot{V}_{4,5} &\leq -\underline{\sigma}(\widetilde{k}_i)\underline{\sigma}(\eta_5)\|\widetilde{x}_i\|^2 - \underline{\sigma}(\eta_6)\|\widetilde{E}_i\|^2 + E_M^2\|\widetilde{E}_i\| + \overline{\sigma}(\eta_6)E_M^1\|\widetilde{E}_i\| \\
&\leq -\chi_{4,1}^{\mathrm{T}}H_{4,1}\chi_{4,1} + h_{4,1}\chi_{4,1}
\end{aligned}$$

where

$$H_{4,1} = \begin{bmatrix} \underline{\sigma}(\eta_5)\underline{\sigma}(\widetilde{k}_i) & 0 \\ 0 & \underline{\sigma}(\eta_6) \end{bmatrix}, \; h_{4,1} = \begin{bmatrix} 0 & E_M^2 + \overline{\sigma}(\eta_6)E_M^1 \end{bmatrix}, \; \chi_{4,1} = \begin{bmatrix} \|\widetilde{x}_i\| \\ \|\widetilde{E}_i\| \end{bmatrix}$$

By Lemma 3.1, both $\|\widetilde{x}_i\|$ and $\|\widetilde{E}_i\|$ are UUB within the following neighbourhoods, respectively:

$$\begin{aligned}
\Omega_{\widetilde{x}}^2 &= \left\{ \widetilde{x}_i \middle| \|\widetilde{x}_i\| \leq \frac{E_M^2 + \overline{\sigma}(\eta_6)E_M^1}{\underline{\sigma}(H_{4,1})} \right\} \\
\Omega_{\widetilde{E}} &= \left\{ \widetilde{E}_i \middle| \|\widetilde{E}_i\| \leq \frac{E_M^2 + \overline{\sigma}(\eta_6)E_M^1}{\underline{\sigma}(H_{4,1})} \right\}
\end{aligned}$$

which completes the proof. □

After modifying the observer design, it is also essential to update the formation control law to achieve the boundedness of the formation tracking error.

5.4.2 Observer-based robust formation controller

Although the CIDA proposed in Section 5.3 works, it does require some preliminary information that is hard to obtain (such as the value of τ_i Assumption 5.2). Hence, it is vital to find an alternative method that could increase the practicality of the control design. To ease the requirement on the accessible information, Assumption 5.2 is further modified as follows:

Assumption 5.7. *There is an unknown positive constant τ_i and a finite time t_s for the ith agent such that the following inequality is satisfied when $t \geq t_s$*

$$|g_i^{-1}(t)(\dot{x}_{di}(t) - f_i(x_i(t)) - \varpi_i(t))| \leq \tau_i \mathbf{1}_{n\times 1}$$

where $\tau_i < U_{Mi}$ and $\mathbf{1}_{n\times 1}$ is an n-dimensional column vector whose every entry is one.

Inspired by the auxiliary variable design (Han *et al.* 2019), a new adaptive auxiliary variable ξ_i is defined for the ith agent, which further leads to the following nominal controller design:

$$u_i^{\text{nom}} = \widehat{g}_i^{-1}(\dot{x}_{di} - k_e e_{xi} - \widehat{u}_i - k_\xi \xi_i) \tag{5.40}$$

where k_e and k_ξ are both positive definite diagonal matrices.

The adaptive law of the auxiliary variable is set as

$$\dot{\xi}_i = \eta_7 \widehat{g}_i (u_i^{\text{nom}} - \mathcal{S}(u_i^{\text{nom}}, U_{Mi})) - \eta_8 \xi_i \tag{5.41}$$

where η_7 and η_8 are both positive definite diagonal matrices. Accordingly, the formation control law is given as

$$u_i = \mathcal{S}(u_i^{\text{nom}}, U_{Mi}) \tag{5.42}$$

Based on the above discussions, the observer-based design presented in this chapter can be illustrated as the diagram in Figure 5.9, and final result of the observer-based formation controller is given as the following theorem:

Theorem 5.5. *Consider a cluster of nonlinear first-order agents* (5.4) *with actuator saturation* (5.2), *where Assumption 5.1, 5.6 and 5.7 hold. By the adaptive observer* (5.36), *the estimation tuning law* (5.39), *the auxiliary tuning law* (5.41) *and the compensated formation control law* (5.42), *then ξ_i, e_x and δ_x are all semi-globally UUB if the controller parameters are chosen*

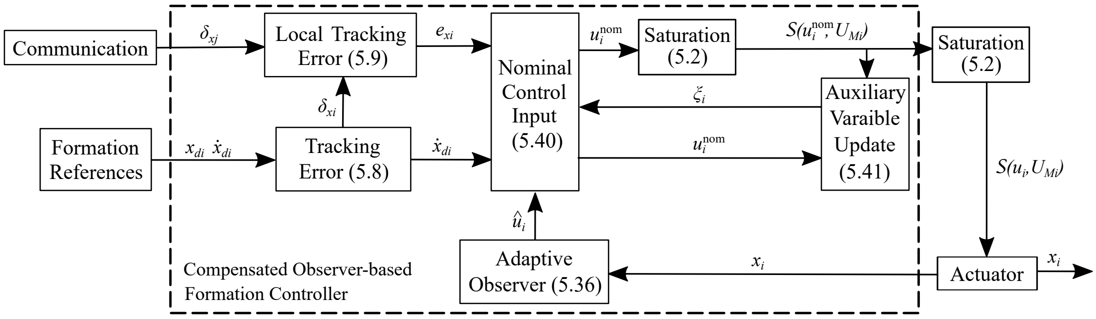

Figure 5.9. Compensated observer-based formation controller for physical experiments.

properly such that the following matrix is positive definite:

$$H_{4,2} = \begin{bmatrix} \underline{\sigma}(Q)\underline{\sigma}(k_e)/2 & -\mathcal{K}_1/2 & -\overline{\sigma}(Q)/4 & 0 & -\overline{\sigma}(Q)/4 \\ -\mathcal{K}_1/2 & \underline{\sigma}(\eta_8) & -\mathcal{K}_2/2 & 0 & 0 \\ -\overline{\sigma}(Q)/4 & -\mathcal{K}_2/2 & \underline{\sigma}(\eta_7 k_\xi) & 0 & 0 \\ 0 & 0 & 0 & \underline{\sigma}(\eta_5)\underline{\sigma}(\widetilde{K}) & 0 \\ -\overline{\sigma}(Q)/4 & 0 & 0 & 0 & \underline{\sigma}(\eta_4) \end{bmatrix}$$

where

$$\mathcal{K}_1 = \overline{\sigma}(Q)\overline{\sigma}(k_\xi)/2, \ \mathcal{K}_2 = \overline{\sigma}(\eta_8 k_\xi) + \overline{\sigma}(\eta_7)$$

Proof. Consider the following Lyapunov candidates:

$$V_e = \frac{1}{2}e_x^{\mathrm{T}} P \otimes I_n e_x, \ V_\xi = \frac{1}{2}\xi^{\mathrm{T}}\xi, \ V_\zeta = \frac{1}{2}\zeta^{\mathrm{T}}\zeta, \ V_o = \frac{1}{2}\widetilde{x}^{\mathrm{T}}\eta_5 \otimes I_N \widetilde{x} + \frac{1}{2}\widetilde{E}^{\mathrm{T}}\widetilde{E}$$

where

$$\xi = [\xi_1^{\mathrm{T}}, \xi_2^{\mathrm{T}}, \ldots, \xi_N^{\mathrm{T}}]^{\mathrm{T}}, \qquad u^{\mathrm{nom}} = [(u_1^{\mathrm{nom}})^{\mathrm{T}}, (u_2^{\mathrm{nom}})^{\mathrm{T}}, \ldots, (u_N^{\mathrm{nom}})^{\mathrm{T}}]^{\mathrm{T}}$$
$$u^{\mathrm{diff}} = u^{\mathrm{nom}} - \mathcal{S}(u^{\mathrm{nom}}), \qquad \zeta = \widehat{g}u^{\mathrm{diff}}$$

According to (5.41), the time derivative of ξ is given as

$$\begin{aligned} V_\xi &= \xi^{\mathrm{T}}\dot{\xi} \\ &= \xi^{\mathrm{T}}(\eta_7 \otimes I_N)\zeta - \xi^{\mathrm{T}}(\eta_8 \otimes I_N)\xi \\ &\leq \overline{\sigma}(\eta_7)\|\xi\|\|\zeta\| - \underline{\sigma}(\eta_8)\|\xi\|^2 \end{aligned}$$

Accordingly, the time derivative of V_ζ is given as

$$\dot{V}_\zeta = \zeta^{\mathrm{T}} d(\widehat{g}u^{\mathrm{com}})/dt + \zeta^{\mathrm{T}}(\dot{\widehat{g}}\mathcal{S}(u) - g\dot{\mathcal{S}})$$

$$
\begin{aligned}
&= \zeta^{\mathrm{T}}[\ddot{x}_d - k_e(L+B)\otimes I_n(g\mathcal{S}(u)+w-\dot{x}_d) - k_\xi \otimes I_n(\eta_7 \otimes I_n\zeta - \eta_8 \otimes I_n\xi) - \dot{\hat{u}}] \\
&\quad + \zeta^{\mathrm{T}}(\dot{g}\mathcal{S}(u) - g\dot{\mathcal{S}})
\end{aligned}
$$

where $\dot{\mathcal{S}} = d\mathcal{S}(u)/dt$.

According to the boundedness of the saturation phenomenon, there exist two positive constants that satisfy $\|\mathcal{S}(u)\| \le \mathcal{S}_M^1$ and $\|\dot{\mathcal{S}}\| \le \mathcal{S}_M^2$. Hence, we can rewrite $\dot{V}_\zeta$ as

$$
\begin{aligned}
\dot{V}_\zeta \le\ & x_M^2\|\zeta\| + \overline{\sigma}(k_e)\overline{\sigma}(L+B)(g_M^1 S_M^1 + w_{M,1} + x_M^1)\|\zeta\| - \underline{\sigma}(\eta_7 k_\xi)\|\zeta\|^2 \\
&+ \overline{\sigma}(\eta_8 k_\xi)\|\zeta\|\|\xi\| + \hat{u}_M^1\|\zeta\| + (g_M^2 S_M^1 + g_M^1 S_M^2)\|\zeta\|
\end{aligned}
$$

where $\|w\| \le w_M^1$ and $\|\dot{w}\| \le w_M^2$.

By the results obtained in the observer design, we have

$$
\dot{V}_o \le -\underline{\sigma}(\eta_5)\underline{\sigma}(\widetilde{K})\|\tilde{x}\|^2 - \underline{\sigma}(\eta_6)\|\widetilde{E}\|^2 + \|\widetilde{E}\|(w_{M,2} + \overline{\sigma}(\eta_6)w_{M,1})
$$

where $\widetilde{K} = \mathrm{diag}\{\tilde{k}_1, \tilde{k}_2, \ldots, \tilde{k}_N\}$.

Meanwhile, the time derivative of V_e is obtained as

$$
\begin{aligned}
\dot{V}_e &= e_x^{\mathrm{T}}(P(L+B))\otimes I_n(g\mathcal{S}(u)+w-\dot{x}_d) \\
&= e_x^{\mathrm{T}}(P(L+B))\otimes I_n(\hat{g}u^{\mathrm{nom}} + E - \dot{x}_d - \zeta) \\
&\le -\frac{1}{2}\underline{\sigma}(Q)\underline{\sigma}(k_e)\|e_x\|^2 + \frac{1}{2}\overline{\sigma}(Q)\|e_x\|\|\widetilde{E}\| + \frac{1}{2}\overline{\sigma}(Q)\epsilon_M\|e_x\| + \frac{1}{2}\overline{\sigma}(Q)\overline{\sigma}(k_\xi)\|e_x\|\|\xi\| \\
&\quad + \frac{1}{2}\overline{\sigma}(Q)\|e_x\|\|\zeta\|
\end{aligned}
$$

where $\|\hat{u} - E\| \le \|\widetilde{E}\| + \epsilon_M$ and ϵ_M is a positive bounded constant.

Accordingly, if define $V_{4,6} = V_e + V_\zeta + V_\xi + V_o$, then we have

$$
\begin{aligned}
\dot{V}_{4,6} \le\ & -\frac{1}{2}\underline{\sigma}(Q)\underline{\sigma}(k_e)\|e_x\|^2 + \frac{1}{2}\overline{\sigma}(Q)\|\tilde{w}\|\|e_x\| + \frac{1}{2}\overline{\sigma}(Q)\overline{\sigma}(k_\xi)\|e_x\|\|\xi\| + \frac{1}{2}\overline{\sigma}(Q)\|e_x\|\|\zeta\| \\
&+ \frac{1}{2}\overline{\sigma}(Q)\epsilon_M\|e_x\| - \underline{\sigma}(\eta_8)\|\xi\|^2 + \overline{\sigma}(\eta_7)\|\xi\|\|\zeta\| - \underline{\sigma}(\eta_7 k_\xi)\|\zeta\|^2 + \overline{\sigma}(\eta_8 k_\xi)\|\zeta\|\|\xi\| \\
&+ \Delta_\zeta\|\zeta\| - \underline{\sigma}(\eta_5)\underline{\sigma}(\widetilde{K})\|\tilde{x}\|^2 - \underline{\sigma}(\eta_6)\|\tilde{w}\|^2 + \Delta_w\|\tilde{w}\|
\end{aligned}
$$

where

$$
\begin{aligned}
\Delta_\zeta &= x_M^2 + \hat{u}_M^1 + g_M^2 S_M^1 + g_M^1 S_M^2 + \overline{\sigma}(k_e)\overline{\sigma}(L+B)(g_M^1 S_M^1 + w_{M,1} + x_M^1) \\
\Delta_w &= w_{M,2} + \overline{\sigma}(\eta_6)w_{M,1}
\end{aligned}
$$

then one has

$$\dot{V}_{4,6} \leq -\chi_{4,2}^{\mathrm{T}} H_{4,2} \chi_{4,2} + h_{4,2} \chi_{4,2}$$

where

$$\chi_{4,2} = \begin{bmatrix} \|e_x\| & \|\xi\| & \|\zeta\| & \|\tilde{x}\| & \|\tilde{w}\| \end{bmatrix}^{\mathrm{T}},$$
$$h_{4,2} = \begin{bmatrix} \overline{\sigma}(Q)\epsilon_M/2 & 0 & \Delta_\zeta & 0 & \Delta_w \end{bmatrix}$$

Hence, by Lemma 2.1, $\|e_x\|$, $\|\xi\|$ and $\|\zeta\|$ are semi-globally UUB within the following regions, respectively:

$$\Omega_e^4 = \left\{ e_x \middle| \|e_x\| \leq \frac{\overline{\sigma}(h_{4,2})}{\underline{\sigma}(H_{4,2})} \right\},\ \Omega_\xi^1 = \left\{ \xi \middle| \|\xi\| \leq \frac{\overline{\sigma}(h_{4,2})}{\underline{\sigma}(H_{4,2})} \right\},\ \Omega_\zeta^1 = \left\{ \zeta \middle| \|\zeta\| \leq \frac{\overline{\sigma}(h_{4,2})}{\underline{\sigma}(H_{4,2})} \right\}$$

Similar result is also obtained for δ_x:

$$\Omega_\delta^4 = \left\{ \delta_x \middle| \|\delta_x\| \leq \frac{\overline{\sigma}(h_{4,2})}{\underline{\sigma}(H_{4,2})\underline{\sigma}(L+B)} \right\}$$

which completes the proof. □

5.4.3 Simulations results and discussions

To validate the new observer-based compensated controller design (5.42), the example of a three-wheel ODR cluster is employed for comparative numerical simulations. Still, consider the first-order model presented in Section 5.3. Suppose that the cluster contains three ODRs with the directed topology shown in Figure 5.10.

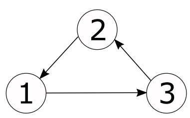

Figure 5.10. The communication topology among 3 ODRs in the experiment.

The initial states and the ODR parameter values are given in Table 5.3.

The system formation reference is chosen as a time-varying circular formation whose centre moves in a sine wave trajectory, which is abstracted as the following expression:

$$x_{di}(t) = \left[\frac{4}{5}\cos\left(\frac{\pi}{18}t + \frac{2i}{3}\pi\right) + \frac{1}{5}\sin\left(\frac{\pi}{15}t\right), \frac{4}{5}\sin\left(\frac{\pi}{18}t + \frac{2i}{3}\pi\right) + \frac{4}{5} - t, 0 \right]^{\mathrm{T}} \quad (5.43)$$

5.4.3 Simulations results and discussions

Table 5.3. Model parameters and initial states of three saturated first-order ODRs.

Robot number	Model parameters		Initial states					
	R_i(m)	$\widehat{R}_i$(m)	p_i^x(m)	p_i^y(m)	θ_i(rad)	$\widehat{p}_i^x$(m)	$\widehat{p}_i^y$(m)	$\widehat{\theta}_i$(rad)
1	0.134	0.13	-0.6	0.3	$-\pi/4$	-0.6	0.3	$-\pi/4$
2	0.128	0.13	0.1	1.4	$\pi/5$	0.1	1.4	$\pi/5$
3	0.126	0.13	1.1	0	$\pi/10$	1.1	0	$\pi/10$

The uncertain term w_i is chosen as

$$w_i = \left[\frac{2}{25}\cos\left(\frac{1}{2}t + \frac{i\pi}{2}\right), \frac{9}{100}\sin\left(\frac{1}{5}t + \frac{i\pi}{3}\right), \frac{2}{25}\sin\left(\frac{1}{10}t + \frac{i\pi}{4}\right)\right]^{\mathrm{T}}$$

The saturation limit is chosen as $U_{Mi} = 0.2$, and the error sensitivity of individual agents is chosen as $b_i = 0.5$. The first item to justify is the adaptive observer's stability. With the parameters chosen as $\eta_5 = \text{diag}\{15, 15, 6\}$, $\eta_6 = \text{diag}\{0.8, 0.8, 0.8\}$ and $\widetilde{k}_i = \text{diag}\{8, 8, 2\}$, the estimation performance of the adaptive observer (5.36) embedded in each agent is shown in Figure 5.11. It is observed that the estimation error of (5.36) is bounded such that $\|E_i - \widehat{u}_i\| \leq 2.1 \times 10^{-3}$ is achived for all agents, which validates Theorem 5.4.

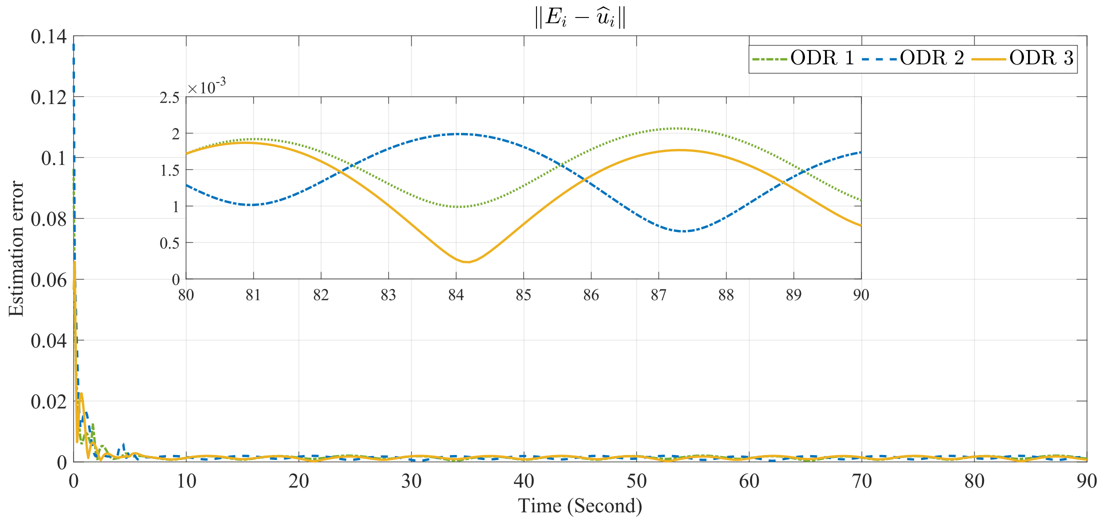

Figure 5.11. Estimation performance of the proposed adaptive observer.

To show the necessity and merits of the control law presented in Theorem 5.5, comparative simulations based on the following three designs are conducted:

1. The observer-based formation controller (OBFC) which employs the adaptive observer (5.36) by having $u_i = \mathcal{S}(u_i^{\text{ob}}, U_{Mi})$, where

$$u_i^{\text{ob}} = \widehat{g}_i^{-1}(\dot{x}_{di} - k_e e_{xi} - \widehat{u}_i)$$

2. The compensated formation controller (CFC) which only employs the auxiliary variable ξ_i by having $u_i = \mathcal{S}(u_i^{\text{com}}, U_{Mi})$, where

$$u_i^{\text{com}} = \widehat{g}_i^{-1}(\dot{x}_{di} - k_e e_{xi} - k_\xi \xi_i)$$

3. The compensated observer-based formation controller (COBFC) which employs both the adaptive observer (5.36) and the auxiliary variable ξ_i, which further leads to the design in (5.42).

The parameter values in the above three designs are selected as $k_e = \text{diag}\{1, 1, 0.5\}$, $k_\xi = \text{diag}\{2, 2, 2\}$, $\eta_7 = \text{diag}\{6, 6, 1\}$ and $\eta_8 = \text{diag}\{0.5, 0.5, 0.5\}$. The propagation of the error-related norms are presented in Figure 5.12. As shown in the results, the tracking errors e_x and δ_x will have a smaller bounded region if the adaptive observer is employed to compensate for the uncertain factors inside the system.

In specific, the trends of e_x in each state channel is provided in Figure 5.13. After comparing the results of COBFC and OBFC, it is observed that implementing the auxiliary variable ξ will help attenuate the oscillation of system states. However, the performance of the compensation term can still be improved by exploring more parameter settings.

The control input is also recorded in Figure 5.14, where the control input is restricted within the saturation limit as what's declared in Theorem 5.5.

The formation statuses of the entire system in time $t = 0$s and $t = 90$s are also provided in Figure 5.15, where all three robots are able to maintain bounded tracking error around their desired trajectories (see dotted lines) to achieve a time-varying circular formation (see the purple dash-dotted line), which validates the effectiveness of Theorem 5.5.

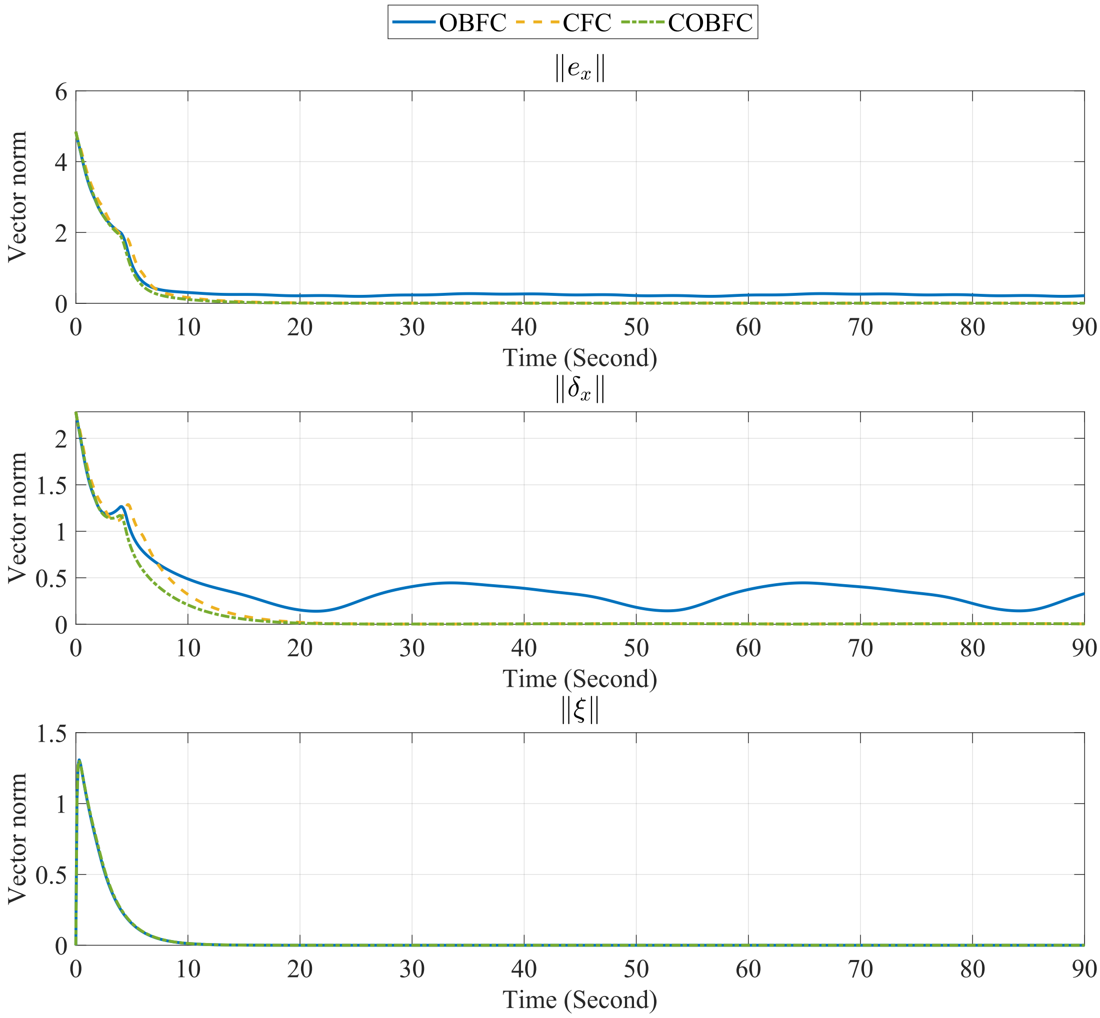

Figure 5.12. Performance comparison among COBFC, OBFC and CFC.

5.4.4 Practical experiments and results

To further prove the effectiveness of the observer-based formation control scheme in practice, three ODRs (see Figure 5.16) are developed and employed to carry out physical experiments. It is seen that the physical structure of the ODRs satisfies the theoretical analysis provided in Chapter 2, which means the dynamic model should match the one provided in Section 5.3.

The OptiTrack system is deployed to act as the feedback of each individual ODR. The distributed communication among robots are carried out in the internet layer on computers, and the useful information is sent to each ODR through WiFi by using the Transmission Control Protocol.

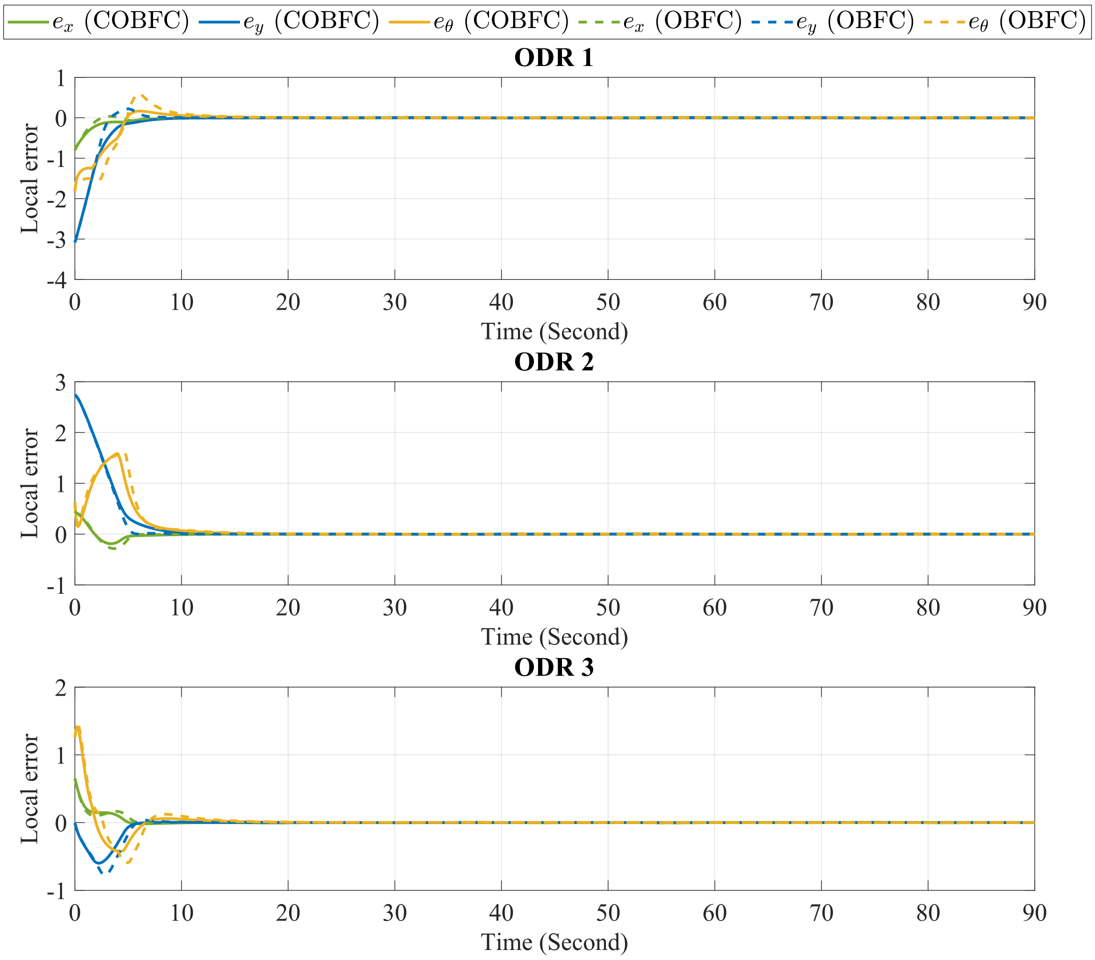

Figure 5.13. Comparison of e_x between COBFC and OBFC.

Although it is impossible to know the specific value of E_i in the experiment, it is reasonable to record the value of $\|\widetilde{x}_i\|$ instead to illustrate that the estimation error of the adaptive observer is bounded. The trends of $\|\widetilde{x}_i\|$ of each individual ODR is recorded in Figure 5.17. It is observed that the value of $\|\widetilde{x}_i\|$ is UUB such that $\|\widetilde{x}_i\| \leq 10^{-2}$ is satisfied for every ODR, which further proves the validity of Theorem 5.4 in practice.

The propagation of the local tracking errors are provided in Figure 5.18. If the auxiliary variable is not implemented by setting $\xi_i = [0, 0, 0]^{\mathrm{T}}$ for each agent, then the propagation of the local tracking error contains state fluctuation with high amplitudes. On the other hand, although the state fluctuation phenomenon is not ruled out after employing the auxiliary variable ξ_i, the amplitudes of the fluctuation is remarkably decreased, which justifies the necessity of including ξ_i in the controller design.

Correspondent to the simulation results, the norms of e_x, δ_x and ξ are also recorded in Figure 5.19. Although CFC is able to maintain the boundedness of each state, it can

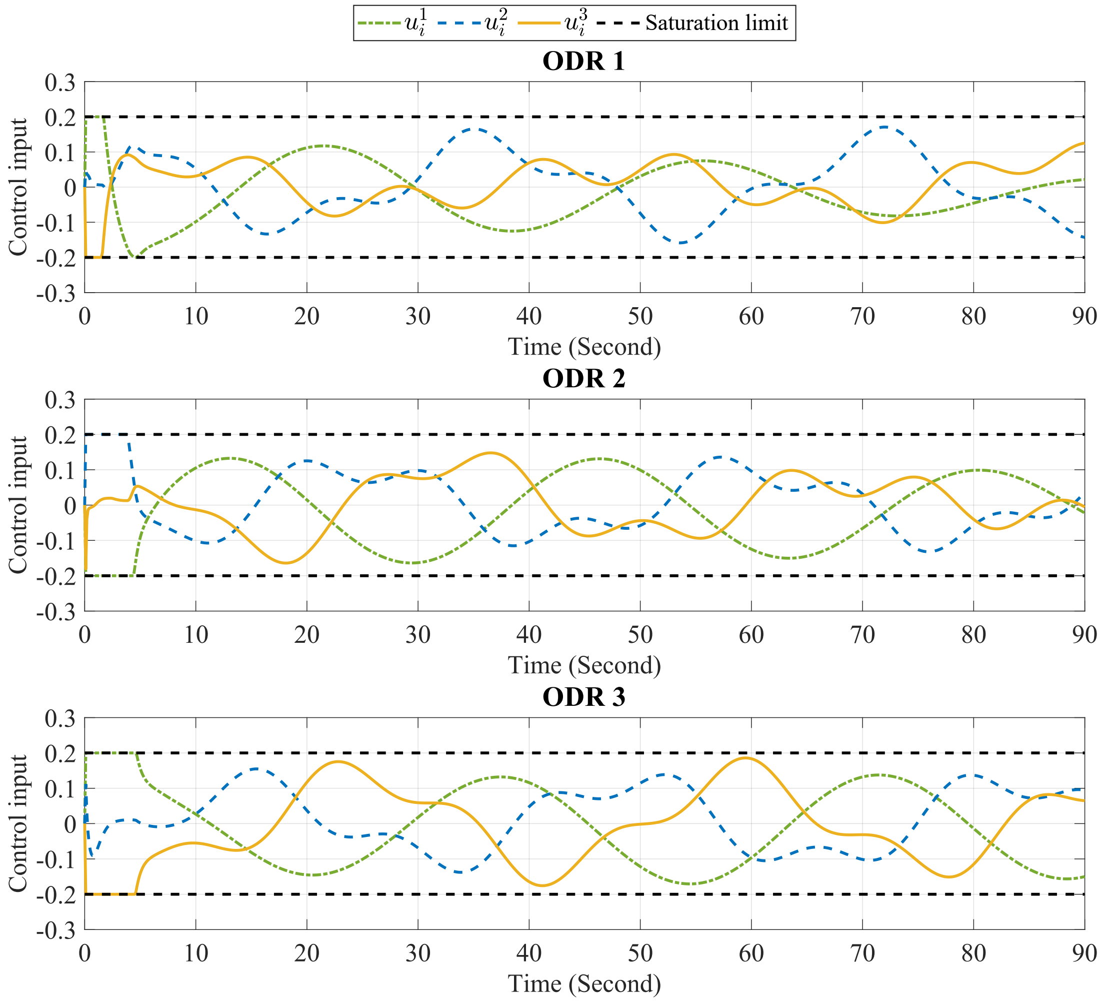

Figure 5.14. Control input of the COBFC scheme.

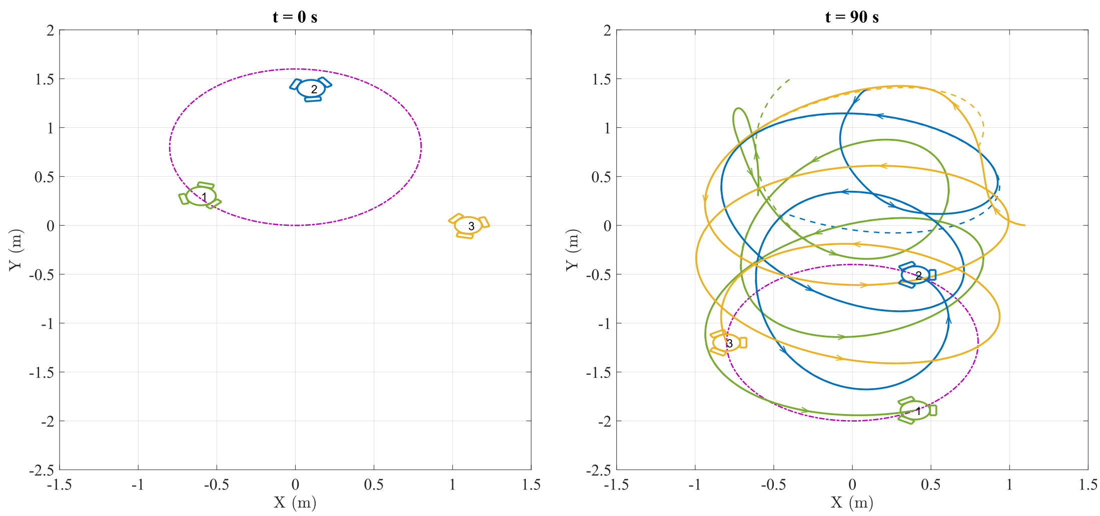

Figure 5.15. System trajectories of COBFC in simulation.

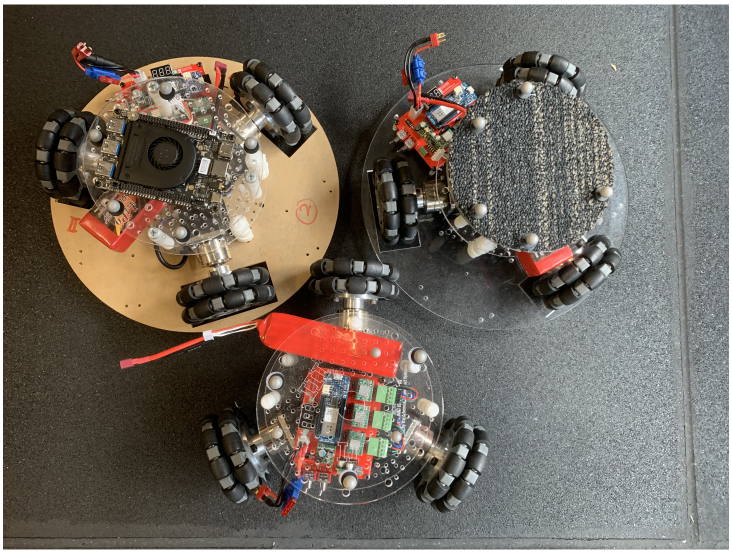

Figure 5.16. Photo of 3 ODRs in the lab.

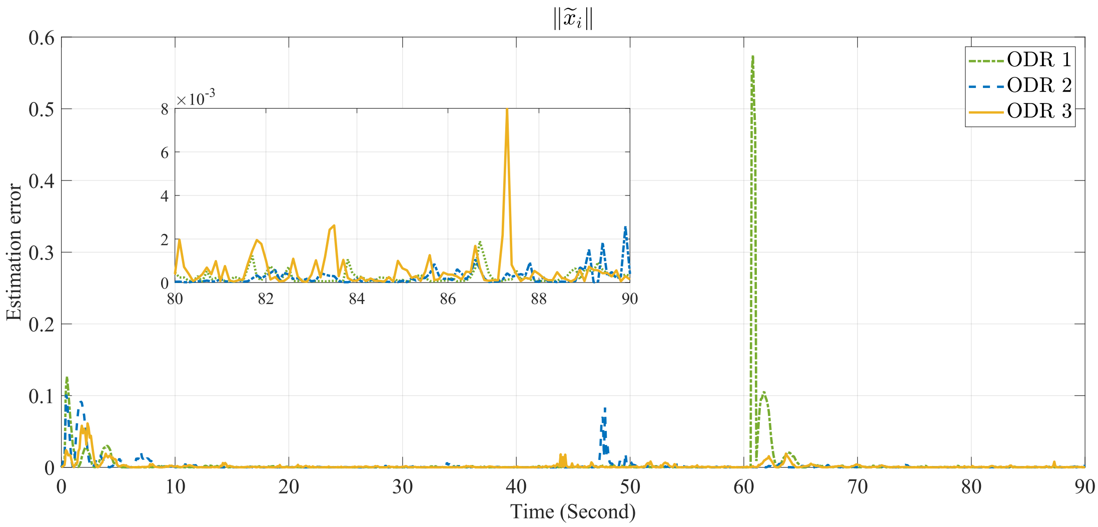

Figure 5.17. Boundedness of $\|\tilde{x}_i\|$ in the experiment.

only ensure $\|e_x\| \leq 2 \times 10^{-1}$. However, the tracking precision is increased by at least 60% if the adaptive observer is implemented (see the results of COBFC and OBFC), which validates the necessity of employing the observer design and the stability of the observer-based control scheme.

The control input of each motor is also recorded and presented in Figure 5.20, where the amplitudes of any arbitrary input is restricted within the actuator saturation limit U_{Mi}.

Note that there are several remarkable boost of the system states in Figures 5.17-5.20 (see around 18s, 38s, 45s and 60s). The corresponding reason is that sometimes one or

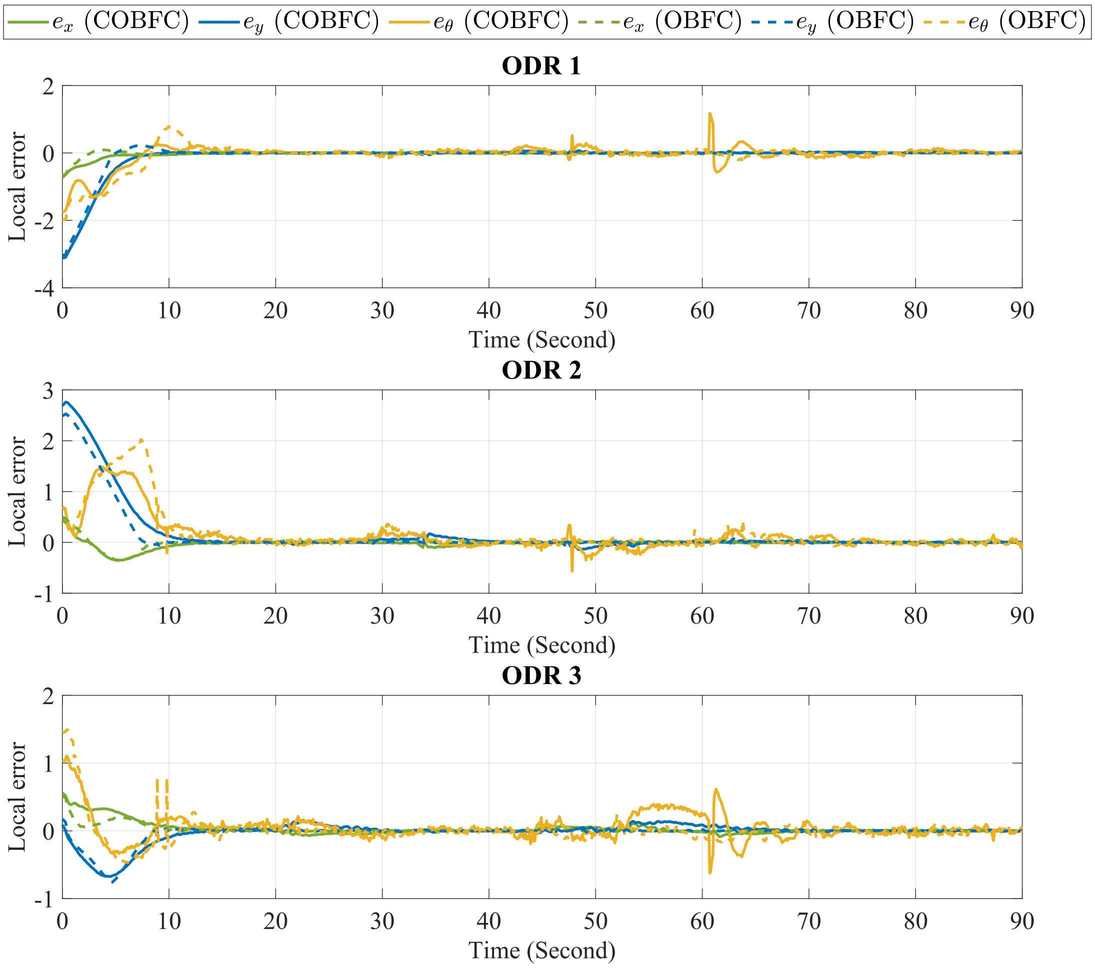

Figure 5.18. Effectiveness of the auxiliary variable in the experiment.

several ODRs may enter the blind area of the OptiTrack system because there are only eight cameras covering the lab (about 24m^2), and the measurement of the ODR states will then change abruptly. However, the stability of the system will not be affected by the occasional faults in the feedback because the error states will still converge to a bounded neighbourhood. Hence, the proposed adaptive observer and the observer-based compensated controller is proved to be robust in practice.

The system formation in time $t = 0$s, $t = 60$s and $t = 90$s is recorded in Figure 5.21, where all three ODRs are able to track their desired trajectories within bounded error to form a time-varying circular formation (see the purple dash-dotted circle). The video for the physical experiment of the COBFC design is uploaded in link `https://youtu.be/ZB1qV9C7WSM`.

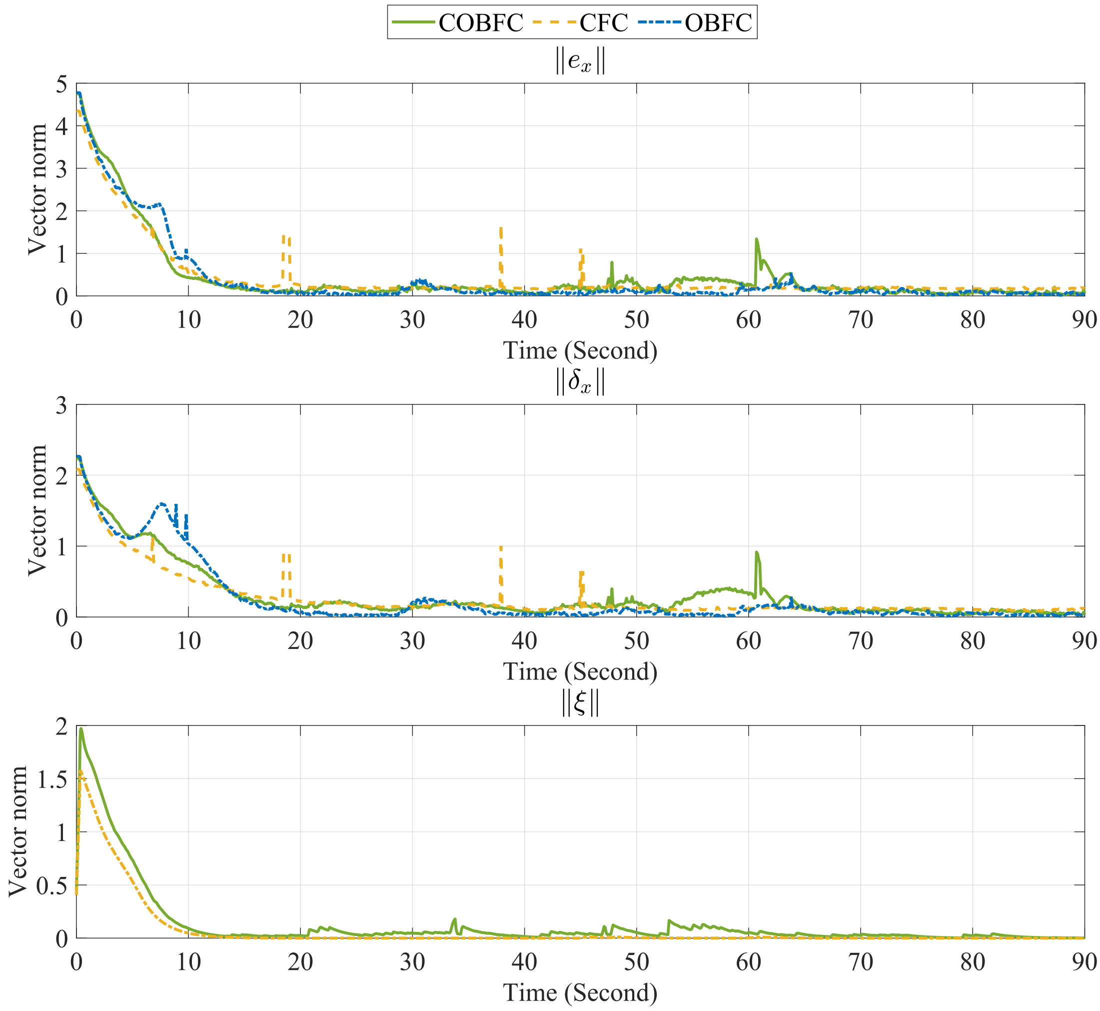

Figure 5.19. Performance comparisons among COBFC, OBFC and CFC.

5.5 Chapter summary

The first main focus of this chapter is the implementation of three-layer NNs in the formation tracking problem of uncertain and saturated first-order multi-agent systems. First, a fully local-error-related cooperative tuning law for unsaturated agents was proposed to avoid the divergence of the weight estimation error. After introducing the actuator saturation phenomenon along with the input coupling phenomenon into the system dynamics, two correlated problems including the slow convergence of cooperative neural estimation and the reverse effect were discussed. The three-layer NN was further modified into an observer to achieve semi-global finite-time convergence regardless of each agent's formation tracking error. A control input distribution algorithm was then developed to attenuate the reverse effect caused by coupled and

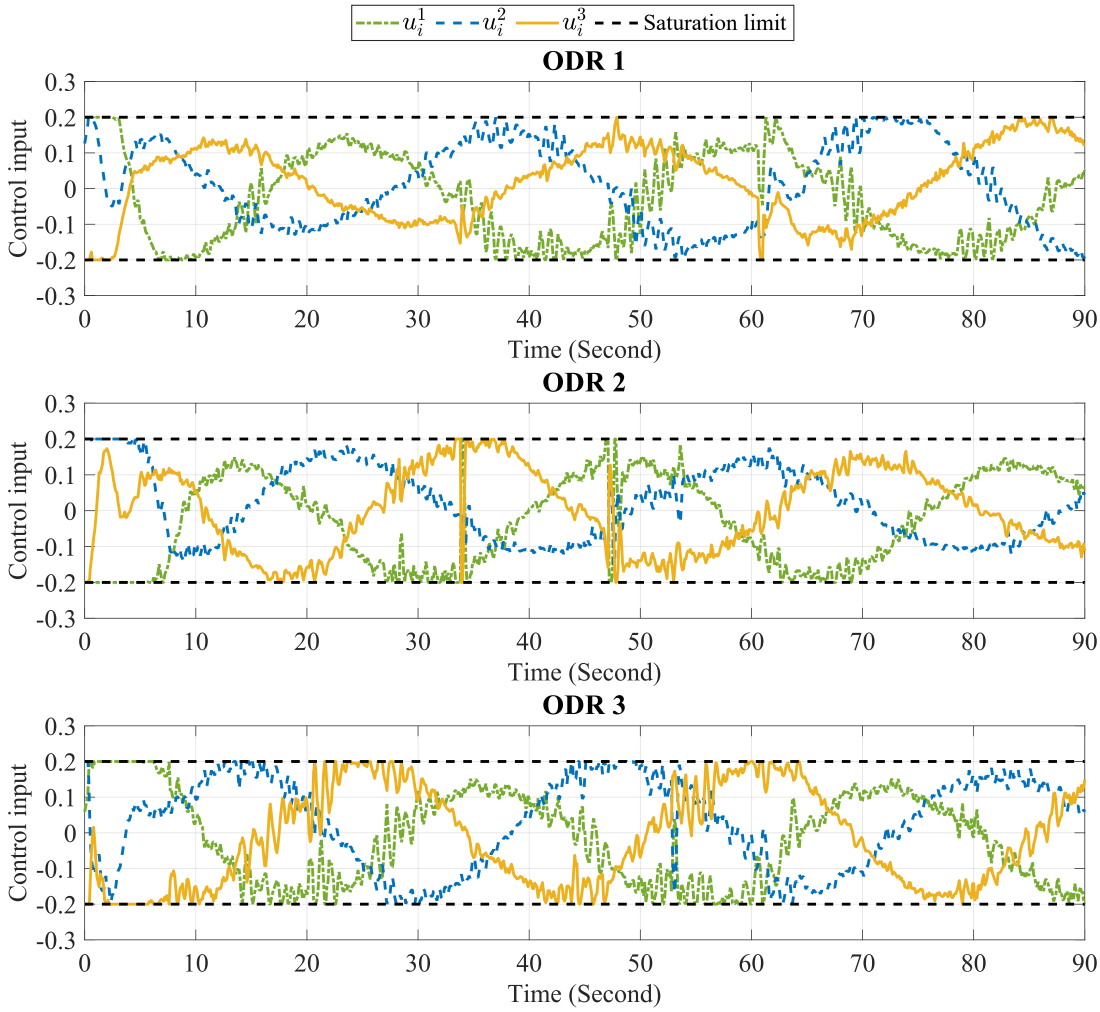

Figure 5.20. Control input of the COBFC scheme in the experiment.

saturated control inputs. Simulation examples are given to show the effectiveness and advantages of the proposed new designs compared with some existing results.

Following the above results in uncertainty approximation, a new adaptive variable is employed to replace the NNs in the observer structure to achieve global stability. An adaptive auxiliary variable is also added into the controller design to attenuate the state fluctuation led by the reverse effect. The corresponding observer-based compensated formation controller is first validated by the Lyapunov stability theory and numerical simulations. To further prove the practicality of the design, physical experiments that includes three networked ODRs are conducted to illustrate the robustness of the formation tracking process.

In the next chapter, the study of the effect of the actuator saturation phenomenon is extended to nonlinear second-order agent clusters. A new method of implementing

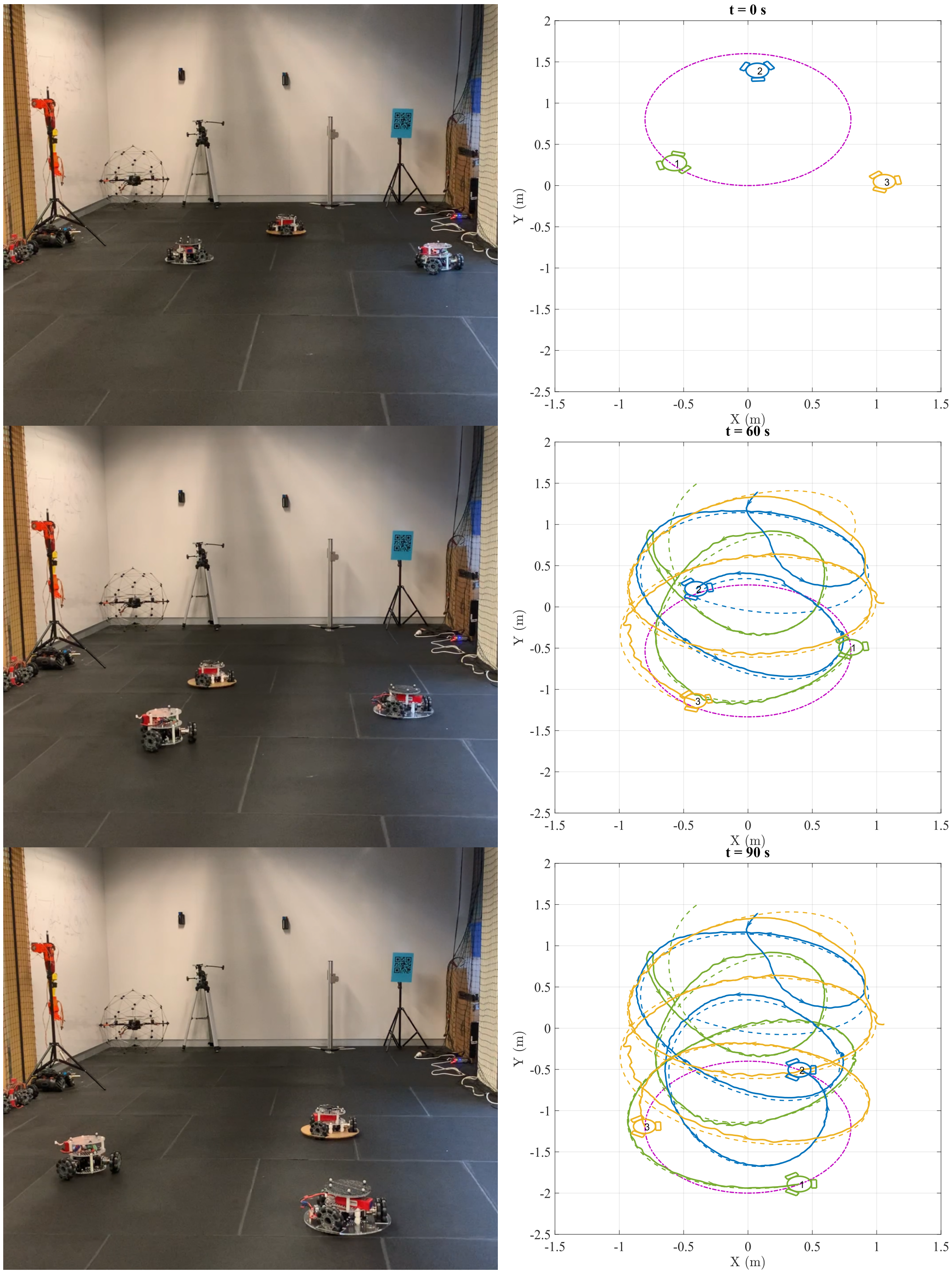

Figure 5.21. Formation status and trajectories of individual ODRs in the experiment.

the linear programming technique to regulate the nominal control input is developed to reduce the state oscillations in the formation tracking process.

Chapter 6

Formation Control of Second-Order Agents with Input Saturation

---

AFTER analysing the effect of actuator saturation on first-order systems, it is also necessary to extend the same issue to second-order systems. Hence, the robust formation control problem for a group of saturated non-linear second-order agents is discussed in this chapter. To carry out the uncertainty estimation process without prior knowledge of the uncertain function, new observer structures that combine the neural network estimation with the sliding mode technique are proposed. A finite-time estimation sliding surface is then defined to obtain finite-time characteristics. Both the adaptive windup compensator and the linear programming technique are employed to attenuate the state fluctuation phenomenon and further construct the observer-based formation controller. A multiple omni-directional robot system is used in the simulations to illustrate the effectiveness of the proposed adaptive observer and the observer-based robust formation controller.

6.1 Introduction

After investigating the effect of actuator saturation on the cooperative first-order agent clusters, it is also essential to extend the same topic to second-order agent clusters. Although the approach to design a saturated formation controller is proposed in the previous chapter, it is still essential to investigate the effect of an extra layer of integration and the corresponding mitigation.

Similar to the previous chapters, the unknown factors such as modelling uncertainty and external disturbances are considered to ensure the robustness of our controllers. Currently, a part of researchers choose to employ switching function (Yang *et al.* 2012) to passively reject the influence of uncertain terms, while the others implement different estimation techniques such as NNs (Fei *et al.* 2020) and observers (Xu *et al.* 2020) to approximate and compensate for uncertain factors to further obtain adaptive controllers.

The sliding mode observer was first proposed to perform finite-time uncertainty estimation for systems with arbitrary order (Levant 2003). The super-twisting-algorithm-based approach (Chalanga *et al.* 2016) is found to have high approximation precision for both matched disturbances (Dou *et al.* 2021) and mismatched disturbances (Mondal *et al.* 2017a). The same structure was further modified by Sun et al. to achieve fixed-time estimation (Sun *et al.* 2018). However, prior knowledge of the uncertain term's Lipschitz constant is essential to ensure the convergence of estimation error, which makes this structure too conservative for certain practical scenarios.

As mentioned in Chapter 5, employing the cooperative tuning approach for NNs is not a suitable choice for systems with actuator saturation. Hence, we only consider the neural-based observer structure for second-order agents that are affected by input saturation. Although there have been several neural-based observer designs developed in the previous chapters, the finite-time convergence of the NN weight has not yet been achieved. Hence, it is essential to analyse if there is an approach to integrate the sliding mode technique with the neural-based estimation structure such that these two schemes can compensate for each other's shortcomings.

Regarding a saturated system with second-order or higher-order dynamics, the state windup phenomenon is commonly seen. Ding and Zheng found out that large error overshoot is expected if we implement a linear sliding surface to design the controller

(Ding and Zheng 2015). To attenuate the state overshoot phenomenon, a saturation function was then employed to construct a saturated sliding surface (Ding and Zheng 2015) for continuous-time sliding mode controller design. To achieve faster error convergence, a nonsingular saturated terminal sliding surface (Ding and Zheng 2016) was further proposed to ensure finite-time stability. Although the discontinuous sliding surfaces (Ding and Zheng 2015, Ding and Zheng 2016) proposed by Ding and Zheng are helpful for reducing the amplitude of the overshoot, the state windup phenomenon is still obvious and the discontinuous sliding surface design has introduced complexity into the stability analysis.

Other than modifying the sliding surface, some researchers choose to employ auxiliary variables to act as the overshoot compensator. Cui et al. introduced a set of fractional tuning laws for the auxiliary variable that is used to compensate for the state windup issue in the SMC scheme (Cui *et al.* 2016). Although the fractional design (Cui *et al.* 2016) is found to be effective, the fact that it uses the value of the auxiliary variable as a denominator in the tuning law may lead to the singular issue. Regarding an electric machine set, Han et al. proposed an adaptive compensator (Han *et al.* 2019) design that is free of the singular issue to attenuate the windup phenomenon. However, the design introduced by Han et al. can only be used for discrete-time systems. Hence, it is essential to investigate if there is a nonsingular tuning approach for the windup compensator in continuous-time systems. Besides, the reverse effect defined in Chapter 5 is also considered in the current chapter.

Motivated by the above gaps, this chapter mainly focuses on providing analysis and solutions to the following issues:

1. How to integrate the sliding mode technique with the NN approximation approach to shorten the convergence time of the estimation error?
2. How to let NNs obtain finite-time characteristics in an observer structure?
3. How to attenuate the state oscillation led by the state windup phenomenon and the reverse effect simultaneously?

The contents in this chapter are organised as follows. The system modelling of a cluster of nonlinear second-order agents with actuator saturation and the problem formulation are given Section 6.2. A brief introduction about the two-layer NN estimation is given in Section 6.3. The development of the finite-time neural-based sliding mode observer, the algorithm-and-observer-based robust formation controller design is introduced in Section 6.4, where both the theoretical analysis and numerical simulation results are given to illustrate the effectiveness of the proposed control scheme. The final conclusions are drawn in Section 6.5.

6.2 System modelling and problem formulation

Consider a multi-agent system consists of $N(N \in \mathbb{R}^+)$ agents that have the following nonlinear second-order dynamics:

$$\begin{cases} \dot{x}_i = v_i \\ \dot{v}_i = f_i(x_i, v_i) + g_i(x_i, v_i)\mathcal{S}(u_i, U_{Mi}) + \bar{w}_i, \quad i = 1, 2, \ldots, N \end{cases} \tag{6.1}$$

where $x_i \in \mathbb{R}^n$ denotes the accessible position information of the ith agent, $v_i \in \mathbb{R}^n$ denotes the known velocity information, $f_i(x_i, v_i) \in \mathbb{R}^n$ is the unknown function in agent dynamics, $\bar{w}_i \in \mathbb{R}^n$ is the external disturbance, $g_i(x_i, v_i) \in \mathbb{R}^{n \times n}$ is the known control gain matrix, $u_i \in \mathbb{R}^n$ represents the control input vector, $\mathcal{S}(u_i, U_{Mi}) \in \mathbb{R}^n$ is the saturated control input and U_{Mi} is the known constant saturation limit. If define $\mathcal{S}(u_i(j), U_{Mi})$ to be the jth element of $\mathcal{S}(u_i, U_{Mi})$, then we have the following expression:

$$\mathcal{S}(u_i(j), U_{Mi}) = \begin{cases} u_i(j) & |u_i(j)| \leq U_{Mi} \\ \text{sign}(u_i(j))U_{Mi} & |u_i(j)| > U_{Mi} \end{cases} \tag{6.2}$$

Without loss of generality, we use g_i to represent $g_i(x_i, v_i)$, if not specially stated otherwise. If we have $w_i = f_i(x_i, v_i) + \bar{w}_i$ to represent the overall uncertainty, then we obtain an alternative expression of (6.1) as follows:

$$\begin{cases} \dot{x}_i = v_i \\ \dot{v}_i = g_i\mathcal{S}(u_i, U_{Mi}) + w_i, \quad i = 1, 2, \ldots, N \end{cases} \tag{6.3}$$

Define $x = [x_1^{\mathrm{T}}, x_2^{\mathrm{T}}, \ldots, x_N^{\mathrm{T}}]^{\mathrm{T}}$, $v = [v_1^{\mathrm{T}}, v_2^{\mathrm{T}}, \ldots, v_N^{\mathrm{T}}]^{\mathrm{T}}$, $g = \text{diag}\{g_1, g_2, \ldots, g_N\}$, $w = [w_1^{\mathrm{T}}, w_2^{\mathrm{T}}, \ldots, w_N^{\mathrm{T}}]^{\mathrm{T}}$ and $\mathcal{S}(u) = [\mathcal{S}^{\mathrm{T}}(u_1, U_{M1}), \mathcal{S}^{\mathrm{T}}(u_2, U_{M2}), \ldots, \mathcal{S}^{\mathrm{T}}(u_N, U_{MN})]^{\mathrm{T}}$, we then obtain the cluster's dynamics as

$$\begin{cases} \dot{x} = v \\ \dot{v} = g\mathcal{S}(u) + w \end{cases} \tag{6.4}$$

The position reference of the ith agent is denoted as $x_{di} \in \mathbb{R}^n$. The main goal of this chapter is to construct a controller such that the reference tracking error of each agent is semi-globally UUB when the actuator is saturated, which is equivalent to the following inequality:

$$\lim_{t \to \infty} ||x_i(t) - x_{di}(t)|| \leq \nu_\delta^s, \ \forall x_i(t_0) \in \Omega_x, \ i = 1, 2, \ldots, N \tag{6.5}$$

The following assumptions are made regarding the agent cluster in (6.4).

Assumption 6.1. *The formation reference x_{di} and its derivatives $\dot{x}_{di}$ and $\ddot{x}_{di}$ remain bounded and known throughout the formation tracking process. The initial state of the ith agent satisfies $x_i(t_0) \in \Omega_x$ and $v_i(t_0) \in \Omega_v$, where Ω_x and Ω_v are both compact sets.*

Assumption 6.2. *Consider the ith saturated agent in* (6.3)*, the unknown function w_i is bounded for the ith agent when $t \geq t_0$, and there is a finite time $t_s \geq t_0$ such that the following inequality exists satisfied when $t \geq t_s$:*

$$\tau_i \mathbf{1}_{n\times 1} > |g_i^{-1}(\ddot{x}_{di} - w_i)|$$

where τ_i is an unknown positive constant that satisfies $\tau_i < U_{Mi}$ and $\mathbf{1}_{n\times 1}$ is an n-dimensional column vector whose every entry is 1.

Assumption 6.3. *The control gain matrix is bounded such that there are positive constants g_M^1 and g_M^2 that satisfy the following inequalities:*

$$\|g\|_F \leq g_M^1, \ \|\dot{g}\|_F \leq g_M^2$$

Remark 6.1. *Notice that Assumption 6.2 is made to ensure that the formation tracking process is feasible to the saturated agents in* (6.4) *after a finite amount of time. In an ideal situation where $u_i = g_i^{-1}(t)(\ddot{x}_{di}(t) - w_i(t))$, we then have $\ddot{x}_i = \ddot{x}_{di}$, meaning that the agent can successfully track the acceleration reference. However, it is still necessary to have a residual amount of control input to reduce the value of $\|x_i(t) - x_{di}(t)\|$ when $\|x_i(t_0) - x_{di}(t_0)\| > \nu_\delta^s$, where $x_i(t_0)$ is the initial position of the ith agent, $v_i(t_0)$ is the initial agent velocity and $x_{di}(t_0)$ is the initial position reference of the ith agent. Hence, we have $\tau_i < U_{Mi}$ to offer redundancy in the control input for error reduction. The time t_s is defined to mark the time when the formation tracking task is feasible to each agent in* (6.4).

6.3 Two-layer neural networks

In this chapter, two-layer NNs are implemented to construct sliding mode observers for each agent to estimate the unknown function w_i:

$$w_i = W_i^{\mathrm{T}} \mathcal{T}(Y_i) + \epsilon_i,\ i = 1, 2, \ldots, N$$

where $Y_i = [x_i^{\mathrm{T}}, v_i^{\mathrm{T}}]^{\mathrm{T}} \in \mathbb{R}^{2n}$ is the input vector of the NN for the ith agent, $W_i \in \mathbb{R}^{2n \times n}$ is the unknown weight matrix that represents the set of optimal coefficients to estimate, $\epsilon_i \in \mathbb{R}^n$ is the bounded network bias that satisfies $\|\epsilon_i\| \leq \epsilon_M$, ϵ_M is a small positive number, $\mathcal{T}(\cdot)$ is the hyperbolic function, and the jth element of $\mathcal{T}(Y_i)$ is expressed as

$$\mathcal{T}(Y_i(j)) = \frac{e^{Y_i(j)} - e^{-Y_i(j)}}{e^{Y_i(j)} + e^{-Y_i(j)}}$$

where $Y_i(j)$ is the jth element of Y_i. The NN estimation $\widehat{w}_i$ is given as

$$\widehat{w}_i = \widehat{W}_i^{\mathrm{T}} \mathcal{T}(Y_i) \tag{6.6}$$

where $\widehat{W}_i$ is the estimated weight matrix.

Define $\widetilde{w}_i^N = w_i - \widehat{w}_i$ as the estimation error of the NN, then we have its expression as follows:

$$\widetilde{w}_i^N = \widetilde{W}_i^{\mathrm{T}} \mathcal{T}(Y_i) + \epsilon_i \tag{6.7}$$

where $\widetilde{W}_i = W_i - \widehat{W}_i$ is the estimation error of the weight matrix.

Assumption 6.4. *The optimal weight W_i is bounded such that $\|W_i\|_F \leq W_M$ is satisfied for all $i \in [1, N]$.*

6.4 Observer-based formation control scheme

6.4.1 Neural-based sliding mode observer design

In most previous works, sliding mode observer (Fei *et al.* 2021b, Dou *et al.* 2021) is one popular approach for system uncertainty estimation. For a nominal second-order system with matched disturbance (6.3), if we define $\widehat{v}_i$ as the observer's estimation of state v_i, the observer usually employs the following design:

$$\begin{cases} \dot{\gamma}_{i,1} = \mu_{i,1} + g_i u_i,\ \dot{\gamma}_{i,2} = \mu_{i,2},\ \ldots, \dot{\gamma}_{i,k} = \mu_{i,k} \\ \mu_{i,1} = -\alpha_{i,1}\beta_{i,w}^{\frac{1}{k}} \mathrm{sgn}^{\frac{k-1}{k}}(\gamma_{i,1} - v_i) + \gamma_{i,2} \\ \qquad\vdots \\ \mu_{i,k-1} = -\alpha_{i,k-1}\beta_{i,w}^{\frac{1}{2}} \mathrm{sgn}^{\frac{1}{2}}(\gamma_{i,k-1} - \mu_{i,k-2}) + \gamma_{i,k} \\ \mu_{i,k} = -\alpha_{i,k}\beta_{i,w} \mathrm{sgn}(\gamma_{i,k} - \mu_{i,k-1}), \\ \widehat{v}_i = \gamma_{i,1}, \widehat{w}_i = \gamma_{i,2} \end{cases}$$

where k is a positive number that satisfies $k \geq 2$, $\alpha_{i,j}(j \in [1,k])$ is a positive number and $\beta_{i,w}$ is the Lipschitz constant of the $(k-2)$th derivative of the unknown function w_i. The term $\mathrm{sgn}^{m_1}(\bar{\gamma})$ has the following expression

$$\mathrm{sgn}^{m_1}(\bar{\gamma}) = [\mathrm{sign}(\bar{\gamma}(1))|\bar{\gamma}(1)|^{m_1}, \mathrm{sign}(\bar{\gamma}(2))|\bar{\gamma}(2)|^{m_1}, \ldots, \mathrm{sign}(\bar{\gamma}(m_2)|\bar{\gamma}(m_2)|^{m_1}]^{\mathrm{T}}$$

where $\bar{\gamma} \in \mathbb{R}^{m_2 \times 1}$, $\bar{\gamma}(k)$ is the kth element of $\bar{\gamma}$, $m_1 \in \mathbb{R}^+$ and $m_2 \in \mathbb{R}^+$. Such design follows the idea of augmenting the system and implement the sliding mode approaching law on each first-order subsystem to achieve precise state tracking. Due to the implementation of function $\mathrm{sgn}^{m_1}(\bar{\gamma})$, the above method is also referred as super-twisting-based observer (Chalanga *et al.* 2016). Although this observer design is easy to be implemented, there is one severe issue:

Problem 6.1. *Its requirement of knowing the Lipschitz constant in advance is hard to satisfy for practical scenarios. Hence, how to estimate the unknown factors without any priori knowledge has become a gap to fill.*

To solve Problem 6.1, it is reasonable to employ NNs for the adaptive estimation of w_i without any prior knowledge of its Lipschitz constant. The method of tuning NN weight with local formation tracking error (Lewis *et al.* 2013) is found to be effective for MASs with ideal actuators. However, using terms correlated with reference tracking error to tune the NN weight will potentially prolong the converging time of estimation error when the actuator saturation phenomenon exists because the weight tuning process will not settle before the tracking error converges. Therefore, the structure of neural-based observers (Liu *et al.* 2013) is proposed so that the estimation process can work independently from the reference tracking process. For a nominal second-order system (6.3) with velocity measurement, we have the nominal expression of neural-based observer as

$$\begin{cases} \dot{\widehat{x}}_i = \dot{\widehat{v}}_i + \alpha_{i,1}(x_i - \widehat{x}_i) \\ \dot{\widehat{v}}_i = \alpha_{i,2}(v_i - \widehat{v}_i) + g_i\mathcal{S}(u_i, U_{Mi}) + \widehat{W}_i^{\mathrm{T}}\mathcal{T}(Y_i) \end{cases} \tag{6.8}$$

where $\widehat{x}_i$ is the estimation of state x_i and $\widehat{v}_i$ represents the estimation of state v_i.

Although the Lipschitz constant is not required in (6.8) because of the implementation of NN, it is hard to obtain finite-time characteristics in such structure. Meanwhile, the approximation accuracy of (6.8) also has high dependency on the estimation precision of the NN if we only employ the NN output as the estimation of w_i.

To reduce the dependency on the NN estimation accuracy, the method of turning the estimation problem into a tracking problem regarding the following imaginary second-order system is proposed:

$$\begin{cases} \dot{\widehat{x}}_i = \widehat{v}_i \\ \dot{\widehat{v}}_i = g_i\mathcal{S}(u_i, U_{Mi}) + \widehat{u}_i \end{cases} \tag{6.9}$$

where $\widehat{u}_i$ is the imaginary control input of the system. In this imaginary system, g_iu_i is treated as the known system dynamics. If we define $\widetilde{x}_i = x_i - \widehat{x}_i$ and $\widetilde{v}_i = v_i - \widehat{v}_i$ to represent the position and velocity tracking errors of the imaginary system regarding the actual system (6.3), respectively, we can then have the tracking error dynamics of system (6.9) as

$$\begin{cases} \dot{\widetilde{x}}_i = \widetilde{v}_i \\ \dot{\widetilde{v}}_i = w_i - \widehat{u}_i \end{cases} \tag{6.10}$$

In theory, when $\|\widetilde{x}_i\| = 0$ and $\|\widetilde{v}_i\| = 0$ are satisfied simultaneously, we also have $\|w_i - \widehat{u}_i\| = 0$. Hence, the final goal of the observer design is abstracted as designing an imaginary control input $\widehat{u}_i$ to achieve the semi-global uniform ultimate boundedness of the error states $\widetilde{x}_i$ and $\widetilde{v}_i$. Based on the observation errors $\widetilde{x}_i$ and $\widetilde{v}_i$, the estimation sliding surface of the observer is defined as

$$\widetilde{s}_i = \widetilde{v}_i + \widetilde{\lambda}_{i,1}\widetilde{x}_i \tag{6.11}$$

where $\widetilde{\lambda}_{i,1} \in \mathbb{R}^+$ represents the slope of the sliding surface.

Accordingly, the derivative of the estimation sliding surface $\widetilde{s}_i$ is given as

$$\dot{\widetilde{s}}_i = \dot{\widetilde{v}}_i + \widetilde{\lambda}_{i,1}\dot{\widetilde{x}}_i = w_i - \widehat{u}_i + \widetilde{\lambda}_{i,1}\widetilde{v}_i$$

Based on our previous analysis of the NN-based estimation (6.6) and the observer sliding surface design (6.11), we propose the following imaginary control input design for the neural-based sliding observer (6.9):

$$\widehat{u}_i = \widehat{W}_i^{\mathrm{T}} \mathcal{T}(Y_i) + \widetilde{\lambda}_{i,1}\widetilde{v}_i + \widetilde{c}_{i,1}\widetilde{s}_i + \widetilde{x}_i \tag{6.12}$$

where $\widetilde{c}_{i,1} \in \mathbb{R}^+$ is the imaginary controller's sensitivity to $\widetilde{s}_i$. The update law of the NN is chosen as

$$\dot{\widehat{W}}_i = \eta_1 \mathcal{T}(Y_i)\widetilde{s}_i^{\mathrm{T}} - \eta_2 \widehat{W}_i \tag{6.13}$$

where $\eta_1 \in \mathbb{R}^+$ indicates the NN's sensitivity to $\widetilde{s}_i$ and $\eta_2 \in \mathbb{R}^+$ is the damper constant that can prevent the divergence of weight matrix $\widehat{W}_i$.

Theorem 6.1. *Consider the imaginary second-order system* (6.9) *under Assumption 6.4. By the estimation sliding surface* (6.11)*, the sliding-variable-based tuning law* (6.13) *and the imaginary control input design* (6.12)*, we have that the states $\widetilde{s}_i$, $\widetilde{x}_i$ and $\widetilde{W}_i$ are all semi-globally UUB if the NN compact set conditions are satisfied for all agents when $t \geq t_0$.*

Proof. Consider the following continuous Lyapunov candidate:

$$V_{5,1} = \frac{1}{2}\widetilde{s}_i^{\mathrm{T}}\widetilde{s}_i + \frac{1}{2\eta_1}\mathrm{tr}\{\widetilde{W}_i^{\mathrm{T}}\widetilde{W}_i\} + \frac{1}{2}\widetilde{x}_i^{\mathrm{T}}\widetilde{x}_i$$

Then the time derivative of $V_{5,1}$ is obtained as

$$\begin{aligned}
\dot{V}_{5,1} &= \widetilde{s}_i^{\mathrm{T}}\dot{\widetilde{s}}_i - \frac{1}{\eta_1}\mathrm{tr}\{\widetilde{W}_i^{\mathrm{T}}\dot{\widehat{W}}_i\} + \widetilde{x}_i^{\mathrm{T}}\dot{\widetilde{x}}_i \\
&= \widetilde{s}_i^{\mathrm{T}}(w_i - \widehat{u}_i + \widetilde{\lambda}_{i,1}\widetilde{v}_i) - \frac{1}{\eta_1}\mathrm{tr}\{\widetilde{W}_i^{\mathrm{T}}\dot{\widehat{W}}_i\} + \widetilde{x}_i^{\mathrm{T}}(\widetilde{s}_i - \widetilde{\lambda}_{i,1}\widetilde{x}_i) \\
&= \widetilde{s}_i^{\mathrm{T}}(\widetilde{W}_i^{\mathrm{T}}\mathcal{T}(Y_i) + \epsilon_i - \widetilde{c}_{i,1}\widetilde{s}_i) - \mathrm{tr}\{\widetilde{W}_i^{\mathrm{T}}(\mathcal{T}(Y_i)\widetilde{s}_i^{\mathrm{T}} - \eta_2\widehat{W}_i/\eta_1)\} - \widetilde{\lambda}_{i,1}\widetilde{x}_i^{\mathrm{T}}\widetilde{x}_i \\
&\leq -\widetilde{c}_{i,1}\|\widetilde{s}_i\|^2 + \epsilon_M\|\widetilde{s}_i\| + \frac{\eta_2}{\eta_1}W_M\|\widetilde{W}_i\|_F - \frac{\eta_2}{\eta_1}\|\widetilde{W}_i\|_F^2 - \widetilde{\lambda}_{i,1}\|\widetilde{x}_i\|^2 \\
&\leq -\begin{bmatrix}\|\widetilde{s}_i\| & \|\widetilde{W}_i\|_F & \|\widetilde{x}_i\|\end{bmatrix}\begin{bmatrix}\widetilde{c}_{i,1} & 0 & 0 \\ 0 & \eta_2/\eta_1 & 0 \\ 0 & 0 & \widetilde{\lambda}_{i,1}\end{bmatrix}\begin{bmatrix}\|\widetilde{s}_i\| \\ \|\widetilde{W}_i\|_F \\ \|\widetilde{x}_i\|\end{bmatrix} \\
&\quad + \begin{bmatrix}\epsilon_M & \eta_2 W_M/\eta_1 & 0\end{bmatrix}\begin{bmatrix}\|\widetilde{s}_i\| \\ \|\widetilde{W}_i\|_F \\ \|\widetilde{x}_i\|\end{bmatrix}
\end{aligned} \tag{6.14}$$

Define

$$H_{5,1} = \begin{bmatrix} \widetilde{c}_{i,1} & 0 & 0 \\ 0 & \eta_2/\eta_1 & 0 \\ 0 & 0 & \widetilde{\lambda}_{i,1} \end{bmatrix},\ h_{5,1} = \begin{bmatrix} \epsilon_M & \eta_2 W_M/\eta_1 & 0 \end{bmatrix},\ \chi_{5,1} = \begin{bmatrix} \|\widetilde{s}_i\| \\ \|\widetilde{W}_i\|_F \\ \|\widetilde{x}_i\| \end{bmatrix}$$

then (6.14) is modified as

$$\begin{aligned} \dot{V}_{5,1} &\leq -\chi_{5,1}^{\mathrm{T}} H_{5,1}\chi_{5,1} + h_{5,1}\chi_{5,1} \\ &\leq -\underline{\sigma}(H_{5,1})\|\chi_{5,1}\|^2 + \|h_{5,1}\|\|\chi_{5,1}\| \end{aligned}$$

Hence, the time derivative $\dot{V}_{5,1}$ is negative when the following condition is met:

$$\|\chi_{5,1}\| > \frac{\|h_{5,1}\|}{\underline{\sigma}(H_{5,1})}$$

By the characteristics of matrix norm and Lemma 2.1, we have that the states $\widetilde{s}_i$, $\widetilde{W}_i$ and $\widetilde{x}_i$ are semi-globally UUB within the following neighbourhood, respectively:

$$\begin{aligned} \Omega_{\widetilde{s}} &= \left\{ \widetilde{s}_i \middle| \|\widetilde{s}_i\| \leq \frac{\eta_1\epsilon_M + \eta_2 W_M}{\eta_1\underline{\sigma}(H_1)} \right\} \\ \Omega_{\widetilde{W}} &= \left\{ \widetilde{W}_i \middle| \|\widetilde{W}_i\|_F \leq \frac{\eta_1\epsilon_M + \eta_2 W_M}{\eta_1\underline{\sigma}(H_1)} \right\} \\ \Omega_{\widetilde{x}}^3 &= \left\{ \widetilde{x}_i \middle| \|\widetilde{x}_i\| \leq \frac{\eta_1\epsilon_M + \eta_2 W_M}{\eta_1\underline{\sigma}(H_1)} \right\} \end{aligned} \tag{6.15}$$

which completes the proof. □

Remark 6.2. *Note that NNs with three or more layers (Liu* et al. *2013) are often found to have higher estimation precision over two-layer NNs. Besides,* (6.13) *is not the optimal tuning law because we have* $\dot{\widehat{W}}_i = -\eta_2\widehat{W}_i$ *when* $\|\widetilde{s}_i\| = 0$*, which further leads to a potential divergence issue. However, the neural-based observer structure in* (6.9) *is still expected to have robust performance because the final estimation* (6.12) *is not fully dependent on the output of the NN. The error-related terms such as* $\widetilde{\lambda}_{i,1}\widetilde{v}_i$ *,*$\widetilde{c}_{i,1}\widetilde{s}_i$ *and* $\widetilde{x}_i$ *are able to compensate for the network bias* ϵ_i *and further leads to* $\|w_i - \widehat{u}_i\| \leq \epsilon_M$*. Hence, we can still ensure that the estimation error of structure* (6.9) *will be bounded within a small neighbourhood around zero while the structure's simplicity is maintained by employing two-layer NNs instead of multi-layer NNs.*

6.4.2 Practical finite-time neural-based sliding mode observer

It is undeniable that the performance of an observer-based controller is correlated with the characteristic of the observer. Hence, it is vital to design an observer with finite error converging time. To acquire finite-time characteristics, the previous linear sliding surface is modified into a finite-time sliding surface for the observer as follows:

$$\widetilde{s}_i = \widetilde{v}_i + \widetilde{\lambda}_{i,1}\widetilde{x}_i + \widetilde{\lambda}_{i,2}\widetilde{x}_i^p \tag{6.16}$$

where $\widetilde{\lambda}_{i,2}$ is a positive constant, $p = p_1/p_2 \in (0,1)$, p_1 and p_2 are both positive odd number and $p_1 < p_2$. Define $\widetilde{x}_i(j)$ to be the jth element in $\widetilde{x}_i$, then we have $\widetilde{x}_i^p = [\widetilde{x}_i^p(1), \widetilde{x}_i^p(2), \ldots, \widetilde{x}_i^p(n)]^{\mathrm{T}}$.

The time derivative of the terminal sliding surface (6.16) is expressed as

$$\dot{\widetilde{s}}_i = \dot{\widetilde{v}}_i + \widetilde{\lambda}_{i,1}\widetilde{v}_i + p\widetilde{\lambda}_{i,2}\mathrm{diag}\{\widetilde{x}_i^{p-1}\}\widetilde{v}_i$$

It is observed that there is a potential singular issue when $\|\widetilde{x}_i\| \to 0$. Inspired by Wang et al. (Wang *et al.* 2018b) and Feng et al. (Feng *et al.* 2013), a saturation function is implemented to avoid singularity, and the controller design is given as

$$\widehat{u}_i = \widehat{W}_i^{\mathrm{T}}\mathcal{T}(Y_i) + \widetilde{c}_{i,1}\widetilde{s}_i + \widetilde{c}_{i,2}\widetilde{s}_i^p + \widetilde{x}_i + \widetilde{\lambda}_{i,1}\widetilde{v}_i + p\widetilde{\lambda}_{i,2}\mathrm{diag}\{\mathcal{S}(\widetilde{x}_i^{p-1}, h)\}\widetilde{v}_i \tag{6.17}$$

where h is a positive constant.

Before presenting the theorem for the practical finite-time observer design, let us first recall some useful results.

Lemma 6.1. (Sun *et al.* 2021a) *For any variables ζ_1 and ζ_2, we have*

$$|\zeta_1|^{\bar{\zeta}_1}|\zeta_2|^{\bar{\zeta}_2} \le \frac{\bar{\zeta}_1}{\bar{\zeta}_1+\bar{\zeta}_2}\bar{\zeta}_3|\zeta_1|^{\bar{\zeta}_1+\bar{\zeta}_2} + \frac{\bar{\zeta}_2}{\bar{\zeta}_1+\bar{\zeta}_2}\bar{\zeta}_3^{-\bar{\zeta}_1/\bar{\zeta}_2}|\zeta_1|^{\bar{\zeta}_1+\bar{\zeta}_2}$$

where $\bar{\zeta}_1$, $\bar{\zeta}_2$ and $\bar{\zeta}_3$ are all positive constants.

Definition 6.1. (Sun *et al.* 2021a) *Consider a vector X whose equilibrium point is $\|X\| = 0$ and its correlated continuous Lyapunov function $V(X)$. Then vector X is said to be semi-globally practically finite-time bounded (SGPFTB) if there exists a positive scalar b_X and a finite converging time $t_{\mathrm{set}} < \infty$ such that $\|X\| \le b_X$ for all $t \ge t_{\mathrm{set}}$ and $X(t_0) \in \Omega_V^X$.*

Lemma 6.2. (Sun *et al.* 2021a) *Suppose there exists scalars $\bar{\beta}_1 > 0$, $\bar{\alpha}_1 \in (0,1)$ and $\bar{\gamma}_1 > 0$. Consider a vector X that satisfies $X(t_0) \in \Omega_V^X$ and its correlated continuous Lyapunov function $V(X)$ that satisfies the following inequality:*

$$\dot{V}(X) \le -\bar{\beta}_1 V^{\bar{\alpha}_1}(X) + \bar{\gamma}_1,\ t \ge t_0$$

Then X is considered to be SGPFTB within the residual region of

$$\Omega_X = \left\{ X \middle| V(X) \leq \left(\frac{\bar{\gamma}_1}{(1-\bar{\beta}_3)\bar{\beta}_1} \right)^{1/\alpha_1} \right\}$$

where $\bar{\beta}_3 \in (0,1)$. The finite convergence time t_{set} is provided as

$$t_{\text{set}} \leq \frac{1}{\bar{\beta}_1 \bar{\beta}_3 (1-\bar{\alpha}_1)} \left[V^{1-\bar{\alpha}}(X(t_0)) - \left(\frac{\bar{\gamma}_1}{(1-\bar{\beta}_3)\bar{\beta}_1} \right)^{(1-\bar{\alpha}_1)/\bar{\alpha}_1} \right]$$

The following theorem summarises the development of the finite-time neural-based sliding mode observer:

Theorem 6.2. *Consider the imaginary second-order system* (6.9) *under Assumption 6.4. By the estimation sliding surface design* (6.16)*, the sliding-variable-based tuning law* (6.13) *and the imaginary control input* (6.17)*, we have the following results if the NN compact set conditions are satisfied for all agents when $t \geq t_0$:*

1. *The error-related vectors $\widetilde{W}_i$, $\widetilde{s}_i$ and $\widetilde{x}_i$ are all semi-globally UUB.*
2. *The error-related vectors $\widetilde{W}_i$, $\widetilde{s}_i$ and $\widetilde{x}_i$ are all SGPFTB if $2\widetilde{c}_{i,1} - 1 > 0$.*

Proof. This proof contains two parts, the semi-global uniform ultimate boundedness of $\widetilde{W}_i$, $\widetilde{s}_i$ and $\widetilde{x}_i$ are proved in the Part 6.2.1 while their finite-time characteristics are addressed in Part 6.2.2.

Part 6.2.1. Consider the following continuous Lyapunov candidate for the imaginary system (6.9):

$$V_{5,1} = \frac{1}{2}\widetilde{s}_i^{\mathrm{T}}\widetilde{s}_i + \frac{1}{2\eta_1}\mathrm{tr}\{\widetilde{W}_i^{\mathrm{T}}\widetilde{W}_i\} + \frac{1}{2}\widetilde{x}_i^{\mathrm{T}}\widetilde{x}_i \tag{6.18}$$

Then $\dot{V}_{5,1}$ is given as

$$\begin{aligned}
\dot{V}_{5,1} &= \widetilde{s}_i^{\mathrm{T}}\dot{\widetilde{s}}_i - \frac{1}{\eta_1}\mathrm{tr}\{\widetilde{W}_i^{\mathrm{T}}\dot{\widehat{W}}_i\} + \widetilde{x}_i^{\mathrm{T}}\widetilde{v}_i \\
&= \widetilde{s}_i^{\mathrm{T}}(w_i - \widehat{u}_i + \widetilde{\lambda}_{i,1}\widetilde{v}_i + p\widetilde{\lambda}_{i,2}\mathrm{diag}\{\widetilde{x}_i^{p-1}\}\widetilde{v}_i) - \mathrm{tr}\{\widetilde{W}_i^{\mathrm{T}}\mathcal{T}(Y_i)\widetilde{s}_i^{\mathrm{T}} - \eta_2\widehat{W}_i/\eta_1\} \\
&\quad + \widetilde{x}_i^{\mathrm{T}}(\widetilde{s}_i - \widetilde{\lambda}_{i,1}\widetilde{x}_i - \widetilde{\lambda}_{i,2}\widetilde{x}_i^p) \\
&= \widetilde{s}_i^{\mathrm{T}}\epsilon_i - \widetilde{c}_{i,1}\widetilde{s}_i^{\mathrm{T}}\widetilde{s}_i - \widetilde{c}_{i,2}\widetilde{s}_i^{\mathrm{T}}\widetilde{s}_i^p + \widetilde{s}_i^{\mathrm{T}}\widetilde{\lambda}_{i,2}\mathrm{diag}\{\widetilde{x}_i^{p-1} - \mathcal{S}(\widetilde{x}_i^{p-1}, h)\}\widetilde{v}_i - \widetilde{\lambda}_{i,1}\widetilde{x}_i^{\mathrm{T}}\widetilde{x}_i - \widetilde{\lambda}_{i,2}\widetilde{x}_i^{\mathrm{T}}\widetilde{x}_i^p \\
&\quad - \frac{\eta_2}{\eta_1}\mathrm{tr}\{\widetilde{W}_i^{\mathrm{T}}(W_i - \widetilde{W}_i)\}
\end{aligned} \tag{6.19}$$

According to Wang et al. (Wang *et al.* 2018b) and Feng et al. (Feng *et al.* 2013), the system is said to enter the singular region when $\mathcal{S}(\widetilde{x}_i^{p-1}, h) \neq \widetilde{x}_i^{p-1}$. However, it is proved that the state $\widetilde{x}_i$ is expected to escape the singular region monotonically, meaning that the singular region does not affect the stability of the method and (6.19) is further reduced as

$$\begin{aligned}\dot{V}_{5,1} \leq& -\widetilde{c}_{i,1}\|\widetilde{s}_i\|^2 - \widetilde{c}_{i,2}\|\widetilde{s}_i\|^{p+1} + \epsilon_M\|\widetilde{s}_i\| - \frac{\eta_2}{\eta_1}\|\widetilde{W}_i\|_F^2 + \frac{\eta_2}{\eta_1}W_M\|\widetilde{W}_i\|_F - \widetilde{\lambda}_{i,1}\|\widetilde{x}_i\|^2 \\ &- \widetilde{\lambda}_{i,2}\|\widetilde{x}_i\|^{p+1} \\ \leq& -\chi_{5,1}^{\mathrm{T}}H_{5,1}\chi_{5,1} + h_{5,1}\chi_{5,1}\end{aligned} \tag{6.20}$$

Hence, by Lemma 2.1, we have that $\widetilde{s}_i$, $\widetilde{x}_i$ and $\widetilde{W}_i$ are semi-globally UUB within the neighbourhood presented in (6.15).

Part 6.2.2. Still, we consider the Lyapunov function $V_{5,1}$ and the inequality presented in (6.20). By using Young's inequality, we have

$$\epsilon_M\|\widetilde{s}_i\| \leq \frac{1}{2}\epsilon_M^2 + \frac{1}{2}\|\widetilde{s}_i\|^2,\ \frac{\eta_2}{\eta_1}W_M\|\widetilde{W}_i\|_F \leq \frac{\eta_2}{2\eta_1}W_M^2 + \frac{\eta_2}{2\eta_1}\|\widetilde{W}_i\|_F^2$$

Then we can rewrite (6.20) as

$$\begin{aligned}\dot{V}_{5,1} \leq& -\frac{2\widetilde{c}_{i,1}-1}{2}\|\widetilde{s}_i\|^2 - \widetilde{c}_{i,2}\|\widetilde{s}_i\|^{p+1} + \frac{1}{2}\epsilon_M^2 - \frac{\eta_2}{2\eta_1}\|\widetilde{W}_i\|_F^2 + \frac{\eta_2}{2\eta_1}W_M^2 - \widetilde{\lambda}_{i,1}\|\widetilde{x}_i\|^2 \\ &- \widetilde{\lambda}_{i,2}\|\widetilde{x}_i\|^{p+1}\end{aligned}$$

By Lemma 6.1, choose $\bar{\zeta}_1 = 1-p$, $\bar{\zeta}_2 = 1+p$, $\zeta_1 = 1$ and $\zeta_2 = \|\widetilde{s}_i\|$, then one has

$$\|\widetilde{s}_i\|^{1+p} \leq \frac{1-p}{2}\left(\frac{2}{1+p}\right)^{(p+1)/(p-1)} + \|\widetilde{s}_i\|^2$$

Similarly results are also obtained for $\|\widetilde{x}_i\|$ and $\|\widetilde{W}_i\|_F$ as follows, respectively:

$$\|\widetilde{x}_i\|^{1+p} \leq \frac{1-p}{2}\left(\frac{2}{p+1}\right)^{(p+1)/(p-1)} + \|\widetilde{x}_i\|^2$$
$$\|\widetilde{W}_i\|_F^{p+1} \leq \frac{1-p}{2}\left(\frac{2}{p+1}\right)^{(p+1)/(p-1)} + \|\widetilde{W}_i\|_F^2$$

Define Δ_V^1 to be a positive constant as follows

$$\Delta_V^1 = \left(\frac{(1-p)(2\widetilde{c}_{i,1}-1)}{4} + \frac{\widetilde{\lambda}_{i,1}(1-p)}{2} + \frac{\eta_2(1-p)}{4\eta_1}\right)\left(\frac{2}{p+1}\right)^{(p+1)/(p-1)}$$

$$+\frac{1}{2}\epsilon_M^2+\frac{\eta_2}{2\eta_1}W_M^2$$

Then we have

$$\dot{V}_{5,1}\leq-\frac{2\widetilde{c}_{i,1}+2\widetilde{c}_{i,2}-1}{2}\|\widetilde{s}_i\|^{1+p}-\frac{\eta_2}{2\eta_1}\|\widetilde{W}_i\|_F^{1+p}-(\widetilde{\lambda}_{i,1}+\widetilde{\lambda}_{i,2})\|\widetilde{x}_i\|^{1+p}+\Delta_V^1$$

Based on the format of $V_{5,1}$, we have the following transformations

$$\|\widetilde{s}_i\|^{1+p}=2^{(1+p)/2}\left(\frac{1}{2}\|\widetilde{s}_i\|^2\right)^{(1+p)/2}$$
$$\|\widetilde{W}_i\|_F^{1+p}=(2\eta_1)^{(1+p)/2}\left(\frac{1}{2\eta_1}\|\widetilde{W}_i\|_F^2\right)^{(1+p)/2}$$
$$\|\widetilde{x}_i\|^{1+p}=2^{(1+p)/2}\left(\frac{1}{2}\|\widetilde{x}_i\|^2\right)^{(1+p)/2}$$

Hence, $\dot{V}_{5,1}$ has the following alternative expression:

$$\dot{V}_{5,1}\leq-\beta_1V_{5,1}^{(1+p)/2}+\Delta_V^1$$

where

$$\beta_1=2^{(p-1)/2}\min\{2\widetilde{c}_{i,1}+2\widetilde{c}_{i,2}-1,\eta_2\eta_1^{(p-1)/2},2(\widetilde{\lambda}_{i,1}+\widetilde{\lambda}_{i,2})\}$$

By Lemma 6.2, with $2\widetilde{c}_{i,1}-1>0$, we have that $\widetilde{W}_i$, $\widetilde{s}_i$ and $\widetilde{x}_i$ are all SGPFTB, which completes the proof.

□

After illustrating the development of the neural-based sliding mode observer, we now focus on the cooperative formation control problem regarding (6.4).

6.4.3 Robust formation control via linear programming

With the definition of δ_{xi} and δ_{vi} in (2.8), the cluster expression of the error dynamics is written as follows:

$$\begin{cases}\dot{\delta}_x=\delta_v\\ \dot{\delta}_v=-\ddot{x}_d+g\mathcal{S}(u)+w\end{cases}$$

where $\delta_x = [\delta_{x1}^{\mathrm{T}}, \delta_{x2}^{\mathrm{T}}, \ldots, \delta_{xN}^{\mathrm{T}}]^{\mathrm{T}} \in \mathbb{R}^{nN}$, $\delta_v = [\delta_{v1}^{\mathrm{T}}, \delta_{v2}^{\mathrm{T}}, \ldots, \delta_{vN}^{\mathrm{T}}]^{\mathrm{T}} \in \mathbb{R}^{nN}$, and $x_d = [x_{d1}^{\mathrm{T}}, x_{d2}^{\mathrm{T}}, \ldots, x_{dN}^{\mathrm{T}}]^{\mathrm{T}} \in \mathbb{R}^{nN}$.

With the definition of local errors as mentioned in (2.12), the following sliding surface is defined for the controller construction:

$$s_i = e_{vi} + \lambda_i e_{xi} \tag{6.21}$$

where $\lambda_i \in \mathbb{R}^+$ indicates the slope of the sliding surface.

Define $\Lambda = \mathrm{diag}\{\lambda_1, \lambda_2, \ldots, \lambda_N\} \in \mathbb{R}^{N\times N}$, then the cluster is expressed as

$$\dot{S} = (L+B) \otimes I_n(-\ddot{x}_d + g\mathcal{S}(u) + w + \Lambda \otimes I_n \delta_v)$$

where $e_x = [e_{x1}^{\mathrm{T}}, e_{x2}^{\mathrm{T}}, \ldots, e_{xN}^{\mathrm{T}}]^{\mathrm{T}} \in \mathbb{R}^{nN}$, $x_d = [x_{d1}^{\mathrm{T}}, x_{d2}^{\mathrm{T}}, \ldots, x_{dN}^{\mathrm{T}}]^{\mathrm{T}} \in \mathbb{R}^{nN}$ and $S = [s_1^{\mathrm{T}}, s_2^{\mathrm{T}}, \ldots, s_N^{\mathrm{T}}]^{\mathrm{T}} \in \mathbb{R}^{nN}$.

Suppose that the actuator is ideal instead of saturated, we then construct the following nominal sliding mode controller for the ith agent:

$$u_i^{\mathrm{nom}} = g_i^{-1}(\ddot{x}_{di} - \widehat{u}_i - c_i s_i - \lambda_i \delta_{vi} - \delta_{xi}) \tag{6.22}$$

where $c_i \in \mathbb{R}^+$ denotes the controller's sensitivity to the value of sliding variable s_i.

However, regarding a second-order system (6.3) with actuator saturation, the controller design u_i^{nom} will lead to the state windup issue (Cui *et al.* 2016, Ding and Zheng 2016), which indicates that u_i^{nom} is inadequate. To ease the state windup phenomenon, the method of employing auxiliary variables (Cui *et al.* 2016, Han *et al.* 2019) is commonly used. Inspired by the discrete-time compensator design (Han *et al.* 2019) proposed by Han et al., a new compensator design is developed for continuous-time systems.

Define an auxiliary vector $\xi_i \in \mathbb{R}^n$ for the ith agent to act as the anti-windup compensator. Then we modify the previous nominal sliding mode controller into the following form:

$$u_i^{\mathrm{com}} = g_i^{-1}(\ddot{x}_{di} - \widehat{u}_i - c_i s_i - \lambda_i \delta_{vi} - \delta_{xi} - c_i \xi_i) \tag{6.23}$$

To make the vector ξ_i adaptive, we choose the following tuning law:

$$\dot{\xi}_i = \eta_3 g_i u_i^{\mathrm{diff}} - \eta_4 \xi_i \tag{6.24}$$

where $u_i^{\text{diff}} = u_i^{\text{com}} - \mathcal{S}(u_i^{\text{com}}, U_{Mi})$ denotes the difference between the desired compensated control input u_i^{com} and the actual capability of the saturated actuator, $\eta_3 \in \mathbb{R}^+$ is the auxiliary variable's sensitivity to u_i^{diff} and $\eta_4 \in \mathbb{R}^+$ is the self-converging speed of ξ_i.

As mentioned in Chapter 5, employing saturation phenomenon to the control input arbitrarily is insufficient. Hence, it is still essential to make modification to the compensated nominal control input in (6.23) to conquer the following problem:

Problem 6.2. *The amplitude of* (6.23) *is not bounded and may exceed the saturation limitation. Hence, how to reduce the scenarios where the reverse effect is triggered and attenuate state chattering and oscillation is an important issue to investigate.*

To deal with Problem 6.2, the linear programming method is employed to regulate u_i^{com} to further obtain a new control input u_i^{reg}. The goal of employing the linear programming method lies in the following three parts:

1. Ensure that the amplitudes of the elements in u_i^{reg} do not exceed the saturation limitation U_{Mi}. In other words, we have $u_i^{\text{reg}} = \mathcal{S}(u_i^{\text{reg}}, U_{Mi})$.
2. Attenuate the reverse effect by reducing the circumstances when $\text{sign}(g_i u_i) \neq \text{sign}(g_i \mathcal{S}(u_i))$.
3. Minimise the difference between $g_i u_i^{\text{com}}$ and $g_i u_i^{\text{reg}}$.

Normally, a linear programming problem contains two important parts, the restrictions of the variables and the cost function to maximise or minimise. The optimisation restrictions are usually expressed as follows:

$$\begin{aligned} &\mathcal{A}\mathcal{X} \leq \mathcal{B} \\ &\mathcal{A}_{\text{eq}}\mathcal{X} = \mathcal{B}_{\text{eq}} \\ &\mathcal{B}_l \leq \mathcal{X} \leq \mathcal{B}_u \end{aligned} \tag{6.25}$$

where $\mathcal{X} \in \mathbb{R}^n$ is the vector to be optimised, $\mathcal{A}$ and $\mathcal{A}_{\text{eq}}$ are $n \times n$ matrices, $\mathcal{B}$, $\mathcal{B}_{\text{eq}}$, $\mathcal{B}_l$ and $\mathcal{B}_u$ are $n \times 1$ vectors.

To achieve $u_i^{\text{reg}} = \mathcal{S}(u_i^{\text{reg}}, U_{Mi})$, it is vital to have $-U_{Mi}\mathbf{1}_{n\times 1} \leq u_i^{\text{reg}} \leq U_{Mi}\mathbf{1}_{n\times 1}$. Because the output of the linear programming algorithm is u_i^{reg}, the upper and lower bounds of u_i^{reg} are chosen as $\mathcal{B}_l = -U_{Mi}\mathbf{1}_{n\times 1}$ and $\mathcal{B}_u = U_{Mi}\mathbf{1}_{n\times 1}$, respectively.

To attenuate the reverse effect, it is essential to have a case by case discussion to obtain the optimisation restrictions $\mathcal{A}$, $\mathcal{B}$, $\mathcal{A}_{\text{eq}}$ and $\mathcal{B}_{\text{eq}}$.

1. Define $g_i(j)$ to be the jth row in matrix g_i. When $g_i(j)u_i^{\text{com}} = 0$, we can use equation $\mathcal{A}_{\text{eq}}\mathcal{X} = \mathcal{B}_{\text{eq}}$ to express our expectation by having $g_i(j)u_i^{\text{reg}} = 0$.

2. When $g_i(j)u_i^{\text{com}} \neq 0$, there are two restrictions that can be given in the form of $\mathcal{A}\mathcal{X} \leq \mathcal{B}$. First, to ensure $\text{sign}(g_i(j)u_i^{\text{reg}}) \neq -\text{sign}(g_i(j)u_i^{\text{com}})$, we need to have $-\text{sign}(g_i(j)u_i^{\text{com}})g_i(j)u_i^{\text{reg}} \leq 0$.

   Besides, the overall effect of u_i^{reg} should be less than the one of u_i^{com} to reduce state oscillation. Hence, we also have

$$\text{sign}(g_i(j)u_i^{\text{com}})g_i(j)u_i^{\text{reg}} \leq \text{sign}(g_i(j)u_i^{\text{com}})g_i(j)u_i^{\text{com}}$$

The last element to confirm is the cost function to minimise, which is the difference between $g_iu_i^{\text{com}}$ and $g_iu_i^{\text{reg}}$. With the conditions that $g_i(j)u_i^{\text{reg}} = 0$ when $g_i(j)u_i^{\text{com}} = 0$ and $\text{sign}(g_i(j)u_i^{\text{reg}}) \neq -\text{sign}(g_i(j)u_i^{\text{com}})$ when $g_i(j)u_i^{\text{com}} \neq 0$, we construct the following cost function to illustrate the difference between $g_iu_i^{\text{com}}$ and $g_iu_i^{\text{reg}}$:

$$\Xi_1(u_i^{\text{reg}}) = \sum_{j=1}^{n} \text{sign}(g_i(j)u_i^{\text{com}})(g_i(j)u_i^{\text{com}} - g_i(j)u_i^{\text{reg}}) \tag{6.26}$$

Although the value of $g_iu_i^{\text{com}}$ is time-varying, as long as we know $\text{sign}(g_iu_i^{\text{com}})$, the specific value of $g_iu_i^{\text{com}}$ does not affect the final result of the optimisation. Hence, we can simplify the cost function as

$$\Xi_2(u_i^{\text{reg}}) = -\sum_{j=1}^{n} \text{sign}(g_i(j)u_i^{\text{com}})g_i(j)u_i^{\text{reg}} \tag{6.27}$$

Accordingly, we can summarise the problem formulation of the linear programming process as finding the vector u_i^{reg} that minimise the difference between $g_i(j)u_i^{\text{reg}}$ and $g_i(j)u_i^{\text{com}}$, which has the following mathematical expression:

$$u_i^{\text{reg}} = \text{argmin}_U \Xi_2(U), \text{ when } \mathcal{A}U \leq \mathcal{B},\ \mathcal{A}_{\text{eq}}U = \mathcal{B}_{\text{eq}} \text{ and } \mathcal{B}_l \leq U \leq \mathcal{B}_u \tag{6.28}$$

The detailed steps of the linear programming process is illustrated in in Algorithm 3. Although linear programming is an optimisation tool, it is only employed as an

Algorithm 3: Linear-programming-based control input regulation algorithm (LPB-CIRA)

Input: u_i^{com}, g_i
Output: u_i^{reg}
$\mathcal{B}_l = -U_{Mi}\mathbf{1}_{n\times 1}$;
$\mathcal{B}_u = U_{Mi}\mathbf{1}_{n\times 1}$;
if $u_i^{\text{com}} \neq \mathcal{S}(u_i^{\text{com}}, U_{Mi})$ **then**
  for $j = 1 : n$ **do**
    if $g_i(j)u_i^{\text{com}} = 0$ **then**
      $\mathcal{B}_{\text{tem}} = 0$;
      $\mathcal{A}_{\text{tem}} = g_i(j)$;
      Add $\mathcal{A}_{\text{tem}}$ and $\mathcal{B}_{\text{tem}}$ to $\mathcal{A}_{\text{eq}}$ and $\mathcal{B}_{\text{eq}}$, respectively;
    else
      $\mathcal{B}_{\text{tem}} = g_i(j)u_i^{\text{com}}$;
      $\mathcal{A}_{\text{tem}} = \text{sign}(g_i(j)u_i^{\text{com}})g_i(j)$;
      Add $\mathcal{A}_{\text{tem}}$ and $\mathcal{B}_{\text{tem}}$ to $\mathcal{A}$ and $\mathcal{B}$, respectively;
      $\mathcal{B}_{\text{tem}} = 0$;
      $\mathcal{A}_{\text{tem}} = -\text{sign}(g_i(j)u_i^{\text{com}})g_i(j)$;
      Add $\mathcal{A}_{\text{tem}}$ and $\mathcal{B}_{\text{tem}}$ to $\mathcal{A}$ and $\mathcal{B}$, respectively;
    end
  end
  Obtain $u_i^{\text{reg}} = \arg\min_{\mathcal{X}} \Xi_2(\mathcal{X})$ that subjects to (6.25);
else
  $u_i^{\text{reg}} = u_i^{\text{com}}$;
end
Return u_i^{reg}

attachment for the sliding mode controller in (6.23), which makes it different from the conventional optimal controller. Hence, to avoid misleading, Algorithm 3 is named as the linear-programming-based control input regulation algorithm (LPBCIRA) to better illustrate its purpose.

Based on our discussions on the finite-time sliding mode observer (6.17), the sliding surface (6.21), the adaptive auxiliary variable (6.24), the compensated controller design

(6.23) and the LPBCIRA (Algorithm 3), we have the overall system diagram in Figure 6.1.

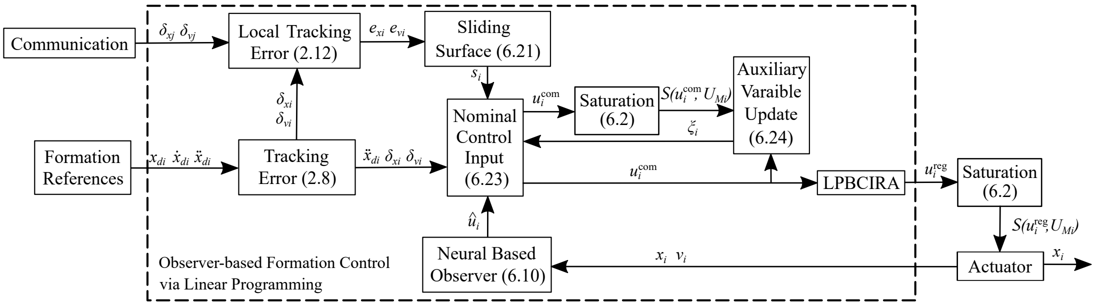

Figure 6.1. Observer-based formation control via linear programming.

The following theorem summarises the proposed robust sliding mode formation controller design:

Theorem 6.3. *Consider a cluster of saturated second-order agents* (6.4) *under Assumptions 6.1- 6.4. By the finite-time sliding mode observer* (6.17)*, the sliding surface design* (6.21)*, the anti-windup compensator ξ_i, the auxiliary variable tuning law* (6.24)*, the compensated nominal formation controller* (6.23) *and the LPBCIRA (Algorithm 3), the states δ_x, e_x and S are all semi-globally UUB if the NN compact set conditions are satisfied for all agents when $t \geq t_0$ and the parameters of the observer-based controller are chosen properly such that the following matrix is positive definite:*

$$H_{5,2} = \begin{bmatrix} \underline{\sigma}(QC)/2 & 0 & -\overline{\sigma}(QC)/4 & -\mathcal{K}_4/2 & 0 & -\overline{\sigma}(Q)\mathcal{T}_M/4 & 0 \\ 0 & \underline{\sigma}(P\Lambda) & 0 & -\mathcal{K}_3/2 & 0 & 0 & 0 \\ -\overline{\sigma}(QC)/4 & 0 & \eta_4 & -\mathcal{K}_5/2 & 0 & 0 & 0 \\ -\mathcal{K}_4/2 & -\mathcal{K}_3/2 & -\mathcal{K}_5/2 & \underline{\sigma}(C) & 0 & -\mathcal{K}_1/2 & 0 \\ 0 & 0 & 0 & 0 & \underline{\sigma}(\widetilde{C}) & 0 & 0 \\ -\overline{\sigma}(Q)\mathcal{T}_M/4 & 0 & 0 & -\mathcal{K}_1/2 & 0 & \eta_2/\eta_1 & 0 \\ 0 & 0 & 0 & 0 & 0 & 0 & \underline{\sigma}(\widetilde{\Lambda}) \end{bmatrix}$$

where

$$\mathcal{K}_1 = \mathcal{T}_M \frac{\overline{\sigma}(Q)}{2}, \; \mathcal{K}_2 = \frac{\overline{\sigma}(Q)\overline{\sigma}(C)}{2} + \frac{1}{\underline{\sigma}(L+B)}$$
$$\mathcal{K}_3 = \overline{\sigma}(C) + \frac{\overline{\sigma}(\Lambda)}{\underline{\sigma}(L+B)}, \; \mathcal{K}_4 = \frac{\overline{\sigma}(Q)}{2} + \mathcal{K}_2$$
$$\mathcal{K}_5 = \eta_3 + \frac{\overline{\sigma}(Q)\overline{\sigma}(C)}{2}$$
$$\widetilde{C} = \mathrm{diag}\{\widetilde{c}_{1,1}, \widetilde{c}_{2,1}, \ldots, \widetilde{c}_{N,1}\}$$

$$\widetilde{\Lambda} = \mathrm{diag}\{\widetilde{\lambda}_{1,1}, \widetilde{\lambda}_{2,1}, \ldots, \widetilde{\lambda}_{N,1}\}$$

Proof. Note that our final design u_i^{reg} is based on the compensated controller design u_i^{com}. Meanwhile, based on the restrictions of the linear programming algorithm process, we get that u_i^{reg} is a stable and valid design if and only if u_i^{com} is capable of ensuring the semi-global uniform ultimate boundedness of the error-related states. Hence, this proof is carried out based on the condition that $u_i = u_i^{\mathrm{com}}$.

Define $\xi = [\xi_1^{\mathrm{T}}, \xi_2^{\mathrm{T}}, \ldots, \xi_N^{\mathrm{T}}]^{\mathrm{T}}$, $u^{\mathrm{diff}} = [(u_1^{\mathrm{diff}})^{\mathrm{T}}, (u_2^{\mathrm{diff}})^{\mathrm{T}}, \ldots, (u_N^{\mathrm{diff}})^{\mathrm{T}}]^{\mathrm{T}} \in \mathbb{R}^{nN}$, $\mathcal{S}(u^{\mathrm{com}}) = [\mathcal{S}_1^{\mathrm{T}}(u_1^{\mathrm{com}}, U_{M1}), \mathcal{S}_2^{\mathrm{T}}(u_2^{\mathrm{com}}, U_{M2}), \ldots, \mathcal{S}_N^{\mathrm{T}}(u_N^{\mathrm{com}}, U_{MN})]^{\mathrm{T}}$, $\widehat{u} = [\widehat{u}_1^{\mathrm{T}}, \widehat{u}_2^{\mathrm{T}}, \ldots, \widehat{u}_N^{\mathrm{T}}]^{\mathrm{T}}$, $\kappa = gu^{\mathrm{diff}}$ and $C = \mathrm{diag}\{c_1, c_2, \ldots, c_N\} \in \mathbb{R}^{N\times N}$, then consider the following Lyapunov candidates for the system (6.4):

$$V_{5,2} = \frac{1}{2}S^{\mathrm{T}}P \otimes I_n S + \frac{1}{2}e_x^{\mathrm{T}}P \otimes I_n e_x,\ V_\xi = \frac{1}{2}\xi^{\mathrm{T}}\xi,\ V_\kappa = \frac{1}{2}\kappa^{\mathrm{T}}\kappa$$

According to (6.24), we have the time derivative of V_ξ as

$$\begin{aligned}\dot{V}_\xi &= \xi^{\mathrm{T}}\dot{\xi} \\ &= \xi^{\mathrm{T}}(\eta_3 g u^{\mathrm{diff}} - \eta_4 \xi) \\ &\leq \eta_3\|\xi\|\|\kappa\| - \eta_4\|\xi\|^2\end{aligned}$$

For $V_{5,2}$, the time derivative is obtained as

$$\begin{aligned}\dot{V}_{5,2} &= S^{\mathrm{T}}P \otimes I_n\dot{S} + e_x^{\mathrm{T}}P \otimes I_n\dot{e}_x \\ &= S^{\mathrm{T}}(P(L+B)) \otimes I_n(-\ddot{x}_d + g\mathcal{S}(u^{\mathrm{com}}) + w + \Lambda \otimes I_n\delta_v) + e_x^{\mathrm{T}}P \otimes I_n(S - \Lambda \otimes I_n e_x) \\ &= S^{\mathrm{T}}(P(L+B)) \otimes I_n(-\ddot{x}_d + gu^{\mathrm{com}} - gu^{\mathrm{diff}} + w + \Lambda \otimes I_n\delta_v) + e_x^{\mathrm{T}}P \otimes I_n(S \\ &\quad - \Lambda \otimes I_n e_x) \\ &= S^{\mathrm{T}}(P(L+B)) \otimes I_n(\widetilde{w}^O - C \otimes I_n S - C \otimes I_n\xi - \kappa) - e_x^{\mathrm{T}}(P\Lambda) \otimes I_n e_x\end{aligned}$$

where $\widetilde{w}^O = w - \widehat{u}$. By the finite-time characteristics of design (6.17), we have that the estimation error states $\widetilde{x}_i$, $\widetilde{s}_i$ and $\widetilde{W}_i$ are all SGPFTB. Hence, it is reasonable to have that $\widetilde{w}^O$ is bounded when $t \geq t_o$ such that $\|\widetilde{w}^O\| \leq \|\widetilde{W}\|_F\|\mathcal{T}(Y)\| + \bar{\epsilon}_M$, where $\widetilde{W} = \mathrm{diag}\{\widetilde{W}_1, \widetilde{W}_2, \ldots, \widetilde{W}_N\}$ and $\bar{\epsilon}_M$ is a bounded positive constant.

Besides, we get that the fictitious control input $\widehat{u}_i$ is bounded when $t \geq t_o$ such that there is $\|\dot{\widehat{u}}\| \leq \widehat{u}_M^1$, where $\widehat{u} = [\widehat{u}_1^{\mathrm{T}}, \widehat{u}_2^{\mathrm{T}}, \ldots, \widehat{u}_N^{\mathrm{T}}]^{\mathrm{T}}$. We then have the following alternative expression for $\dot{V}_2$ when $t \geq \max(t_o, t_s)$:

$$\dot{V}_{5,2} \leq -\frac{1}{2}\underline{\sigma}(QC)\|S\|^2 - \underline{\sigma}(P\Lambda)\|e_x\|^2 + \frac{1}{2}\overline{\sigma}(Q)\mathcal{T}_M\|\widetilde{W}\|_F\|S\| + \frac{1}{2}\overline{\sigma}(Q)\bar{\epsilon}_M\|S\| + \frac{1}{2}\overline{\sigma}(QC)\|S\|\|\xi\| + \frac{1}{2}\overline{\sigma}(Q)\|S\|\|\kappa\|$$

where $\|\mathcal{T}(Y)\| \leq \mathcal{T}_M$ is applied.

Regarding V_κ, we have

$$\begin{aligned}\dot{V}_\kappa &= \kappa^{\mathrm{T}} d(gu^{\mathrm{com}})/dt + \kappa^{\mathrm{T}}(\dot{g}\mathcal{S}(u) - g\dot{\mathcal{S}}) \\ &= \kappa^{\mathrm{T}}[\dddot{x}_d - \widehat{u}_M^1 - (C(L+B)) \otimes I_n(\widetilde{W}^{\mathrm{T}}\mathcal{T}(Y) + \epsilon - C \otimes I_n S - \delta_x - C \otimes I_n\xi - \kappa) - \Lambda \\ &\quad \otimes I_n(-\ddot{x}_d + g\mathcal{S}(u) + w) - (L+B)^{-1} \otimes I_n(S - \Lambda \otimes I_n e_x)] - \kappa^{\mathrm{T}} g\dot{\mathcal{S}} - \kappa^{\mathrm{T}}\dot{g}\mathcal{S}(u)\end{aligned}$$

where

$$\dot{\mathcal{S}} = d\mathcal{S}(u)/dt,\ \widetilde{S} = [\widetilde{s}_1^{\mathrm{T}}, \widetilde{s}_2^{\mathrm{T}}, \ldots, \widetilde{s}_N^{\mathrm{T}}]^{\mathrm{T}}$$
$$\widetilde{x} = [\widetilde{x}_1^{\mathrm{T}}, \widetilde{x}_2^{\mathrm{T}}, \ldots, \widetilde{x}_N^{\mathrm{T}}]^{\mathrm{T}},\ \widetilde{v} = [\widetilde{v}_1^{\mathrm{T}}, \widetilde{v}_2^{\mathrm{T}}, \ldots, \widetilde{v}_N^{\mathrm{T}}]^{\mathrm{T}}$$

To analyse the derivative of V_κ more conveniently, we separate the above Lyapunov function into two parts:

$$\begin{aligned}V_\kappa^1 &= -\kappa^{\mathrm{T}} g\dot{\mathcal{S}} - \kappa^{\mathrm{T}}\dot{g}\mathcal{S}(u) \\ V_\kappa^2 &= \kappa^{\mathrm{T}}[\dddot{x}_d - \hat{\dot{u}} - (C(L+B)) \otimes I_n(\widetilde{w}^O + \epsilon - C \otimes I_n S - \delta_x - C \otimes I_n\xi - \kappa) - \Lambda \otimes I_n \\ &\quad (-\ddot{x}_d + g\mathcal{S}(u) + w) - (L+B)^{-1} \otimes I_n(S - \Lambda \otimes I_n e_x)]\end{aligned}$$

According to the boundedness of the saturation phenomenon, there exist two positive constants that satisfy $\|\mathcal{S}(u)\| \leq \mathcal{S}_M^1$ and $\|\dot{\mathcal{S}}\| \leq \mathcal{S}_M^2$. By Assumption 7.4, it is reasonable to have $\|\ddot{x}_d\| \leq x_M^1$ and $\|\dddot{x}_d\| \leq x_M^2$, where x_M^1 and x_M^2 are both positive constants. By applying inequality scaling, we have the following equations when $t \geq t_o$:

$$\begin{aligned}V_\kappa^1 &\leq \|\kappa\|(g_M^1\mathcal{S}_M^2 + g_M^2\mathcal{S}_M^1) \\ V_\kappa^2 &\leq \|\kappa\|x_M^2 + \widehat{u}_M^1\|\kappa\| + \frac{\overline{\sigma}(Q)}{2}\|\kappa\|(\mathcal{T}_M\|\widetilde{W}\|_F + \bar{\epsilon}_M + \overline{\sigma}(C)\|S\| + \overline{\sigma}(C)\|\xi\|) + \overline{\sigma}(C)\|e_x\| \\ &\quad + \overline{\sigma}(\Lambda)(x_M^1 + g_M^1 S_M^1 + w_M)\|\kappa\| + \frac{1}{\underline{\sigma}(L+B)}\|\kappa\|(\|S\| + \overline{\sigma}(\Lambda)\|e_x\|) - \underline{\sigma}(C)\|\kappa\|^2\end{aligned}$$

where w_M is a positive constant that satisfies $\|w\| \leq w_M$.

Hence, we further have the norm expression of $\dot{V}_\kappa$ as follows:

$$\dot{V}_\kappa \leq -\underline{\sigma}(C)\|\kappa\|^2 + \mathcal{K}_1\|\kappa\|\|\widetilde{W}\|_F + \mathcal{K}_2\|\kappa\|\|S\| + \mathcal{K}_3\|\kappa\|\|e_x\| + \frac{\overline{\sigma}(Q)\overline{\sigma}(C)}{2}\|\kappa\|\|\xi\|$$

$$+ \Delta_\kappa \|\kappa\|$$

where Δ_κ is a positive constant that is given as

$$\Delta_\kappa = \overline{\sigma}(\Lambda)(x_M^1 + g_M^1 S_M^1 + w_M) + x_M^2 + \widehat{u}_M^1 + \frac{\overline{\sigma}(Q)}{2}\bar{\epsilon}_M + g_M^1 \mathcal{S}_M^2 + g_M^2 \mathcal{S}_M^1$$

To justify the closed-loop stability of the observer-based scheme, the observation errors are also considered in the tracking process. Accordingly, consider the following Lyapunov candidate for the observer design:

$$V_o = \frac{1}{2}\widetilde{S}^{\mathrm{T}}\widetilde{S} + \frac{1}{2\eta_1}\mathrm{tr}\{\widetilde{W}^{\mathrm{T}}\widetilde{W}\} + \frac{1}{2}\widetilde{x}^{\mathrm{T}}\widetilde{x} \tag{6.29}$$

Similar to the proofs of Theorems 6.1 and 6.2, we have

$$\dot{V}_o \leq \begin{bmatrix} \|\widetilde{S}\| \\ \|\widetilde{W}\|_F \\ \|\widetilde{x}\| \end{bmatrix}^{\mathrm{T}} \begin{bmatrix} \underline{\sigma}(\widetilde{C}) & 0 & 0 \\ 0 & \eta_2/\eta_1 & 0 \\ 0 & 0 & \underline{\sigma}(\widetilde{\Lambda}) \end{bmatrix} \begin{bmatrix} \|\widetilde{S}\| \\ \|\widetilde{W}\|_F \\ \|\widetilde{x}\| \end{bmatrix} + \begin{bmatrix} \bar{\epsilon}_M & \eta_2 W_M/\eta_1 & 0 \end{bmatrix} \begin{bmatrix} \|\widetilde{S}\| \\ \|\widetilde{W}\|_F \\ \|\widetilde{x}\| \end{bmatrix}$$

Therefore, it is reasonable to combine $V_{5,2}$, V_ξ, V_κ and V_o as follows to analyse the stability of the closed-loop observer-based scheme:

$$V_{5,3} = V_{5,2} + V_\xi + V_\kappa + V_o$$

Then we have the following time derivative:

$$\dot{V}_{5,3} \leq -\chi_{5,2}^{\mathrm{T}} H_{5,2} \chi_{5,2} + h_{5,2}\chi_{5,2}$$

where

$$\chi_{5,2} = \begin{bmatrix} \|S\| & \|e_x\| & \|\xi\| & \|\kappa\| & \|\widetilde{S}\| & \|\widetilde{W}\|_F & \|\widetilde{x}\| \end{bmatrix}^{\mathrm{T}}$$
$$h_{5,2} = \begin{bmatrix} \frac{1}{2}\overline{\sigma}(Q)\bar{\epsilon}_M & 0 & 0 & \Delta_\kappa & \bar{\epsilon}_M & \eta_2 W_M/\eta_1 & 0 \end{bmatrix}$$

According to the preliminary condition of Theorem 6.3, matrix H_2 is positive definite, which means that $\dot{V}_3$ will remain negative until $\|\chi_2\| \leq \|h_2\|/\underline{\sigma}(H_2)$. Hence, by Lemma 2.1 and the fact that the NN estimation approach is only valid semi-globally, the semi-global uniform ultimate boundedness of $\|S\|$, $\|e_x\|$, $\|\xi\|$, $\|\kappa\|$, $\|\widetilde{S}\|$, $\|\widetilde{W}\|_F$ and $\|\widetilde{x}\|$ are proved simultaneously.

Hence, the stability of the design u_i^{com} is proved. Based on the discussion presented in the first half of the proof and the fact that employing LPBCIRA does not affect the stability of u_i^{com}, the design u_i^{reg} can also achieve the semi-global uniform ultimate boundedness of the error-related variables S, e_x and δ_x, which completes the proof. □

Remark 6.3. *Note that although both the state windup issue and the reverse effect can introduce oscillation into the system states, they share different triggering reasons and illustrations. The state windup issue only exists if one of the following two conditions is met:*

1. *The investigated system is a first-order system with input saturation and integration-based structures such as the proportional–integral–derivative control scheme are used (Bohn and Atherton 1995).*
2. *The investigated system is a second-order or higher-order system with input saturation (Han* et al. *2019).*

However, the reverse effect defined in this chapter is caused by the combination of the input saturation and the input coupling effect. In terms of the system performance, state windup issue usually appears as fluctuations around the neighbourhood of $\|\delta_{xi}\| = 0$, while the oscillation caused by the reverse effect is more disarray. Corresponding discussion will be extended in Section 6.4.4 along with the simulation results.

Remark 6.4. *To attenuate the reverse effect, one of the linear programming restriction is chosen as $-\text{sign}(g_i(j)u_i^{\text{com}})g_i(j)u_i^{\text{reg}} \leq 0$ when $g_i(j)u_i^{\text{com}} \neq 0$. Take the circumstance when $\text{sign}(g_i(j)u_i^{\text{com}}) > 0$ as an example, we have $-g_i(j)u_i^{\text{reg}} \leq 0$, which is equivalent to $g_i(j)u_i^{\text{reg}} \geq 0$. In theory, if we want to fully avoid the reverse effect, we need to ensure that $g_i(j)u_i^{\text{reg}} > 0$ when $\text{sign}(g_i(j)u_i^{\text{com}}) > 0$. However, there is a chance that the linear programming approach cannot find out its optimal solution because the boundary of the solution region is not available when we do not include the points on line $g_i(j)u_i^{\text{reg}} = 0$. Hence, what the LPBCIRA can do is to ensure that the following equation is satisfied:*

$$\text{sign}(g_i(j)u_i^{\text{reg}}) = \begin{cases} 0 \text{ or } \text{sign}(g_i(j)u_i^{\text{com}}), & \text{when } \text{sign}(g_i(j)u_i^{\text{com}}) \neq 0 \\ 0, & \text{when } \text{sign}(g_i(j)u_i^{\text{com}}) = 0 \end{cases}$$

Remark 6.5. *The linear cost function to minimise was first chosen as $\Xi_1(u_i^{\text{reg}})$ to indicate the overall effort difference between u_i^{reg} and u_i^{com}. We choose to add up the effort difference in each channel directly without applying any weight to illustrate that every channel is treated with the same amount of importance.*

Table 6.1. Parameters and initial states of saturated second-order ODRs.

Robot number	Model parameters			System initial states			Observer initial states		
	m_i(kg)	R_i(m)	$I_i(\mathrm{kg}\cdot\mathrm{m}^2)$	p_i^x(m)	p_i^y(m)	θ_i(rad)	$\widehat{p}_i^x$(m)	$\widehat{p}_i^y$(m)	$\widehat{\theta}_i$(rad)
1	3.0	0.20	0.08	3.4	0.5	$\pi/5$	3.0	0.8	$\pi/6$
2	3.2	0.22	0.10	1.2	1.5	$-\pi/3$	1.5	1.8	$-\pi/5$
3	2.8	0.21	0.07	-0.8	1.2	$\pi/6$	-1.1	1.0	$\pi/7$
4	2.6	0.19	0.05	-1.0	-0.8	$\pi/4$	-1.2	-1.0	$\pi/3$
5	3.1	0.23	0.09	1.6	-0.3	$-\pi/4$	1.3	0.0	$-\pi/5$
6	2.9	0.18	0.06	3.2	-0.8	$\pi/6$	3.1	-1.0	$\pi/5$

6.4.4 Simulation results and discussions

To justify the effectiveness of the finite-time neural-based sliding mode observer (6.17), the windup compensating auxiliary variable ξ_i, the compensated sliding mode formation controller (6.23), the LPBCIRA (Algorithm 3) and the linear-programming-based sliding mode formation controller u_i^{reg}, comparative simulations regarding a multi-robot system are conducted.

Consider a cluster of three-wheel ODRs (Fei *et al.* 2020). Based on the discussion in Chapter 2, the dynamics of the ith robot is given as

$$\begin{cases} \dot{x}_i = v_i \\ \dot{v}_i = M_i T_s(\theta_i, R_i)\mathcal{S}(u_i, U_{Mi}) + w_i \end{cases} \tag{6.30}$$

where $x_i = [p_i^x, p_i^y, \theta_i]^{\mathrm{T}}$, $M_i = \mathrm{diag}\{1/m_i, 1/m_i, 1/I_i\}$, m_i is the mass of the robot, I_i is the inertia of the robot, $u_i = [F_i^1, F_i^2, F_i^3]^{\mathrm{T}}$ is the force vector of the three motors and R_i is the radius of the robot. The parameter values of each robot are given in Table 6.1.

The desired formation is chosen as a time-varying circular formation to test the system's performance when a set of complex references is given. The specific expression of the formation reference is given as

$$x_{di}(t) = \left[\cos\left(\frac{1}{10}t\right) + 2\cos\left(\frac{1}{10}t + \frac{i\pi}{3}\right), -\sin\left(\frac{1}{10}t\right) + 2\sin\left(\frac{1}{10}t + \frac{i\pi}{3}\right), 0\right]^{\mathrm{T}} \tag{6.31}$$

6.4.4 Simulation results and discussions

The unknown nonlinear term w_i is chosen as follows to ensure the diversity of nonlinearities:

$$w_i = \frac{1}{5}\left[\frac{1}{2}\sin(p_i^x) + \frac{3}{5}\sin\left(\frac{3}{5}t + \frac{i\pi}{5}\right), -\frac{3}{5}e^{-|p_i^y - 1|} + \frac{4}{5}\sin\left(\frac{2}{5}t + \frac{i\pi}{5}\right),\right.$$
$$\left.\frac{1}{5}\cos(\theta_i) + \frac{2}{5}\sin\left(\frac{1}{2}t + \frac{i\pi}{5}\right)\right]^{\mathrm{T}}$$

The communication topology is chosen as the directed graph shown in Figure 6.2, and the value of b_i is set as $b_i = 2$.

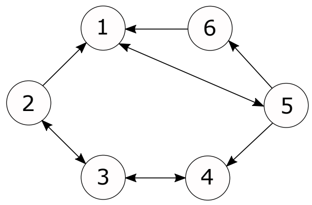

Figure 6.2. Communication topology of the multi-ODR system.

The first thing to justify is the necessity and advantages of developing the neural-based sliding mode observer. Regarding the ODR cluster, suppose that the control input is selected as $u_i = u_i^{\mathrm{nom}}$, which does not lead to the divergence of the system states and satisfy that $x_i \in \Omega_x$ and $v_i \in \Omega_v$. With the neural updating parameters chosen as $\eta_1 = 10$ and $\eta_2 = 1$, we have the following four designs to offer comparative results:

1. The cooperatively tuned NN estimation (CTNNE) (Lewis *et al.* 2013) where the tuning law is chosen as

$$\dot{\widehat{W}}_i = \eta_1 \mathcal{T}(Y_i) s_i^{\mathrm{T}} - \eta_2 \widehat{W}_i$$

2. The observer-based NN estimation (OBNNE-1) where the observer structure (6.9) is implemented with the linear sliding surface design (6.11), the adaptive weight update law (6.13) and the imaginary control input (6.12). The output of the NN is used as the estimation of w_i, which leads to $\widetilde{w} = [(\widetilde{w}_1^N)^{\mathrm{T}}, (\widetilde{w}_2^N)^{\mathrm{T}}, \ldots, (\widetilde{w}_N^N)^{\mathrm{T}}]^{\mathrm{T}}$. The related parameter values are chosen as $\widetilde{\lambda}_{i,1} = 2$ and $\widetilde{c}_{i,1} = 3$ by Theorem 6.1.

3. The observer-based NN estimation (OBNNE-2) where the observer structure (6.9) is implemented with the linear sliding surface design (6.11), the adaptive weight update law (6.13) and the imaginary control input (6.12). The imaginary control input $\widehat{u}_i$ is chosen as the estimation of w_i, leading to $\widetilde{w} = \widetilde{w}^O$. The related parameter values are chosen as $\widetilde{\lambda}_{i,1} = 2$ and $\widetilde{c}_{i,1} = 3$ by Theorem 6.1.

4. The observer-based finite-time NN estimation (OBFTNNE) where the observer structure (6.9) is implemented with the finite-time sliding surface design (6.16), the adaptive weight update law (6.13) and the imaginary control input (6.17). The imaginary control input $\widehat{u}_i$ is chosen to act as the estimation of w_i, leading to $\widetilde{w} = \widetilde{w}^O$. The related parameter values are chosen as $\widetilde{\lambda}_{i,1} = 1.5$, $\widetilde{\lambda}_{i,2} = 0.5$ $p_1 = 3$, $p_2 = 5$, $h = 1$, $\widetilde{c}_{i,1} = 3$ and $\widetilde{c}_{i,2} = 3$ by Theorem 6.2.

The propagation of observation error norm correlated with different designs are illustrated in Figure 6.3, where the finite settling time t_{set} and the ultimate bounded region $\widetilde{w}_M$ of each approach are recorded in Table 6.2. For each method, we have that $\|\widetilde{w}\| \leq \widetilde{w}_M$ when $t \geq t_{\text{set}}$.

The propagation of observation error norm correlated with different designs are illustrated in Figure 6.3, where the finite settling time t_{set} and the ultimate bounded region $\widetilde{w}_M$ of each approach are recorded in Table 6.2. For each method, we have that $\|\widetilde{w}\| \leq \widetilde{w}_M$ when $t \geq t_{\text{set}}$.

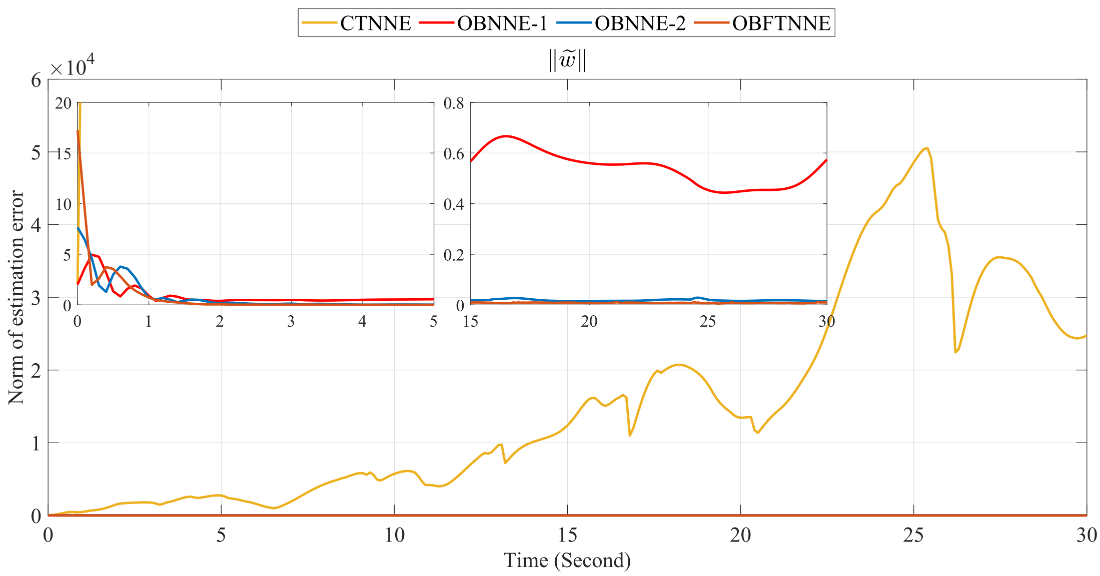

Figure 6.3. Estimation accuracy comparison of four estimation techniques.

It is observed in Figure 6.3 that although the CTNNE method works fine for system without input saturation (Lewis *et al.* 2013), the estimation error norm did not converge and even goes up to 6×10^4 when the actuator is saturated. Such finding illustrates that the NN tuning method that involves variables related to reference tracking errors (Lewis *et al.* 2013) is not suitable for systems with input saturation.

Table 6.2. Comparison of the estimation error and the converging time.

Criteria	Estimation techniques			
	CTNNE	OBNNE-1	OBNNE-2	OBFTNNE
t_{set} (s)	–	1.5	7.7	4.2
$\widetilde{w}_M$	6.00×10^4	6.67×10^{-1}	2.85×10^{-2}	1.12×10^{-2}

On the contrary, the norm of the estimation error is expected to converge to a small neighbourhood around 0 if we implement the neural-based observer structure (6.9), which indicates the necessity of developing the neural-based sliding mode observer. In specific, if we only use the output of NNs to act as our estimation of the uncertainty (OBNNE-1) (Liu *et al.* 2013), $\|\widetilde{w}\|$ is bounded within 6.67×10^{-1}. Although such result is acceptable, the estimation accuracy will increase remarkably by 96% as the value of $\widetilde{w}_M$ dropped from 6.67×10^{-1} to 2.85×10^{-2} if we adopt the OBNNE-2 design. Such result justified the validity of Theorem 6.1 and the analyse provided in Remark 6.2. Regarding the OBFTNNE, although it did not make a huge difference in the precision perspective ($\widetilde{w}_M = 1.12 \times 10^{-2}$), it shortened the error converging time significantly from 7.7s to 4.2s, meaning that Theorem 6.2 is also valid.

To illustrate the performance of the auxiliary variable and the proposed observer-based controller, we have the following three designs for comparison:

1. The nominal formation controller (NFC) where $u_i = \mathcal{S}(u_i^{\text{nom}}, U_{Mi})$.

2. The compensated formation controller (CFC) where the auxiliary variable ξ_i is employed, the tuning law of ξ_i is chosen as (6.24) and $u_i = \mathcal{S}(u_i^{\text{com}}, U_{Mi})$. The tuning parameters of the auxiliary variable is set as $\eta_3 = 1$ and $\eta_4 = 0.5$.

3. The linear-programming-based compensated formation controller (LPBCFC) in which the auxiliary variable ξ_i is employed, the tuning law of ξ_i is chosen as (6.24), the LPBCIRA is used and $u_i = u_i^{\text{reg}}$. The tuning parameters of the auxiliary variable is set as $\eta_3 = 1$ and $\eta_4 = 0.5$.

In the above three designs, the parameter of the controller is chosen as $c_i = 2$ and $\lambda_i = 2$. The actuator saturation limitation is set as $U_{Mi} = 1$. To illustrate that both the state windup and the reverse effect exist in the multi-ODR cluster, we first have a look at the propagation of the sliding variable s_i. If we employ the NFC design, then we have the trend of s_i as shown in Figure 6.4. It is found that there are two different kinds of state fluctuation according to Remark 6.3:

1. One kind of regulated oscillation around the value of equilibrium point of $s_i = [0,0,0]^{\mathrm{T}}$. (See s_x and s_y of ODR one, two, five and six.)

2. One kind of disarray fluctuation without any specific characteristics. (See s_θ of all ODRs).

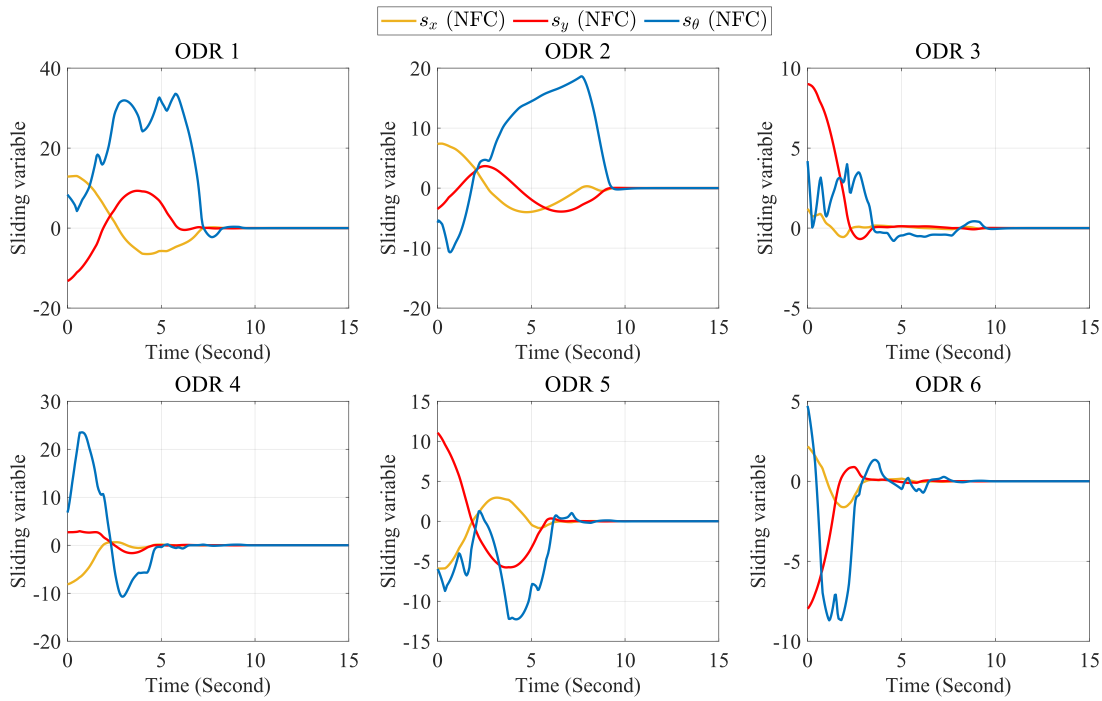

Figure 6.4. Propagation of s_i (NFC).

The first phenomenon is caused by the state windup issue (Han *et al.* 2019), while the second one is the illustration of the reverse effect in Definition 5.1. After employing the auxiliary variable to compensate for the windup issue, we have the CFC design, whose trends of s_i are given as the dotted lines in Figure 6.5.

Compared with the results of NFC, the auxiliary variable is found to be effective for attenuating the windup phenomenon (see s_x and s_y of ODR one, two, five and six in Figures 6.4-6.5). However, every ODR with the CFC design still experiences state fluctuation in the channel of s_θ, indicating the existence of the reverse effect.

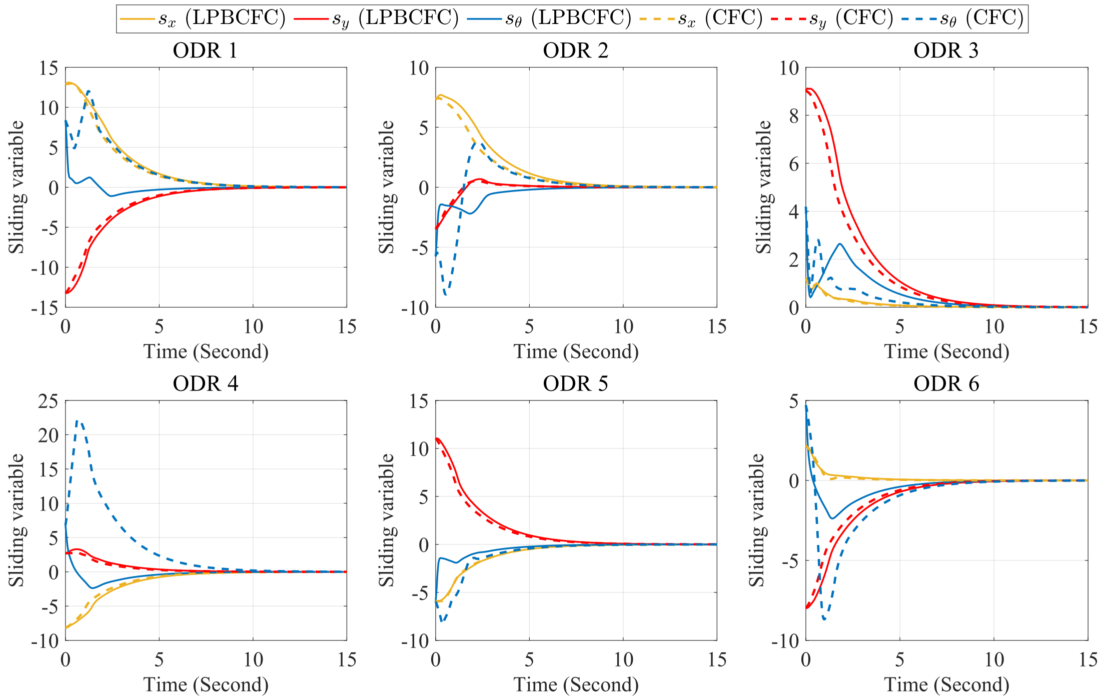

Figure 6.5. Propagation of s_i (CFC and LPBCFC).

After implementing the LPBCIRA, the amplitudes of the state fluctuation phenomenon is significantly reduced for each ODR (see the curves of LPBCFC in Figure 6.5). Similar results are also obtained in the perspective of e_x (see Figure 6.6), indicating the effectiveness of the LPBCIRA (Algorithm 3).

However, note that the LPBCFC design can not fully avoid the state fluctuation because of the following two reasons:

1. The norm of the initial estimation error of the neural-based observer is not zero, and it takes the observer a finite period of time (t_{set}) to ensure that the estimation error is bounded within a small neighbourhood around zero. Hence, it is possible that the control input u_i^{com} will lead to state fluctuation when $t < t_{\text{set}}$.

2. The implementation of the auxiliary variable ξ_i does not guarantee that the system is free of the windup phenomenon. Hence, state overshoots may still exist (see s_y of ODR two and s_θ of ODR six).

To show that the system is affected by the input saturation phenomenon and the LPBCIRA is able to maintain u_i^{reg} within the saturation limitation, the control inputs of LPBCFC are provided in Figure 6.7, where we see that the value of each channel in u_i^{reg} is restricted within the neighbourhood of $[-1, 1]$.

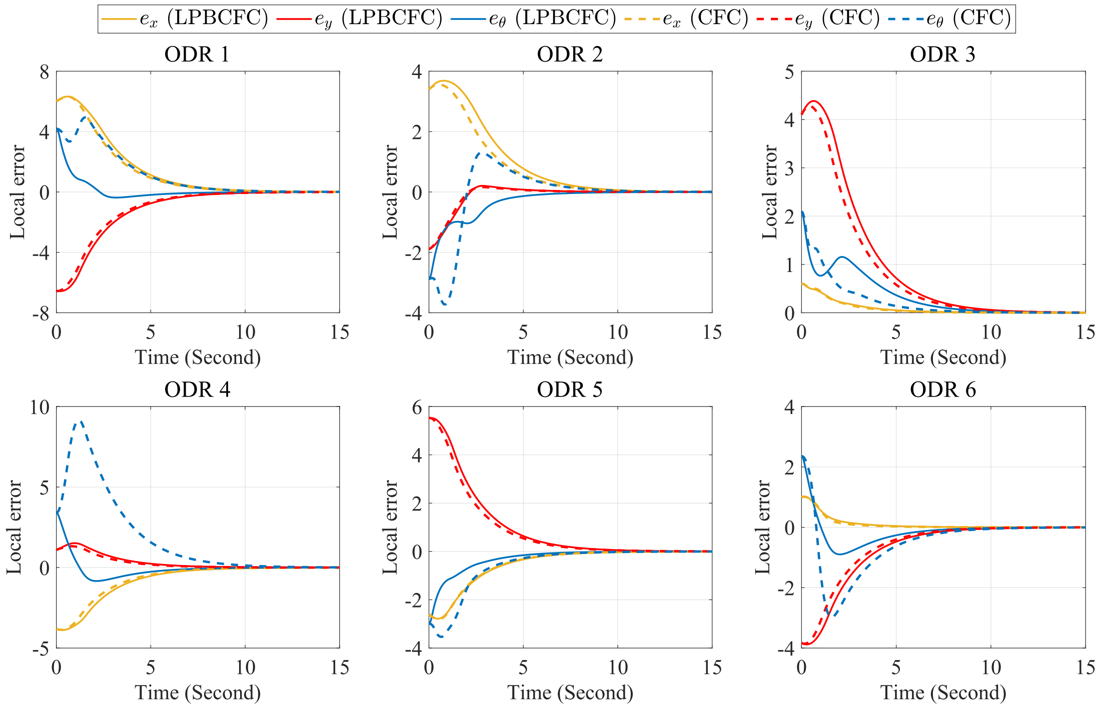

Figure 6.6. Propagation of e_{xi} (CFC and LPBCFC).

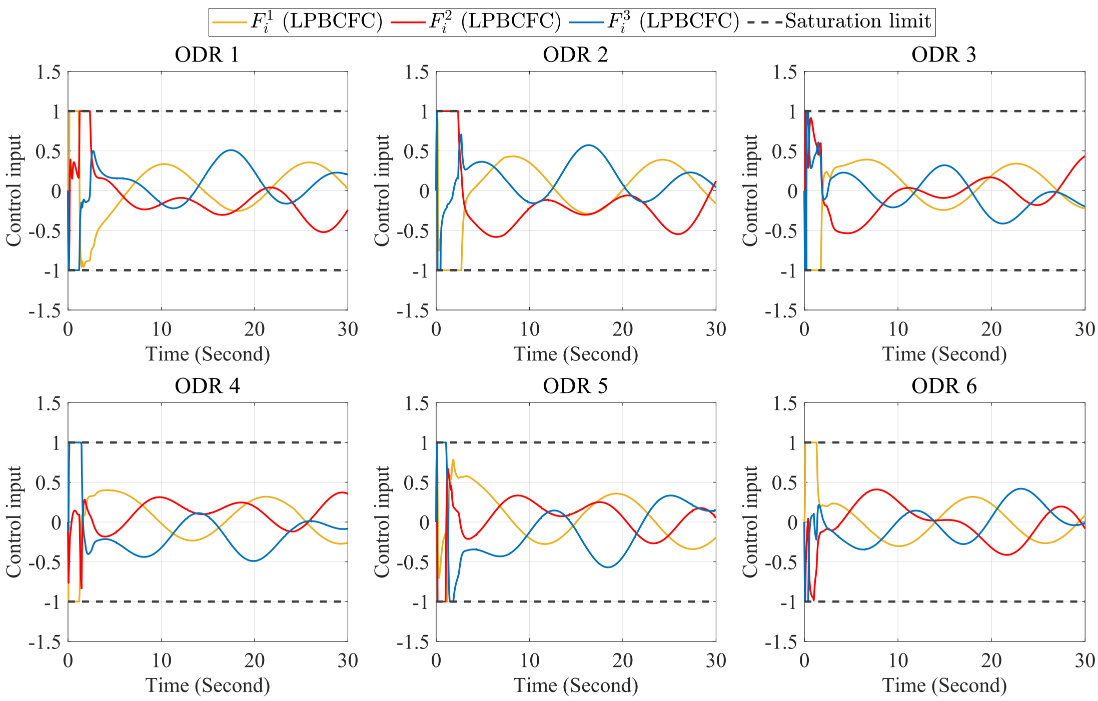

Figure 6.7. Control input of the LPBCFC scheme.

To offer intuitive comparison, the trends of $\|S\|$, $\|e_x\|$, $\|\delta_x\|$ and $\|\xi\|$ are also recorded and presented in Figure 6.8, where more chattering is expected if the NFC design is employed. Although the results of CFC and LPBCFC look similar, the CFC design still experiences state fluctuation when $t \in [0, 5]$, which is significantly attenuated if the LPBCFC design is employed. Regarding the specific bounded region of each vector, all three methods achieve the same result because the actual control input of LPBCFC and CFC will converge to u_i^{nom} ultimately. From the simulation data, we have the semi-globally UUB region of $\|S\| \le 2.7 \times 10^{-3}$, $\|e_x\| \le 8.3 \times 10^{-4}$, $\|\delta_x\| \le 3.1 \times 10^{-4}$ and $\|\xi\| \to 0$ when $t \to +\infty$, which further proves the validity of Theorem 6.3.

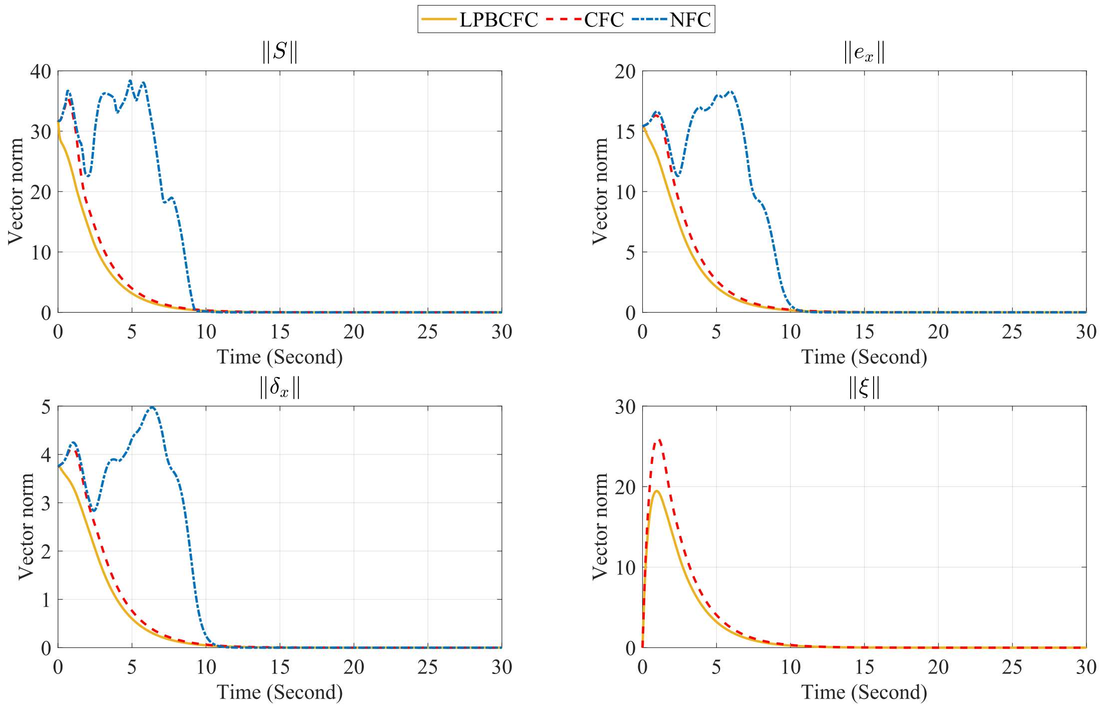

Figure 6.8. Comparison of the propagation of vector norms.

Although the trend of $\|e_x\|$ can illustrate the difference between the current system formation and the expected system formation, it can only justify the short-term effect of the state fluctuation phenomenon instead of the ling-term one. Hence, we define a positive scalar Δ_e as the absolute formation tracking error as follows within the period of $[t_0, t_n]$:

$$\Delta_e = \int_{t_0}^{t_n} \|e_x(\tau)\|_1 d\tau \tag{6.32}$$

where t_n denotes the current time. Here, we can treat Δ_e as the overall cost that memorise how much formation error has the system had.

Besides, we also define a positive scalar Δ_u as the following integration form to record how much effort has the control input made regarding the multiple ODR system from

t_0 to t_n:

$$\Delta_u = \int_0^{t_n} \|u(\tau)\|_1 d\tau \tag{6.33}$$

The trends of Δ_e and Δ_u are recorded in Figure 6.9 simultaneously. We see that without the implementation of the auxiliary variable and the LPBCIRA, the NFC design makes the most overall effort while having the worst performance ($\Delta_e > 300$). Although the CFC design and the LPBCFC design share little difference in the perspective of Δ_u (less than three), their difference in Δ_e is remarkable (more than 30). Such result indicates that the LPBCFC design tends to make the right effort that reduces the system formation error rather than making the maximum effort regardless of the system behaviour. The difference between the LPBCFC and CFC also shows that there are two kinds of state fluctuation phenomenon for cluster (6.4), further proves the validity of the statements made in Remark 6.3 and Theorem 6.3.

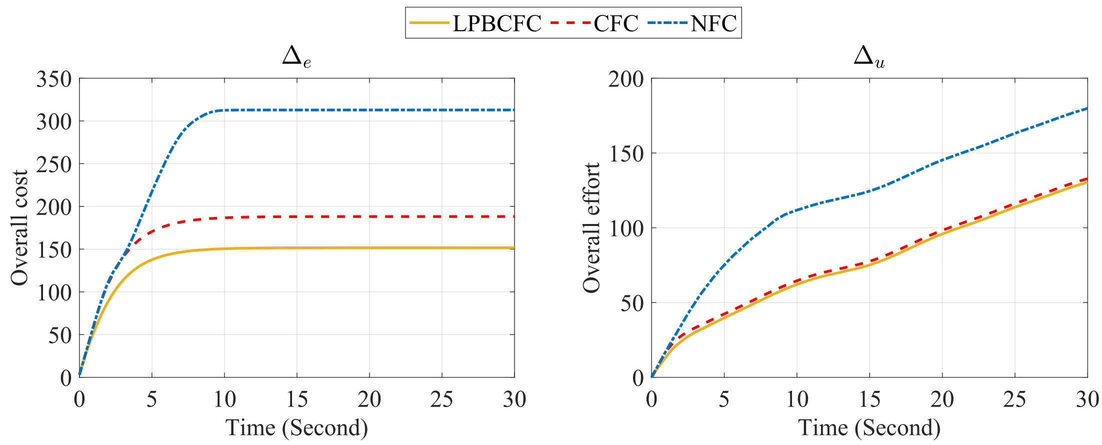

Figure 6.9. Overall cost and overall effort.

The formation status of the multi-ODR system is presented in Figure 6.10. It is observed that the system is able to track the predefined trajectories (dotted curves) to further form a rotating circular formation (dash-dotted curve), whose centre is also spinning in a circular trajectory.

6.5 Chapter summary

In this chapter, we have addressed the formation control problem for saturated second-order multi-agent systems with system uncertainties. New neural-based sliding mode

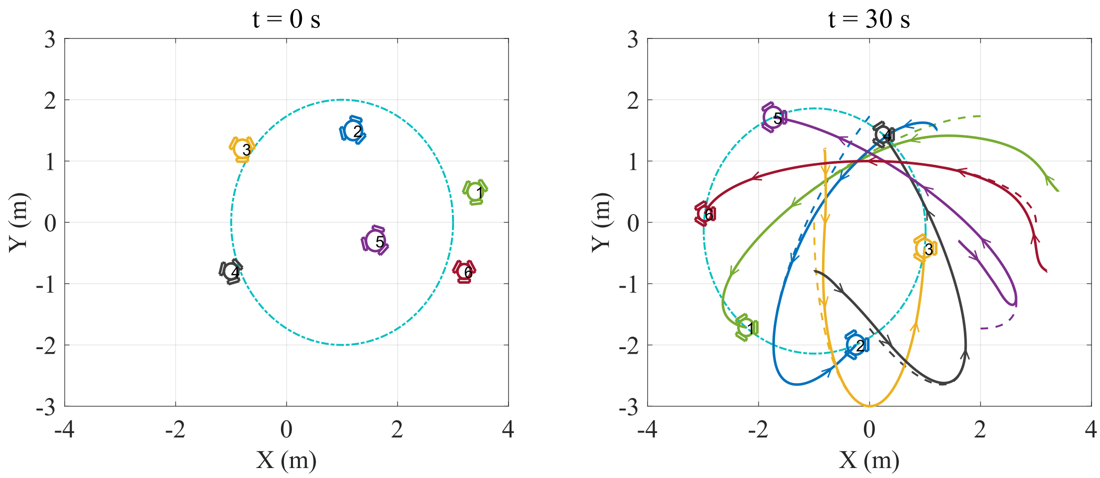

Figure 6.10. System formation status while applying the LPBCFC design.

observer designs are proposed for nominal second-order systems and finite-time characteristics have been achieved. A set of adaptive auxiliary variables is employed in the SMC scheme to attenuate the state windup phenomenon. The linear programming technique is further employed to attenuate the state fluctuation led by the reverse effect. Simulations are conducted to provide comparative results that illustrate the necessity and the effectiveness of the proposed observer designs and the robust formation control law.

In the next chapter, a new hierarchical formation control structure is developed to avoid the coupling phenomenon between the inter-agent communication and the low-level motion dynamics. Analysis and designs regarding a multi-UAV system and a mixed-order MAS are conducted to illustrate the merits of using the hierarchical structure. Two-layer NNs are also employed to ensure the robustness of the controller designs.

Chapter 7

Hierarchical Formation Control of Multi-Agent Systems

CURRENTLY, most of the formation control algorithms are developed in a single-layer structure that couples the inter-agent communication with the specific motion dynamics. Although such method is valid, its corresponding stability analysis is hard to conduct when individual agents acquire complex dynamics. Therefore, it is essential to develop a multi-layer formation control structure that separates the multi-agent communication and the motion control. In this chapter, the hierarchical control scheme is discussed regarding the formation control issue of multi-agent systems. First, the example of a multi-quadcopter system is employed to investigate the hierarchical formation control design for unified-order multi-agent systems with complex and heterogeneous dynamics. After that, the formation control problem is further expanded to mixed-order multi-agent systems, and a neural-based hierarchical formation control structure is proposed for a mixed-order cluster that contains both first-order agents and second-order agents. Both theoretical analysis and simulations are conducted to prove the effectiveness of the proposed schemes.

7.1 Introduction

The control problem of networked MASs is first discussed by Olfati-Saber and Murray (Olfati-Saber and Murray 2004), where the agent states achieve a consensus value correlated with the initial state values ultimately. Since then, most of the research works in the field of MAS are developed in the similar fashion (Shi and Yan 2020, Sun *et al.* 2021b), where local errors are defined with the implementation of the Laplacian matrix and further employed in the construction of motion control laws. Although such method is proved to be effective and valid by using the Lyapunov stability theory, it does increase the complexity of the stability analysis by introducing the Laplacian matrix into the Lyapunov candidates (Lewis *et al.* 2013).

Among the many kinds of robots that are investigated, the motion control of uncrewed grounded vehicles are comparatively easy (Fei *et al.* 2021a, Wang *et al.* 2019) because no guidance law is needed. On the contrary, the control problem of UAVs are more complex because it is essential to design separate control laws for the position loop and the attitude loop. The movement of quadcopters is analysed based on an ideal second-order dynamics and time-varying formation tracking process is achieved by a Riccati-based approach (Dong *et al.* 2018). Both UAVs and uncrewed grounded vehicles are modelled with a double-integrator structure by Ren et al. to achieve robust three-dimensional formation control (Ren *et al.* 2022). However, it is worth mentioning that Dong et al. ignored the coupling phenomenon between the position loop and the attitude loop. Although Ren et al. employed the popular two-loop controller design, chattering is observed in different system states because of the coupling between the inter-agent communication and the under-actuated UAV model. Hence, it is essential to discuss if employing a multi-layer formation control scheme can reduce the complexity of the multi-UAV cluster formation control design.

Apart from unified-order MASs, mixed-order MASs have attracted massive interests because of the implementation of hybrid-robot systems in practical scenarios (Shi and Yan 2020). The cooperative consensus tracking problem was discussed for mixed-order MASs (Li *et al.* 2019c) that contain both first-order and second-order agents, and the error-related sliding variables were defined to construct neural adaptive consensus control laws. Corresponding results are further extended to systems with agents that have higher-order dynamics (Li *et al.* 2022). However, the idea of directly building up the overall system model with the specific agent dynamics (Li *et al.* 2019c, Li *et al.*

2022) is found to be problematic while designing the controller and analysing system stability due to the mismatch in dynamics. Hence, how to avoid the state mismatch among agents caused by the difference in dynamics orders has became a challenge.

Motivated by the above discussions, the following issues are investigated in this chapter:

1. How to design a hierarchical formation control scheme for unified-order MASs with complex agent dynamics?

2. How to construct a hierarchical formation control scheme for mixed-order MASs?

3. How to implement NNs in the hierarchical control structure to estimate the unknown factors in the system dynamics?

The contents in this chapter are organised as follows. The development of the neural-based sliding mode observer and the observer-based hierarchical formation control scheme for a multi-UAV cluster are given in Section 7.2. The development of the observer-based hierarchical formation control scheme for mixed-order MASs is presented in Section 7.3. The final conclusions are drawn in Section 7.4.

7.2 Hierarchical design for unified-order vehicle clusters

7.2.1 System modelling and problem formulation

Consider a distributed heterogeneous multi-drone system consists of $N(N > 1)$ UAVs, where the dynamics of the ith UAV is expressed as follows (Ren *et al.* 2022, Fei *et al.*

Table 7.1. Parameter definitions.

Term(s)	Definition
$K_{i,x}$, $K_{i,y}$, $K_{i,z}$, $K_{i,\phi}$, $K_{i,\theta}$, $K_{i,\psi}$	Aerodynamic drag coefficients
$\varpi_{i,x}$, $\varpi_{i,y}$, $\varpi_{i,z}$, $\varpi_{i,\phi}$, $\varpi_{i,\theta}$, $\varpi_{i,\psi}$	External disturbances
$J_{i,x}$, $J_{i,y}$, $J_{i,z}$	Moments of inertia around the axis
m_i	The mass of the UAV
g	The gravity constant
v_i	The drag force coefficient

2022b):

$$\begin{cases} \ddot{p}_i^x = \dfrac{\cos(\phi_i)\sin(\theta_i)\cos(\psi_i) + \sin(\phi_i)\sin(\psi_i)}{m_i}(u_{i,1} + u_{i,2} + u_{i,3} + u_{i,4}) + \varpi_{i,x} - \dfrac{K_{i,x}}{m_i}\dot{p}_i^x \\ \ddot{p}_i^y = \dfrac{\cos(\phi_i)\sin(\theta_i)\sin(\psi_i) - \sin(\phi_i)\cos(\psi_i)}{m_i}(u_{i,1} + u_{i,2} + u_{i,3} + u_{i,4}) + \varpi_{i,y} - \dfrac{K_{i,y}}{m_i}\dot{p}_i^y \\ \ddot{p}_i^z = \dfrac{\cos(\phi_i)\cos(\theta_i)}{m_i}(u_{i,1} + u_{i,2} + u_{i,3} + u_{i,4}) + \varpi_{i,z} - \dfrac{K_{i,z}}{m_i}\dot{p}_i^z - g \\ \ddot{\phi}_i = -\dfrac{K_{i,\phi}}{J_{i,x}}\dot{\phi}_i + \dfrac{J_{i,y} - J_{i,z}}{J_{i,x}}\dot{\theta}_i\dot{\psi}_i + \dfrac{R_i}{J_{i,x}}(-u_{i,2} + u_{i,4}) + \varpi_{i,\phi} \\ \ddot{\theta}_i = -\dfrac{K_{i,\theta}}{J_{i,y}}\dot{\theta}_i + \dfrac{J_{i,z} - J_{i,x}}{J_{i,y}}\dot{\phi}_i\dot{\psi}_i + \dfrac{R_i}{J_{i,y}}(-u_{i,1} + u_{i,3}) + \varpi_{i,\theta} \\ \ddot{\psi}_i = -\dfrac{K_{i,\psi}}{J_{i,z}}\dot{\psi}_i + \dfrac{J_{i,x} - J_{i,y}}{J_{i,z}}\dot{\phi}_i\dot{\theta}_i + \dfrac{v_i}{J_{i,z}}(-u_{i,1} + u_{i,2} - u_{i,3} + u_{i,4}) + \varpi_{i,\psi}, \quad i \in [1, N] \end{cases} \tag{7.1}$$

where p_i^x, p_i^y and p_i^z represent the global coordinates of the ith UAV, ϕ_i, θ_i and ψ_i denote the roll angle, pitch angle and yaw angle, respectively, $u_{i,j}(j \in [1, 4])$ represents the combined thrust or force provided by the jth motor, R_i is the distance between the centre of the drone and the centre of the rotor, and the rest of the parameters are defined in Table 7.1.

For the sake of simplicity, the following definitions are made to divide the control input of the system into T_i, $\tau_{i,1}$, $\tau_{i,2}$ and $\tau_{i,3}$:

$$\begin{aligned} T_i &= u_{i,1} + u_{i,2} + u_{i,3} + u_{i,4}, \quad & \tau_{i,1} &= -u_{i,2} + u_{i,4} \\ \tau_{i,2} &= -u_{i,1} + u_{i,3}, & \tau_{i,3} &= -u_{i,1} + u_{i,2} - u_{i,3} + u_{i,4} \end{aligned} \tag{7.2}$$

Due to the strong coupling between channels, the position channel and the attitude channel should not be combined into an overall second-order model (Du *et al.* 2017). Instead, design and analysis based on individual loops are required. Define $x_{i,p} = [p_i^x, p_i^y, p_i^z]^{\mathrm{T}}$ and $v_{i,p} = [\dot{p}_i^x, \dot{p}_i^y, \dot{p}_i^z]^{\mathrm{T}}$. We then have the dynamics of the position loop as

$$\begin{cases} \dot{x}_{i,p} = v_{i,p} \\ \dot{v}_{i,p} = f_{i,p} + g_{i,p} T_i + \varpi_{i,p} - \bar{g}_p, \quad i \in [1, N] \end{cases} \tag{7.3}$$

for which we have the following equations:

$$f_{i,p} = -[K_{i,x}\dot{p}_i^x/m_i, K_{i,y}\dot{p}_i^y/m_i, K_{i,z}\dot{p}_i^z/m_i]^{\mathrm{T}}, \ \varpi_{i,p} = [\varpi_{i,x}, \varpi_{i,y}, \varpi_{i,z}]^{\mathrm{T}}, \ \bar{g}_p = [0, 0, g]^{\mathrm{T}}$$
$$g_{i,p} = \left[\frac{\cos(\phi_i)\sin(\theta_i)\cos(\psi_i)+\sin(\phi_i)\sin(\psi_i)}{m_i} \quad \frac{\cos(\phi_i)\sin(\theta_i)\sin(\psi_i)-\sin(\phi_i)\cos(\psi_i)}{m_i} \quad \frac{\cos(\phi_i)\cos(\theta_i)}{m_i}\right]^{\mathrm{T}}$$

If we have $w_{i,p} = f_{i,p} + \varpi_{i,p}$ as the overall system uncertainties in the position loop, (7.3) can be simplified to the following version:

$$\begin{cases} \dot{x}_{i,p} = v_{i,p} \\ \dot{v}_{i,p} = g_{i,p} u_i + w_{i,p}, \quad i \in [1, N] \end{cases} \tag{7.4}$$

Similarly, if define $x_{i,a} = [\phi_i, \theta_i, \psi_i]^{\mathrm{T}}$ and $v_{i,a} = [\dot{\phi}_i, \dot{\theta}_i, \dot{\psi}_i]^{\mathrm{T}}$, then the dynamics in the attitude loop has the following expression:

$$\begin{cases} \dot{x}_{i,a} = v_{i,a} \\ \dot{v}_{i,a} = g_{i,a} \tau_i + w_{i,a}, \quad i \in [1, N] \end{cases} \tag{7.5}$$

where $w_{i,a} = f_{i,a} + \varpi_{i,a}$, $\varpi_{i,a} = [\varpi_{i,\phi}, \varpi_{i,\theta}, \varpi_{i,\psi}]^{\mathrm{T}}$ and

$$f_{i,a} = \begin{bmatrix} (J_{i,y} - J_{i,z})\dot{\theta}_i\dot{\psi}_i/J_{i,x} - K_{i,\phi}\dot{\phi}_i/J_{i,x} \\ (J_{i,z} - J_{i,x})\dot{\phi}_i\dot{\psi}_i/J_{i,y} - K_{i,\theta}\dot{\theta}_i/J_{i,y} \\ (J_{i,x} - J_{i,y})\dot{\phi}_i\dot{\theta}_i/J_{i,z} - K_{i,\psi}\dot{\psi}_i/J_{i,z} \end{bmatrix}, \ g_{i,a} = \begin{bmatrix} \frac{R_i}{J_{i,x}} & 0 & 0 \\ 0 & \frac{R_i}{J_{i,y}} & 0 \\ 0 & 0 & \frac{v_i}{J_{i,z}} \end{bmatrix}, \ \tau_i = \begin{bmatrix} \tau_{i,1} \\ \tau_{i,2} \\ \tau_{i,3} \end{bmatrix}$$

For the sake of convenience while analysing the cluster formation tracking behaviour in later parts, it is still necessary to have a unified cluster dynamics expression. For the ith UAV, define $x_i = [x_{i,p}^{\mathrm{T}}, x_{i,a}^{\mathrm{T}}]^{\mathrm{T}}$ and $v_i = [v_{i,p}^{\mathrm{T}}, v_{i,a}^{\mathrm{T}}]^{\mathrm{T}}$, then the following simplified version is obtained:

$$\begin{cases} \dot{x}_i = v_i \\ \dot{v}_i = u_i + w_i - \bar{g}_i, \quad i \in [1, N] \end{cases} \tag{7.6}$$

where we have $u_i = [(g_{i,p}T_i)^{\mathrm{T}}, (g_{i,a}\tau_i)^{\mathrm{T}}]^{\mathrm{T}}$, $w_i = [w_{i,p}^{\mathrm{T}}, w_{i,a}^{\mathrm{T}}]^{\mathrm{T}}$ and $\bar{g}_i = [\bar{g}_p^{\mathrm{T}}, 0, 0, 0]^{\mathrm{T}}$.

To obtain the cluster expression, we define $x = [x_1^{\mathrm{T}}, x_2^{\mathrm{T}}, \ldots, x_N^{\mathrm{T}}]^{\mathrm{T}}$, $v = [v_1^{\mathrm{T}}, v_2^{\mathrm{T}}, \ldots, v_N^{\mathrm{T}}]^{\mathrm{T}}$, $u = [u_1^{\mathrm{T}}, u_2^{\mathrm{T}}, \ldots, u_N^{\mathrm{T}}]^{\mathrm{T}}$, $w = [w_1^{\mathrm{T}}, w_2^{\mathrm{T}}, \ldots, w_N^{\mathrm{T}}]^{\mathrm{T}}$ and $\bar{g} = [\bar{g}_1^{\mathrm{T}}, \bar{g}_2^{\mathrm{T}}, \ldots, \bar{g}_N^{\mathrm{T}}]$, which further lead to

$$\begin{cases} \dot{x} = vs. \\ \dot{v} = u + w - \bar{g} \end{cases} \tag{7.7}$$

There are two sets of reference for each UAV to follow, the position reference and the attitude reference. Throughout this section, we use $x_{i,p}^d \in \mathbb{R}^3$ and $\psi_i^d \in \mathbb{R}^1$ to represent the position reference and the desired yaw angle for the ith UAV, respectively. The goal of this article is to achieve semi-global uniform ultimate boundedness for each UAV's position tracking error and attitude tracking error, which is illustrated as

$$\lim_{t\to\infty} \|x_{i,p} - x_{i,p}^d\| \le \nu_p^s, \quad \lim_{t\to\infty} \|\psi_i - \psi_i^d\| \le \nu_a^s, \ \forall x_i(t_0) \in \Omega_x \tag{7.8}$$

where both ν_p^s and ν_a^s are small positive constants.

The communication graph of the multi-UAV system (7.7) is chosen as a strongly connected graph, and the following assumptions are made for the multi-UAV system (7.7):

Assumption 7.1. *The trajectory reference $x_{i,p}^d$ and its derivatives $\dot{x}_{i,p}^d$ and $\ddot{x}_{i,p}^d$ are all bounded and accessible to the ith UAV. The yaw angle reference ψ_i^d is bounded and known to the ith UAV.*

7.2.2 Two-layer neural networks for uncrewed aerial vehicles

In this subsection, two-layer NNs are employed to estimate the overall system uncertainty w_i. According to the universal approximation theorem, a two-layer NN can be used to approximate the unknown function when the network compact set conditions are satisfied (Li *et al.* 2022). Hence, the uncertainty w_i is expressed as the following form:

$$w_i = W_i^{\mathrm{T}}\varphi(x_i, v_i) + \epsilon_i, \ i = 1, 2, \ldots, n$$

where $\varphi(\cdot)$ is the activation function vector of the NN, W_i is the optimal weight matrix, ϵ_i is the bounded network approximation bias that satisfies $\|\epsilon_i\| \le \epsilon_M$ and ϵ_M is a bounded positive number. To reduce the complexity of the NN design, we chose the activation function as the identity function, which further leads to $\varphi(x_i, v_i) = [x_i^{\mathrm{T}}, v_i^{\mathrm{T}}]^{\mathrm{T}} \in \mathbb{R}^{12\times 1}$, $W_i \in \mathbb{R}^{12\times 6}$ and $\epsilon_i \in \mathbb{R}^6$.

For the ith UAV, the NN estimation of w_i is given as

$$\widehat{w}_i = \widehat{W}_i^{\mathrm{T}} \varphi(x_i, v_i) \tag{7.9}$$

where $\widehat{W}_i$ denotes the estimated weight matrix.

Define $\widetilde{W}_i = W_i - \widehat{W}_i$ and $\widetilde{w}_i = w_i - \widehat{w}_i$. Then the estimation error $\widetilde{w}_i$ is given as

$$\widetilde{w}_i = \widetilde{W}_i^{\mathrm{T}} \varphi(x_i, v_i) + \epsilon_i$$

The following assumption is made to ensure the boundedness of the NN output:

Assumption 7.2. *The optimal weight matrix W_i is bounded such that $\|W_i\|_{\mathrm{F}} \leq W_M$ is met for each UAV, where W_M is a positive constant.*

Remark 7.1. *In a practical task, the external disturbance may include functions that do not use the system states x_i and v_i as variables. For example, the external disturbance $\bar{w}_i$ can be a function that only relates to the task time t (such as $\bar{w}_i = sin(t)$). However, since the system states x_i and v_i are correlated with external variables such as t, and therefore can be expressed as a function whose variables include the external variables, the external variables can also be seen as a function that uses the system states x_i and v_i as its variables. Hence, we are still able to employ the NN to perform a unified estimation of $\bar{w}_i$, which validates the implementation of* (7.9).

7.2.3 Overview of the observer-based hierarchical control scheme

In this section, the robust formation control problem of multi-UAV systems is considered when each UAV contains model uncertainty. To reduce the complexity of the controller design, a hierarchical two-level formation controller design is proposed to separate the concerns.

In high-level designs, virtual agents are generated according to the second-order nominal model of UAVs to act as the reference generators that provide feasible commends to the low-level design, and the low-level controllers are responsible for the actual motion control of physical UAVs. A new neural-based observer design is also proposed in this section for the estimation and compensation of the nonlinear model uncertainties.

7.2.4 High-level design for unified-order vehicle clusters

To ensure that the formation controller of each UAV is offered with a sufficient number of state references, each high-level virtual agent is defined to have the homogeneous second-order dynamics as follows:

$$\begin{cases} \dot{\bar{x}}_i = \bar{v}_i, \\ \dot{\bar{v}}_i = \mathcal{S}(\bar{u}_i, \bar{U}_{Mi}) \end{cases} \tag{7.10}$$

where $\bar{x}_i \in \mathbb{R}^n$ and $\bar{v}_i \in \mathbb{R}^n$ are the position and velocity information of the virtual agent, respectively, $\bar{u}_i \in \mathbb{R}^n$ is the control input of the virtual agent, and $\mathcal{S}(\bar{u}_i, \bar{U}_{Mi}) \in \mathbb{R}^n$ is the actuator saturation phenomenon. Define $\mathcal{S}(\bar{u}_i(j), \bar{U}_{Mi})$ to be the jth element of $\mathcal{S}(\bar{u}_i, \bar{U}_{Mi})$. Then we have

$$\mathcal{S}(\bar{u}_i(j), \bar{U}_{Mi}) = \begin{cases} \bar{u}_i(j) & |u_i(j)| \leq \bar{U}_{Mi} \\ \text{sign}(\bar{u}_i(j))\bar{U}_{Mi} & |\bar{u}_i(j)| > \bar{U}_{Mi} \end{cases} \tag{7.11}$$

where $\bar{U}_{Mi}$ is a positive constant that represents the saturation limitation.

Accordingly, we have the following cluster expression:

$$\begin{cases} \dot{\bar{x}} = \bar{v}, \\ \dot{\bar{v}} = \mathcal{S}(\bar{u}) \end{cases} \tag{7.12}$$

where

$$\mathcal{S}(\bar{u}) = [\mathcal{S}^{\mathrm{T}}(\bar{u}_1, \bar{U}_{M1}), \mathcal{S}^{\mathrm{T}}(\bar{u}_2, \bar{U}_{M2}), \ldots, \mathcal{S}^{\mathrm{T}}(\bar{u}_N, \bar{U}_{MN})]^{\mathrm{T}}$$
$$\bar{x} = [\bar{x}_1^{\mathrm{T}}, \bar{x}_2^{\mathrm{T}}, \ldots, \bar{x}_N^{\mathrm{T}}]^{\mathrm{T}}, \ \bar{v} = [\bar{v}_1^{\mathrm{T}}, \bar{v}_2^{\mathrm{T}}, \ldots, \bar{v}_N^{\mathrm{T}}]^{\mathrm{T}}$$

Regarding the virtual system (7.10), we define the high-level tracking errors $\bar{\delta}_{xi}$ and $\bar{\delta}_{vi}$ as

$$\begin{cases} \bar{\delta}_{xi} = \bar{x}_i - x_{i,p}^d \\ \bar{\delta}_{vi} = \bar{v}_i - \dot{x}_{i,p}^d \end{cases} \tag{7.13}$$

The tracking error dynamics for the ith virtual agent is given as

$$\begin{cases} \dot{\bar{\delta}}_{xi} = \bar{\delta}_{vi} \\ \dot{\bar{\delta}}_{vi} = \mathcal{S}(\bar{u}_i, \bar{U}_{Mi}) - \ddot{x}_{i,p}^d \end{cases}$$

Then we have the virtual local formation tracking errors $\bar{e}_{xi}$ and $\bar{e}_{vi}$ as follows, respectively:

$$\begin{cases} \bar{e}_{xi} = \sum_{j=1}^{N} l_{ij}\bar{\delta}_{xj} + b_i\bar{\delta}_{xi} \\ \bar{e}_{vi} = \sum_{j=1}^{N} l_{ij}\bar{\delta}_{vj} + b_i\bar{\delta}_{vi} \end{cases} \tag{7.14}$$

where b_i is the ith diagonal element of B. Define $\bar{\lambda}_i$ to be a positive constant. Then the virtual sliding surface is designed as

$$\bar{s}_i = \bar{e}_{vi} + \bar{\lambda}_i\bar{\mathcal{S}}(\bar{e}_{xi}, \bar{\tau}_e, \bar{\psi}_e) \tag{7.15}$$

where $\bar{\tau}_e$ is a positive constant, $\bar{\psi}_e$ is a very small positive constant and $\bar{\mathcal{S}}(\bar{e}_{xi}, \bar{\tau}_e, \bar{\psi}_e) \in \mathbb{R}^n$ is a bounded smooth projection function whose jth element is expressed as

$$\bar{\mathcal{S}}(\bar{e}_{xi}(j), \bar{\tau}_e, \bar{\psi}_e) = \begin{cases} \bar{\tau}_e + \bar{\psi}_e\left(1 - \exp\left(\dfrac{\bar{\tau}_e - \bar{e}_{xi}(j)}{\bar{\psi}_e}\right)\right), & \text{if } \bar{e}_{xi}(j) > \bar{\tau}_e \\ \bar{e}_{xi}(j), & \text{if } |\bar{e}_{xi}(j)| \leq \bar{\tau}_e \\ \bar{\psi}_e\left(\exp\left(\dfrac{\bar{\tau}_e + \bar{e}_{xi}(j)}{\bar{\psi}_e}\right) - 1\right) - \bar{\tau}_e, & \text{if } \bar{e}_{xi}(j) < -\bar{\tau}_e \end{cases} \tag{7.16}$$

Then we have the time derivative of the virtual sliding surface as

$$\dot{\bar{s}}_i = \dot{\bar{e}}_{vi} + \bar{\lambda}_i \mathrm{diag}\{\bar{\mathcal{S}}_d(\bar{e}_{xi}, \bar{\tau}_e, \bar{\psi}_e)\}\bar{e}_{vi} \tag{7.17}$$

where the jth element in $\bar{\mathcal{S}}_d(\bar{e}_{xi}, \bar{\tau}_e, \bar{\psi}_e)$ has the following expression:

$$\bar{\mathcal{S}}_d(\bar{e}_{xi}(j), \bar{\tau}_e, \bar{\psi}_e) = \begin{cases} \exp\left(\dfrac{\bar{\tau}_e - \bar{e}_{xi}(j)}{\bar{\psi}_e}\right), & \text{if } \bar{e}_{xi}(j) > \bar{\tau}_e \\ 1, & \text{if } |\bar{e}_{xi}(j)| \leq \bar{\tau}_e \\ \exp\left(\dfrac{\bar{\tau}_e + \bar{e}_{xi}(j)}{\bar{\psi}_e}\right), & \text{if } \bar{e}_{xi}(j) < -\bar{\tau}_e \end{cases}$$

Define $\bar{S} = [\bar{s}_1^{\mathrm{T}}, \bar{s}_2^{\mathrm{T}}, \ldots, \bar{s}_N^{\mathrm{T}}]^{\mathrm{T}}$, $\bar{e}_x = [\bar{e}_{x1}^{\mathrm{T}}, \bar{e}_{x2}^{\mathrm{T}}, \ldots, \bar{e}_{xN}^{\mathrm{T}}]^{\mathrm{T}}$, $\bar{e}_v = [\bar{e}_{v1}^{\mathrm{T}}, \bar{e}_{v2}^{\mathrm{T}}, \ldots, \bar{e}_{vN}^{\mathrm{T}}]^{\mathrm{T}}$ and $\bar{\Lambda} = \mathrm{diag}\{\bar{\lambda}_1, \ldots, \bar{\lambda}_N\}$. Then the cluster expression is obtained as

$$\bar{S} = \bar{e}_v + (\bar{\Lambda} \otimes I_3)\bar{\mathcal{S}}(\bar{e}_x, \bar{\tau}_e, \bar{\psi}_e)$$

Based on the discussions about the tracking error (7.13) and the sliding surface design (7.15) of the virtual system (7.10), we have the nominal high-level controller design as follows:

$$\bar{u}_i^{\mathrm{nom}} = \ddot{x}_{i,p}^{d} - \bar{c}_i\bar{s}_i - \bar{\lambda}_i \mathrm{diag}\{\bar{\mathcal{S}}_d(\bar{e}_{xi}, \bar{\tau}_e, \bar{\psi}_e)\}\bar{\delta}_{vi} - \bar{k}_i\bar{\delta}_{xi}$$

where $\bar{c}_i$ and $\bar{k}_i$ are both positive constants.

To ensure that the amplitudes of the control input stay within the saturation limitation, we have the following saturated high-level formation controller:

$$\bar{u}_i = \bar{\mathcal{S}}(\bar{u}_i^{\text{nom}}, \bar{\tau}_u, \bar{\psi}_u) \tag{7.18}$$

where $\bar{\tau}_u$ and $\bar{\psi}_u$ are both positive constants.

Now we are ready to present our result within high-level controller design:

Theorem 7.1. *Consider the virtual cluster* (7.10), *where Assumption 7.1 holds. By the sliding surface design* (7.15) *and the sliding mode controller* (7.18), *the variables $\bar{S}$, $\bar{e}_x$ and $\bar{\delta}_x$ are all UUB.*

Proof. Consider a Lyapunov candidate as follows:

$$V_{6,1} = \frac{1}{2}\bar{S}^{\mathrm{T}} P \otimes I_3 \bar{S} + \frac{1}{2}\bar{e}_x^{\mathrm{T}}(P\bar{K}) \otimes I_3 \bar{e}_x$$

where $\bar{K} = \mathrm{diag}\{\bar{k}_1, \bar{k}_2, \ldots, \bar{k}_N\}$.

The time derivative of $V_{6,1}$ is given as

$$\begin{aligned}
\dot{V}_{6,1} &= \bar{S}^{\mathrm{T}} P \otimes I_3 \dot{\bar{S}} + \bar{e}_x^{\mathrm{T}}(P\bar{K}) \otimes I_3 \dot{\bar{e}}_x \\
&= \bar{S}^{\mathrm{T}} P \otimes I_3 (\dot{\bar{e}}_v + \bar{\Lambda} \otimes I_3 \mathrm{diag}\{\bar{\mathcal{S}}_d(\bar{e}_x, \bar{\tau}_e, \bar{\psi}_e)\}\bar{e}_v) + \bar{e}_x^{\mathrm{T}}(P\bar{K}) \otimes I_3 (\bar{S} \\
&\quad - (\bar{\Lambda} \otimes I_3)\bar{\mathcal{S}}(\bar{e}_x, \bar{\tau}_e, \bar{\psi}_e)) \\
&= \bar{S}^{\mathrm{T}}(P(L+B)) \otimes I_3 (\dot{\bar{\delta}}_v + \bar{\Lambda} \otimes I_3 \mathrm{diag}\{\bar{\mathcal{S}}_d(\bar{e}_x, \bar{\tau}_e, \bar{\psi}_e)\}\bar{\delta}_v) + \bar{e}_x^{\mathrm{T}}(P\bar{K}) \otimes I_3 \bar{S} \\
&\quad - \bar{e}_x^{\mathrm{T}}(P\bar{K}\bar{\Lambda}) \otimes I_3 \bar{\mathcal{S}}(\bar{e}_x, \bar{\tau}_e, \bar{\psi}_e)
\end{aligned}$$

First, we rule out the saturation phenomenon (7.11) and have $\bar{u}_i = \bar{u}_i^{\text{nom}}$ instead to test if the nominal controller is able to ensure the uniform ultimate boundedness of both $\bar{s}_i$ and $\bar{e}_{xi}$. Then we have the modified version of $\dot{V}_{6,1}$ as

$$\begin{aligned}
\dot{V}_{6,1} &= -\bar{S}^{\mathrm{T}}(P(L+B)\bar{C}) \otimes I_3 \bar{S} - \bar{S}^{\mathrm{T}}(P\bar{K}) \otimes I_3 \bar{e}_x + \bar{e}_x^{\mathrm{T}}(P\bar{K}) \otimes I_3 \bar{S} \\
&\quad - \bar{e}_x^{\mathrm{T}}(P\bar{K}\bar{\Lambda}) \otimes I_3 \bar{\mathcal{S}}(\bar{e}_x, \bar{\tau}_e, \bar{\psi}_e) \\
&= -\bar{S}^{\mathrm{T}}(P(L+B)\bar{C}) \otimes I_3 \bar{S} - \bar{e}_x^{\mathrm{T}}(P\bar{K}\bar{\Lambda}) \otimes I_3 \bar{\mathcal{S}}(\bar{e}_x, \bar{\tau}_e, \bar{\psi}_e)
\end{aligned}$$

By Lemma 2.3 and the inequality that $\bar{\mathcal{S}}(\bar{e}_x, \bar{\tau}_e, \bar{\psi}_e) \leq \bar{e}_x$, we have the following norm form:

$$\dot{V}_{6,1} \leq -\frac{1}{2}\underline{\sigma}(Q\bar{C})\|\bar{S}\|^2 - \underline{\sigma}(P\bar{K}\bar{\Lambda})\|\bar{\mathcal{S}}(\bar{e}_x, \bar{\tau}_e, \bar{\psi}_e)\|^2$$

Hence, we get that $\dot{V}_{6,1}$ will remain negative until $\|\bar{S}\| = \|\bar{\mathcal{S}}(\bar{e}_x, \bar{\tau}_e, \bar{\psi}_e)\| = 0$ is achieved. By the characteristics of the smooth projection function $\bar{\mathcal{S}}(\bar{e}_x, \bar{\tau}_e, \bar{\psi}_e)$, $\|\bar{e}_x\|$ will also converge to the value of zero. According to (7.14), we have that $\|\bar{\delta}_x\| = 0$ is ultimately achieved as well. By the definition of UUB (Lewis *et al.* 2013), we have that $\|\bar{S}\|$, $\|\bar{e}_x\|$ and $\|\bar{\delta}_x\|$ are all UUB, which indicates that the design of $\bar{u}_i^{\mathrm{nom}}$ is able to achieve convergence of the virtual tracking error.

If we recall the saturation phenomenon (7.11) and the saturated controller design (7.18), similar results are also expected and the states $\|\bar{S}\|$, $\|\bar{e}_x\|$ and $\|\bar{\delta}_x\|$ are all UUB, which completes the proof.

□

Remark 7.2. *The virtual high-level agent* (7.10) *is constructed with a saturation phenomenon* (7.11) *to ensure that the states $\bar{x}_i$, $\bar{v}_i$ and $\bar{u}_i$ are a set of suitable and feasible reference vectors to prevent the low-level UAVs from causing aggressive motion and create large pitch angles or rotational angles* (Tang *et al.* 2018).

7.2.5 Neural-based observer design for unified-order vehicle clusters

Differently from the high-level design, it is vital to consider the system uncertainties w_i for the low-level design. To maintain the robustness of the formation tracking process, one popular way is to employ the neural-based observer designs (Liu *et al.* 2013, Fei *et al.* 2021a) to estimate the unknown terms and then perform compensation in the controller design. On the basis of the work proposed by Fei et al. (Fei *et al.* 2021a), the sliding mode technique is integrated with an artificial NN to approximate the unknown factor w_i in system (7.6).

Although the sliding mode structures (Liu *et al.* 2013, Fei *et al.* 2021a) are effective for an arbitrary kind of uncertainty, the design of only using the NN output as the estimation value relies too much on the accuracy of the NN. In other words, if we were to use the FTDO designs (Liu *et al.* 2013, Fei *et al.* 2021a), then the norm of the difference between $\widehat{w}_i$ and w_i would be no less than ϵ_M, which illustrates their limitation. To overcome this weakness, we propose to have an alternative way of analysing the problem. First, we build up an imaginary second-order observation system according to the actual system

(7.6):

$$\begin{cases} \dot{\widehat{x}}_i = \widehat{v}_i \\ \dot{\widehat{v}}_i = g_i u_i + \widehat{u}_i \end{cases} \tag{7.19}$$

where $\widehat{u}_i$ is the imaginary control input, and vectors $\widehat{x}_i$ and $\widehat{v}_i$ represent our estimations of states x_i and v_i, respectively. As u_i is the to be designed controller and g_i is known in advance, the term $g_i u_i$ is treated as the known dynamics for the imaginary system. By comparing the difference between the imaginary system (7.19) and the actual UAV dynamics (7.6), we have the following tracking error dynamics for the imaginary system:

$$\begin{cases} \dot{\widetilde{x}}_i = \widetilde{v}_i \\ \dot{\widetilde{v}}_i = w_i - \widehat{u}_i \end{cases} \tag{7.20}$$

where $\widetilde{x}_i = x_i - \widehat{x}_i$ and $\widetilde{v}_i = v_i - \widehat{v}_i$ are applied.

In theory, we have $w_i = \widehat{u}_i$ when both $\|\widetilde{x}_i\| = 0$ and $\|\widetilde{v}_i\| = 0$ are satisfied. Hence, our goal of building up an adaptive observer to estimate w_i is also equivalent to designing a tracking controller $\widehat{u}_i$ that reduces the value of $\|\widetilde{x}_i\|$ and $\|\widetilde{v}_i\|$ as much as possible. To achieve the uniformly ultimate boundedness of $\widetilde{x}_i$ and $\widetilde{v}_i$, we define the observation sliding surface as

$$\widetilde{s}_i = \widetilde{v}_i + \widetilde{\lambda}_i \widetilde{x}_i \tag{7.21}$$

where $\widetilde{\lambda}_i$ is a positive constant.

We have the derivative of the observation sliding surface as

$$\dot{\widetilde{s}}_i = \dot{\widetilde{v}}_i + \widetilde{\lambda}_i \dot{\widetilde{x}}_i = w_i - \widehat{u}_i + \widetilde{\lambda}_i \widetilde{v}_i$$

Based on our previous discussion about the artificial NN estimation of w_i (7.9), we have the following neural adaptive sliding mode controller design for the imaginary system:

$$\widehat{u}_i = \widehat{W}_i^{\mathrm{T}} \varphi(x_i, v_i) + \widetilde{\lambda}_i \widetilde{v}_i + \widetilde{c}_i \widetilde{s}_i + \widetilde{k}_i \widetilde{x}_i \tag{7.22}$$

where $\widetilde{c}_i$ and $\widetilde{k}_i$ are both positive constants, and the update law of the NN is

$$\dot{\widehat{W}}_i = \eta_1 \varphi(x_i, v_i) \widetilde{s}_i^{\mathrm{T}} - \eta_2 \|\widetilde{s}_i\| \widehat{W}_i \tag{7.23}$$

where η_1 and η_2 are both positive constants.

Now we are ready to present our result of the neural-based sliding mode observer design.

Theorem 7.2. *Consider the system of* (7.19)*, where Assumption 7.2 is satisfied. By the observation sliding variable* (7.21)*, the NN estimation* (7.21)*, the adaptive neural weight tuning law* (7.23) *and the imaginary control input* (7.22)*, we have that the error states* $\widetilde{s}_i$*,* $\widetilde{x}_i$ *and* $\widetilde{W}_i$ *are all semi-globally UUB if the compact set conditions of NNs hold when* $t \geq t_0$*.*

Proof. Consider the following Lyapunov candidate:

$$V_{6,2} = \frac{1}{2}\widetilde{s}_i^{\mathrm{T}}\widetilde{s}_i + \frac{1}{2\eta_1}\mathrm{tr}\{\widetilde{W}_i^{\mathrm{T}}\widetilde{W}_i\} + \frac{\widetilde{k}_i}{2}\widetilde{x}_i^{\mathrm{T}}\widetilde{x}_i$$

Then the derivative of $V_{6,2}$ is obtained as follows:

$$\begin{aligned}
\dot{V}_{6,2} &= \widetilde{s}_i^{\mathrm{T}}\dot{\widetilde{s}}_i - \frac{1}{\eta_1}\mathrm{tr}\{\widetilde{W}_i^{\mathrm{T}}\dot{\widehat{W}}_i\} + \widetilde{k}_i\widetilde{x}_i^{\mathrm{T}}\dot{\widetilde{x}}_i \\
&= \widetilde{s}_i^{\mathrm{T}}(w_i - \widehat{u}_i + \widetilde{\lambda}_i\widetilde{v}_i) - \frac{1}{\eta_1}\mathrm{tr}\{\widetilde{W}_i^{\mathrm{T}}\dot{\widehat{W}}_i\} + \widetilde{k}_i\widetilde{x}_i^{\mathrm{T}}(\widetilde{s}_i - \widetilde{\lambda}_i\widetilde{x}_i) \\
&= \widetilde{s}_i^{\mathrm{T}}(\widetilde{W}_i^{\mathrm{T}}\varphi(x_i, v_i) + \epsilon_i - \widetilde{c}_i\widetilde{s}_i) - \frac{1}{\eta_1}\mathrm{tr}\{\widetilde{W}_i^{\mathrm{T}}(\eta_1\varphi(x_i, v_i)\widetilde{s}_i^{\mathrm{T}} - \eta_2\|\widetilde{s}_i\|\widehat{W}_i)\} - \widetilde{k}_i\widetilde{\lambda}_i\widetilde{x}_i^{\mathrm{T}}\widetilde{x}_i \\
&= -\widetilde{c}_i\widetilde{s}_i^{\mathrm{T}}\widetilde{s}_i - \widetilde{k}_i\widetilde{\lambda}_i\widetilde{x}_i^{\mathrm{T}}\widetilde{x}_i + \widetilde{s}_i^{\mathrm{T}}\epsilon_i + \frac{\eta_2}{\eta_1}\|\widetilde{s}_i\|\mathrm{tr}\{\widetilde{W}_i^{\mathrm{T}}(W_i - \widetilde{W}_i)\}
\end{aligned} \tag{7.24}$$

We can further modify (7.24) into the following norm form:

$$\begin{aligned}
\dot{V}_{6,2} &\leq -\widetilde{c}_i\|\widetilde{s}_i\|^2 - \widetilde{k}_i\widetilde{\lambda}_i\|\widetilde{x}_i\|^2 + \|\widetilde{s}_i\|\epsilon_M + \frac{\eta_2}{\eta_1}\|\widetilde{s}_i\|\|\widetilde{W}_i\|_{\mathrm{F}}(W_M - \|\widetilde{W}_i\|_{\mathrm{F}}) \\
&\leq -\widetilde{c}_i\|\widetilde{s}_i\|^2 - \widetilde{k}_i\widetilde{\lambda}_i\|\widetilde{x}_i\|^2 + \|\widetilde{s}_i\|\epsilon_M - \frac{\eta_2}{\eta_1}\|\widetilde{s}_i\|(\|\widetilde{W}_i\|_{\mathrm{F}}^2 - W_M\|\widetilde{W}_i\|_{\mathrm{F}} + \frac{W_M^2}{4} - \frac{W_M^2}{4}) \\
&\leq -\widetilde{c}_i\|\widetilde{s}_i\|^2 - \widetilde{k}_i\widetilde{\lambda}_i\|\widetilde{x}_i\|^2 + \|\widetilde{s}_i\|\epsilon_M - \frac{\eta_2}{\eta_1}\|\widetilde{s}_i\|(\|\widetilde{W}_i\|_{\mathrm{F}}^2 - \frac{W_M}{2})^2 + \frac{\eta_2 W_M^2}{4\eta_1}\|\widetilde{s}_i\| \\
&\leq -\widetilde{c}_i\|\widetilde{s}_i\|^2 - \widetilde{k}_i\widetilde{\lambda}_i\|\widetilde{x}_i\|^2 + \|\widetilde{s}_i\|\epsilon_M + \frac{\eta_2 W_M^2}{4\eta_1}\|\widetilde{s}_i\| \\
&\leq -\chi_{6,1}^{\mathrm{T}}H_{6,1}\chi_{6,1} + \mathcal{H}_{6,1}\chi_{6,1}
\end{aligned}$$

where

$$\chi_{6,1} = \begin{bmatrix} \|\widetilde{s}_i\| \\ \|\widetilde{x}_i\| \end{bmatrix}, \ \mathcal{H}_{6,1} = \begin{bmatrix} \epsilon_M + \eta_2 W_M^2/4\eta_1 & 0 \end{bmatrix}$$

$$H_{6,1} = \begin{bmatrix} \widetilde{c}_i & 0 \\ 0 & \widetilde{k}_i\widetilde{\lambda}_i \end{bmatrix}$$

Hence, $\dot{V}_{6,1}$ is said to be negative when the following condition is met:

$$\|\chi_{6,1}\| > \frac{4\eta_1\epsilon_M + \eta_2 W_M^2}{4\eta_1\underline{\sigma}(H_{6,1})}$$

By Definition 2.1, we have that the vector χ_1 is semi-globally UUB within the following neighbourhood:

$$\Omega_\chi^1 = \left\{ \chi_{6,1} \middle| \|\chi_{6,1}\| \leq \frac{4\eta_1\epsilon_M + \eta_2 W_M^2}{4\eta_1\underline{\sigma}(H_{6,1})} \right\}$$

Hence, the error states $\widetilde{s}_i$ and $\widetilde{x}_i$ are both semi-globally UUB. According to the Lyapunov stability theory extension (Kim and Lewis 1999), the correlated state $\widetilde{W}_i$ is also semi-globally UUB, which completes the proof. □

As a result, we are confident to have $\|\widetilde{w}_i\| \leq \widetilde{w}_M$, where $\widetilde{w}_M$ is a positive constant, to support the theorems in the low-level formation controller design.

7.2.6 Low-level design for unified-order vehicle clusters

Regarding the low-level design, we need to first focus on the position loop to provide an essential reference for the attitude control loop (Du *et al.* 2017). Accordingly, the position loop dynamics (7.4) and the attitude loop dynamics (7.5) of the ith UAV are investigated for the low-level designs.

By Theorem 7.1, we have that the states $\bar{x}_i$, $\bar{v}_i$ and $\bar{u}_i$ will converge to $x_{i,p}^d$, $\dot{x}_{i,p}^d$ and $\ddot{x}_{i,p}^d$, respectively. Hence, it is reasonable to use states $\bar{x}_i$, $\bar{v}_i$ and $\bar{u}_i$ to act as the references for the ith low-level system. Define $\delta_{xi,p}$ and $\delta_{vi,p}$ to be the low-level reference tracking errors as follows:

$$\begin{cases} \delta_{xi,p} = x_{i,p} - \bar{x}_i \\ \delta_{vi,p} = v_{i,p} - \bar{v}_i, \ i \in [1, N]. \end{cases} \tag{7.25}$$

Then we have the tracking error dynamics as

$$\begin{cases} \dot{\delta}_{xi,p} = \delta_{vi,p} \\ \dot{\delta}_{vi,p} = g_{i,p}u_i + w_{i,p} - \bar{u}_i - \bar{g}_p, \ i \in [1, N] \end{cases} \tag{7.26}$$

Different from the nominal system designs (Fei *et al.* 2021b, Fei *et al.* 2021a), we did not design u_i directly from the perspective of (7.26). Instead, we first define $u_{i,p} = g_{i,p}u_i$ to denote the nominal control input of the position loop. Then (7.26) can be rewritten as

$$\begin{cases} \dot{\delta}_{xi,p} = \delta_{vi,p} \\ \dot{\delta}_{vi,p} = u_{i,p} + w_{i,p} - \bar{u}_i - \bar{g}_p, \ i \in [1, N] \end{cases} \tag{7.27}$$

The position loop sliding surface is constructed as follows:

$$s_{i,p} = \delta_{vi,p} + \lambda_i^p \delta_{xi,p} \tag{7.28}$$

where λ_i^p is a positive constant.

The time derivative of the sliding surface is given as

$$\dot{s}_{i,p} = \dot{\delta}_{vi,p} + \lambda_i^p \delta_{vi,p} = u_{i,p} + w_{i,p} - \bar{u}_i + \lambda_i^p \delta_{vi,p} - \bar{g}_p$$

By the neural-based observer design, we have $\widehat{u}_i = \widehat{w}_i$, where $\widehat{w}_i = [\widehat{w}_{i,p}^{\mathrm{T}}, \widehat{w}_{i,a}^{\mathrm{T}}]^{\mathrm{T}}$ represents our estimation of the system uncertainty w_i.

Based on the discussion about the neural-based observer (7.22) and the potential-based position loop sliding variable (7.28), we have the following nominal controller design:

$$u_{i,p} = \bar{u}_i - \widehat{w}_{i,p} - \lambda_i^p \delta_{vi,p} - k_i^p \delta_{xi,p} - c_i^p s_{i,p} + \bar{g}_p \tag{7.29}$$

where $k_i^p \in \mathbb{R}^+$ and $c_i^p \in \mathbb{R}^+$.

Now we are ready to present our results in the low-level nominal controller design for the position loop (7.4) of the ith UAV.

Theorem 7.3. *Consider the nominal position loop dynamics of the ith UAV* (7.4)*, where Assumptions 7.1-7.2 are satisfied. By the neural-based observer* (7.22) *and the nominal control law* (7.29)*, the states $\delta_{xi,p}$ and $s_{i,p}$ are both semi-globally UUB if the compact set conditions of NNs hold when $t \geq t_0$.*

Proof. Consider the following Lyapunov candidate for the ith UAV:

$$V_{i,p} = \frac{1}{2} s_{i,p}^{\mathrm{T}} s_{i,p} + \frac{k_i^p}{2} \delta_{xi,p}^{\mathrm{T}} \delta_{xi,p} \tag{7.30}$$

The time derivative of the Lyapunov candidate (7.30) is given as

$$\begin{aligned}
\dot{V}_{i,p} &= s_{i,p}^{\mathrm{T}} \dot{s}_{i,p} + k_i^p \delta_{xi,p}^{\mathrm{T}} \dot{\delta}_{xi,p} \\
&= s_{i,p}^{\mathrm{T}} (\dot{\delta}_{vi,p} + \lambda_i^p \delta_{vi,p}) + k_i^p \delta_{xi,p}^{\mathrm{T}} (s_{i,p} - \lambda_i^p \delta_{xi,p}) \\
&= s_{i,p}^{\mathrm{T}} (u_{i,p} + w_{i,p} - \bar{u}_i - \bar{g}_p + \lambda_i^p \delta_{vi,p}) + k_i^p \delta_{xi,p}^{\mathrm{T}} (s_{i,p} - \lambda_i^p \delta_{xi,p}) \\
&= s_{i,p}^{\mathrm{T}} (\widetilde{w}_{i,p} - k_i^p \delta_{xi,p} - c_i^p s_{i,p}) - k_i^p \lambda_i^p \delta_{xi,p}^{\mathrm{T}} \delta_{xi,p} + k_i^p \delta_{xi,p}^{\mathrm{T}} s_{i,p} \\
&\leq -c_i^p \|s_{i,p}\|^2 + \|s_{i,p}\| \widetilde{w}_M - k_i^p \lambda_i^p \|\delta_{xi,p}\|^2
\end{aligned}$$

where $\widetilde{w}_{i,p} = w_{i,p} - \widehat{w}_{i,p}$.

Alternatively, we have the following matrix form:

$$\dot{V}_{i,p} \leq -\chi_{6,2}^{\mathrm{T}} H_{6,2} \chi_{6,2} + \mathcal{H}_{6,2} \chi_{6,2}$$

where

$$\chi_{6,2} = \begin{bmatrix} \|s_{i,p}\| \\ \|\delta_{xi,p}\| \end{bmatrix}, \ \mathcal{H}_{6,2} = \begin{bmatrix} \widetilde{w}_M & 0 \end{bmatrix}, \ H_{6,2} = \begin{bmatrix} c_i^p & 0 \\ 0 & k_i^p \lambda_i^p \end{bmatrix}$$

Hence, $\dot{V}_{i,p}$ is guaranteed to be negative within the following region:

$$\|\chi_{6,2}\| > \frac{\widetilde{w}_M}{\underline{\sigma}(H_{6,2})}$$

By Definition 2.1, we have that the vector χ_2 is semi-globally UUB within the following region:

$$\Omega_\chi^2 = \left\{ \chi_{6,2} \middle| \|\chi_{6,2}\| \leq \frac{\widetilde{w}_M}{\underline{\sigma}(H_{6,2})} \right\}$$

As in the case of $\|\chi_2\|$, the values of $\|s_{i,p}\|$ and $\|\delta_{xi,p}\|$ are both semi-globally UUB, which completes the proof.

□

After obtaining the nominal control $u_{i,p}$, the next step is to use the flight control techniques to calculate the reference for the row angle and the yaw angle. Inspired by (Ren *et al.* 2022), with $u_{i,p} = [u_{i,x}, u_{i,y}, u_{i,z}]^{\mathrm{T}}$, we have a new guidance law for T_i^d:

$$\begin{cases} T_i^d = \dfrac{m_i u_{i,z}}{\cos(\phi_i)\cos(\theta_i)} \\ \phi_i^d = \arcsin\left(\dfrac{(u_{i,x}\sin(\psi_i^d) - u_{i,y}\cos(\psi_i^d))}{(u_{i,x}^2 + u_{i,y}^2 + u_{i,z}^2)^{1/2}} \right) \\ \theta_i^d = \arctan\left(\dfrac{u_{i,x}\cos(\psi_i^d) + u_{i,y}\sin(\psi_i^d)}{u_{i,z}} \right) \end{cases} \tag{7.31}$$

After both ϕ_i^d and θ_i^d are calculated, we can use the conventional approach of calculating the slope between the current value and the previous value to get the value of $\dot{\phi}_i^d$, $\ddot{\phi}_i^d$, $\dot{\theta}_i^d$, $\ddot{\theta}_i^d$, $\dot{\psi}_i^d$ and $\ddot{\psi}_i^d$ as follows:

$$\xi_{i,1} = \begin{cases} [0,0,0]^{\mathrm{T}} & t \leq t_{\text{step}} \\ \dfrac{x_{i,a}^d(t) - x_{i,a}^d(t - t_{\text{step}})}{t_{\text{step}}} & t > t_{\text{step}} \end{cases} \tag{7.32}$$

where $\xi_{i,1}$ is the estimation of $\dot{x}_{i,a}^d$, t represents the current time and t_{step} is the control step size. Similarly, we have the following structure to get the second-order derivative as

$$\xi_{i,2} = \begin{cases} [0,0,0]^{\mathrm{T}} & t \leq 2t_{\text{step}} \\ \dfrac{\xi_{i,1}(t) - \xi_{i,1}(t - t_{\text{step}})}{t_{\text{step}}} & t > 2t_{\text{step}} \end{cases} \tag{7.33}$$

Accordingly, we have $\xi_{i,1} = \dot{x}_{i,a}^d$ and $\xi_{i,2} = \ddot{x}_{i,a}^d$ when $t > 2t_{\text{step}}$. Similarly to the position loop, define $\delta_{xi,a}$ and $\delta_{vi,a}$ to be the reference tracking errors in the attitude loop, which further leads to

$$\begin{cases} \delta_{xi,a} = x_{i,a} - x_{i,a}^d \\ \delta_{vi,a} = v_{i,a} - \dot{x}_{i,a}^d, \ i \in [1, N] \end{cases} \tag{7.34}$$

If we define $u_{i,a} = g_{i,a} u_i$ to be the nominal control input for the attitude loop, we have the error dynamics as follows:

$$\begin{cases} \dot{\delta}_{xi,a} = \delta_{vi,a} \\ \dot{\delta}_{vi,a} = u_{i,a} + w_{i,a} - \ddot{x}_{i,a}^d, \ i \in [1, N] \end{cases} \tag{7.35}$$

Differently from the position loop, the vector $\delta_{vi,a}$ cannot be directly obtained because $\dot{x}_{i,a}^d$ is unknown to the ith UAV. Instead, the UAV can only gain access to the estimated error vector $\widehat{\delta}_{vi,a}$ as

$$\widehat{\delta}_{vi,a} = v_{i,a} - \xi_{i,1}$$

Accordingly, we have the actual sliding surface for the attitude loop as $s_{i,a} = \delta_{vi,a} + \lambda_i^a \delta_{xi,a}$, and the estimated sliding variable is given as

$$\widehat{s}_{i,a} = \widehat{\delta}_{vi,a} + \lambda_i^a \delta_{xi,a} \tag{7.36}$$

where λ_i^a is a positive constant. The time derivative of the actual sliding surface $s_{i,a}$ is

$$\dot{s}_{i,a} = \dot{\delta}_{vi,a} + \lambda_i^a \delta_{vi,a} = u_{i,a} + w_{i,a} - \ddot{x}_{i,a}^d + \lambda_i^a \delta_{vi,a}$$

Based on our discussion about the neural-based observer (7.22) and the estimated attitude loop sliding variable (7.36), we have the following nominal controller design:

$$u_{i,a} = \xi_{i,2} - \widehat{w}_{i,a} - \lambda_i^a \widehat{\delta}_{vi,a} - k_i^a \delta_{xi,a} - c_i^a \widehat{s}_{i,a} \tag{7.37}$$

where k_i^a and c_i^a are both positive constants.

Now we are ready to present the result of the low-level nominal controller design for the attitude loop of the ith UAV:

Theorem 7.4. *Consider the nominal attitude loop dynamics of the ith UAV* (7.5)*, where Assumptions 7.1-7.2 are satisfied. By the neural-based observer* (7.22)*, the first-order differentiator* (7.32)*, the second-order differentiator* (7.33) *and the nominal control law* (7.37)*, the states* $\delta_{xi,a}$ *and* $s_{i,a}$ *are both semi-globally UUB if the compact set conditions of NNs hold when* $t \geq t_0$.

Proof. Consider the following Lyapunov candidate.

$$V_{i,a} = \frac{1}{2} s_{i,a}^{\mathrm{T}} s_{i,a} + \frac{k_i^a}{2} \delta_{xi,a}^{\mathrm{T}} \delta_{xi,a}$$

Then we have the time derivative of $V_{i,a}$ as

$$\begin{aligned}
\dot{V}_{i,a} &= s_{i,a}^{\mathrm{T}} \dot{s}_{i,a} + k_i^a \delta_{xi,a}^{\mathrm{T}} \dot{\delta}_{xi,a} \\
&= s_{i,a}^{\mathrm{T}} (\dot{\delta}_{vi,a} + \lambda_i^a \delta_{vi,a}) + k_i^a \delta_{xi,a}^{\mathrm{T}} (s_{i,a} - \lambda_i^a \delta_{xi,a}) \\
&= s_{i,a}^{\mathrm{T}} (u_{i,a} + w_{i,a} - \ddot{x}_{i,a}^d + \lambda_i^a \delta_{vi,a}) + k_i^a \delta_{xi,a}^{\mathrm{T}} (s_{i,a} - \lambda_i^a \delta_{xi,a}) \\
&= s_{i,a}^{\mathrm{T}} (\widetilde{w}_{i,a} - k_i^a \delta_{xi,a} - c_i^a \widehat{s}_{i,a} + \xi_{i,2} - \ddot{x}_{i,a}^d + \lambda_i^a (\delta_{vi,a} - \widehat{\delta}_{vi,a})) - k_i^a \lambda_i^a \delta_{xi,a}^{\mathrm{T}} \delta_{xi,a} + k_i^a \delta_{xi,a}^{\mathrm{T}} s_{i,a}
\end{aligned} \tag{7.38}$$

where $\widetilde{w}_{i,p} = w_{i,p} - \widehat{w}_{i,p}$. We have $\xi_{i,1} = \dot{x}_{i,a}^d$, $\xi_{i,2} = \ddot{x}_{i,a}^d$, $\delta_{vi,a} = \widehat{\delta}_{vi,a}$ and $s_{i,a} = \widehat{s}_{i,a}$ when $t > 2t_{\text{step}}$. Therefore, (7.38) is rewritten as

$$\begin{aligned}
\dot{V}_{i,a} &= s_{i,a}^{\mathrm{T}} (\widetilde{w}_{i,a} - c_i^a s_{i,a}) - k_i^a \lambda_i^a \delta_{xi,a}^{\mathrm{T}} \delta_{xi,a} \\
&\leq -c_i^a \|s_{i,a}\|^2 + \widetilde{w}_M \|s_{i,a}\| - k_i^a \lambda_i^a \|\delta_{xi,a}\|^2
\end{aligned}$$

Similarly, we also have the following matrix form:

$$\dot{V}_{i,a} \leq -\chi_{6,3}^{\mathrm{T}} H_{6,3} \chi_{6,3} + \mathcal{H}_{6,3} \chi_{6,3}$$

where

$$\chi_{6,3} = \begin{bmatrix} \|s_{i,a}\| \\ \|\delta_{xi,a}\| \end{bmatrix}, \ \mathcal{H}_{6,3} = \begin{bmatrix} \widetilde{w}_M & 0 \end{bmatrix}, \ H_{6,3} = \begin{bmatrix} c_i^a & 0 \\ 0 & k_i^a \lambda_i^a \end{bmatrix}$$

Hence, $\dot{V}_{i,a}$ is negative within the following region:

$$\|\chi_3\| > \frac{\widetilde{w}_M}{\underline{\sigma}(H_{6,3})}$$

By Definition 2.1, we have that the vector χ_3 is semi-globally UUB within the following region:

$$\Omega_\chi^3 = \left\{ \chi_{6,3} \middle| \|\chi_{6,3}\| \leq \frac{\widetilde{w}_M}{\underline{\sigma}(H_{6,3})} \right\}$$

As in the case of $\|\chi_{6,3}\|$, the values of $\|s_{i,a}\|$ and $\|\delta_{xi,a}\|$ are both semi-globally UUB, which completes the proof. $\square$

As the position loop and the attitude loop are strongly coupled, a subtle fluctuation in the output of any part of the controller design can lead to oscillation in the system states. Regarding the designs covered by Theorems 7.1-7.4, there are two factors that can lead to potential oscillations in the system's control input:

1. The values of θ_i^d and ψ_i^d are not guaranteed to be smooth because they are generated by the reverse calculation (7.31). Hence, the output values of the direct derivative structures (7.32) and (7.33) can be filled with chattering because of the discontinuity of their input.

2. Before $\|\widehat{W}_i - W_i\|_{\mathrm{F}}$ is settled within a neighbourhood around 0, the output of the NN is usually filled with oscillations (Fei *et al.* 2021a).

Before introducing the saturated and smoothed differentiator, it is essential to first make the following assumption:

Assumption 7.3. *The vectors $\dot{x}_{i,a}^d$ and $\ddot{x}_{i,a}^d$ are both bounded such that $\lim_{t\to+\infty} |\dot{x}_{i,a}^d| \leq \xi_M^1 \mathbf{1}_3$ and $\lim_{t\to+\infty} |\ddot{x}_{i,a}^d| \leq \xi_M^2 \mathbf{1}_3$ are met simultaneously.*

Consequently, we have the saturated and smoothed differentiator designs, as shown in Algorithm 4, where l_ξ is initially set as zero. Accordingly, we have

$$\begin{aligned} \xi_{i,1} &= \mathcal{D}(t_{\text{step}}, t_{\text{diff}}, x_{i,a}^d, t, \xi_M^1) \\ \xi_{i,2} &= \mathcal{D}(2t_{\text{step}}, t_{\text{diff}}, \xi_{i,1}, t, \xi_M^2) \end{aligned} \tag{7.39}$$

where t_{diff} is the differentiate step size.

To reduce the negative effect brought about by the fluctuations in the NN's output, the following observation introduction function is proposed to smoothly introduce the uncertainty estimations $\widehat{\varpi}_{i,p}$ and $\widehat{\varpi}_{i,a}$ into the low-level controller designs.

$$\bar{f}(t) = 1 - \frac{\exp(-\gamma_1(t-\gamma_2))}{1+\exp(-\gamma_1(t-\gamma_2))} \tag{7.40}$$

where γ_1 and γ_2 are both positive constants.

Hence, instead of using $\widehat{\varpi}_{i,p}$ and $\widehat{\varpi}_{i,a}$ directly, we have the following smoothed position controller and attitude controller:

$$u_{i,p}^s = \bar{u}_i - \bar{f}(t)\widehat{\varpi}_{i,p} - \lambda_i^p \delta_{vi,p} - k_i^p \delta_{xi,p} - c_i^p s_{i,p} + \bar{g}_p \tag{7.41}$$

Algorithm 4: Saturated and smoothed differentiator $\mathcal{D}(t_{\text{delay}}, t_{\text{diff}}, \xi_{\text{in}}^+, t, \xi_M)$

Input: t_{delay}, t_{diff}, ξ_{in}^+, t, ξ_M
Output: ξ_{out}^+
if $t \leq t_{\text{delay}}$ **then**
  $\xi_{\text{out}}^+ = [0, 0, 0]^{\text{T}}$;
else
  if $t \geq l_\xi t_{\text{diff}}$ **then**
    $\xi_{\text{out}}^+ = (\xi_{\text{in}}^+ - \xi_{\text{in}}^-)/t_{\text{diff}}$;
    $l_\xi = l_\xi + 1$;
  else
    $\xi_{\text{out}}^+ = \xi_{\text{out}}^-$;
  end
end
$\xi_{\text{out}}^- = \xi_{\text{out}}^+$;
$\xi_{\text{in}}^- = \xi_{\text{in}}^+$;
$\xi_{\text{out}}^+ = \mathcal{S}(\xi_{\text{out}}^+, \xi_M)$;
Return ξ_{out}^+ ;

$$u_{i,a}^s = \xi_{i,2} - \bar{f}(t)\widehat{w}_{i,a} - \lambda_i^a \widehat{\delta}_{vi,a} - k_i^a \delta_{xi,a} - c_i^a \widehat{s}_{i,a} \tag{7.42}$$

Ultimately, we have the following motion controller design:

$$\begin{aligned} T_i &= \frac{\bar{g}_p^{\text{T}} u_{i,p}^s}{g\cos(\phi_i)\cos(\theta_i)} \\ \tau_i &= g_{i,a}^{-1} u_{i,a} \end{aligned} \tag{7.43}$$

In all, the hierarchical formation controller is illustrated as Figure 7.1. Now the overall hierarchical design can be summarised as the following theorem:

Theorem 7.5. *Consider a group of UAVs* (7.7) *with a strongly connected communication topology, where Assumptions 7.1–7.3 are satisfied. By the high-level formation controller in* (7.18)*, the smoothed low-level position loop controller in* (7.41)*, the smoothed low-level attitude formation controller in* (7.42) *and the actual motion controller in* (7.43)*, the values of* $\|x_{i,p} - x_{i,p}^d\|$ *and* $\|\psi_i - \psi_i^d\|$ *are both semi-globally UUB if the compact set conditions of NNs hold when* $t \geq t_0$.

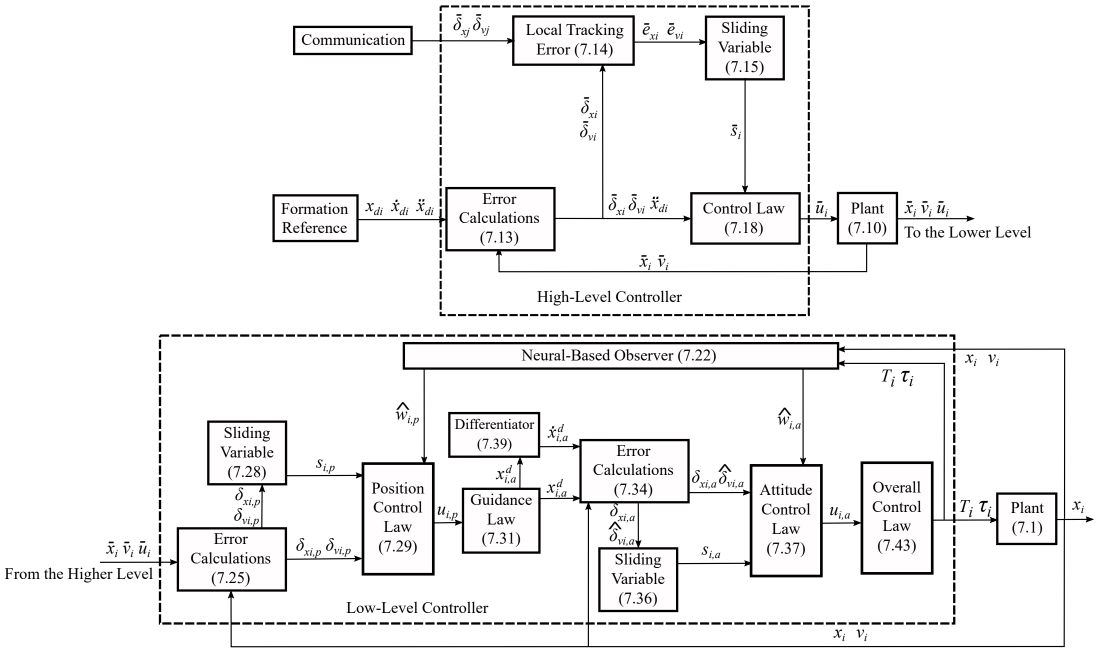

Figure 7.1. Hierarchical formation control scheme for multi-UAV clusters.

Proof. By Theorem 7.1, one has

$$\lim_{t\to+\infty}\|\bar{x}_i - x^d_{i,p}\| = 0,\ \lim_{t\to+\infty}\|\bar{v}_i - \dot{x}^d_{i,p}\| = 0,\ \lim_{t\to+\infty}\|\bar{v}_i - \ddot{x}^d_{i,p}\| = 0 \tag{7.44}$$

Since the value of the introduction function (7.40) will converge to 1 ultimately, the result and analysis related to Theorem 7.3 remain the same.

Although the smoothed design in Algorithm 4 will lead to differences between the set $\{\xi_{i,1}, \xi_{i,2}\}$ and $\{\dot{x}^d_{i,a}, \ddot{x}^d_{i,a}\}$, the difference should be small and bounded if the value of t_{diff} is chosen properly. Suppose we have $\|\xi_{i,1} - \dot{x}^d_{i,a}\| \leq \tilde{\xi}^1_M$ and $\|\xi_{i,2} - \ddot{x}^d_{i,a}\| \leq \tilde{\xi}^2_M$, similar to the proof of Theorem 7.4. We have that

$$\lim_{t\to+\infty}\|x_{i,a} - x^d_{i,a}\| \leq \frac{\widetilde{w}_M + (\lambda^a_i + c^a_i)\tilde{\xi}^1_M + \tilde{\xi}^2_M}{\underline{\sigma}(H_{6,3})} \tag{7.45}$$

where $\tilde{\xi}^1_M$ and $\tilde{\xi}^2_M$ are both small positive constants.

With the actual motion controller chosen as (7.43), we have that:

$$\lim_{t\to+\infty}\|x_{i,p} - \bar{x}_i\| \leq \frac{\widetilde{w}_M + (\lambda^a_i + c^a_i)\tilde{\xi}^1_M + \tilde{\xi}^2_M}{\underline{\sigma}(H_{6,3})}$$

$$\lim_{t\to+\infty}\|x_{i,a} - x^d_{i,a}\| \leq \frac{\widetilde{w}_M + (\lambda^a_i + c^a_i)\tilde{\xi}^1_M + \tilde{\xi}^2_M}{\underline{\sigma}(H_{6,3})}$$

which matches the goal of this section (7.8) and concludes the proof.

□

Table 7.2. UAV system parameters.

Robot number	1	2	3	4	5	6
m_i(kg)	2.08	2.10	2.11	2.10	2.09	2.12
R_i(m)	0.29	0.31	0.30	0.32	0.34	0.33
$J_{i,x}(\mathrm{Ns}^2/\mathrm{rad})$	1.25	1.23	1.24	1.23	1.24	1.25
$J_{i,y}(\mathrm{Ns}^2/\mathrm{rad})$	1.24	1.25	1.24	1.26	1.23	1.26
$J_{i,z}(\mathrm{Ns}^2/\mathrm{rad})$	2.50	2.52	2.51	2.49	2.50	2.53
$K_i(\mathrm{Ns}^2/\mathrm{rad})$	1.2×10^{-2}	1.3×10^{-2}	1.4×10^{-2}	1.1×10^{-2}	1.2×10^{-2}	1.3×10^{-2}
v_i	5.1×10^{-2}	5.2×10^{-2}	4.9×10^{-2}	5.1×10^{-2}	4.8×10^{-2}	5.3×10^{-2}

7.2.7 Simulation results and discussion

To justify the performance of the proposed hierarchical formation controller design, comparative simulations based on a multi-UAV system were conducted.

Consider a multi-UAV system that contains six heterogeneous UAVs whose dynamics are expressed as (7.1). The system's parameter values are given in Table 7.2, where we have $K_i = K_{i,x} = K_{i,y} = K_{i,z} = K_{i,\phi} = K_{i,\theta} = K_{i,\psi}$.

The gravity constant g was set to $g = 9.81$. The communication topology of the system was chosen as shown in Figure 7.2, and we used $b_i = 1$ for $i \in [1, 6]$.

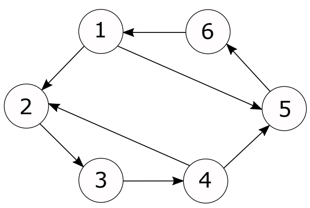

Figure 7.2. Communication topology of the multi-UAV cluster.

The initial states are chosen as $x_{1,p} = \hat{x}_{1,p} = \bar{x}_1 = [4, 1, 0]^{\mathrm{T}}$, $x_{2,p} = \hat{x}_{2,p} = \bar{x}_2 = [1, 2, 0]^{\mathrm{T}}$, $x_{3,p} = \hat{x}_{3,p} = \bar{x}_3 = [-2, -4, 0]^{\mathrm{T}}$, $x_{4,p} = \hat{x}_{4,p} = \bar{x}_4 = [-4, -1, 0]^{\mathrm{T}}$, $x_{5,p} = \hat{x}_{5,p} = \bar{x}_5 = [-1.5, -1, 0]^{\mathrm{T}}$ and $x_{6,p} = \hat{x}_{6,p} = \bar{x}_6 = [0, -1, 0]^{\mathrm{T}}$. All the other states were set as zero vectors or zero matrices when $t = 0$.

7.2.7 Simulation results and discussion

The position reference for the ith UAV was chosen as

$$x_{i,p}^{d} = \left[3\cos\left(\frac{2}{25}t + \frac{i-1}{3}\pi\right),\ 3\sin\left(\frac{2}{25}t + \frac{i-1}{3}\pi\right),\ \frac{1}{2} + \frac{3}{20}t\right]^{\mathrm{T}} \tag{7.46}$$

The reference of the yaw angle was chosen as $\psi_i^d = 0$. The system uncertainties were chosen as follows:

$$\bar{\varpi}_{i,p} = \left[\frac{3}{5}\sin\left(\frac{3}{10}t + \frac{i\pi}{6}\right),\ \frac{4}{5}\sin\left(\frac{1}{5}t + \frac{i\pi}{5}\right),\ \frac{9}{10}\sin\left(\frac{1}{5}t + \frac{i\pi}{4}\right)\right]^{\mathrm{T}}$$
$$\bar{\varpi}_{i,a} = \left[\frac{1}{10}\sin\left(\frac{1}{2}t - \frac{i\pi}{6}\right),\ \frac{2}{25}\sin\left(\frac{3}{5}t - \frac{i\pi}{5}\right),\ \frac{3}{50}\sin\left(\frac{2}{5}t - \frac{i\pi}{4}\right)\right]^{\mathrm{T}}$$

The parameters of the high level controller were chosen as $\bar{U}_{Mi} = 0.2$, $\bar{\tau}_e = 0.5$, $\bar{\psi}_e = 0.05$, $\bar{c}_i = 1$, $\bar{\lambda}_i = 2$, $\bar{k}_i = 1.5$, $\bar{\tau}_u = 0.19$ and $\bar{\psi}_u = 0.01$. To illustrate the effectiveness of the high-level formation controller (7.18), the norms of the high-level error-related vectors $\bar{\delta}_{xi}$ and $\bar{s}_i$ are given in Figures 7.3 and 7.4, respectively.

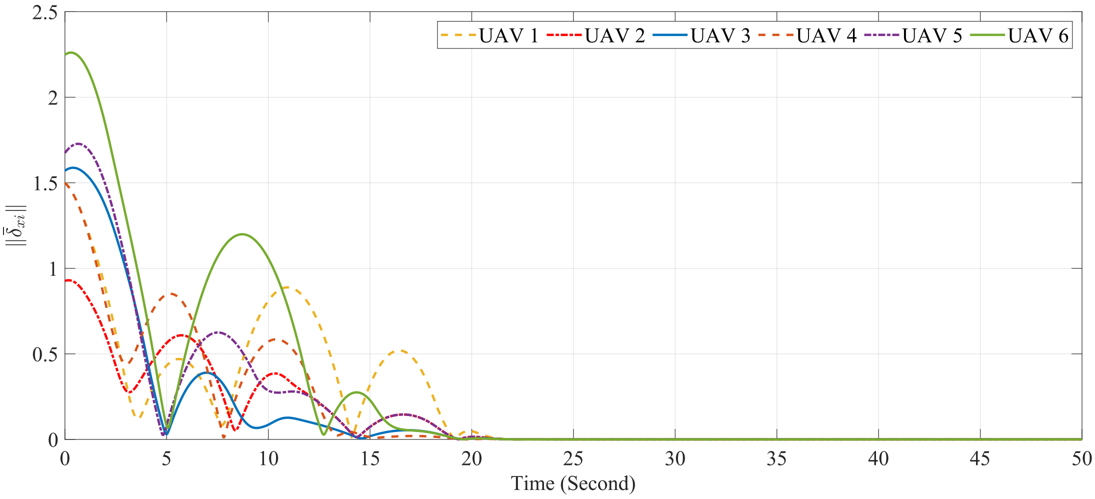

Figure 7.3. Norms of high-level tracking errors (Multi-UAV cluster).

Although the performance of the sliding mode controller (7.18) was affected by the saturation phenomenon (7.11) and obvious state overshoots can be noted, the uniform ultimate boundedness of both $\bar{\delta}_{xi}$ and $\bar{s}_i$ was still achieved simultaneously, which validates the results presented in Theorem 7.1.

The parameters of the neural-based observer were selected as $\widetilde{\lambda}_i = 2$, $\widetilde{c}_i = 4$, $\widetilde{k}_i = 4$, $\eta_1 = 20$ and $\eta_2 = 0.5$. Define $\|\widetilde{x}\|$, $\|\widetilde{s}\|$ and $\|\widetilde{d}\|$ as follows to represent the overall state

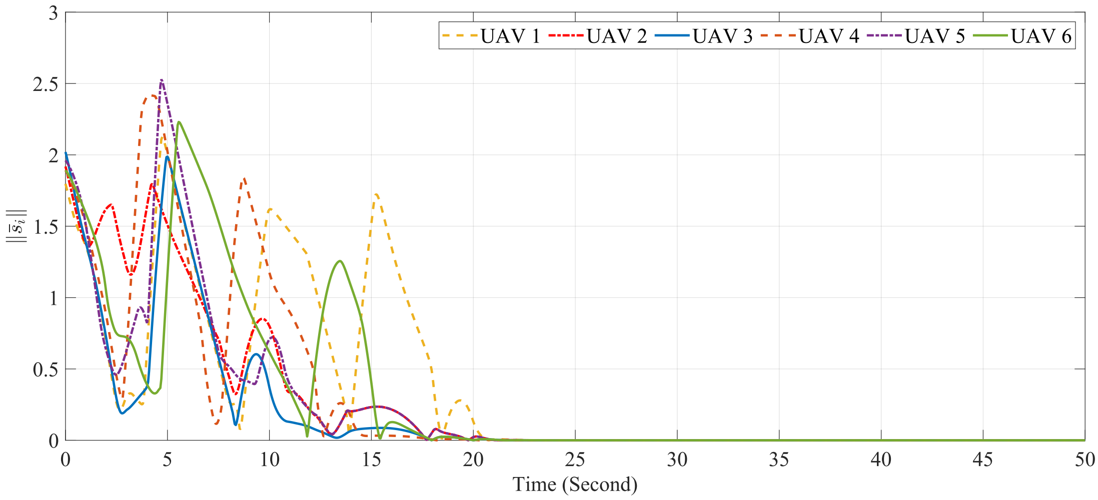

Figure 7.4. Norms of high-level sliding variables (Multi-UAV cluster).

observation error norm, overall observation sliding variable norm and uncertainty estimation error norm, respectively.

$$\|\tilde{x}\| = \sqrt{\sum_{i=i}^{N} \|\tilde{x}_i\|^2},\ \|\tilde{s}\| = \sqrt{\sum_{i=i}^{N} \|\tilde{s}_i\|^2},\ \|\tilde{w}\| = \sqrt{\sum_{i=i}^{N} \|\tilde{w}_i\|^2}$$

Then we have the values of $\|\tilde{x}\|$, $\|\tilde{s}\|$ and $\|\tilde{d}\|$ as shown in Figure 7.5, where it is found that all three norms are semi-globally UUB for 2×10^{-3}. Hence, Theorem 7.2 was verified. However, both overshooting and chattering were observed in the output of the neural-based observer within the first two seconds, which validates our motivation of employing the observation introduction function (7.40).

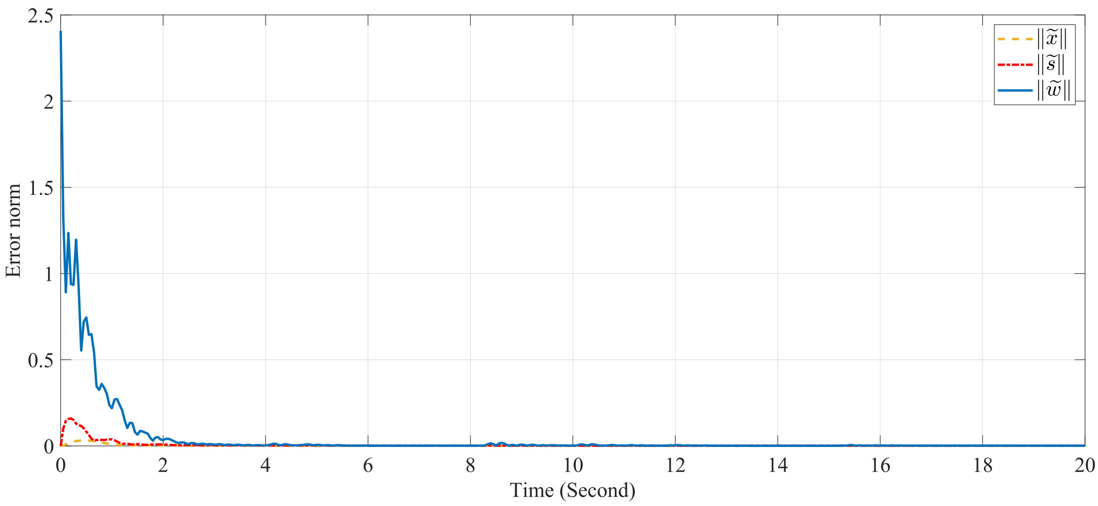

Figure 7.5. Effectiveness of the neural-based observer.

The parameters of the low-level position controller are chosen as $\lambda_i^p = 2$, $c_i^p = 2$ and $k_i^p = 2$. And the parameters of the low-level attitude controller are selected as $\lambda_i^a = 2$, $c_i^a = 4$ and $k_i^a = 4$. To illustrate the stability of our low-level controller design, we define error norm vectors $\|\delta_{x,a}\|$, $\|\delta_{x,p}\|$, $\|s_a\|$ and $\|s_p\|$ as follows:

$$\|\delta_{x,a}\| = \sqrt{\sum_{i=i}^{N} \|\delta_{xi,a}\|^2},\ \|\delta_{x,p}\| = \sqrt{\sum_{i=i}^{N} \|\delta_{xi,p}\|^2},\ \|s_a\| = \sqrt{\sum_{i=i}^{N} \|s_{i,a}\|^2},\ \|s_p\| = \sqrt{\sum_{i=i}^{N} \|s_{i,p}\|^2}$$

The trends of $\|\delta_{x,a}\|$, $\|\delta_{x,p}\|$, $\|s_a\|$ and $\|s_p\|$ are recorded in Figure 7.6, where they are semi-globally UUB for 4×10^{-4}, 7×10^{-4}, 3×10^{-4} and 1.5×10^{-3}. Hence, both Theorem 7.3 and 7.4 are valid.

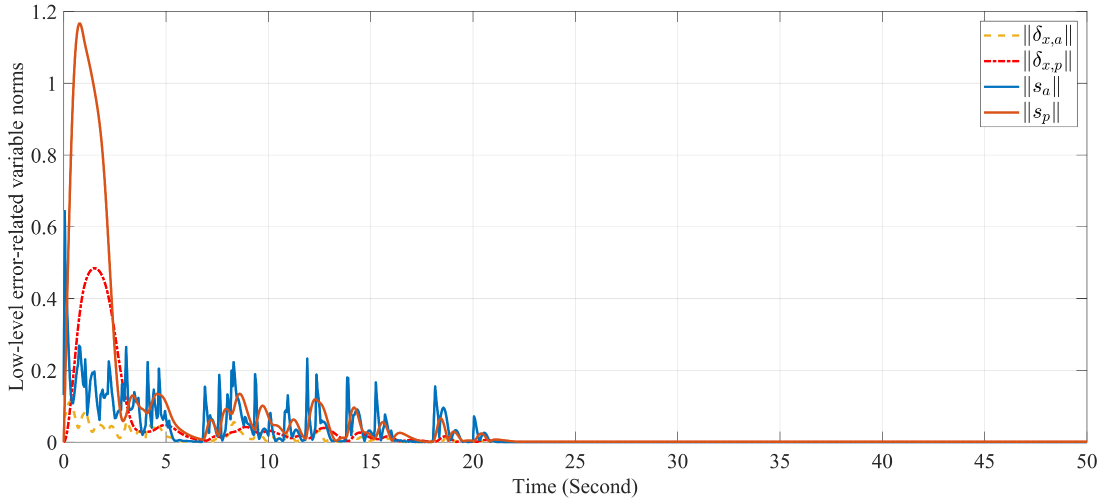

Figure 7.6. Effectiveness of the low-level controller (Multi-UAV cluster).

To prove that the observation introduction function (7.40)) and the saturated differentiator (Algorithm 4) help attenuate the chattering in the control input, the following two comparative simulations were conducted:

1. The original controller (TOC) where both (7.32) and (7.33) are employed to provide the derivatives of the attitude reference $x_{i,a}^d$. The derivatives are saturated with $\xi_{i,1} = \mathcal{S}(\xi_{i,1}, 0.2)$ and $\xi_{i,2} = \mathcal{S}(\xi_{i,2}, 0.1)$.

2. The smoothed controller (TSC) where the introduction function (7.40) is used with $\gamma_1 = 4$ and $\gamma_2 = 2$, and the attitude reference derivatives are obtained as

$$\xi_{i,1} = \mathcal{D}(t_{\text{step}}, 10t_{\text{step}}, x_{i,a}^d, t, 0.2),\ \xi_{i,2} = \mathcal{D}(2t_{\text{step}}, 10t_{\text{step}}, \xi_{i,1}, t, 0.1)$$

where the overall controller is chosen simultaneously with (7.43). Furthermore, we have the results shown in Figures 7.7 and 7.8.

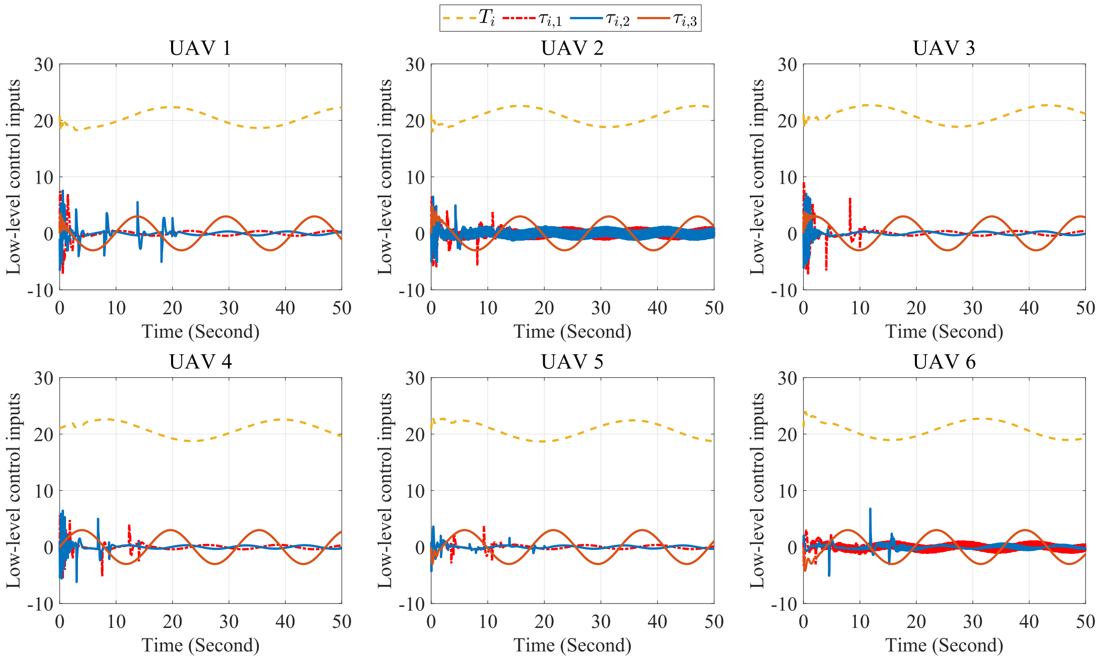

Figure 7.7. Control input of the TOC scheme.

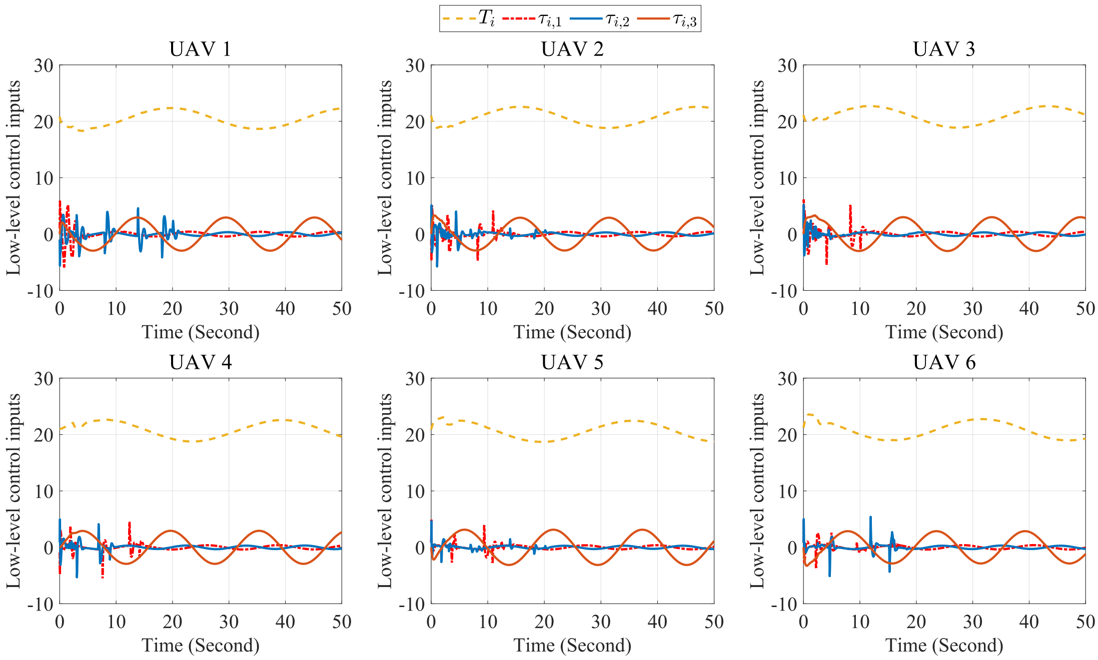

Figure 7.8. Control input of the TSC scheme.

As the introduction function (7.40) is not used in the TOC design, more chattering was observed in the control input for the first four seconds. Besides, the TSC design was found to have smoother control input ultimately (see UAVs two and six) due to the implementation of the smoothed differentiator (Algorithm 4). Therefore, the effectiveness of the TSC design and its superiority over the TOC design are both illustrated.

Finally, define $x_p^d = [x_{1,p}^d, x_{2,p}^d, \ldots, x_{N,p}^d]^{\mathrm{T}}$ and $x_p = [x_{1,p}, x_{2,p}, \ldots, x_{N,p}]^{\mathrm{T}}$ to represent the overall formation reference and the actual position of the multi-UAV system, respectively. Then we have the norm of the overall reference tracking error of the system with TSC design, as shown in Figure 7.9, where the semi-global uniform ultimate boundedness of $\|x_p - x_p^d\|$ proves the validity of Theorem 7.5.

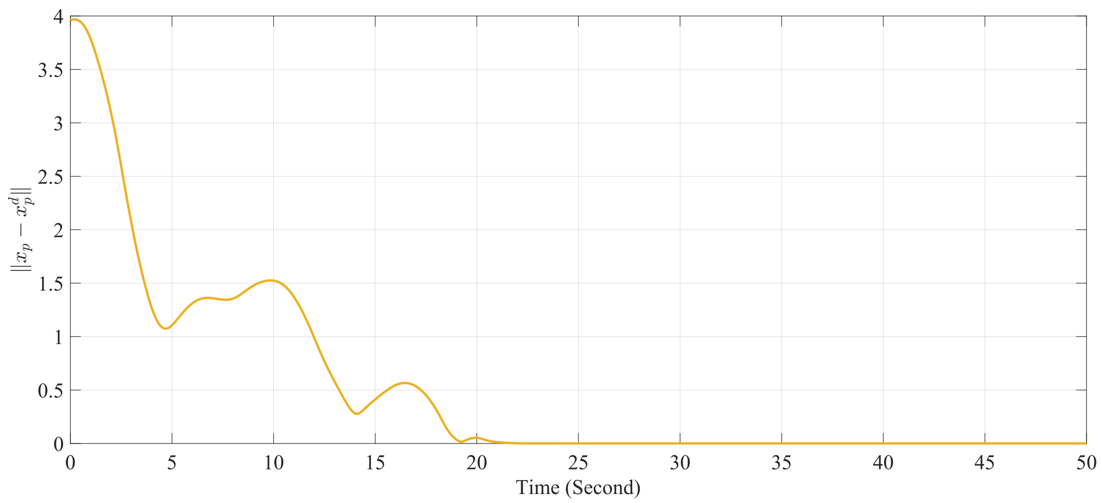

Figure 7.9. Norm of the overall reference tracking error.

The trajectories of all UAVs are given in Figure 7.10 to illustrate the movement and formation status of the entire system. According to (7.46), the desired formation is a rotating circle that keeps on elevating (see the dotted grey circle). In Figure 7.10, each UAV successfully reached its position reference within bounded error to form the desired formation, which illustrates the effectiveness of the proposed design structure in Figure 7.1. The angular status of each UAV is also given in Figure 7.11 to indicate that the saturation phenomenon employed in the higher level helps restrict the pitch and roll angle within $[-30°, 30°]$ to further reduce the aggressive motion of each UAV.

7.3 Hierarchical scheme for mixed-order vehicle clusters

In the previous section, although each UAV has heterogeneous dynamics because of the differences in the parameter values, all UAVs are modelled in a double-integrator

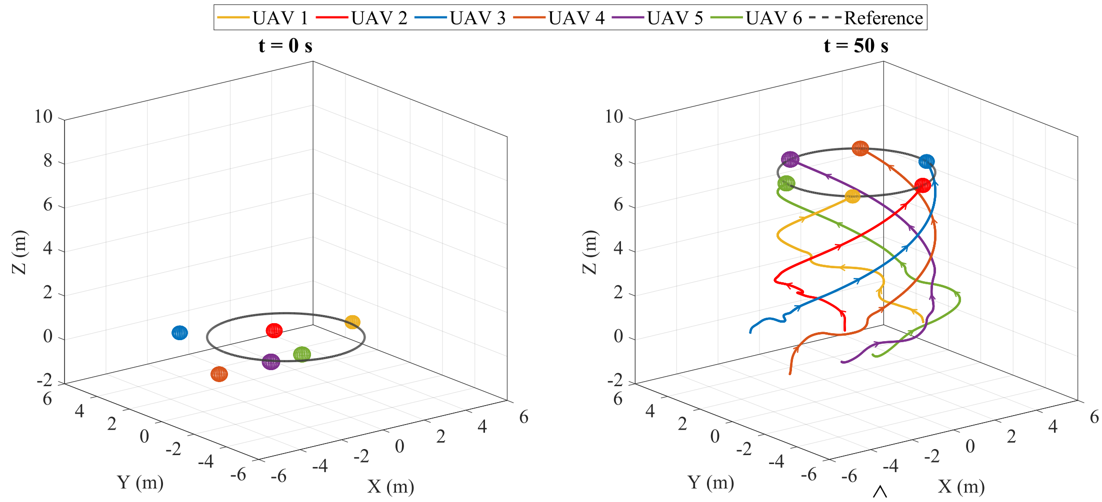

Figure 7.10. Illustration of system formation and individual trajectories (Multi-UAV cluster).

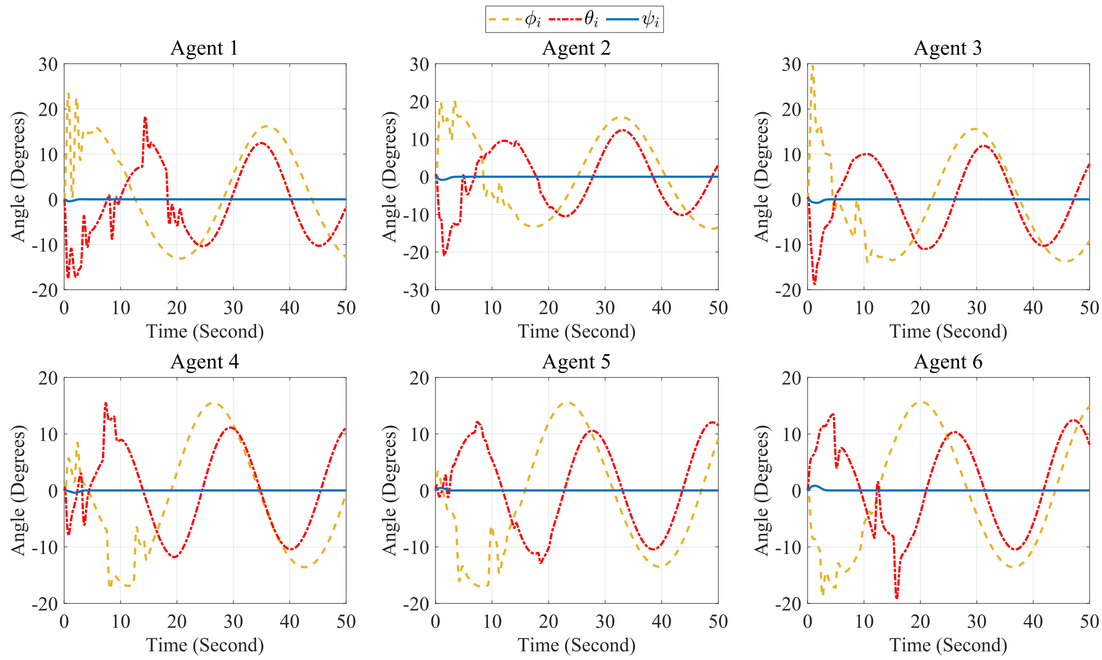

Figure 7.11. Trends of angular states.

structure. Therefore, it is essential to extend the formation control problem to a MAS that contains agents with different order dynamics (Li *et al.* 2019c) to increase the practicality of the control scheme.

7.3.1 System modelling and problem formulation

Consider a mixed-order MAS with $N(N \in \mathbb{R}^+)$ agents, where $N_1(N_1 \in \mathbb{R}^+)$ agents have first-order dynamics, and $N_2(N_2 \in \mathbb{R}^+)$ agents have second-order dynamics. The dynamics of a first-order agent is expressed as

$$\dot{x}_i = f_i + g_i u_i + \bar{w}_i, \quad i = 1, 2, \ldots, N_1 \tag{7.47}$$

and the dynamics of a second-order agent is written as

$$\begin{cases} \dot{x}_i = v_i \\ \dot{v}_i = f_i + g_i u_i + \bar{w}_i, \quad i = N_1 + 1, N_1 + 2, \ldots, N \end{cases} \tag{7.48}$$

where $x_i \in \mathbb{R}^n$ denotes the position information of the ith agent, $v_i \in \mathbb{R}^n$ denotes the velocity information of the ith second-order agent, $f_i \in \mathbb{R}^n$ is the unknown function in agent dynamics, $\bar{w}_i \in \mathbb{R}^n$ is the external disturbance, $g_i \in \mathbb{R}^{n\times n}$ is the known control gain matrix, $u_i \in \mathbb{R}^n$ represents the control input vector, and $N = N_1 + N_2$. If we have $w_i = f_i + \bar{w}_i$ to be the overall uncertainty for the system, an alternative expression for (7.47) is obtained as follows:

$$\dot{x}_i = g_i u_i + w_i, \quad i = 1, 2, \ldots, N_1 \tag{7.49}$$

Similarly, (7.48) is rewritten as

$$\begin{cases} \dot{x}_i = v_i \\ \dot{v}_i = g_i u_i + w_i, \quad i = N_1 + 1, N_1 + 2, \ldots, N \end{cases} \tag{7.50}$$

The position reference of the ith agent is denoted as $x_{di} \in \mathbb{R}^n$. The reference vector x_{di} and its time derivatives $\dot{x}_{di}$ and $\ddot{x}_{di}$ are all known to the ith agent. The goal of this section is to achieve the semi-global uniform ultimate boundedness of each agent's reference tracking error, which is abstracted as the following inequality:

$$\lim_{t\to\infty} ||x_i(t) - x_{di}(t)|| \leq \nu_\delta^s, \ \forall x_i(t_0) \in \Omega_x, \ i = 1, 2, \ldots, N \tag{7.51}$$

The communication graph of the mixed-order MAS is chosen as a strongly connected graph.

Assumption 7.4. *The state vectors x_i, v_i and w_i are all bounded. The formation reference x_{di} and its derivatives also remain bounded throughout the formation tracking process.*

7.3.2 Two-layer neural network design for mixed-order clusters

In this section, a two-layer NN is implemented to estimate the unknown function w_i for each individual agent:

$$w_i = W_i^{\mathrm{T}} \varphi_i + \epsilon_i,\ i = 1, 2, \ldots, N$$

where $\varphi_i \in \mathbb{R}^m$ is the input vector of the two-layer NN for the ith agent, m is a positive constant, $W_i \in \mathbb{R}^{m \times n}$ represents the optimal weight, and $\epsilon_i \in \mathbb{R}^n$ is the bounded network bias that satisfies $\|\epsilon_i\| \le \epsilon_M$, in which ϵ_M is a small positive number.

The input vector is chosen as $\varphi_i = x_i$ for the ith first-order agent, while it is set as $\varphi_i = [x_i^{\mathrm{T}}, v_i^{\mathrm{T}}]^{\mathrm{T}}$ for the ith second-order agent. The NN estimation $\widehat{w}_i$ is given as

$$\widehat{w}_i = \widehat{W}_i^{\mathrm{T}} \varphi_i \tag{7.52}$$

where $\widehat{W}_i$ is the estimated weight matrix.

Define $\widetilde{w}_i = w_i - \widehat{w}_i$ and $\widetilde{W}_i = W_i - \widehat{W}_i$. We have the following expression for the estimation error:

$$\widetilde{w}_i = \widetilde{W}_i^{\mathrm{T}} \varphi_i + \epsilon_i$$

Assumption 7.5. *The optimal weight W_i is bounded such that $\|W_i\|_F \le W_M$ for all $i \in [1, N]$.*

7.3.3 Dynamics mismatch in mixed-order multi-agent systems

In some previous works, an overall system dynamics is first constructed to obtain the error dynamics for the whole cluster to further carry out the controller design and its stability analysis (Fei *et al.* 2020, Li *et al.* 2019c, Li *et al.* 2022, Fei *et al.* 2021b). Taking the aforementioned mixed-order systems that contains both first-order agents (7.49) and second-order agents (7.50) as an example, we normally define the position tracking error of the ith agent as

$$\delta_{xi} = x_i - x_{di},\ i \in [1, N]$$

Due to the restrictions of the system model, the velocity tracking error is defined as follows:

$$\delta_{vi} = \begin{cases} 0_{n\times 1}, & i \in [1, N_1] \\ v_i - \dot{x}_{di}, & i \in [N_1 + 1, N] \end{cases}$$

Accordingly, the local formation tracking error e_{xi} and the local speed tracking error e_{vi} are given as follows:

$$\begin{cases} e_{xi} = \sum_{j=1}^{N} a_{ij}(\delta_{xi} - \delta_{xj}) + b_i\delta_{xi} = \sum_{j=1}^{N} l_{ij}\delta_{xj} + b_i\delta_{xi} \\ e_{vi} = \sum_{j=1}^{N} a_{ij}(\delta_{vi} - \delta_{vj}) + b_i\delta_{vi} = \sum_{j=1}^{N} l_{ij}\delta_{vj} + b_i\delta_{vi} \end{cases}$$

Such analysis is useful for systems that only contains agents with unified orders such as the second-order MASs (Fei *et al.* 2020, Fei *et al.* 2021b). However, the very basic and simple rules of $\dot{e}_{xi} = e_{vi}$ and $\dot{\delta}_{xi} = \delta_{vi}$ are in fact invalid for first-order agents in mixed-order systems, which further leads to the issue of variable mismatch.

Hence, instead of using the specific agent dynamics directly, we propose to first construct an extra virtual agent on top of each actual agent dynamics to further perform hierarchical control (Sharma *et al.* 2021). The virtual agents are treated as high-level reference generators for the actual agents, which are considered as low-level systems in the hierarchical design.

7.3.4 High-level design for mixed-order vehicle clusters

To ensure that the formation controller of each agent is offered with sufficient amount of state references, each high-level virtual agent is defined to have the homogeneous second-order dynamics as follows:

$$\begin{cases} \dot{\bar{x}}_i = \bar{v}_i \\ \dot{\bar{v}}_i = \bar{u}_i \end{cases} \tag{7.53}$$

where $\bar{x}_i \in \mathbb{R}^n$ and $\bar{v}_i \in \mathbb{R}^n$ are the position and velocity information of the virtual agent, respectively, and $\bar{u}_i \in \mathbb{R}^n$ is the control input of the virtual agent.

Define $\bar{x} = [\bar{x}_1^{\mathrm{T}}, \bar{x}_2^{\mathrm{T}}, \ldots, \bar{x}_N^{\mathrm{T}}]^{\mathrm{T}}$, $\bar{v} = [\bar{v}_1^{\mathrm{T}}, \bar{v}_2^{\mathrm{T}}, \ldots, \bar{v}_N^{\mathrm{T}}]^{\mathrm{T}}$ and $\bar{u} = [\bar{u}_1^{\mathrm{T}}, \bar{u}_2^{\mathrm{T}}, \ldots, \bar{u}_N^{\mathrm{T}}]^{\mathrm{T}}$, then the dynamics of the virtual cluster is given as

$$\begin{cases} \dot{\bar{x}} = \bar{v} \\ \dot{\bar{v}} = \bar{u} \end{cases} \tag{7.54}$$

Regarding the virtual system (7.53), the high-level position tracking error $\bar{\delta}_{xi}$ and velocity tracking error $\bar{\delta}_{vi}$ are defined as follows:

$$\begin{cases} \bar{\delta}_{xi} = \bar{x}_i - x_{di} \\ \bar{\delta}_{vi} = \bar{v}_i - \dot{x}_{di} \end{cases} \tag{7.55}$$

Accordingly, the tracking error dynamics of the ith virtual system is obtained as

$$\begin{cases} \dot{\bar{\delta}}_{xi} = \bar{\delta}_{vi} \\ \dot{\bar{\delta}}_{vi} = \bar{u}_i - \ddot{x}_{di} \end{cases}$$

Then we have the local formation tracking error $\bar{e}_{xi}$ and the local velocity tracking error $\bar{e}_{vi}$ for the ith virtual system (7.53) as follows, respectively:

$$\begin{cases} \bar{e}_{xi} = \sum_{j=1}^{N} a_{ij}(\bar{\delta}_{xi} - \bar{\delta}_{xj}) + b_i\bar{\delta}_{xi} = \sum_{j=1}^{N} l_{ij}\bar{\delta}_{xj} + b_i\bar{\delta}_{xi} \\ \bar{e}_{vi} = \sum_{j=1}^{N} a_{ij}(\bar{\delta}_{vi} - \bar{\delta}_{vj}) + b_i\bar{\delta}_{vi} = \sum_{j=1}^{N} l_{ij}\bar{\delta}_{vj} + b_i\bar{\delta}_{vi} \end{cases} \tag{7.56}$$

where b_i is the ith diagonal element of matrix B. Then we have the following cluster expression:

$$\begin{cases} \bar{e}_x = (L+B) \otimes I_n(\bar{x} - x_d) = (L+B) \otimes I_n\bar{\delta}_x \\ \bar{e}_v = (L+B) \otimes I_n(\bar{v} - \dot{x}_d) = (L+B) \otimes I_n\bar{\delta}_v \end{cases}$$

where $\bar{e}_x = [\bar{e}_{x1}^{\mathrm{T}}, \bar{e}_{x2}^{\mathrm{T}}, \ldots, \bar{e}_{xN}^{\mathrm{T}}]^{\mathrm{T}}$, $\bar{e}_v = [\bar{e}_{v1}^{\mathrm{T}}, \bar{e}_{v2}^{\mathrm{T}}, \ldots, \bar{e}_{vN}^{\mathrm{T}}]^{\mathrm{T}}$, $\bar{\delta}_x = [\bar{\delta}_{x1}^{\mathrm{T}}, \bar{\delta}_{x2}^{\mathrm{T}}, \ldots, \bar{\delta}_{xN}^{\mathrm{T}}]^{\mathrm{T}}$, $\bar{\delta}_v = [\bar{\delta}_{v1}^{\mathrm{T}}, \bar{\delta}_{v2}^{\mathrm{T}}, \ldots, \bar{\delta}_{vN}^{\mathrm{T}}]^{\mathrm{T}}$ and $x_d = [x_{d1}^{\mathrm{T}}, x_{d2}^{\mathrm{T}}, \ldots, x_{dN}^{\mathrm{T}}]^{\mathrm{T}}$ are applied.

Based on (7.13), we have the virtual sliding surface designed as follows:

$$\bar{s}_i = \bar{e}_{vi} + \bar{\lambda}_i\bar{e}_{xi} \tag{7.57}$$

where $\bar{\lambda}_i$ is a positive constant.

Define $\bar{S} = [\bar{s}_1^{\mathrm{T}}, \bar{s}_2^{\mathrm{T}}, \ldots, \bar{s}_N^{\mathrm{T}}]^{\mathrm{T}}$, then the cluster expression is as follows:

$$\bar{S} = (L+B) \otimes I_n(\bar{\delta}_v + \bar{\Lambda} \otimes I_n\bar{\delta}_x)$$

where $\bar{\Lambda} = \mathrm{diag}\{\bar{\lambda}_1, \bar{\lambda}_2, \ldots, \bar{\lambda}_N\}$.

The time derivative of $\bar{S}$ is given as

$$\dot{\bar{S}} = (L+B) \otimes I_n(\bar{u} - \ddot{x}_d + \bar{\Lambda} \otimes I_n\bar{\delta}_v)$$

Based on the discussions about the tracking error (7.13) and the sliding surface design (7.57) of the virtual system (7.53), we have the following high-level controller design:

$$\bar{u}_i = \ddot{x}_{di} - \bar{c}_i \bar{s}_i - \bar{\lambda}_i \bar{\delta}_{vi} - \bar{\delta}_{xi} \tag{7.58}$$

where $\bar{c}_i$ is a positive constant.

Now the result of the unified high-level controller design is given as the following theorem:

Theorem 7.6. *Consider the virtual cluster* (7.53) *where Assumption 7.4 holds, by the sliding surface design* (7.57) *and the sliding mode controller* (7.58)*, the sliding variable $\bar{S}$, the local formation tracking error $\bar{e}_x$ and the high-level reference tracking error $\bar{\delta}_x$ are all UUB.*

Proof. Consider a Lyapunov candidate as follows:

$$V_{6,3} = \frac{1}{2}\bar{S}^{\mathrm{T}} P \otimes I_n \bar{S} + \frac{1}{2}\bar{e}_x^{\mathrm{T}} P \otimes I_n \bar{e}_x$$

By Lemma 2.3, its time derivative is obtained as

$$\begin{aligned}
\dot{V}_{6,3} &= \bar{S}^{\mathrm{T}} P \otimes I_n \dot{\bar{S}} + \bar{e}_x^{\mathrm{T}} P \otimes I_n \dot{\bar{e}}_x \\
&= \bar{S}^{\mathrm{T}} (P(L+B)) \otimes I_n (\bar{u} - \ddot{x}_d + \bar{\Lambda} \otimes I_n \bar{\delta}_v) + \bar{e}_x^{\mathrm{T}} P \otimes I_n (\bar{S} - \bar{\Lambda} \otimes I_n \bar{e}_x) \\
&= -\frac{1}{2}\bar{S}^{\mathrm{T}} Q\bar{C} \otimes I_n \bar{S} - \bar{e}_x^{\mathrm{T}} (P\bar{\Lambda}) \otimes I_n \bar{e}_x \\
&\leq -\frac{1}{2}\underline{\sigma}(Q\bar{C})\|\bar{S}\|^2 - \underline{\sigma}(P\bar{\Lambda})\|\bar{e}_x\|^2
\end{aligned}$$

where $\bar{C} = \mathrm{diag}\{\bar{c}_1, \bar{c}_2, \ldots, \bar{c}_N\}$.

Hence, we get that $\dot{V}_1$ will remain negative until $\|\bar{S}\| = \|\bar{e}_x\| = 0$, which also leads to $\|\bar{\delta}_{xi}\| = 0$. By Lemma 3.1, we get that $\bar{S}$, $\bar{e}_x$ and $\bar{\delta}_{xi}$ are UUB, which completes the proof. □

7.3.5 Low-level design for mixed-order vehicle clusters

From the proof of Theorem 7.6, we see that the states of the virtual agents are expected to converge to the formation reference ultimately. Hence, it is reasonable to use the corresponding states of the virtual agents to act as the reference for the low-level controllers. The high level states $\bar{x}_i$, $\bar{v}_i$ and $\bar{u}_i$ will act as the position reference, velocity reference and acceleration reference for low-level systems, respectively.

Define δ_{xi} and δ_{vi} to be the low-level tracking errors as follows, respectively:

$$\begin{cases} \delta_{xi} = x_i - \bar{x}_i,\ i \in [1, N] \\ \delta_{vi} = v_i - \bar{v}_i,\ i \in [N_1 + 1, N] \end{cases} \tag{7.59}$$

Then the tracking error dynamics for first-order agents is written as

$$\dot{\delta}_{xi} = g_i u_i + w_i - \bar{v}_i,\ i \in [1, N_1]$$

Similarly, the tracking error dynamics for second-order agents is given as

$$\begin{cases} \dot{\delta}_{xi} = \delta_{vi} \\ \dot{\delta}_{vi} = g_i u_i + w_i - \bar{u}_i,\ i \in [N_1 + 1, N] \end{cases}$$

With the NN approximation (7.52), the neural-based controller for the ith first-order agent is expressed as

$$u_i = g_i^{-1}(-\widehat{w}_i + \bar{v}_i - k_i \delta_{xi}) \tag{7.60}$$

A fully error-related weight update law is chosen as follows:

$$\dot{\widehat{W}}_i = \eta_1 \varphi_i \delta_{xi}^{\mathrm{T}} - \eta_2 \|\delta_{xi}\| \widehat{W}_i \tag{7.61}$$

Now the result of the low-level controller design for first-order agents is summarised as the following theorem:

Theorem 7.7. *Consider the ith first-order agent* (7.49) *under Assumptions 7.4 and 7.5, by implementing the neural-based controller designs* (7.60) *and the weight tuning law* (7.61)*, the low-level position tracking error δ_{xi} and the weight estimation error $\widetilde{W}_i$ are semi-globally UUB if the compact set conditions for two-layer NNs are met for each first-order agent when $t \geq t_0$.*

Proof. Consider the following Lyapunov candidate for the ith first-order agent:

$$V_{6,4} = \frac{1}{2}\delta_{xi}^{\mathrm{T}}\delta_{xi} + \frac{1}{2\eta_1}\mathrm{tr}\{\widetilde{W}_i^{\mathrm{T}}\widetilde{W}_i\}$$

Then the time derivative of $V_{6,4}$ is obtained as

$$\begin{aligned} \dot{V}_{6,4} &= \delta_{xi}^{\mathrm{T}}\dot{\delta}_{xi} - \frac{1}{\eta_1}\mathrm{tr}\{\widetilde{W}_i^{\mathrm{T}}\dot{\widehat{W}}_i\} \\ &= \delta_{xi}^{\mathrm{T}}(\widetilde{W}_i^{\mathrm{T}}\varphi_i + \epsilon_i - k_i\delta_{xi}) - \mathrm{tr}\{\widetilde{W}_i^{\mathrm{T}}(\varphi_i\delta_{xi}^{\mathrm{T}} - \eta_2\|\delta_{xi}\|\widehat{W}_i/\eta_1)\} \\ &\leq -k_i\|\delta_{xi}\|^2 + \epsilon_M\|\delta_{xi}\| - \eta_2\|\delta_{xi}\|(\|\widetilde{W}_i\|_F^2 - \|\widetilde{W}_i\|_F W_M)/\eta_1 \end{aligned} \tag{7.62}$$

In the perspective of δ_{xi}, (7.62) is rewritten as

$$\begin{aligned}\dot{V}_{6,4} &\leq -\|\delta_{xi}\|(k_i\|\delta_{xi}\| - \epsilon_M + \eta_2(\|\widetilde{W}_i\|_F^2 - W_M/2)^2/\eta_1 - \eta_2 W_M^2/(4\eta_1)) \\ &\leq -\|\delta_{xi}\|(k_i\|\delta_{xi}\| - \epsilon_M - \eta_2 W_M^2/(4\eta_1))\end{aligned}$$

which indicates that $\dot{V}_{6,4}$ will remain negative when the following inequality is satisfied:

$$\|\delta_{xi}\| > \frac{4\eta_1\epsilon_M + \eta_2 W_M^2}{4k_i\eta_1}$$

By Lemma 2.1, δ_{xi} is proved to be semi-globally UUB within the following neighbourhood:

$$\Omega_\delta^f = \left\{\delta_{xi}\middle| \|\delta_{xi}\| \leq \frac{4\eta_1\epsilon_M + \eta_2 W_M^2}{4k_i\eta_1}\right\}$$

According to the extension of Lyapunov stability (Kim *et al.* 1997), $\|\widetilde{W}_i\|$ is also semi-globally UUB, which completes the proof. □

Regarding second-order agents, the following low-level sliding surface is designed based on the low-level tracking errors δ_{xi} and δ_{vi}:

$$s_i = \delta_{vi} + \lambda_i\delta_{xi} \tag{7.63}$$

where λ_i is a positive constant.

The time derivative of s_i is given as

$$\dot{s}_i = g_i u_i + w_i - \bar{u}_i + \lambda_i\delta_{vi}$$

Accordingly, the low-level neural-based formation controller design is obtained as follows:

$$u_i = g_i^{-1}(-\widehat{w}_i + \bar{u}_i - \lambda_i\delta_{vi} - \delta_{xi} - k_i s_i) \tag{7.64}$$

where the update law of the neural weight is chosen as

$$\dot{\widehat{W}}_i = \eta_1\varphi_i s_i^{\mathrm{T}} - \eta_2\|s_i\|\widehat{W}_i \tag{7.65}$$

Now the result of the low-level controller design for second-order agents is given as the following theorem:

Theorem 7.8. *Consider the ith second-order agent* (7.50) *under Assumptions 7.4 and 7.5, by implementing the neural-based controller designs* (7.64) *and the weight tuning law* (7.65)*, the low-level position tracking error δ_{xi}, the sliding variable s_i and the weight estimation error $\widetilde{W}_i$ are guaranteed to be semi-globally UUB if the compact set conditions for two-layer NNs are met when $t \geq t_0$.*

Proof. Consider the following Lyapunov candidate for the ith second-order agent:

$$V_{6,5} = \frac{1}{2}s_i^{\mathrm{T}}s_i + \frac{1}{2}\delta_{xi}^{\mathrm{T}}\delta_{xi} + \frac{1}{2\eta_1}\mathrm{tr}\{\widetilde{W}_i^{\mathrm{T}}\widetilde{W}_i\}$$

Similar to the proof of Theorem 7.7, the time derivative of $V_{6,5}$ is obtained as

$$\dot{V}_{6,5} \leq -\lambda_i\|\delta_{xi}\|^2 - k_i\|s_i\|^2 + \epsilon_M\|s_i\| - \eta_2\|s_i\|(\|\widetilde{W}_i\|_F^2 - \|\widetilde{W}_i\|_F W_M)/\eta_1$$

which further leads to the semi-globally UUB neighbourhood of $\|s_i\|$ as follows:

$$\Omega_s^s = \left\{ s_i \middle| \|s_i\| \leq \frac{4\eta_1\epsilon_M + \eta_2 W_M^2}{4k_i\eta_1} \right\}$$

In the perspective of δ_{xi}, the alternative form of $\dot{V}_{6,5}$ is given as

$$\dot{V}_{6,5} \leq -\lambda_i\|\delta_{xi}\|^2 + \|s_i\|(\epsilon_M + \eta_2 W_M^2/(4\eta_1))$$

Then we have the bounded region of δ_{xi} as follows:

$$\Omega_\delta^s = \left\{ \delta_{xi} \middle| \|\delta_{xi}\| \leq \frac{4\eta_1\epsilon_M + \eta_2 W_M^2}{4\sqrt{k_i\lambda_i}\eta_1} \right\}$$

By Lemma 2.1 and the Lyapunov stability extension mentioned (Kim *et al.* 1997), $\|\delta_{xi}\|$, $\|s_i\|$ and $\|\widetilde{W}_i\|$ are all semi-globally UUB, which completes the proof. □

7.3.6 Overall system stability analysis for mixed-order vehicle clusters

If we sum up Theorems 7.6-7.8, we obtain an overall hierarchical system design as shown in Figure 7.12.

With the results obtained in Theorems 7.6-7.8, we have the conclusion that both the high-level system and the low-level system are stabilised for an agent with arbitrary dynamics order. Now, we are ready to summarise our result of this section.

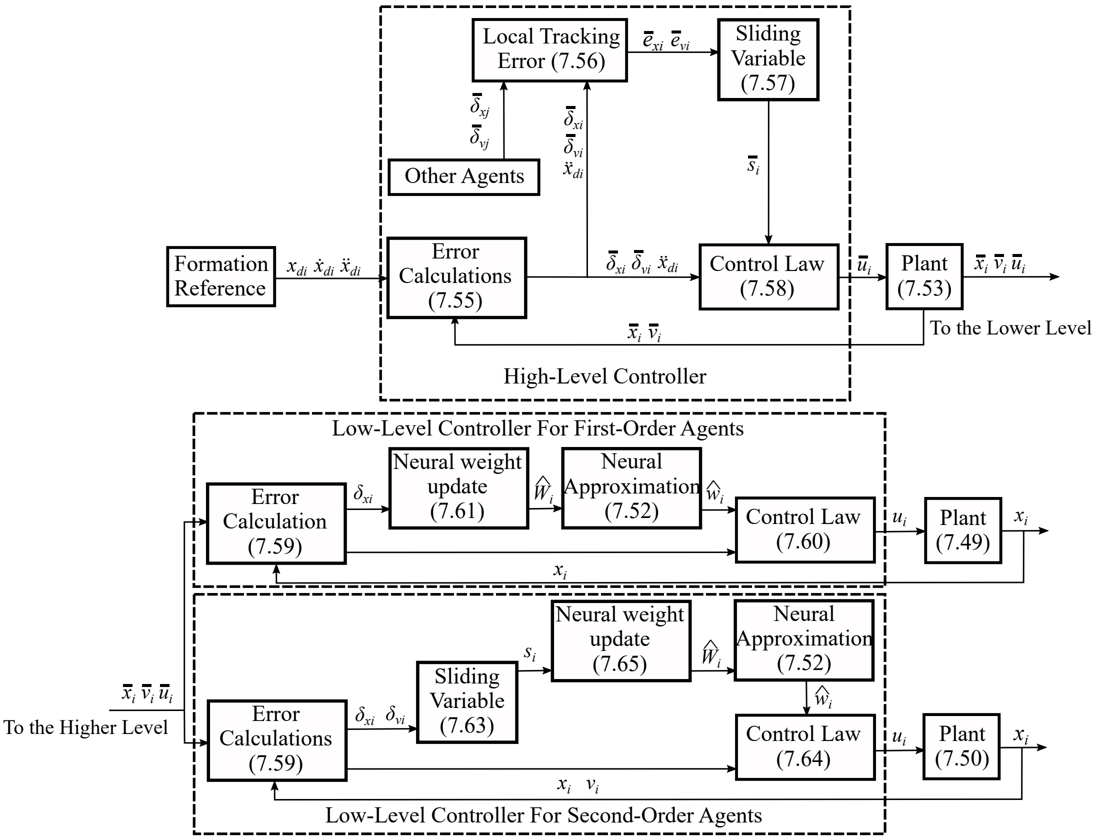

Figure 7.12. Hierarchical formation control scheme for mixed-order MASs.

Theorem 7.9. *Consider a mixed-order MAS with both first-order agents* (7.49) *and second-order agents* (7.50)*, where Assumptions 7.4 and 7.5 hold, by the high-level formation controller* (7.58)*, the reference tracking error norm* $\|x_i - x_{di}\|$ *is semi-globally UUB for the ith agent if*

1. *The low-level controller* (7.60) *is employed for first-order agents*
2. *The low-level controller* (7.64) *is applied for second-order agents*
3. *The compact set conditions of NNs hold when* $t \geq t_0$.

Proof. By Theorem 7.6, we have the following equation:

$$\lim_{t\to\infty} \|\bar{\delta}_{xi}(t)\| = \lim_{t\to\infty} \|\bar{x}_i(t) - x_{di}(t)\| = 0 \tag{7.66}$$

meaning that $\lim_{t\to\infty} \bar{x}_i(t) = x_{di}(t)$.

By Theorem 7.7, we have the following equation for first-order agents:

$$\lim_{t\to\infty} \|\delta_{xi}(t)\| = \lim_{t\to\infty} \|x_i(t) - \bar{x}_i(t)\| \leq \frac{4\eta_1\epsilon_M + \eta_2 W_M^2}{4k_i\eta_1}$$

With (7.66), it is guaranteed that

$$\lim_{t\to\infty} \|x_i(t) - x_{di}(t)\| \leq \frac{4\eta_1\epsilon_M + \eta_2 W_M^2}{4k_i\eta_1}$$

Similarly, the following result is obtained for second-order agents:

$$\lim_{t\to\infty} \|x_i(t) - x_{di}(t)\| \leq \frac{4\eta_1\epsilon_M + \eta_2 W_M^2}{4\sqrt{k_i\lambda_i}\eta_1}$$

By Lemma 2.1, we have that the reference tracking error norm $\|x_i - x_{di}\|$ is semi-globally UUB for both first-order agents and second-order agents, which completes the proof. □

7.3.7 Simulation results and discussion

To illustrate the effectiveness of our proposed hierarchical formation control design, a numerical simulation based on a multi-ODR system is conducted.

The rover cluster contains four ODRs, where two are set to perform motor speed control (first-order agents) and the others are set to perform motor force control (second-order agents). As mentioned in Chapter 2, the dynamics of the ith first-order ODR is set as

$$\dot{x}_i = T_f(\theta_1, R_i)u_i + w_i,\ i = 1, 2$$

where $x_i = [p_i^x, p_i^y, \theta_i]^{\mathrm{T}}$ denotes the position information of the rover, $u_i = [v_i^1, v_i^2, v_i^3]^{\mathrm{T}}$ is the speed vector of three motors, and R_i is the radius of the ith robot.

The dynamics of the ith second-order ODR is given as

$$\begin{cases} \dot{x}_i = v_i \\ \dot{v}_i = M_i T_s(\theta_i, R_i)u_i + w_i,\ i = 3, 4 \end{cases}$$

where v_i is the speed information of the ith rover, $M_i = \mathrm{diag}\{1/m_i, 1/m_i, 1/I_i\}$, m_i is the mass of the robot, I_i is the inertia of the robot, and $u_i = [F_i^1, F_i^2, F_i^3]^{\mathrm{T}}$ is the force vector of the three motors.

The parameters of the ODRs are chosen as $R_1 = 0.25\text{m}$, $R_2 = 0.22\text{m}$, $R_3 = 0.24\text{m}$, $R_4 = 0.28\text{m}$, $m_3 = 3.2\text{kg}$, $m_4 = 3.5\text{kg}$, $I_3 = 0.12\text{kg}\cdot\text{m}^2$ and $I_4 = 0.15\text{kg}\cdot\text{m}^2$. The formation reference for the ith ODR is chosen as follows:

$$x_{di} = \left[\frac{3}{2}\cos\left(\frac{t}{5}+\frac{i\pi}{2}\right)+\frac{t}{10}, \frac{3}{2}\sin\left(\frac{t}{5}+\frac{i\pi}{2}\right)+1, 0\right]^{\mathrm{T}} \tag{7.67}$$

The nonlinear uncertain term w_i is chosen as

$$\begin{aligned} w_i &= [0.1\sin(0.2t)+0.15\tanh(x), 0.15\sin(0.1t)-0.1e^{-|p_{yi}|-2}, 0.05\cos(\theta_1) \\ &\quad -0.1\sin(0.2t)]^{\mathrm{T}},\ i=1,2 \\ w_i &= [0.5\sin(0.4t)+\tanh(x), 0.3\sin(0.5t)-2e^{-|p_{yi}|-1}, 0.2\cos(\theta_1)+\sin(0.2t)]^{\mathrm{T}},\ i=3,4 \end{aligned}$$

By Theorem 7.6, the parameters in (7.58) are chosen as $\bar{c}_i = \bar{\lambda}_i = 2$. By Theorem 7.7 and Theorem 7.8, the parameter values in (7.60) and (7.64) are set as $k_i = \lambda_i = 2$. The weight tuning parameters in (7.61) and (7.65) are set as $\eta_1 = 15$ and $\eta_2 = 0.2$ simultaneously. The communication topology is chosen as the strongly connected directed graph that is shown in Figure 7.13.

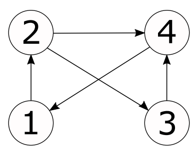

Figure 7.13. Communication topology (Mixed-order multi-ODR cluster).

The initial status of the virtual system and the actual system is set as

$$\begin{aligned} &\bar{x}_1(t_0) = x_1(t_0) = [0.8, 2.3, \pi/6]^{\mathrm{T}}, && \bar{x}_2(t_0) = x_2(t_0) = [-1, 0.5, -\pi/2]^{\mathrm{T}} \\ &\bar{x}_3(t_0) = x_3(t_0) = [-0.6, -1.2, \pi/3]^{\mathrm{T}}, && \bar{x}_4(t_0) = x_4(t_0) = [2.2, 1.5, -\pi/4]^{\mathrm{T}} \end{aligned}$$

To validate the high-level controller design (7.58), the values of $\|\bar{s}_i\|$ and $\|\bar{\delta}_{xi}\|$ are given in Figure 7.14, where the error-related vector norms are all UUB ($\|\bar{s}_i\| \le 6\times10^{-3}$ and $\|\bar{\delta}_{xi}\| \le 4\times10^{-2}$), which validates Theorem 7.6.

Regarding the low-level designs, the norms of δ_{xi} and s_i are given in Figure 7.15, where the boundedness of the vectors ($\|\delta_{xi}\| \le 2\times10^{-3}$ and $\|s_i\| \le 4\times10^{-3}$) are illustrated to further prove the effectiveness of the low-level control schemes mentioned in Theorem 7.7 and Theorem 7.8.

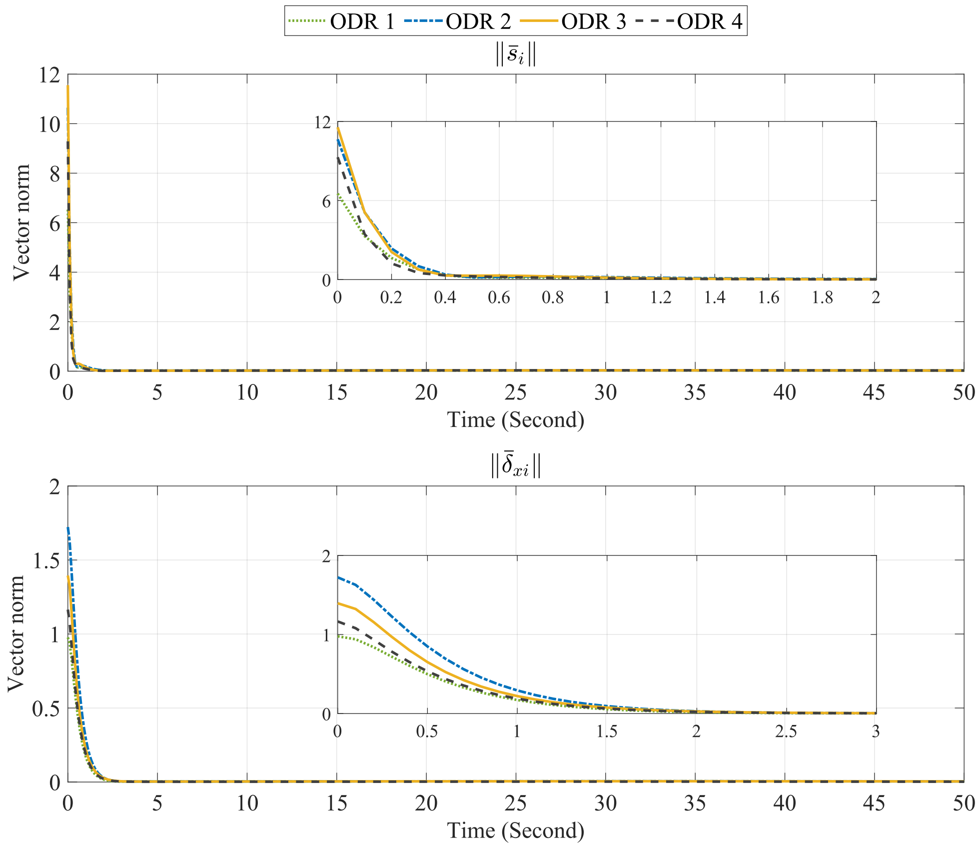

Figure 7.14. Performance of the high-level controller design (Mixed-order multi-ODR cluster).

To illustrate that the NN approximation scheme is valid, the norm of the estimation error of each ODR is recorded in Figure 7.16, where we have $\|\widetilde{w}_i\| \leq 10^{-2}$.

In terms of the overall system performance, the propagation of $\|\bar{\delta}_{xi} + \delta_{xi}\|$ is given in Figure 7.17, where we have $\|\delta_{xi} + \bar{\delta}_{xi}\| \leq 6 \times 10^{-3}$. Hence, we also have $\|x_i - x_{di}\| \leq 6 \times 10^{-3}$, which proves the semi-global boundedness of each ODR's tracking error, the achievement of the main goal in (7.51), and the validity of Theorem 7.9.

According to the formation reference given in (7.67), each ODR is observed to rotate around the centre that travels in a linear trajectory so that the entire system composites a circular formation (see the dash-dotted circle), which is illustrated in Figure 7.18.

7.4 Chapter summary

In this chapter, the hierarchical formation control design is discussed for both unified-order MASs and mixed-order MASs. Regarding the design for unified-order MASs, a

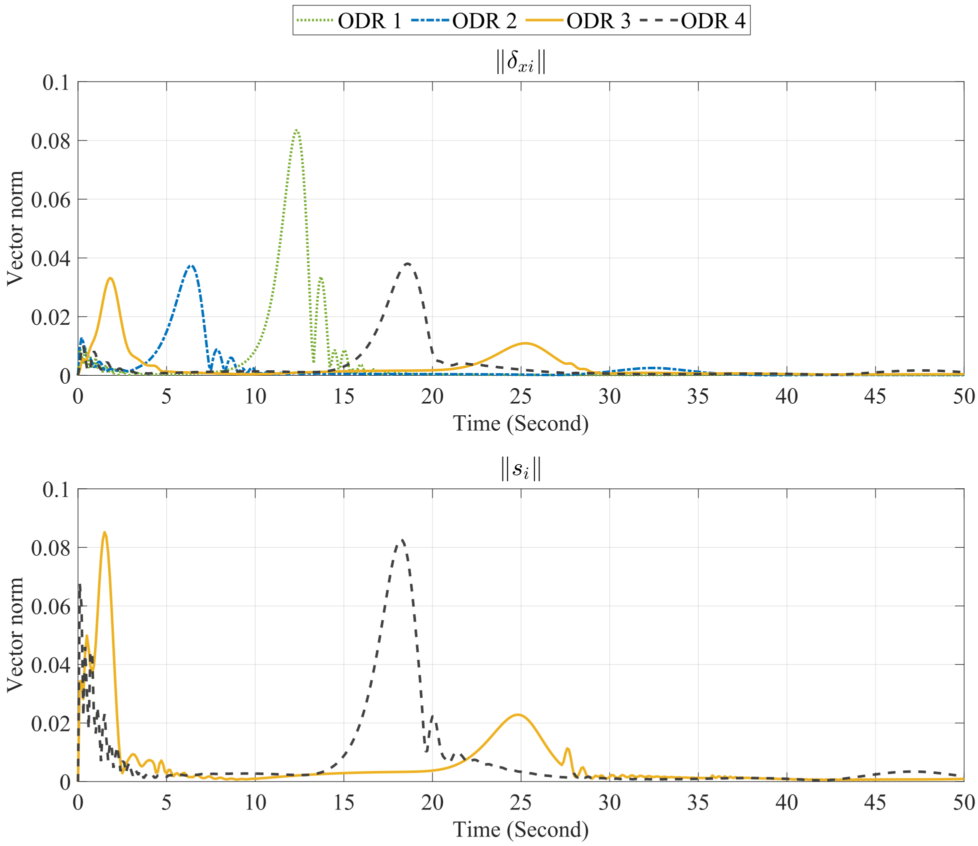

Figure 7.15. Performance of the low-level controller design (Mixed-order multi-ODR cluster).

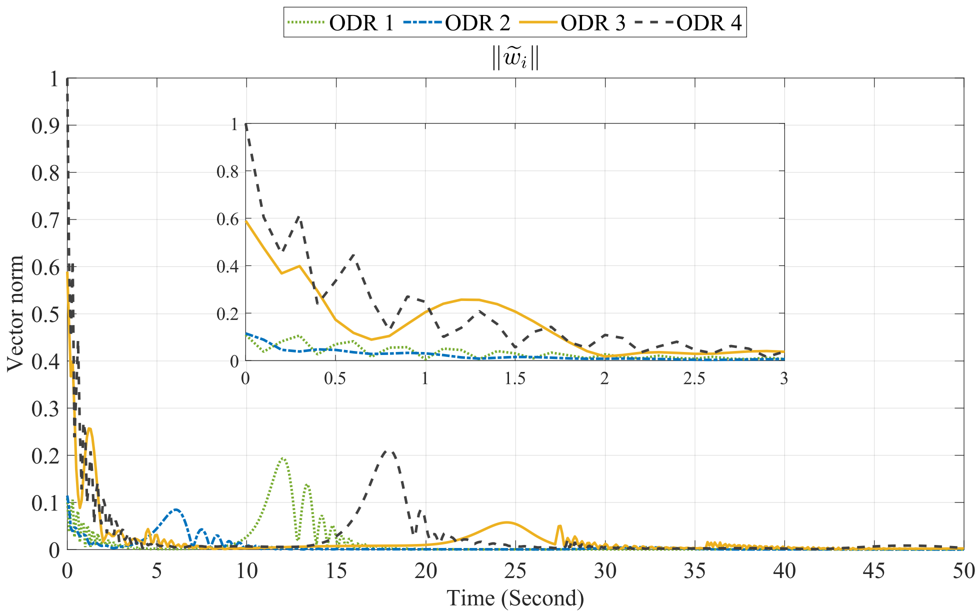

Figure 7.16. Performance of the NN-based estimation in the mixed-order vehicle cluster.

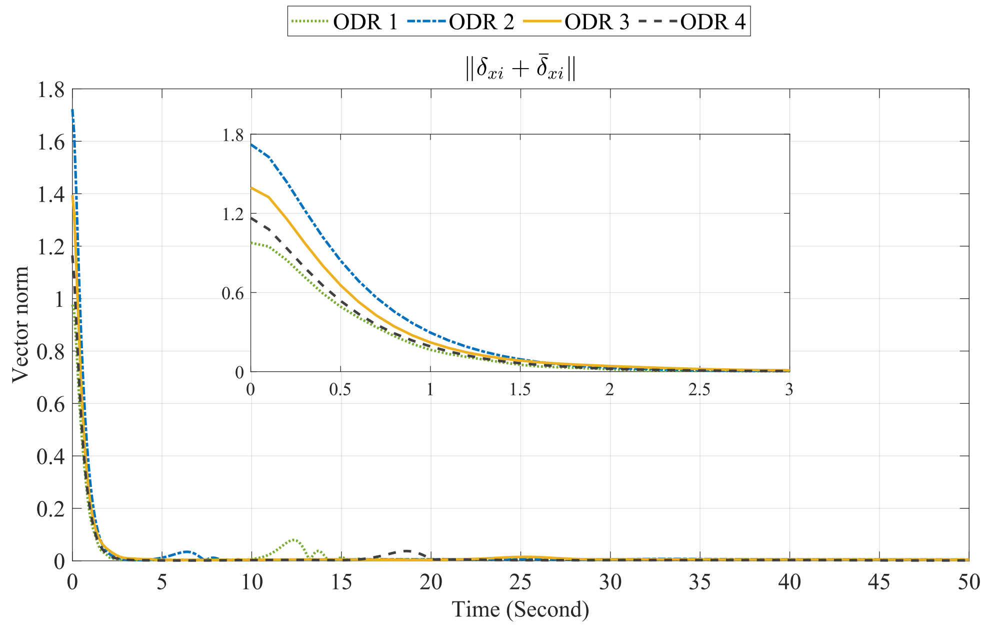

Figure 7.17. Overall tracking error of the mixed-order multi-ODR cluster.

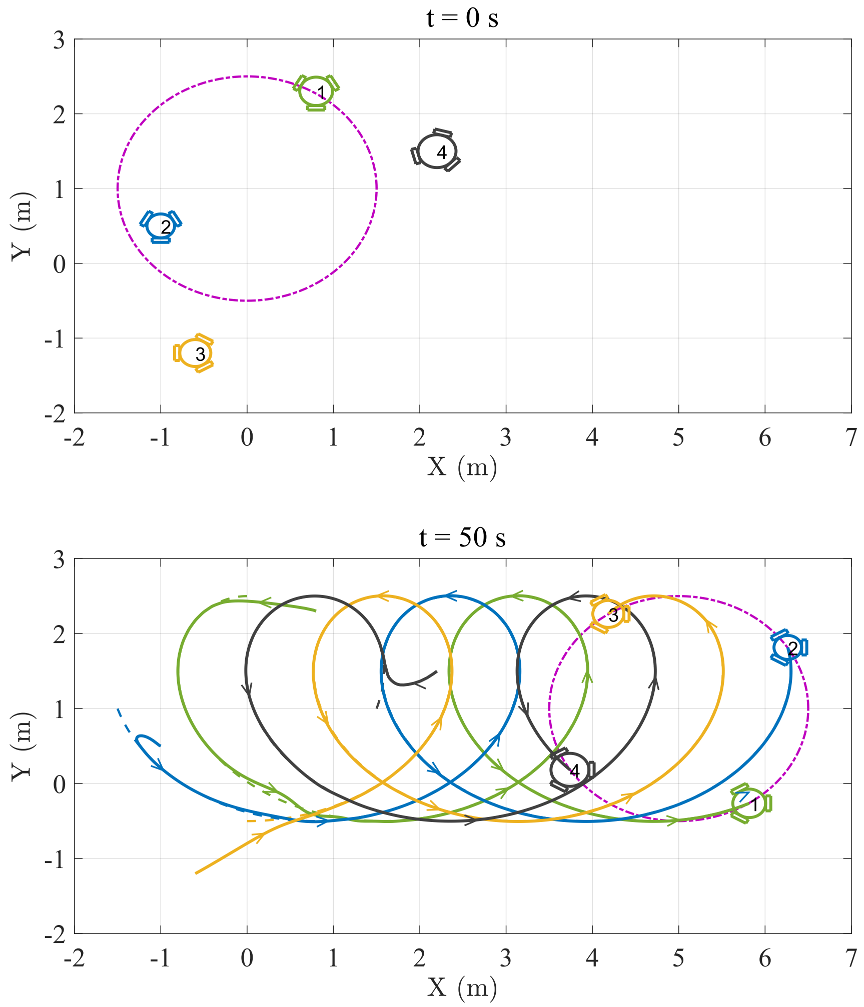

Figure 7.18. System formation status of mixed-order multi-ODR cluster.

neural-based sliding mode observer is proposed for both the position loop and the attitude loop of individual UAVs. To reduce the aggressive behaviours of the multi-UAV cluster, a saturation phenomenon is employed in the high-level formation controller design. An observer-based low-level formation controller is further constructed to ensure the robustness of the formation tracking process.

After expanding the formation control problem to mixed-order MASs, the dynamics mismatch issue is analysed. The cooperatively tuned NNs were then implemented to ensure the boundedness of the reference tracking errors of the MAS. The validity of both designs are both guaranteed by the Lyapunov stability theory, and further illustrated by simulations and corresponding comparisons.

In the next chapter, the conclusions of the thesis are drawn to illustrate the contributions and achievements included in the presented work.

Chapter 8

Conclusions and Future Work

THE research work presented in this thesis concentrates on the robust formation control issue of nonlinear multi-agent systems. The employed methods include sliding mode control, neural network adaptive control and observer-based control. Six general formation control scenarios are investigated and robust controllers are proposed to handle issues such as system uncertainty, actuator saturation, collision avoidance and dynamics mismatch. All methods have been validated by both the Lyapunov stability theory and simulation. In particular, the designs on first-order systems are also verified by physical experiments regarding a robot cluster. This chapter concludes this thesis and provides insights for the gaps that are worthy of investigation in the future.

8.1 Conclusions

8.1.1 Summary of technical chapters

This thesis discusses the development of the robust formation control schemes for nonlinear agent clusters. In Chapter 2, two dynamic sliding mode formation control schemes are proposed to offer unique perspectives in the control design, which offers the method of designing the changing rate of the control input rather than its actual value. Both Chebyshev neural networks and finite-time disturbance observers are proved to be helpful for maintaining the robustness of the dynamic sliding mode control scheme.

To further ensure the safety of the multi-agent systems, static obstacles are considered in Chapter 3, where the artificial potential fields are introduced to generate repulsive force that can drive the agents away from the obstacles. The effect of the distributed information sharing is also analysed to explain why some agents choose to move away from their desired trajectories while the other agents are trying to avoid the obstacles. To attenuate the aforementioned passive correcting behaviour, a reference correction algorithm is developed to modify the reference of each agent when it is unreachable.

In practice, most of the real-time networked multi-agent systems can only carry a limited amount of sensing equipment, which further leads to the issue that every agent can only access a limited amount of information about itself and the other agents around. The restriction on the information availability leads to two issues to solve in Chapter 4, which are the individual adaptive state estimation issue and the collision avoidance among agents. The first gap is filled by constructing a neural-based observer structure that could estimate the unknown agent velocity and disturbances simultaneously. Regarding the collision avoidance problem, the previous idea of building artificial potential fields between the agents that have direct communication is inadequate because those that are not connected in the static communication topology. Therefore, a distance-related time-varying communication topology (inspired by the Bluetooth technique) is introduced to ensure that each agent can exchange information with the ones that are nearby when necessary.

To enhance the practicality of the formation control scheme, the actuator saturation phenomenon is then considered for a cluster of nonlinear first-order agents in Chapter 5. A fully-error-related cooperative tuning method is first presented to avoid the divergence issue of the neural weight. To achieve finite-time neural-based estimation in a system with saturated control input, three-layer neural networks are then embedded into the observer structure. For the agents whose control gain matrix is not diagonal, the combined effect of input saturation and input coupling is analysed. A control input distribution function is then proposed to attenuate the state fluctuation lead by the reverse effect. To increase the practicality of the formation control scheme, the neural network structure is replaced by an adaptive term to obtain an observer with global stability. An adaptive auxiliary variable is then employed to compensate for the state oscillation caused by the reverse effect. To validate the effectiveness of the observer-based compensated formation control scheme, both numerical simulations and physical experiments based on a multi-robot cluster are conducted.

The investigation of the reverse effect is then expended to a cluster of nonlinear second-order agents in Chapter 6. A new structure that integrates the sliding mode control technique and the neural-based approximation approach is first developed to reduce the convergence time of the estimation error and increase the estimation precision. Finite-time sliding surface is then introduced to ensure that the estimation error is bounded within finite time. A nominal sliding mode formation control scheme is first developed on the basis of the auxiliary compensation approach mentioned in Chapter 5. A control input regulation algorithm is then developed by applying the linear programming approach to optimise the nominal control input to avoid the circumstances where the control input triggers the reverse effect.

Although the previous method of considering the communication in the motion control layer is commonly seen, it does introduce complexity and trouble into the stability analysis. In Chapter 7, a new hierarchical formation control structure is proposed for both unified-order multi-agent systems with complex motion dynamics (such as UAVs) and the ones that contain agents with different dynamics orders. A virtual layer is constructed to include the distributed information sharing and further takes the role of a cooperative path planner. The output of the virtual layer is then used as the reference signals for the motion control layer. Such structure is found to achieve a separation of concerns by dividing the inter-agent communication and the motion control into two subsystems.

8.1.2 Specific findings under particular technical topics

There are also some specific findings for several technical topics that are discussed throughout this thesis.

Neural networks in multi-agent systems

Two tuning approaches are investigated and discussed in this thesis, which are the cooperative tuning approach and the observer-based tuning method. Although the adaptive tuning approach (see Chapter 2) is a unique method in the multi-agent structure, it does introduce complex coupling between the inter-agent communication and the motion control process. Particularly when the actuators are restricted by the saturation phenomenon, the cooperative weight tuning law has high chance of introducing oscillations into the system because the saturated control input can not fully reflect the output of the neural network. Hence, such design is not suitable for practical scenarios (see Chapter 5).

On the other hand, the observer-based tuning approach is proved to be effective in both ideal (see Chapter 4) and practical (see Chapters 5 and 6) examples because it has the ability of working separately from the reference tracking process. Hence, employing the neural-based observer structure is more suitable in both theory and practice.

Collision avoidance in multi-agent systems

For an environment that contains static convex obstacles, although the artificial potential fields can help build up safety zones around the obstacles to avoid collision, the local minima issue still remains. The approach of reference adjusting is found to be effective to both reduce the corresponding negative effect and attenuate the passive corrections (see Chapter 3).

Apart from that, static communication topology is found to be insufficient for sharing the essential information involved in the construction of artificial potential fields among agents. One possible approach is to equip agents with range-based communication technique so that they are aware of the information of the agents that have the potential of colliding into (see Chapter 4).

To sum up, the artificial potential field approach is found to be effective for both static and dynamic obstacles if the following two preliminary conditions are met:

1. Each obstacle is convex and could be included in circle or sphere with a fixed radius.

2. The position of each obstacle is known before the construction or update of the artificial potential field.

However, this method is not yet perfect. Its performance when the system is affected by actuator saturation and the local minima issue are issues worthy of investigation, which will be further summarised in the future work.

Actuator saturation in nonlinear systems

There are more issues to consider other than restricting the amplitudes of the control input for nonlinear systems. To start with, any integration process that are included in the position tracking procedure will lead to the famous windup phenomenon. As mentioned in Chapter 6, the windup issue exists for both first-order systems with integration-based control methods (such as the proportional-integral-derivative approach) and higher-order systems. One convenient way is to employ the auxiliary compensation term.

Apart from the windup issue, the reverse effect also exists in systems with coupled and saturated input. To attenuate the corresponding state oscillation, the methods of control input shrinking (see Chapter 5) and linear-programming-based regulation (see Chapter 6) are found to be effective. In comparison, the linear programming approach is found to have better attenuating performance for the reverse effect by minimising the difference between the control performance of the actual control input with the one of the nominal control input.

8.2 Future work

Although plenty of research works have been conducted in the field of multi-agent systems and formation control, there are still some possible gaps to work on in the future, which includes the following aspects.

Mixed-order multi-agent systems

Currently, most of the research works in the area of multi-agent system are based on cluster of agents with unified orders (Fei *et al.* 2021a), which leaves gaps in the study for mixed-order multi-agent systems (Li *et al.* 2022). As mentioned in Chapter 7, analysing the stability of a mixed-order multi-agent system by using a cluster dynamics is not a suitable choice because of the dynamics mismatch issue. Apart from the hierarchical structure presented in Chapter 7, are there any other techniques to solve this issue? Besides, how to employ the event trigger technique to ease the burden in computation and communication in a mixed-order multi-agent structure is also a considerable challenge.

Real-time collision avoidance in practice

Although the collision avoidance issue is discussed in both this thesis (see Chapters 3 and 4) and many research articles (Lee *et al.* 2021, Sharma *et al.* 2021), most of the results are obtained on the basis of ideal actuators that operate without actuator saturation. Besides, most works are carried out in either path planning (Lee *et al.* 2021) or motion control (Sharma *et al.* 2021). Therefore, will the system perform better when collision avoidance algorithms are added in both the path planning layer and the motion control layer?

The local minima issue has remain an open issue for the artificial potential field construction. In practice, not all obstacles are convex, which may trap the robots that enters. Hence, how to build up a memory-based guidance law for the robots to lead themselves out of the local minima issue is a problem worthy of discussion.

Distributed multi-agent learning and optimal control

Machine learning is one popular topic in the recent decade. Although this technique can help achieve the optimal results, it does require massive calculation power because of the many essential iterations to minimise the costs or maximise the rewards. Hence, if an arbitrary task is given for a cluster of intelligent agents, how can they find out the optimal and consensus solution within a short period of time is a challenge to overcome. Also, should the agents just share the raw training data or the trained parameter values?

Bibliography

ANDERSON-B. D., YU-C., FIDAN-B., AND HENDRICKX-J. M. (2008). Rigid graph control architectures for autonomous formations, *IEEE Control Systems Magazine*, **28**(6), pp. 48–63.

BAI-W., ZHOU-Q., LI-T., AND LI-H. (2019). Adaptive reinforcement learning neural network control for uncertain nonlinear system with input saturation, *IEEE Transactions on Cybernetics*, **50**(8), pp. 3433–3443.

BALCH-T., AND ARKIN-R. C. (1998). Behavior-based formation control for multirobot teams, *IEEE Transactions on Robotics and Automation*, **14**(6), pp. 926–939.

BOHN-C., AND ATHERTON-D. (1995). An analysis package comparing pid anti-windup strategies, *IEEE Control Systems Magazine*, **15**(2), pp. 34–40.

CHALANGA-A., KAMAL-S., FRIDMAN-L. M., BANDYOPADHYAY-B., AND MORENO-J. A. (2016). Implementation of super-twisting control: Super-twisting and higher order sliding-mode observer-based approaches, *IEEE Transactions on Industrial Electronics*, **63**(6), pp. 3677–3685.

CHEN-B., AND CHENG-H. H. (2010). A review of the applications of agent technology in traffic and transportation systems, *IEEE Transactions on Intelligent Transportation Systems*, **11**(2), pp. 485–497.

CHEN-B., ZHANG-H., LIU-X., AND LIN-C. (2017). Neural observer and adaptive neural control design for a class of nonlinear systems, *IEEE Transactions on Neural Networks and Learning Systems*, **29**(9), pp. 4261–4271.

CHEN-J., LI-J., ZHANG-R., AND WEI-C. (2019). Distributed fuzzy consensus of uncertain topology structure multi-agent systems with non-identical partially unknown control directions, *Applied Mathematics and Computation*, **362**, p. 124581.

CHEN-K., WANG-J., ZHANG-Y., AND LIU-Z. (2016). Adaptive consensus of nonlinear multi-agent systems with unknown backlash-like hysteresis, *Neurocomputing*, **175**, pp. 698–703.

CHEN-W.-H., YANG-J., GUO-L., AND LI-S. (2015). Disturbance-observer-based control and related methods—An overview, *IEEE Transactions on Industrial Electronics*, **63**(2), pp. 1083–1095.

CHEN-Y., AND SUN-J. (2016). Distributed optimal control for multi-agent systems with obstacle avoidance, *Neurocomputing*, **173**, pp. 2014–2021.

CHEN-Y. Q., AND WANG-Z. (2005). Formation control: a review and a new consideration, *2005 IEEE/RSJ International Conference on Intelligent Robots and Systems*, IEEE, pp. 3181–3186.

CHOY-M. C., SRINIVASAN-D., AND CHEU-R. L. (2003). Cooperative, hybrid agent architecture for real-time traffic signal control, *IEEE Transactions on Systems, Man, and Cybernetics-Part A: Systems and Humans*, **33**(5), pp. 597–607.

CHU-Y., FEI-J., AND HOU-S. (2019). Adaptive global sliding-mode control for dynamic systems using double hidden layer recurrent neural network structure, *IEEE Transactions on Neural Networks and Learning Systems*, **31**(4), pp. 1297–1309.

CUI-R., ZHANG-X., AND CUI-D. (2016). Adaptive sliding-mode attitude control for autonomous underwater vehicles with input nonlinearities, *Ocean Engineering*, **123**, pp. 45–54.

DAI-L., CAO-Q., XIA-Y., AND GAO-Y. (2017). Distributed MPC for formation of multi-agent systems with collision avoidance and obstacle avoidance, *Journal of the Franklin Institute*, **354**(4), pp. 2068–2085.

DING-S., AND ZHENG-W. X. (2015). Robust control of multiple integrators subject to input saturation and disturbance, *International Journal of Control*, **88**(4), pp. 844–856.

DING-S., AND ZHENG-W. X. (2016). Nonsingular terminal sliding mode control of nonlinear second-order systems with input saturation, *International Journal of Robust and Nonlinear Control*, **26**(9), pp. 1857–1872.

DINH-V.-T., NGUYEN-H., SHIN-S.-M., KIM-H.-K., KIM-S.-B., AND BYUN-G.-S. (2012). Tracking control of omnidirectional mobile platform with disturbance using differential sliding mode controller, *International Journal of Precision Engineering and Manufacturing*, **13**(1), pp. 39–48.

DONG-X., HUA-Y., ZHOU-Y., REN-Z., AND ZHONG-Y. (2018). Theory and experiment on formation-containment control of multiple multirotor unmanned aerial vehicle systems, *IEEE Transactions on Automation Science and Engineering*, **16**(1), pp. 229–240.

DONG-X., ZHOU-Y., REN-Z., AND ZHONG-Y. (2016). Time-varying formation tracking for second-order multi-agent systems subjected to switching topologies with application to quadrotor formation flying, *IEEE Transactions on Industrial Electronics*, **64**(6), pp. 5014–5024.

DOU-L., SU-X., ZHAO-X., ZONG-Q., AND HE-L. (2021). Robust tracking control of quadrotor via on-policy adaptive dynamic programming, *International Journal of Robust and Nonlinear Control*, **31**(7), pp. 2509–2525.

DU-H., ZHU-W., WEN-G., AND WU-D. (2017). Finite-time formation control for a group of quadrotor aircraft, *Aerospace Science and Technology*, **69**, pp. 609–616.

ELHAKI-O., AND SHOJAEI-K. (2018). Neural network-based target tracking control of underactuated autonomous underwater vehicles with a prescribed performance, *Ocean Engineering*, **167**, pp. 239–256.

FEI-Y., SHI-P., AND LIM-C.-C. (2020). Neural network adaptive dynamic sliding mode formation control of multi-agent systems, *International Journal of Systems Science*, **51**(11), pp. 2025–2040.

FEI-Y., SHI-P., AND LIM-C.-C. (2021a). Robust and collision-free formation control of multiagent systems with limited information, *IEEE Transactions on Neural Networks and Learning Systems*. doi: 10.1109/TNNLS.2021.3112679.

FEI-Y., SHI-P., AND LIM-C.-C. (2021b). Robust formation control for multi-agent systems: A reference correction based approach, *IEEE Transactions on Circuits and Systems I: Regular Papers*, **68**(6), pp. 2616–2625.

FEI-Y., SHI-P., AND LIM-C.-C. (2022a). Neural-based formation control of uncertain multi-agent systems with actuator saturation, *Nonlinear Dynamics*, **108**, pp. 3693–3709.

FEI-Y., SUN-Y., AND SHI-P. (2022b). Robust hierarchical formation control of unmanned aerial vehicles via neural-based observers, *Drones*, **6**(2), p. 40.

FENG-Y., YU-X., AND HAN-F. (2013). On nonsingular terminal sliding-mode control of nonlinear systems, *Automatica*, **49**(6), pp. 1715–1722.

FU-M., AND YU-L. (2018). Finite-time extended state observer-based distributed formation control for marine surface vehicles with input saturation and disturbances, *Ocean Engineering*, **159**, pp. 219–227.

GAMBUZZA-L. V., AND FRASCA-M. (2020). Distributed control of multiconsensus, *IEEE Transactions on Automatic Control*, **66**(5), pp. 2032–2044.

GAO-W., AND SELMIC-R. R. (2006). Neural network control of a class of nonlinear systems with actuator saturation, *IEEE Transactions on Neural Networks*, **17**(1), pp. 147–156.

GE-S. S., HANG-C. C., LEE-T. H., AND ZHANG-T. (2013). *Stable adaptive neural network control*, Vol. 13, Springer Science & Business Media.

HAN-J.-S., KIM-T.-I., OH-T.-H., AND LEE-S.-H. (2019). Effective disturbance compensation method under control saturation in discrete-time sliding mode control, *IEEE Transactions on Industrial Electronics*, **67**(7), pp. 5696–5707.

HAN-T., GUAN-Z.-H., CHI-M., HU-B., LI-T., AND ZHANG-X.-H. (2017). Multi-formation control of nonlinear leader-following multi-agent systems, *ISA Transactions*, **69**, pp. 140–147.

HORN-R. A., HORN-R. A., AND JOHNSON-C. R. (1994). *Topics in matrix analysis*, Cambridge University Press.

HOU-Z.-S., AND WANG-Z. (2013). From model-based control to data-driven control: Survey, classification and perspective, *Information Sciences*, **235**, pp. 3–35.

HUANG-X., ZHANG-C., LU-H., AND LI-M. (2016). Adaptive reaching law based sliding mode control for electromagnetic formation flight with input saturation, *Journal of the Franklin Institute*, **353**(11), pp. 2398–2417.

HU-Q., AND JIANG-B. (2017). Continuous finite-time attitude control for rigid spacecraft based on angular velocity observer, *IEEE Transactions on Aerospace and Electronic Systems*, **54**(3), pp. 1082–1092.

KANG-W., AND YEH-H.-H. (2002). Co-ordinated attitude control of multi-satellite systems, *International Journal of Robust and Nonlinear Control: IFAC-Affiliated Journal*, **12**(2-3), pp. 185–205.

KIM-Y. H., AND LEWIS-F. L. (1999). Neural network output feedback control of robot manipulators, *IEEE Transactions on Robotics and Automation*, **15**(2), pp. 301–309.

KIM-Y. H., LEWIS-F. L., AND ABDALLAH-C. T. (1997). A dynamic recurrent neural-network-based adaptive observer for a class of nonlinear systems, *Automatica*, **33**(8), pp. 1539–1543.

KUSHLEYEV-A., MELLINGER-D., POWERS-C., AND KUMAR-V. (2013). Towards a swarm of agile micro quadrotors, *Autonomous Robots*, **35**(4), pp. 287–300.

LEE-D. H., LEE-S. S., AHN-C. K., SHI-P., AND LIM-C.-C. (2021). Finite distribution estimation-based dynamic window approach to reliable obstacle avoidance of mobile robot, *IEEE Transactions on Industrial Electronics*, **68**(10), pp. 9998–10006.

LEE-T.-T., AND JENG-J.-T. (1998). The Chebyshev-polynomials-based unified model neural networks for function approximation, *IEEE Transactions on Systems, Man, and Cybernetics, Part B (Cybernetics)*, **28**(6), pp. 925–935.

LEVANT-A. (2003). Higher-order sliding modes, differentiation and output-feedback control, *International Journal of Control*, **76**(9-10), pp. 924–941.

LEWIS-F. L., ZHANG-H., HENGSTER-MOVRIC-K., AND DAS-A. (2013). *Cooperative control of multi-agent systems: optimal and adaptive design approaches*, Springer Science & Business Media.

LIANG-J., WANG-Z., LIU-Y., AND LIU-X. (2014). State estimation for two-dimensional complex networks with randomly occurring nonlinearities and randomly varying sensor delays, *International Journal of Robust and Nonlinear Control*, **24**(1), pp. 18–38.

LI-B., QIN-K., XIAO-B., AND YANG-Y. (2019a). Finite-time extended state observer based fault tolerant output feedback control for attitude stabilization, *ISA Transactions*, **91**, pp. 11–20.

LI-J., DU-J., AND CHANG-W.-J. (2019b). Robust time-varying formation control for underactuated autonomous underwater vehicles with disturbances under input saturation, *Ocean Engineering*, **179**, pp. 180–188.

LINDSEY-Q., MELLINGER-D., AND KUMAR-V. (2012). Construction with quadrotor teams, *Autonomous Robots*, **33**(3), pp. 323–336.

LIN-H., CHEN-K., AND LIN-R. (2019). Finite-time formation control of unmanned vehicles using nonlinear sliding mode control with disturbances, *International Journal of Innovative Computing, Information and Control*, **15**(6), pp. 2341–2353.

LI-S., AND WANG-X. (2013). Finite-time consensus and collision avoidance control algorithms for multiple AUVs, *Automatica*, **49**(11), pp. 3359–3367.

LIU-D., HUANG-Y., WANG-D., AND WEI-Q. (2013). Neural-network-observer-based optimal control for unknown nonlinear systems using adaptive dynamic programming, *International Journal of Control*, **86**(9), pp. 1554–1566.

LIU-J., AND WANG-X. (2012). *Advanced sliding mode control for mechanical systems*, Springer.

LIU-X., XIAO-J.-W., CHEN-D., AND WANG-Y.-W. (2019). Dynamic consensus of nonlinear time-delay multi-agent systems with input saturation: an impulsive control algorithm, *Nonlinear Dynamics*, **97**(2), pp. 1699–1710.

LIU-Z., LAI-G., ZHANG-Y., AND CHEN-C. L. P. (2015). Adaptive neural output feedback control of output-constrained nonlinear systems with unknown output nonlinearity, *IEEE Transactions on Neural Networks and Learning Systems*, **26**(8), pp. 1789–1802.

LI-X., SHI-P., AND WANG-Y. (2019c). Distributed cooperative adaptive tracking control for heterogeneous systems with hybrid nonlinear dynamics, *Nonlinear Dynamics*, **95**(3), pp. 2131–2141.

LI-X., SHI-P., WANG-Y., AND WANG-S. (2022). Cooperative tracking control of heterogeneous mixed-order multiagent systems with higher-order nonlinear dynamics, *IEEE Transactions on Cybernetics*, **52**(6), pp. 5498–5507.

LI-X., SONG-S., AND GUO-Y. (2018). Robust finite-time tracking control for euler–lagrange systems with obstacle avoidance, *Nonlinear Dynamics*, **93**(2), pp. 443–451.

LI-Z., REN-W., LIU-X., AND FU-M. (2013). Distributed containment control of multi-agent systems with general linear dynamics in the presence of multiple leaders, *International Journal of Robust and Nonlinear Control*, **23**(5), pp. 534–547.

MA-X., SUN-F., LI-H., AND HE-B. (2017). Neural-network-based integral sliding-mode tracking control of second-order multi-agent systems with unmatched disturbances and completely unknown dynamics, *International Journal of Control, Automation and Systems*, **15**(4), pp. 1925–1935.

MENG-W., HE-Z., TEO-R., SU-R., AND XIE-L. (2014). Integrated multi-agent system framework: decentralised search, tasking and tracking, *IET Control Theory & Applications*, **9**(3), pp. 493–502.

MONDAL-A., BHOWMICK-C., BEHERA-L., AND JAMSHIDI-M. (2017a). Trajectory tracking by multiple agents in formation with collision avoidance and connectivity assurance, *IEEE Systems Journal*, **12**(3), pp. 2449–2460.

MONDAL-S., SU-R., AND XIE-L. (2017b). Heterogeneous consensus of higher-order multi-agent systems with mismatched uncertainties using sliding mode control, *International Journal of Robust and Nonlinear Control*, **27**(13), pp. 2303–2320.

OH-K.-K., PARK-M.-C., AND AHN-H.-S. (2015). A survey of multi-agent formation control, *Automatica*, **53**, pp. 424–440.

OLFATI-SABER-R. (2006). Flocking for multi-agent dynamic systems: Algorithms and theory, *IEEE Transactions on Automatic Control*, **51**(3), pp. 401–420.

OLFATI-SABER-R., AND MURRAY-R. M. (2004). Consensus problems in networks of agents with switching topology and time-delays, *IEEE Transactions on Automatic Control*, **49**(9), pp. 1520–1533.

OLFATI-SABER-R., FAX-J. A., AND MURRAY-R. M. (2007). Consensus and cooperation in networked multi-agent systems, *Proceedings of the IEEE*, **95**(1), pp. 215–233.

PEYDAYESH-A., AND AREFI-M. M. (2021). Neuro-adaptive distributed output-feedback containment control for multiagent systems with nonstrict-feedback nonlinear dynamics and input constraints, *International Journal of Robust and Nonlinear Control*, **31**(7), pp. 2465–2490.

QU-Z. (2009). *Cooperative control of dynamical systems: applications to autonomous vehicles*, Springer Science & Business Media.

RADAC-M.-B., AND LALA-T. (2020). Robust control of unknown observable nonlinear systems solved as a zero-sum game, *IEEE Access*, **8**, pp. 214153–214165.

REN-W., AND BEARD-R. W. (2005). Consensus seeking in multiagent systems under dynamically changing interaction topologies, *IEEE Transactions on Automatic Control*, **50**(5), pp. 655–661.

REN-W., BEARD-R. W., AND ATKINS-E. M. (2007). Information consensus in multivehicle cooperative control, *IEEE Control Systems Magazine*, **27**(2), pp. 71–82.

REN-Y., ZHANG-K., JIANG-B., CHENG-W., AND DING-Y. (2022). Distributed fault-tolerant time-varying formation control of heterogeneous multi-agent systems, *International Journal of Robust and Nonlinear Control*, **32**, pp. 2864—2882.

REYNOLDS-C. W. (1987). Flocks, herds and schools: A distributed behavioral model, *Proceedings of the 14th Annual Conference on Computer Graphics and Interactive Techniques*, pp. 25–34.

RICHARD-J.-P. (2003). Time-delay systems: an overview of some recent advances and open problems, *Automatica*, **39**(10), pp. 1667–1694.

ROY-S. (2015). Scaled consensus, *Automatica*, **51**, pp. 259–262.

SHARMA-R. S., MONDAL-A., AND BEHERA-L. (2021). Tracking control of mobile robots in formation in the presence of disturbances, *IEEE Transactions on Industrial Informatics*, **17**(1), pp. 110–123.

SHI-P., AND YAN-B. (2020). A survey on intelligent control for multiagent systems, *IEEE Transactions on Systems, Man, and Cybernetics: Systems*, **51**(1), pp. 161–175.

SHOJAEI-K. (2016). Neural network formation control of underactuated autonomous underwater vehicles with saturating actuators, *Neurocomputing*, **194**, pp. 372–384.

SHTESSEL-Y. B., SHKOLNIKOV-I. A., AND LEVANT-A. (2007). Smooth second-order sliding modes: Missile guidance application, *Automatica*, **43**(8), pp. 1470–1476.

SHTESSEL-Y., EDWARDS-C., FRIDMAN-L., AND LEVANT-A. (2014). *Sliding mode control and observation*, Vol. 10, Springer.

SUN-J., YI-J., PU-Z., AND TAN-X. (2018). Fixed-time sliding mode disturbance observer-based nonsmooth backstepping control for hypersonic vehicles, *IEEE Transactions on Systems, Man, and Cybernetics: Systems*, **50**(11), pp. 4377–4386.

SUN-K., LIU-L., QIU-J., AND FENG-G. (2021a). Fuzzy adaptive finite-time fault-tolerant control for strict-feedback nonlinear systems, *IEEE Transactions on Fuzzy Systems*, **29**(4), pp. 786–796.

SUN-Y., SHI-P., AND LIM-C.-C. (2021b). Event-triggered adaptive leaderless consensus control for nonlinear multi-agent systems with unknown backlash-like hysteresis, *International Journal of Robust and Nonlinear Control*, **31**, pp. 7409–7424.

SUN-Z., PARK-M.-C., ANDERSON-B. D., AND AHN-H.-S. (2017). Distributed stabilization control of rigid formations with prescribed orientation, *Automatica*, **78**, pp. 250–257.

TANG-S., WÜEST-V., AND KUMAR-V. (2018). Aggressive flight with suspended payloads using vision-based control, *IEEE Robotics and Automation Letters*, **3**(2), pp. 1152–1159.

TSAI-C.-C., WU-H.-L., TAI-F.-C., AND CHEN-Y.-S. (2017). Distributed consensus formation control with collision and obstacle avoidance for uncertain networked omnidirectional multi-robot systems using fuzzy wavelet neural networks, *International Journal of Fuzzy Systems*, **19**(5), pp. 1375–1391.

WANG-C., TNUNAY-H., ZUO-Z., LENNOX-B., AND DING-Z. (2019). Fixed-time formation control of multirobot systems: Design and experiments, *IEEE Transactions on Industrial Electronics*, **66**(8), pp. 6292–6301.

WANG-C., ZUO-Z., QI-Z., AND DING-Z. (2018a). Predictor-based extended-state-observer design for consensus of mass with delays and disturbances, *IEEE Transactions on Cybernetics*, **49**(4), pp. 1259–1269.

WANG-X., GUO-J., AND TANG-S. (2018b). Neural network-based multivariable fixed-time terminal sliding mode control for re-entry vehicles, *IET Control Theory & Applications*, **12**(12), pp. 1763–1772.

WEN-G., CHEN-C. P., AND LIU-Y.-J. (2017). Formation control with obstacle avoidance for a class of stochastic multiagent systems, *IEEE Transactions on Industrial Electronics*, **65**(7), pp. 5847–5855.

WIECH-J., EREMEYEV-V. A., AND GIORGIO-I. (2018). Virtual spring damper method for nonholonomic robotic swarm self-organization and leader following, *Continuum Mechanics and Thermodynamics*, **30**(5), pp. 1091–1102.

WOOLDRIDGE-M. (2009). *An introduction to multiagent systems*, John Wiley & Sons.

WU-L.-B., PARK-J. H., XIE-X.-P., REN-Y.-W., AND YANG-Z. (2020). Distributed adaptive neural network consensus for a class of uncertain nonaffine nonlinear multi-agent systems, *Nonlinear Dynamics*, **100**(2), pp. 1243–1255.

XIONG-S., AND HOU-Z. (2021). Data-driven formation control for unknown MIMO nonlinear discrete-time multi-agent systems with sensor fault, *IEEE Transactions on Neural Networks and Learning Systems*. doi: 10.1109/TNNLS.2021.3087481.

XU-W., QU-S., ZHAO-L., AND ZHANG-H. (2020). An improved adaptive sliding mode observer for middle-and high-speed rotor tracking, *IEEE Transactions on Power Electronics*, **36**(1), pp. 1043–1053.

YAN-B., SHI-P., AND LIM-C.-C. (2021). Robust formation control for nonlinear heterogeneous multiagent systems based on adaptive event-triggered strategy, *IEEE Transactions on Automation Science and Engineering*. doi: 10.1109/TASE.2021.3103877.

YANG-J., LI-S., AND YU-X. (2012). Sliding-mode control for systems with mismatched uncertainties via a disturbance observer, *IEEE Transactions on Industrial Electronics*, **60**(1), pp. 160–169.

YANG-J., LI-S., SU-J., AND YU-X. (2013). Continuous nonsingular terminal sliding mode control for systems with mismatched disturbances, *Automatica*, **49**(7), pp. 2287–2291.

YANG-R., LIU-L., AND FENG-G. (2022). Cooperative output tracking of unknown heterogeneous linear systems by distributed event-triggered adaptive control, *IEEE Transactions on Cybernetics*, **52**(1), pp. 3–15.

YU-J., DONG-X., LI-Q., AND REN-Z. (2018). Practical time-varying formation tracking for second-order nonlinear multiagent systems with multiple leaders using adaptive neural networks, *IEEE Transactions on Neural Networks and Learning Systems*, **29**(12), pp. 6015–6025.

YU-J., DONG-X., LI-Q., AND REN-Z. (2019). Practical time-varying formation tracking for high-order nonlinear multi-agent systems based on the distributed extended state observer, *International Journal of Control*, **92**(10), pp. 2451–2462.

ZHANG-R., SONG-B., PEI-Y., AND YUN-Q. (2019). Improved method for subsystems performance trade-off in system-of-systems oriented design of uav swarms, *Journal of Systems Engineering and Electronics*, **30**(4), pp. 720–737.

ZHENG-S., SHI-P., WANG-S., AND SHI-Y. (2021). Adaptive neural control for a class of nonlinear multiagent systems, *IEEE Transactions on Neural Networks and Learning Systems*, **32**(2), pp. 763–776.

ZHOU-J., WEN-C., AND LI-T. (2012). Adaptive output feedback control of uncertain nonlinear systems with hysteresis nonlinearity, *IEEE Transactions on Automatic Control*, **57**(10), pp. 2627–2633.

ZHOU-W., WANG-Y., AHN-C. K., CHENG-J., AND CHEN-C. (2020). Adaptive fuzzy backstepping-based formation control of unmanned surface vehicles with unknown model nonlinearity and actuator saturation, *IEEE Transactions on Vehicular Technology*, **69**(12), pp. 14749–14764.

ZOU-A.-M., AND KUMAR-K. D. (2012). Neural network-based adaptive output feedback formation control for multi-agent systems, *Nonlinear Dynamics*, **70**(2), pp. 1283–1296.

ZOU-A.-M., KUMAR-K. D., AND HOU-Z.-G. (2013). Distributed consensus control for multi-agent systems using terminal sliding mode and Chebyshev neural networks, *International Journal of Robust and Nonlinear Control*, **23**(3), pp. 334–357.

ZOU-A.-M., KUMAR-K. D., HOU-Z.-G., AND LIU-X. (2011). Finite-time attitude tracking control for spacecraft using terminal sliding mode and Chebyshev neural network, *IEEE Transactions on Systems, Man, and Cybernetics, Part B (Cybernetics)*, **41**(4), pp. 950–963.